POLITECNICO DI TORINO

Collegio di Ingegneria Chimica e dei Materiali

Master of Science Course
in Materials Engineering

Master of Science Thesis

Diamond dressing of vitrified grinding wheels

Tutors:
Prof.ssa Salvo Milena (Politecnico di Torino)
Prof. Krajnik Peter (Chalmers university of technology)

Co-Tutor:
Prof. Gobber Federico Simone (Politecnico di Torino)

Candidate:
Nigro Francesco

October 2022

Preface

The following thesis work has been carried out as a project formalized by the IGC (International Grinding Centre). The tests have been run in the Materials Processing Laboratory at Chalmers University of Technology, in the period going from January 2022 to June 2022.
At the end of the work carried out, a debt of gratitude is due to my supervisors, Jeffrey Badger (The Grinding Doc) and Peter Krajnik (Professor at Materials and Manufacturing/Industrial and Materials Science, Chalmers University of Technology), for their guidance during the project and for the maximum availability and kindness shown.
I thank the Ph.D co-supervisor Philipp Hoier (Researcher at Materials and Manufacturing / Industrial and Materials Science, Chalmers University of Technology), whose support has been fundamental during the experimental work and the use of the machine.
In addition, I would like to express my gratitude to my thesis partner, Stefano Vindemmio, and my Italian supervisors at the Polytechnic of Turin, Prof.ssa Milena Salvo (DISAT) and Prof. Federico Simone Gobber (DISAT), for their availability and support.
I thank my parents for the financial and psychological support in my university career. Thanks to them, I was able to concentrate most of my time on studying and to take part to a lot of opportunities, as the Erasmus mobility project.
I would also like to include all the friends who have been close to me over these two.
To all those who have been close to me over these two years, I just want to say THANK YOU**.**

RIASSUNTO

Il lavoro di tesi è stato realizzato come progetto formalizzato dall'IGC (International Grinding Center).
Lo scopo del progetto è fornire una descrizione dettagliata della rettifica e della ravvivatura, concentrandosi sulle definizioni, sui fenomeni coinvolti durante le operazioni, sui diversi tipi di macchine, sulle applicazioni e sulle principali variabili da conoscere per una completa comprensione dei processi.
Vengono presentati precedenti test effettuati da Malkin, Murray e Salmon sugli effetti della ravvivatura rotante sulle prestazioni delle mole, oltre a una definizione del numero di aggressività nei processi di finitura e studi sull'utilità del monitoraggio del segnale di emissione acustica durante la ravvivatura, di Badger et al.
Continuando gli esperimenti citati ed estendendo gli studi a nuove valutazioni, gli obiettivi sono:

- Analizzare gli effetti della ravvivatura diamantata a tuffo sulle prestazioni delle mole vetrificate.
- Stabilire l'importanza del numero di Aggressività di ravvivatura per monitorare i danni termici (chiare correlazioni tra le variabili di ravvivatura e rettifica e il numero di aggressività della ravvivatura) e dimostrare la possibilità di poter valutare l'affilatura della mola.
- La rilevanza del monitoraggio del segnale di emissione acustica nella ravvivatura.

Nella ravvivatura a tuffo diamantato, il rullo viene immerso in una mola senza movimento trasversale. I parametri più importanti per i processi di ravvivatura a tuffo sono: avanzamento radiale, rapporto di velocità e modalità, la quale può essere unidirezionale o anti-direzionale.
I test sono stati eseguiti con condizioni di rettifica fisse e, infine, anche con condizioni di rettifica variabili per vedere gli effetti combinati dei parametri di rettifica e ravvivatura sulla generazione di calore.
Per analizzare gli effetti della ravvivatura a tuffo sulle prestazioni della mola, è stata utilizzata una macchina CNC BLOHM PLANOMAT HP 408 (macchina di ravvivatura e rettifica) e sono stati utilizzati i seguenti materiali:

- **Rullo di ravvivatura diamantato a tuffo**: il diametro del rullo è 150 mm e la larghezza è 12,83 mm. Un rivestimento diamantato di 5 mm di spessore radiale è montato su un corpo in acciaio e il legame per le grane diamantate è un innovativo legame ibrido, grazie al quale viene migliorata la resistenza all'usura.
- **Disco di ravvivatura diamantato**: il disco diamantato è stato utilizzato per eseguire la ravvivatura del profilo e la ravvivatura. Il rivestimento diamantato ha uno spessore radiale di 5 mm ed è montato su un corpo in acciaio. Le grane di diamante sono trattenute dallo stesso legame ibrido del rullo di ravvivatura diamantato. Il diametro è di 125 mm e la larghezza del rivestimento diamantato è di 2 mm.
- **Mola in ossido di Alluminio**: la mola è codificata EWD46G7VHK (spiegazione dettagliata nella sezione 6.2.3.). La larghezza della mola è di 50 mm e il diametro iniziale è di 400 mm. La mola per eseguire l'attività sperimentale è stata profilata in modo da ottenere un gradino largo quanto il rullo di ravvivatura.
- **Pezzi piatti in acciaio:** i pezzi rettificati sono stati prelevati da una barra più grande realizzata in 38MnSiVS5 con durezza 217 HV5. La lunghezza dei pezzi era di 68 cm. Essi sono stati utilizzati per effettuare misurazioni e analizzare l'effetto della ravvivatura a tuffo sulle prestazioni della mole.

Il rullo e il disco di ravvivatura diamantato sono stati acquistati e forniti dall'azienda Meister Abrasives; invece, la mola in ossido di alluminio è stata fornita dall'azienda Hermes Abrasives.
Inoltre, sono stati effettuati studi ed analisi sull'utilità del monitoraggio del segnale di emissione acustica durante l'operazione di rettifica. Ciò è stata possibile in quanto la macchina BLOHM è caratterizzata da un sensore che è in grado di rilevare le emissioni acustiche durante le diverse operazioni svolte.
Infine, è stata eseguita un'analisi al microscopio elettronico a scansione per valutare la topografia della ruota dopo la ravvivatura, evidenziando le differenze tra l'operazione di ravvivatura smussata e affilata.
Di seguito si riporta una discussione e trattazione sul lavoro sperimentale svolto in questo studio per la ravvivatura a tuffo di mole vetrificate e risultati finali ottenuti.

1. Coerenza con i risultati di Malkin a Murray

Alcuni dei risultati sono comparabili con gli esperimenti di Malkin e Murray, in particolare i grafici in cui l'energia specifica è riportata in funzione del numero di Aggressività di ravvivatura e dell'energia specifica di ravvivatura, riportati rispettivamente in Figura 1.
Ciò dimostra che i comportamenti delle variabili sono complessivamente coerenti, nonostante si siano adottate condizioni e strumenti diversi, come rullo di ravvivatura, mola e pezzo in acciaio.
Infatti, nel primo grafico (in alto), i dati presentano lo stesso comportamento e valori simili.
Invece nel secondo grafico in Figura 1 (in basso), la situazione è un po' diversa: considerando il comportamento è possibile affermare sia per i risultati di Malkin e Murray sia per i nuovi esperimenti che ad una maggiore energia specifica di ravvivatura, corrisponde un'energia specifica di rettifica maggiore; ma osservando il valore dei punti dati è più difficile trovare una chiara somiglianza.
Ciò è dovuto a molti fattori coinvolti nelle operazioni eseguite, quali: tipo di materiale, dimensione e tipo della grana della mola, tipo di liquido refrigerante e parametri di rettifica solo per citarne alcuni.
Pertanto, in questo caso, il principale risultato raggiunto è che per una data operazione di rettifica, l'energia specifica di rettifica aumenta con l'energia specifica di ravvivatura.
Per avere un'idea migliore sul motivo della differenza di questi valori, sarebbe necessario eseguire un numero maggiore di prove con una maggiore varietà di parametri di ravvivatura, nonché diverse condizioni di rettifica e vari tipi di mole.

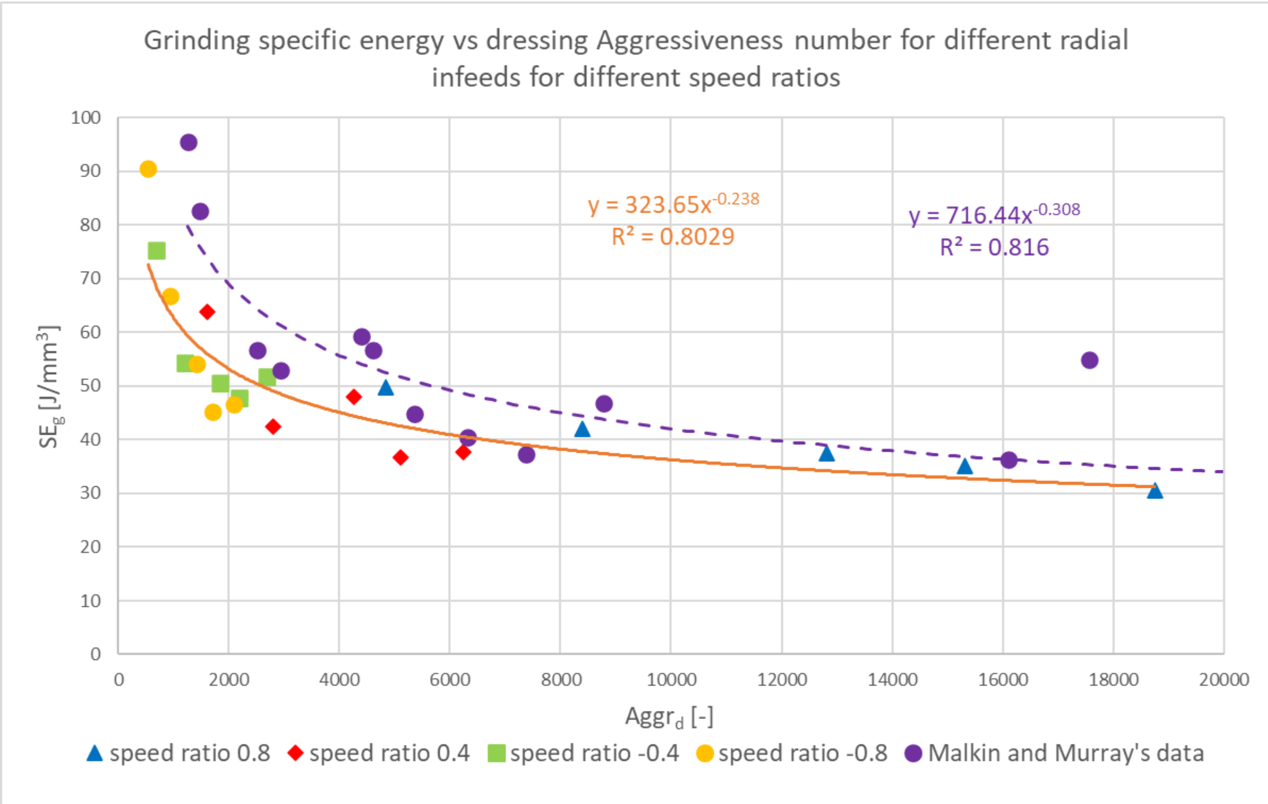

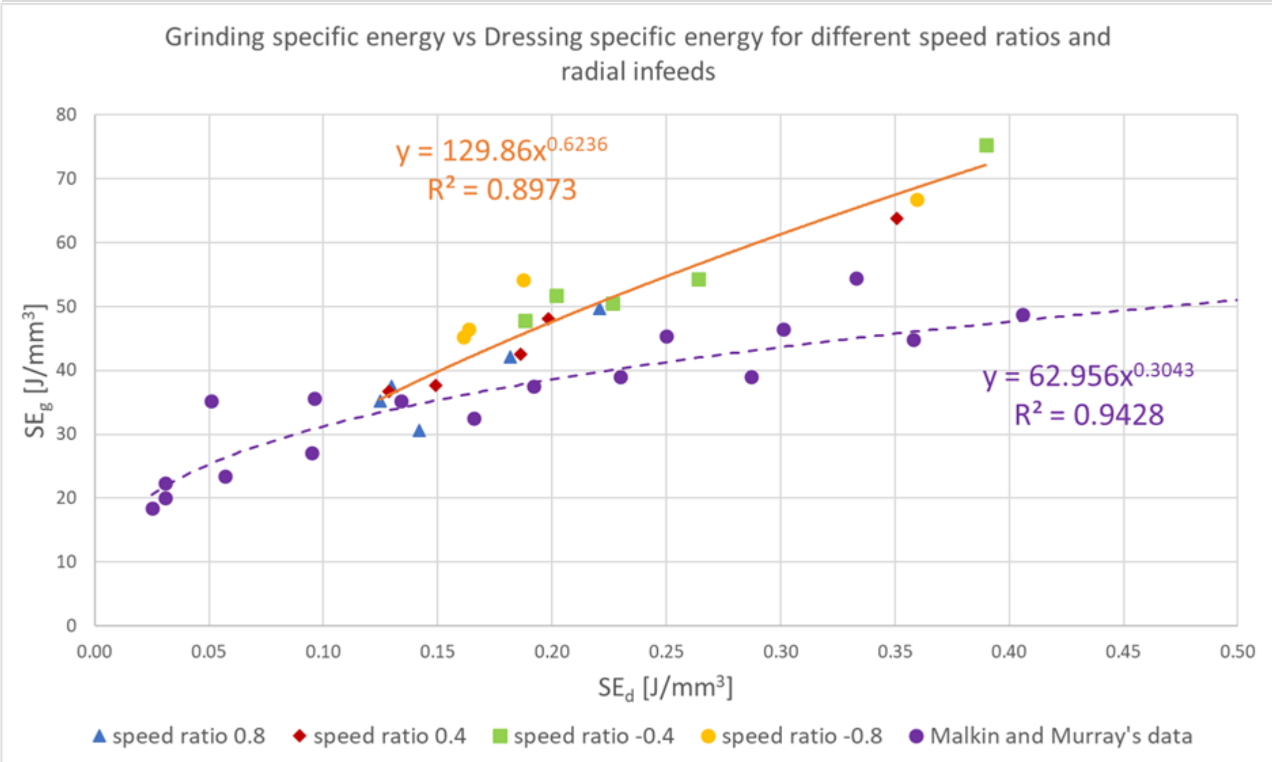

Figura 1: Grafici sperimentali simili ai risultati di Malkin e Murray

2. Importanza del numero di Aggressività

Un secondo risultato importante è l'utilità di definire un numero di aggressività di ravvivatura.
Uno dei principali punti di forza di questo numero adimensionale è che semplicemente osservando l'equazione per la ravvivatura a tuffo, riportata in Equazione 1, è possibile regolare i parametri (rapporto di velocità e avanzamento radiale per giri ruota, sottolineati in blu nell'equazione) in modo da evitare danni termici, come bruciature, le quali influiscono negativamente sulla qualità del pezzo.

$$Aggr_d\ [-] = \frac{1}{1 - \underline{\left(\frac{v_r}{V}\right)}} \cdot \sqrt{\frac{\underline{a_{eff}}}{d_{eq}}} \cdot 10^6$$

Equazione 1: Numero di Aggressività di ravvivatura

Inoltre, una volta fissate le condizioni di rettifica, è possibile stabilire una "regola" per prevedere i danni termici; infatti, la bruciatura è causata da una combinazione di ravvivatura troppo opaca (rapporto di Aggressività di ravvivatura basso) e di Aggressività di rettifica troppo grande (es. elevata velocità di avanzamento del pezzo o grande profondità di taglio).
In Figura 2, per condizioni di rettifica fisse, solo una condizione di ravvivatura (la più smussata) ha portato a bruciatura, quindi è possibile stabilire una soglia.

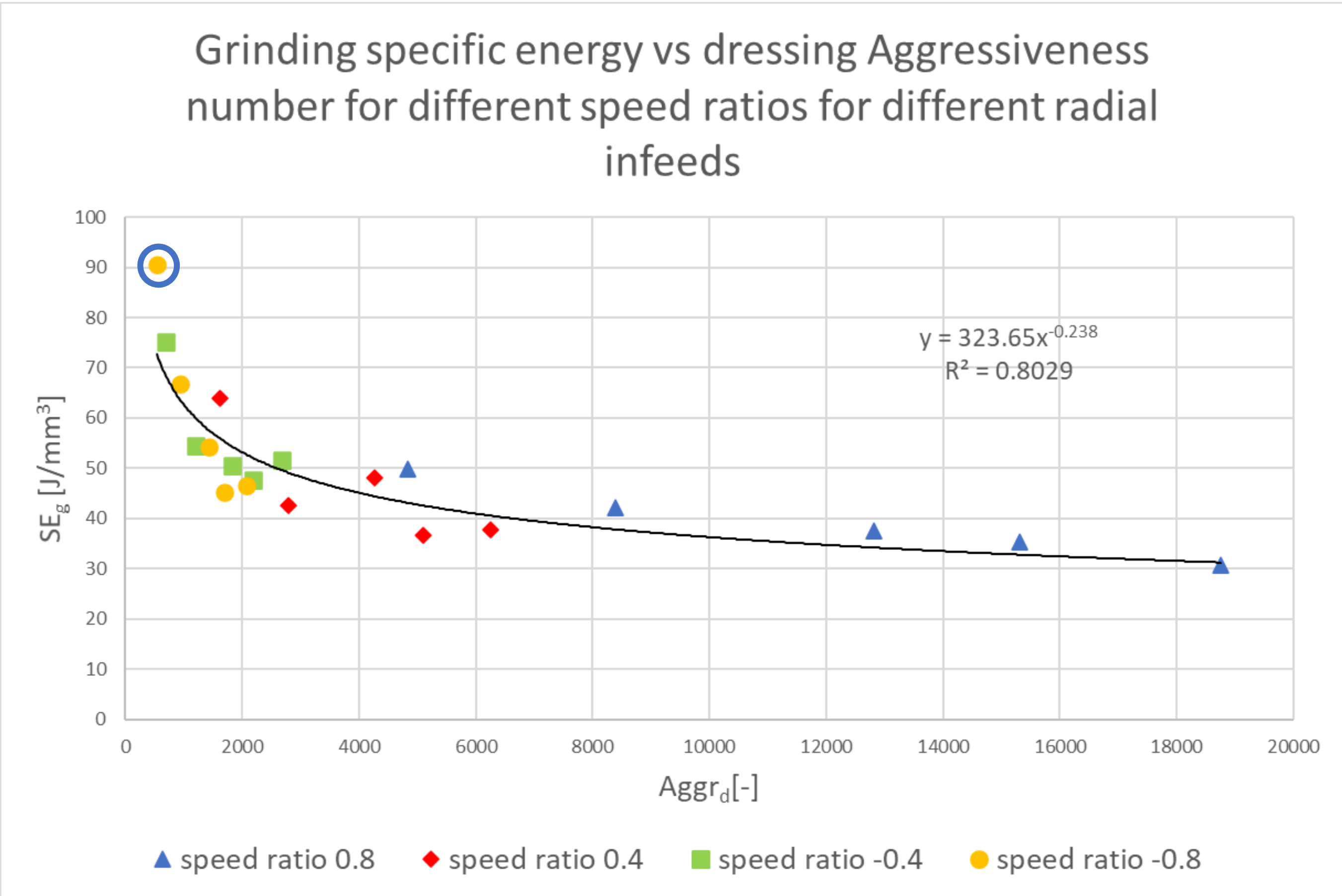

Figura 2: Energia specifica di rettifica vs il numero di aggressività di ravvivatura - soglia di bruciatura

Un ragionamento simile per condizioni variabili di ravvivatura e rettifica viene visualizzato nel grafico in Figura 3 e, ancora una volta, la bruciatura può essere facilmente rilevata, in quanto presenta un andamento differente.

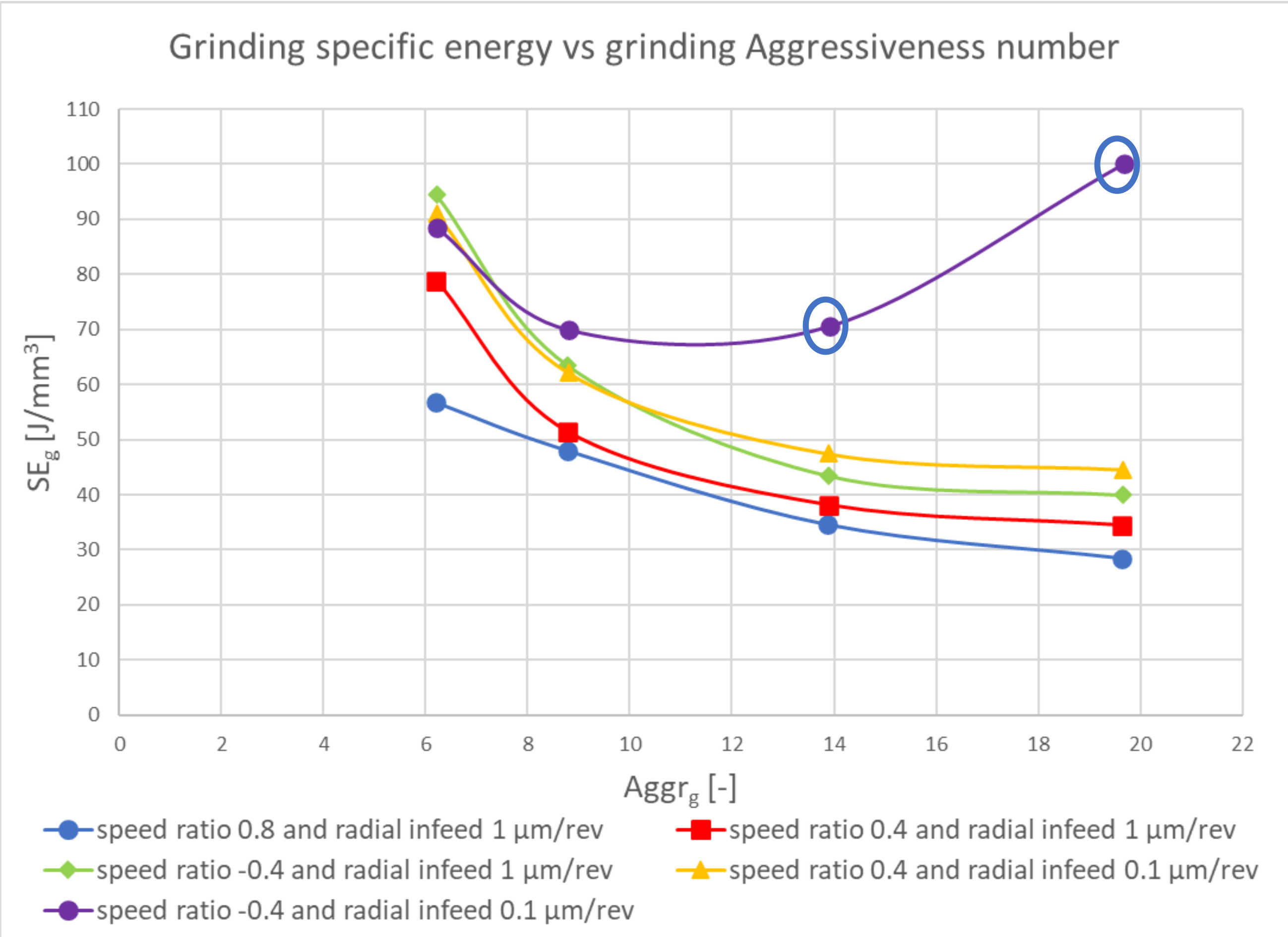

Figura 3: Energia specifica di rettifica vs il numero di Aggressività di rettifica – verifica di bruciatura

Un altro punto chiave raggiunto è che attraverso il numero di Aggressività di ravvivatura è possibile valutare l'affilatura della mola.
Per stabilire se la condizione di ravvivatura è opaca o affilata, quindi se la mola avrebbe aree più o meno appiattite, lo stesso grafico come quello mostrato in Figura 3 può essere utilizzato: una condizione di ravvivatura più smussata porterà a un'energia specifica più elevata e viceversa per condizioni di affilatura.
L'energia specifica (SE) indica l'energia spesa durante l'operazione per unità di volume. Si ottiene mediante l'Equazione 2.

$$SE = \frac{P}{Q} \left[\frac{J}{mm^3}\right]$$

Equazione 2: Energia specifica

In cui:
P è la potenza di rettifica (o di ravvivatura), dato dall' Equazione 3
Q è il tasso di rimozione del materiale, riportato in Equazione 4.

$$P = P_{total} - P_{idle}\ [W]$$

Equazione 3: Potenza di rettifica o di ravvivatura

$$MRR\ \left[\frac{mm^3}{s}\right] = Q = depth\ of\ cut\ [mm] \cdot feedrate\ \left[\frac{mm}{s}\right] \cdot width\ of\ cut\ [mm].$$

Equazione 4: Tasso di asportazione del materiale

Maggiore è la potenza, e di conseguenza l'energia specifica, più inefficiente sarà il processo (si verificherà più sfregamento).
Per tutti i tipi di ravvivatura, c'è un compromesso da fare tra generazione di calore e rugosità superficiale ottenuta durante la rettifica.
In dettaglio, una ravvivatura più affilata produrrà meno calore durante la molatura ma una finitura peggiore, e il contrario per una condizione di ravvivatura opaca.

Inoltre, le immagini SEM hanno rivelato differenze consistenti tra condizione di operazione opaca e affilata, come si può vedere nel confronto in Figura 4 tra due degli zoom su aree smussate e affilate con carico di acciaio: nella condizione opaca, la presenza di acciaio risulta più elevata e il materiale è sostanzialmente fuso, indicando un maggiore sfregamento e aratura rispetto al taglio, quindi una maggiore generazione di calore; nel caso affilato invece, alcuni chip sono visibili per mezzo degli elettroni retro diffusi, quindi i bordi dei grani sono più affilati e si sta verificando il taglio.

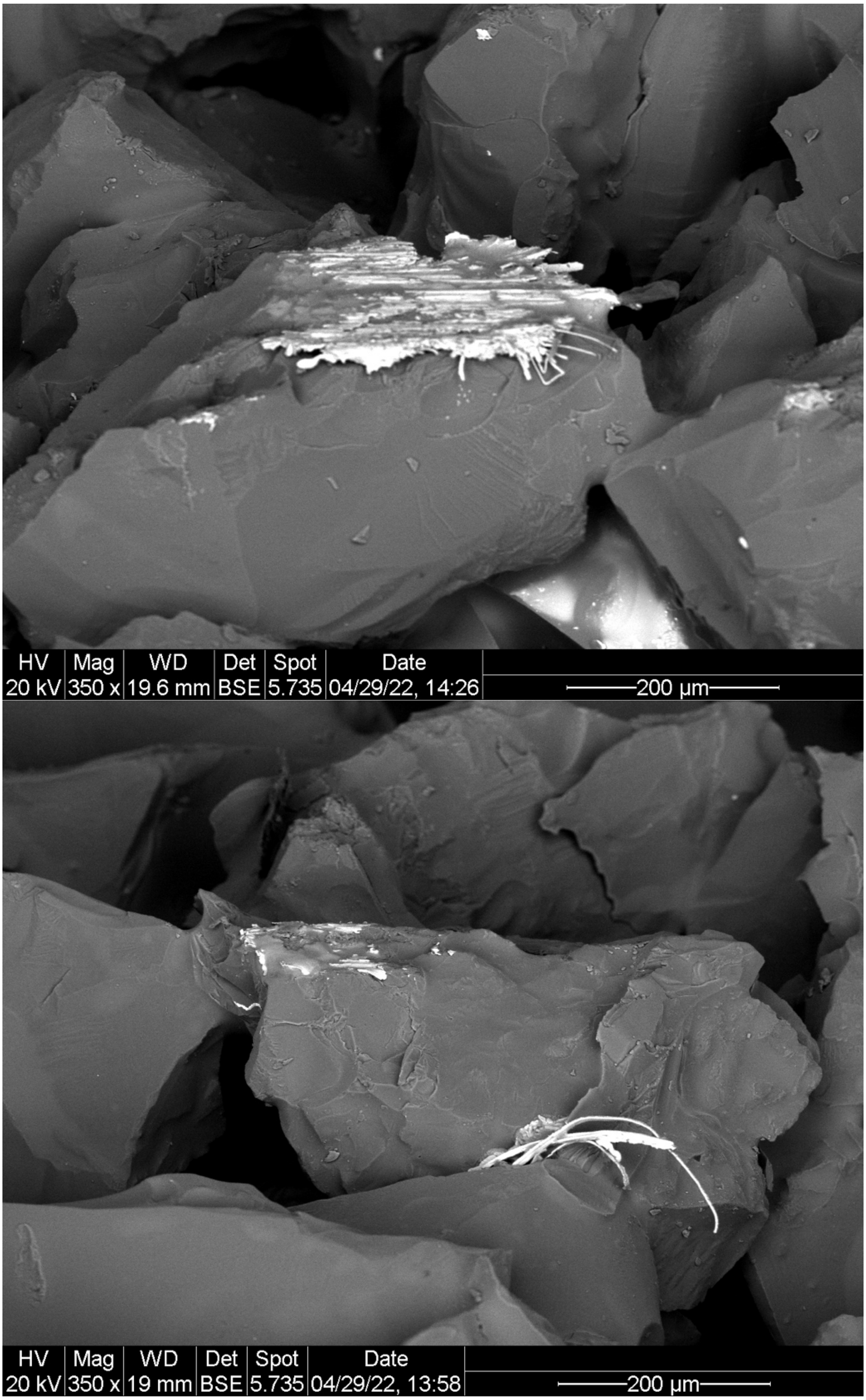

Figura 4: Smussato (sopra) e affilato (sotto) - confronto

3. Segnale di emissione acustica durante la ravvivatura

L'emissione acustica è stata un altro importante fattore di studio nei test.
Tramite il sensore di emissione acustica montato a bordo macchina BLOHM è stato possibile raccogliere i dati AE provenienti dalle operazioni di ravvivatura e trarre conclusioni.
In primo luogo, è stato dimostrato che era possibile trovare una correlazione tra emissione acustica e potere di ravvivatura (Figura 5), o ancora meglio tra le corrispondenti energie specifiche (Figura 6).
In Figura 7 e in Figura 8 si dimostra che la potenza della ravvivatura e l'emissione acustica hanno lo stesso comportamento durante il processo.
Esiste infine la possibilità di definire una potenza "calibrata" di emissione acustica, e in Figura 9 si è notato che la precisione non sarà troppo bassa rispetto a quella derivante dal seguire un andamento della legge di potenza, quello con R^2 più alto.
Il valore dell'emissione acustica è stato espresso in percentuale di un certo valore in Volt, non noto; tuttavia, anche il valore in Volt è stato "calibrato" per avere una correlazione tra AE e potenza di ravvivatura dando una possibile proporzionalità lineare con pendenza prossima a 1: quindi un valore percentuale di emissione acustica corrisponderebbe allo stesso valore in Watt per il potere di ravvivatura.

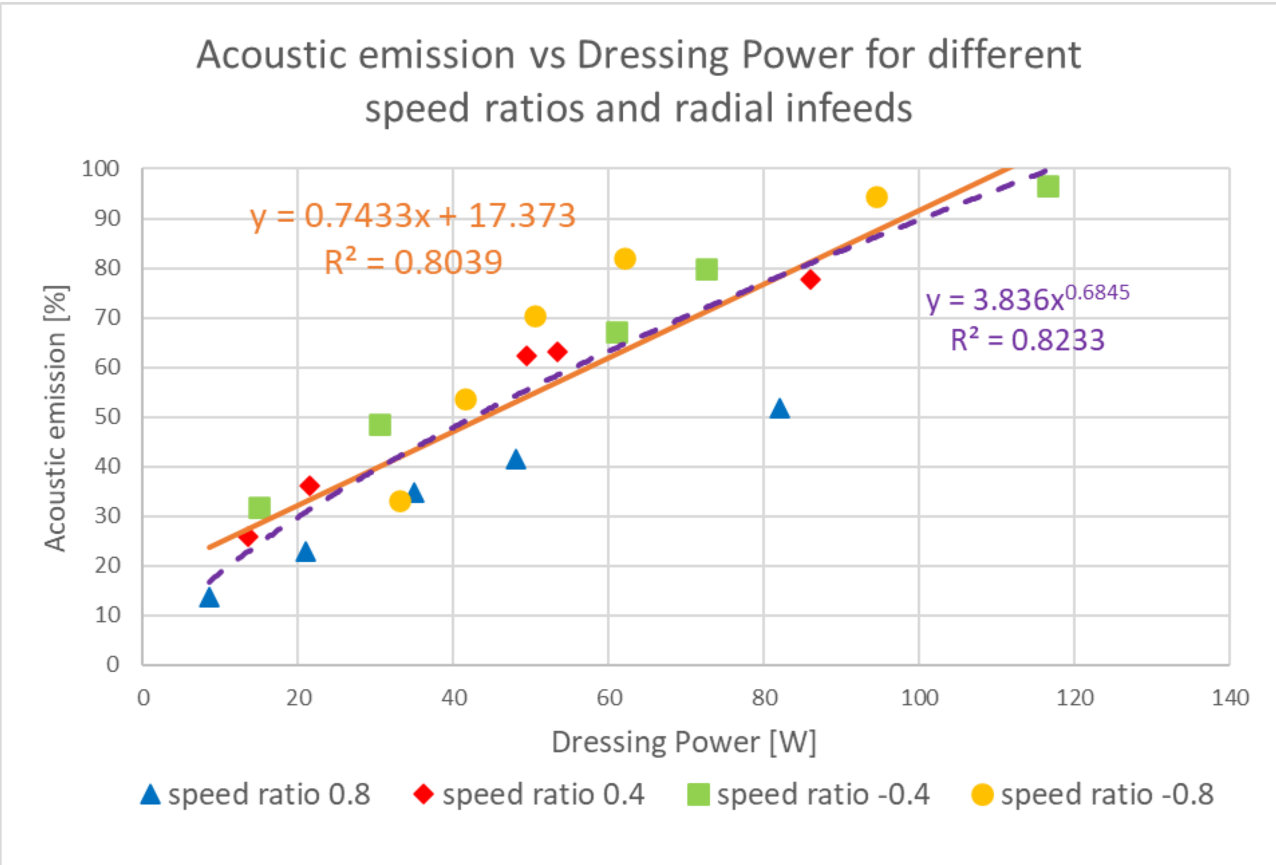

Figura 5: Emissione acustica vs la potenza di ravvivatura per diversi rapporti di velocità: l'andamento legge di potenza

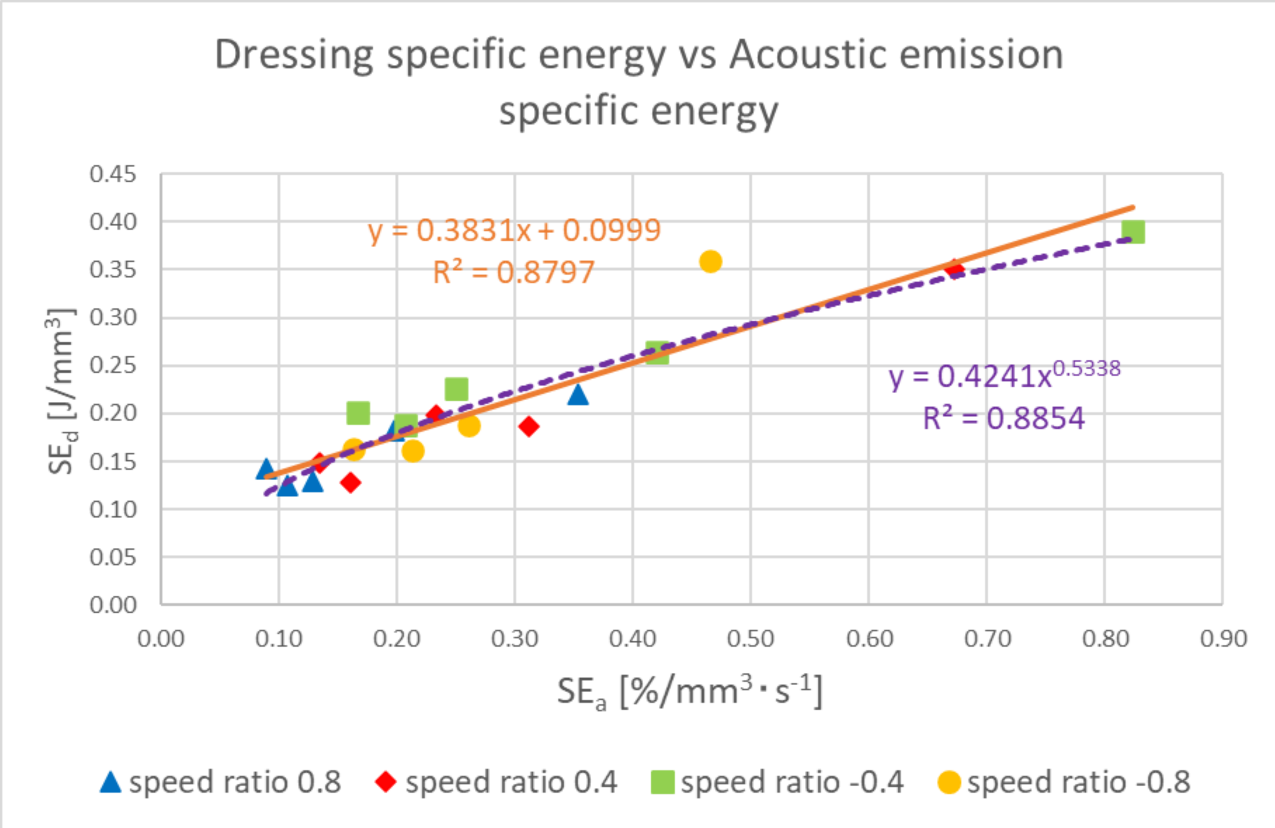

Figura 6: Energia specifica di ravvivatura vs l'energia specifica dell'emissione acustica per diversi rapporti di velocità: andamento lineare e andamento legge di potenza

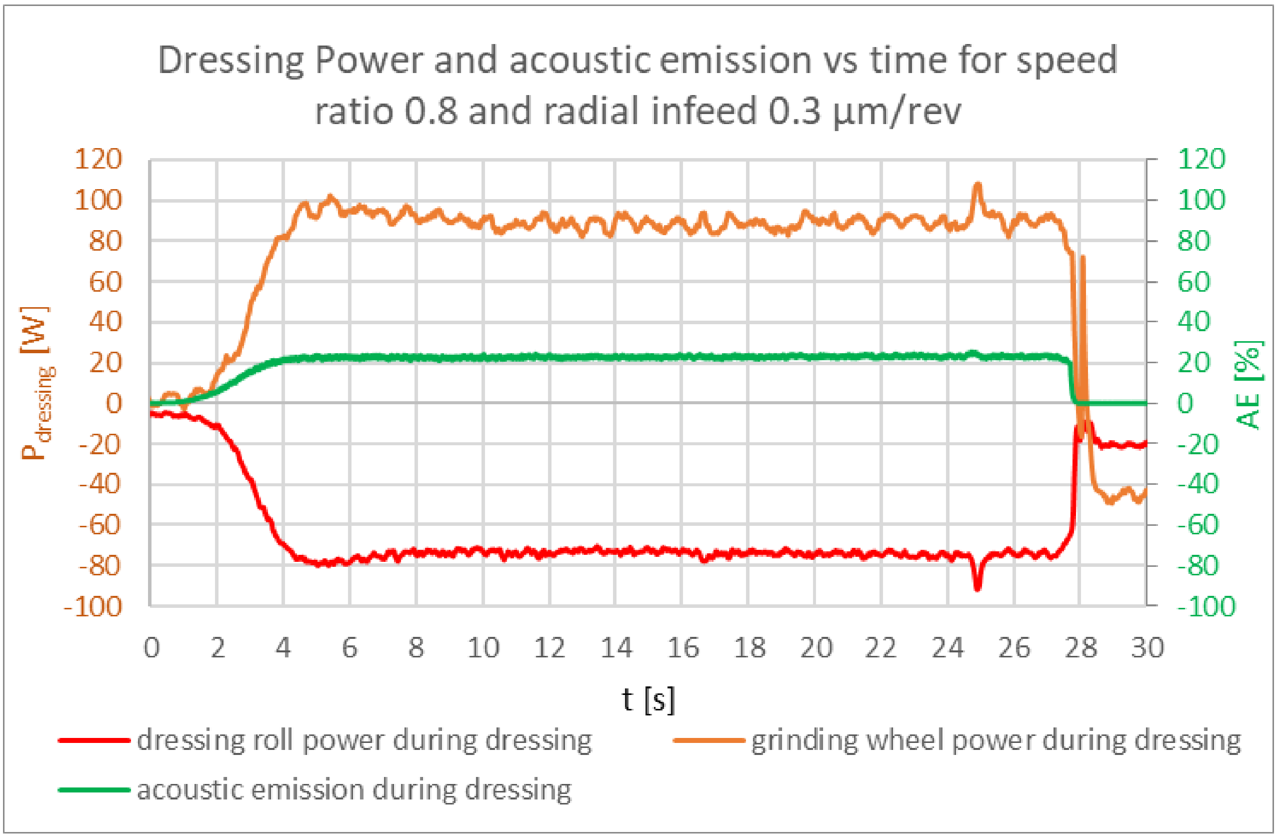

Figura 7: Potenza di ravvivatura e l'emissione acustica sono rappresentate rispetto al tempo con rapporto di velocità 0,8 e alimentazione radiale 0,3 µm/giro

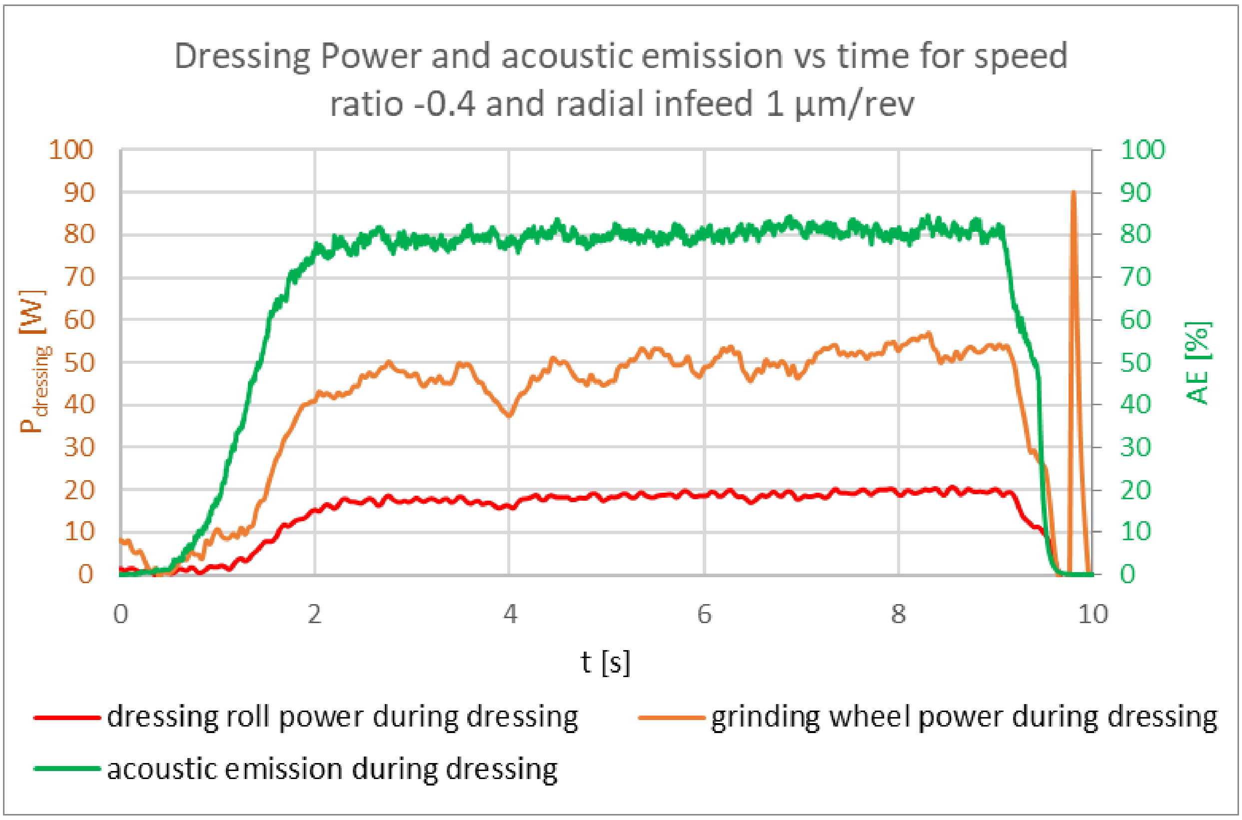

Figura 8: La potenza di ravvivatura e l'emissione acustica sono rappresentate rispetto al tempo con rapporto di velocità -0,4 e alimentazione radiale 1 µm/giro

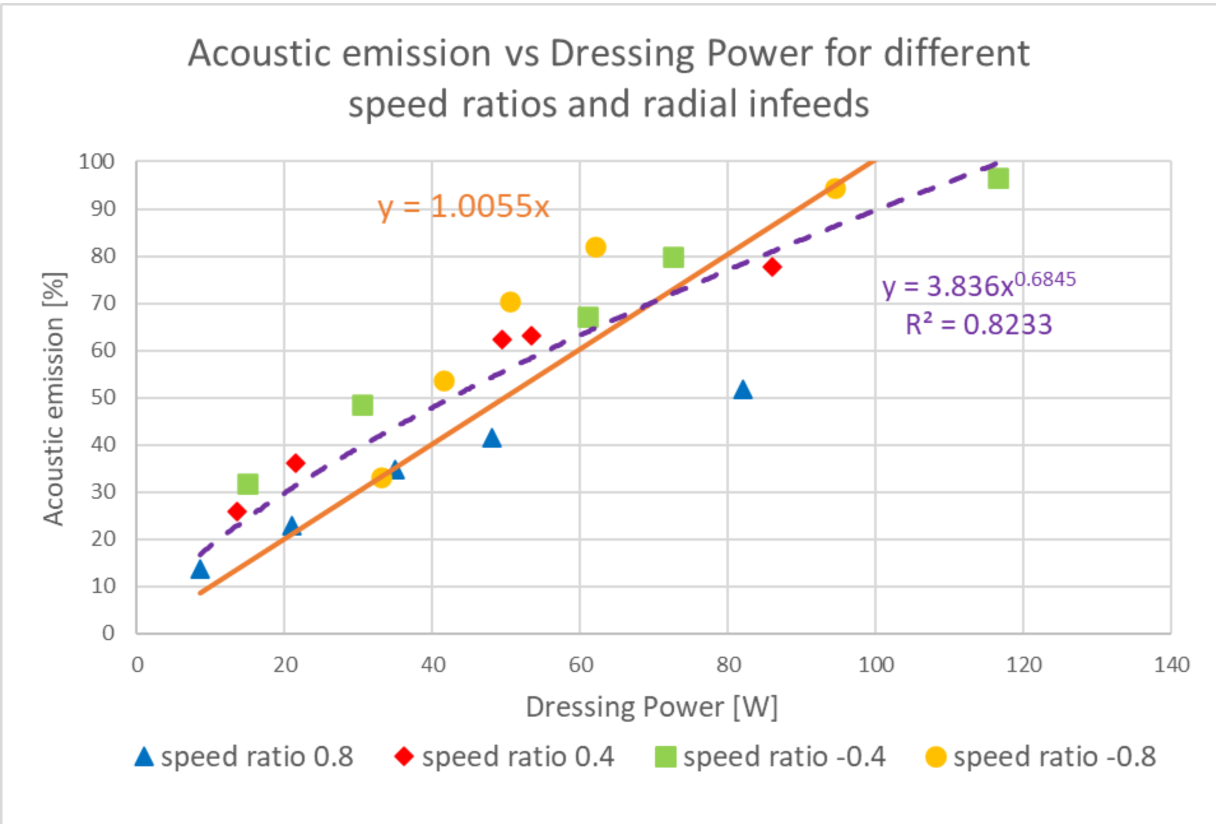

Figura 9: L'emissione acustica viene rappresentata rispetto alla potenza di ravvivatura per diversi rapporti di velocità: linea di tendenza lineare con zero come intercetta e tendenza della legge di potenza

Contents

1. ABSTRACT

The purpose of this project is to collect several dressing data into a unifying theory of aggressiveness and to assess the sharpness of the wheels conditioned with different dressing configurations.
The preparation of grinding tools is the most important enabling factor in the grinding process. Dressing is the process of conditioning the wheel surface to achieve a certain grinding behavior. A high-performing dressing method refers to form-roll plunge dressing, where the diamond roll is plunged into a grinding wheel with no traverse motion. The most important parameters for plunge dressing processes are: radial infeed, speed ratio, and mode (uni- or anti-directional).
The project involves doing experiments using a Blohm industrial grinding and dressing machine, a diamond plunge-roll dresser from Master Abrasives, an aluminum oxide grinding wheel and different flat workpiece to make measurements and analyze the effect of plunge-roll dressing on grinding wheels performance.
A state of art on definition of Aggressiveness number in finishing processes and studies on utility of acoustic emission signal monitoring during dressing, by Badger et al. is reported.
Moreover, scanning electron microscope analysis has been carried out to assess the wheel topography afterwards dressing, underlighting differences between dull and sharp dressing operation.

2 GRINDING PROCESS

2.1. Introduction

Grinding is an important manufacturing process, specifically an abrasive process, that accounts for approximately 20-25% of the total expense for machining operations in industrialized countries. Almost everything we use has been ground at certain point of its production or has been machined by machines that owe their precision to abrasive technologies. [1]

In manufacturing it refers to the removal of metal by abrasion exerted through a rotating abrasive wheel, which is characterized by hard abrasive particles, utilized as cutting medium. The speed of rotation of the grinding wheel, allows to remove a moderate amount of material from the surface of the workpiece to be machined with remarkable precision. By means its characteristics, grinding is a very precise but also expensive process, which makes it suitable only for parts that require a high surface finish. [2]

Therefore, grinding is a material removal process where the abrasive grains act as cutting tools, while the bond acts as a tool holder. Like other machining processes, as milling and turning, grinding is a chip removal process. Abrasive grains of grinding wheels perform in much the same manner as single-point cutting tools, effecting by a multitude of contacts, a multiple-tool cutting action which creates extremely tiny chips similar to those produced in turning. Since cutting edges of the grits are extremely thin, it is possible to remove much smaller chips and refine surface to a much greater accuracy of finish and dimension than with other methods of cutting. [3]

Furthermore, grinding can be likened to the milling process. Cutting occurs on either the periphery or the face of the grinding wheel, similar to peripheral and face milling. Peripherical grinding is more used than face grinding. Despite these similarities, there are relevant differences between grinding and milling:

- The abrasive grains in the wheel are smaller and more numerous than the teeth on a milling cutter.
- Cutting speeds in grinding are higher than in milling.
- The abrasive grits in grinding wheel are randomly oriented and they featured a negative rake angle.
- A grinding wheel is self-sharpening: as the wheel wears, the abrasive particles become dull and either fracture to create fresh cutting edges or are pulled out of the surface of the wheel to expose new grains. [2]

Because heat, small chips, and loose grit are released during grinding, coolants are almost always directed to the interface between the grinding medium and the workpiece. Coolants clean the abrasive wheel in order that it will be free cutting. They are usually water based, with soluble oil additives that prevent rust and add to the cooling effectiveness. Synthetic coolants are also available. [2] [4]
An area where grinding process is unchallenged, it is the machining of extreme hardness or brittleness materials, which for their properties cannot be efficiently shaped by other machining methods. In the production of hardened steel components, such as cutting tools for instance, grinding can be performed on either the annealed or the hardened steel, while other machining methods are usually restricted to the annealed material. Moreover, the machining of non-metallic brittle materials, as ceramics, cemented carbides and glasses, is almost exclusively dependent on abrasive processes. [1]

Therefore, grinding process has the following advantages:

- It is the only way, without considering of lasers and special welding techniques, to machine materials that have a hardness greater than Rockwell C50.

- Different amounts of material may be removed in the process. Parts having high hardness are usually machined or formed in the annealed state, hardened, and then ground.

- Due to the several small cutting edges inherent in the wheel, grinding produces fine finishes. Surface roughness of 0.4 – 2200 micrometers are commonplace.

- Grinding is a fast process which allows to reach accurate dimension, because generally only a small amount of stock is removed. It is possible to grind the workpiece with +- 0.005 mm tolerance.

- Grinding pressure is minimal. This feature allows the magnetic chucks to hold the piece in many grinding operations.

- It is possible to machine non-metallic brittle materials.

Based on the above, grinding offers several excellent advantages, but the workpiece is the deciding factor in the choice of grinding over other metal-working methods.
It should be considered:

- If the drawing defines a specific micro-finish.
- If the part is hardened or soft.
- The precision of the tolerance set for any particular dimension.
- In which shape is workpiece surface before using the grinding process

If the previous examinations favor grinding, then grinding will provide almost any required surface micro-finish, maintain extremely close tolerances, and cutting rapidly and economically.
Moreover, it allows accurate duplication of size and finishes.

If grinding is not required, then the operation is a waste of money. It should be highlighted that grinding, using the proper wheel and machine, will remove stock quickly and will compete favorably with other cutting techniques.

The whole grinding technique is deeper related to the required quality of surface finish. Grit size is a relevant factor in surface finish, but it is not the only one. Others are: wheel speed, feed, dept of cut, wheel balance, type of coolant used if any, type of bond and accuracy of the grinding machine.
Hence, it’s obvious that even if grinding is a science, it is an art too.
Its practice as an art is evident in the work of an expert mechanic who has faced different and numerous grinding problems and who has long practiced skill and common sense in solving them. [2]

2.2. GRINDING WHEELS

The grinding wheels are characterized by three basic elements, as it shown in Figure 1: abrasive particles, bonding material and porosity.
The abrasive particles are the material of great hardness that carries out the removal of shavings. It is held in place in the agglomerate by a bonding material. Porosity is simply constituted by the pores of the abrasive mass: it is important because it allows the coolant to reach the wheel-workpiece interface and ensures space for the formation of chips.
The composition of the grinding wheel and the relative percentages of its three components determine the behavior of the wheel itself in machining. The details of the particular type of wheel are reported on it and follow a standard system of classification and marking of the wheels.
The grinding wheel are classified and chosen for a specific grinding operation by means of four main parameters [2]:

1. **Abrasive Material**
2. **Grain Size**
3. **Bonding Material**
4. **Wheel grade and wheel structure**

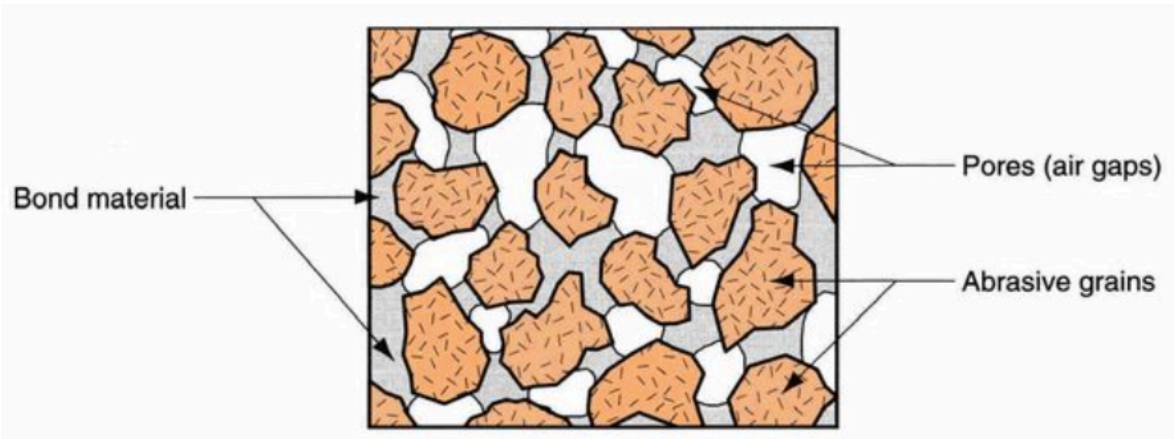

Figure 1: Structure of a grinding wheel

2.2.1. Abrasive Material

Abrasives used in abrasive-machining can be distinguished in:

- *Conventional abrasives*
  - Aluminum oxide Al_2O_3
  - Silicon carbide SiC

- *Superabrasives*
  - Cubic boron nitride cBN
  - Diamond

Cubic boron nitride and diamond are called superabrasive since they are the hardest materials known. These abrasives are much harder than conventional cutting tools materials. Figure 2 shows the four abrasives in their aspect.

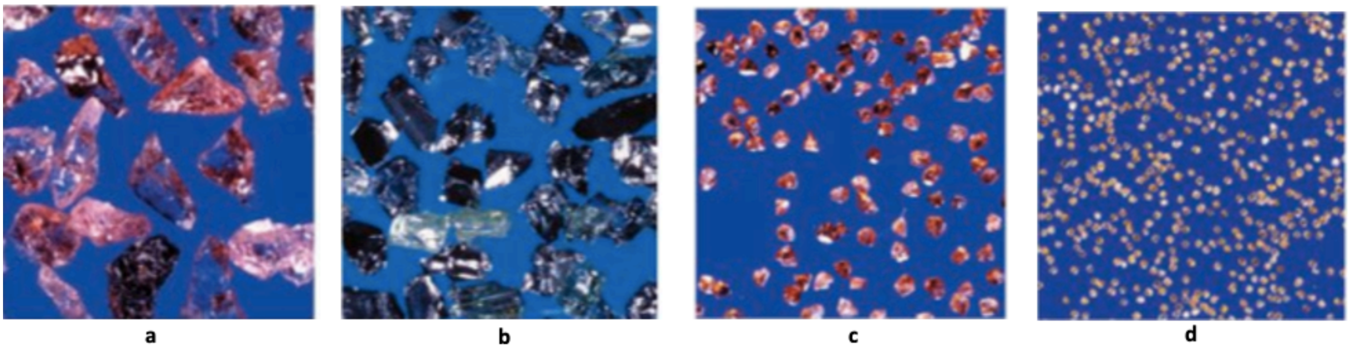

Figure 2: Abrasive Materials - a) Aluminum oxide; b) Silicon carbide; c) Cubic boron nitride; d) Diamond

The abrasives mentioned above are briefly described in the following [5] [6]:

- Aluminum oxide – Most common abrasive material, used to grind steel and other ferrous, high strength alloys. It has a high degree of toughness and in the grinding operation it features a long wheel life but not high efficient grinding. In addition aluminum oxide is used for off-hand and handguide processes for rough-grinding, smoothing and deburring, often in combination with extremely tough zirconia alumina.

- Silicon carbide – Harder then aluminum oxide but less tough. It is used to machine ductile metals, such as aluminum, brass and stainless steel, as well as brittle material. Even if it tends to undergo chemical wear with ferrous metals due to the chemical affinity between the carbon in SiC and the iron in steel, its performance is challenging for creep-feed grinding high alloy steels or generating high quality surfaces.

- Cubic boron nitride – It is the second hardest material after diamond. Compared to diamond, it has greater thermal resistance and chemical wear does not occur when cutting steel.
  It features one hundred times longer wheel lives than aluminum oxide abrasive wheels. With respect its application, cBN grinding wheels are used to machine hard materials and aerospace alloys.

- Diamond – It is the hardest material known, but it subjected to chemical wear when processing steel. Diamonds grinding wheels are used to machine hard abrasive materials, such as ceramics, cemented carbides and glass.

In Figure 3 the Knoop hardness values of the four abrasives are reported.

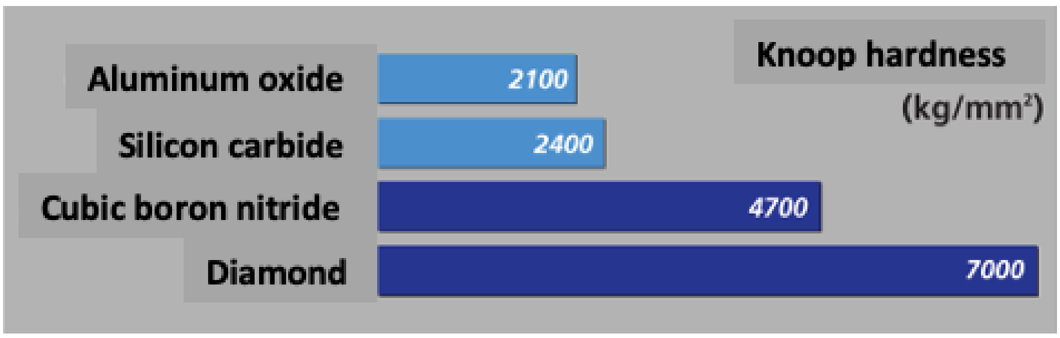

Figure 3: Knoop hardness values of Al_2O_3, SiC, cBN and Diamond

The main properties of an abrasive materials for a grinding wheel are: high hardness, wear resistance, toughness and friability. In particular, friability refers to the ability of an abrasive grain to fracture into smaller pieces. This is a very important property as it is related to the self-sharpening characteristic, which it is fundamental in maintain the sharpness of the abrasives during the grinding operation.
High friability indicates low strength or low fracture resistance of the abrasive, therefore an abrasive particle with high friability will fracture faster under grinding forces than one with low friability. For instance, aluminum oxide has lower friability than silicon carbide, and thus consequently lower tendency to fracture. [2]
The shape and size of the abrasive grain also affect its friability: smaller grains are stronger and less friable than larger ones. [6]

2.2.2. Grain Size

The number relating to the grain size indicates the grain size of the wheel. Since it corresponds to the number of meshes per inch used in sieving, a higher number corresponds to a finer grain size. The coarser grit abrasives are used to have strong stock removal, in the grinding of non-hard materials and when the wheel-workpiece contact surface is large. They produce a rough surface finish and the minimum shape radius achievable with them on the workpiece is superior. On the other hand, fine-grained abrasives are used for high-precision grinding, in the machining of hard materials and when the workpiece-wheel contact area is small. They provide a better finish and allow for smaller shape radii on the piece. [5]
Therefore, harder work materials require smaller grain sizes to cut effectively, while softer materials require larger grit sizes.
Grain sizes used in grinding wheels typically range between 8 and 250. Grit size 8 is very coarse and size 250 is ultrafine, as it shown in Figure 4. [6]

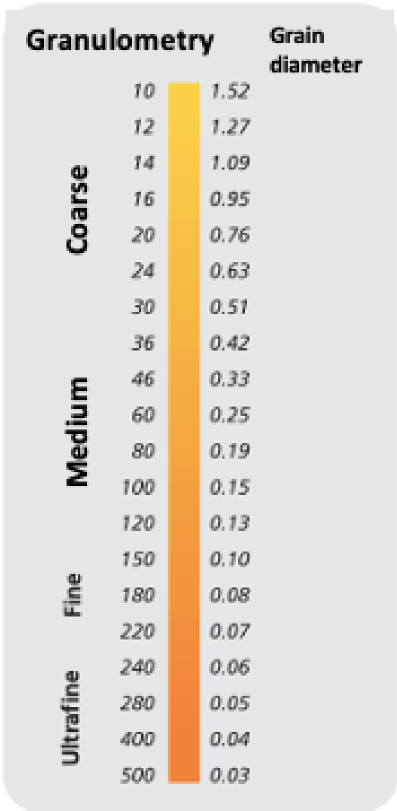

Figure 4: Grain size dimension diagram

2.2.3. Bonding material

The purpose of the bonding material is to retain the individual abrasive grains. The most common types of bonding material are described next.

- Vitrified bond – Most grinding wheels in common use are vitrified bonded wheels. The raw material consist of feldspare (a crystalline mineral) and clays. They are mixed with the abrasives, moistened and molded under pressure into the shape of grinding wheels. Afterwards, these "green" wheels are fired slowly up to a temperature of about 1250°C to fuse the glass and develop structural strength.
  The wheels are then cooled slowly, to prevent thermal cracking, finished to size, inspected for quality and dimensional accuracy and tested for defects.
  Wheels with vitrified bonds are strong, stiff, porous and resistant to acids, oils, water (that might be used in grinding fluids) and elevated temperatures. However, they feature brittleness and lack of resistance to mechanical and thermal shock. To improve their strength, vitrified wheels are also made with steel-backing plates for better structural support of the bonded abrasives.
  The color of the grinding wheel can be modified by adding different elements during its manufacture. [5] [7]

- Resinoid bond – It consist of various thermosetting resin materials, such as phenol formaldehyde.
  Resinoid bond wheels are also called organic wheels since the bond is an organic compound. The manufacturing process for producing them basically consists of:

- Mixing the abrasive with liquid or powdered phenolic resins and additives.
- Pressing the mixture into the shape of a grinding wheel.
- Curing the mixture at temperatures of about 175°C.

Since the elastic modulus of thermosetting resins is lower than that one of glasses, resinoid bond wheels are more flexible than vitrified wheels.
Recently, it has being used polyimide as substitute of phenolic; it features higher toughness and resistance to higher temperatures. Furthermore, these grinding wheels can be also manufactured by means of injection molding technique.
Resin bond has very high strength and is used for rough grinding and cutoff operations. [5] [7]

- Thermoplastic bond – In addition to thermosetting resins, thermoplastic bond are also used to manufacture grinding wheels. They are available with sol-gel abrasives bonded with thermoplastics.

- Rubber bond – Most flexible of the bonding materials and used as a bonding material in cutoff wheels. The manufacturing process consists of:

  - Mixing crude rubber, sulfur and the abrasive grains together.
  - Rolling the mixture into sheets.
  - Cutting out circles.
  - Heating them under pressure to vulcanize the rubber.

  This process allows to produce thin wheels too. [5] [7]

- Metallic bond – Metal, usually bronze, is the common bond material for diamond and cBN grinding wheels. By means of powder metallurgy techniques, the abrasive grains are bonded to the periphery of the wheel. Metal bonding is carried out under high pressure and temperature. The wheel itself may be made of aluminum, bronze, steel, ceramics or composite materials; it depends on the wheel requirements, such as strength, stiffness and dimensional stability.
  Superabrasive wheels may be layered so that a single abrasive layer is brazed to a metal wheel with a particular desired shape. These wheels are lower in cost and are used for small production quantities. [5] [7]

2.2.4. Wheel grade and wheel structure

The **grade** indicates the strength of the grinding wheel, namely how hard the bonding material holds the abrasive grains.
For wheels with vitrified bond, the predicted grade refers to the relative fraction of bonding material and porosity of the wheel for a fixed content of abrasive. The wheels with a high grade are characterized by a greater quantity of bonding material and less porosity, a characteristic that makes them *harder*.
Instead, low grade wheels have less bonding and more porosity, which makes them *softer*. For resinoid bond and metallic bond wheels, which are practically free of natural porosity, the grade is determined by the formulation of the bond.
The high-grade wheels tend to keep their shape well but easily burn because the abrasive grains are not undermined after they are dulled by wear.

The wheels of lower grades, on the other hand, tend to lose their shape more easily but are less prone to burns as the individual abrasive grains are easily undermined and lost once worn, ensuring a self-sharpening effect.
The correct choice of grinding wheel grade depends on numerous variables.
Materials that are more difficult to grind, they quickly cause the wheel to lose sharpness. Hence, they require wheels of a lower grade so that the wheel always remains sharp.
Grinding operations with a large contact arc length require the use of low-grade wheels due to the availability of a large area to distribute the forces on the individual grains.
Therefore, it can be said that the optimal grinding wheel for a given machining is a trade-off between strength and cutting edge: it must be hard enough to maintain its shape but soft enough to allow the replacement of dull grains due to wear.
The hardness scales are not standardized: they are different for each manufacturer. However, within each product family and wheel type, the grade indicates the relative strength of one grade compared to another grade.
To define the grade of a grinding wheel, letters are used as shown in Figure 5.

The **structure** refers to the spacing of the abrasive within the grinding wheel, which is also often referred to as the *volumetric concentration of abrasive in the grinding wheel*. A lower number indicates a higher percentage of abrasive and therefore a more *closed* structure. The higher number, on the other hand, indicates a low percentage of abrasive and a more "open" structure.
Open grinding wheels are used to facilitate chip formation and in operations where cooling is of crucial importance such as creep-feed grinding.
The vitrified bonded wheels have a high natural porosity. Those with a resinoid or metal bond, on the other hand, are almost devoid of natural porosity.
In Figure 6, the different values of the grinding wheel structure and their meaning are displayed. [5] [7]

Figure 5: Grinding wheel grades

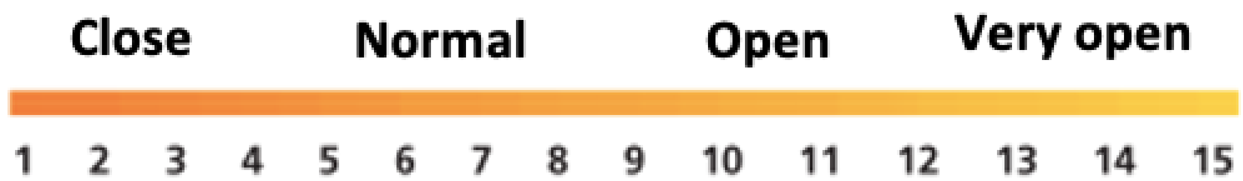

Figure 6: Grinding wheel structure values

2.2.5. Grinding wheel specification

The previous parameters four parameters can be concisely designated in a standard grinding wheel marking system defined by the American National Standards Institute (ANSI).

According to this marking system, numbers and letters are used to specify abrasive type, grit size, grade, structure and bonding material.
Figure 7 presents the marking system for conventional grinding wheels (aluminum oxide and silicon carbide griding wheels) as defined by ANSI, indicating the meaning of every number and letter.
The ANSI Standard for diamond and cubic boron nitride grinding wheels is slightly different than for conventional wheels and it reported in Figure 8. [6] [7]

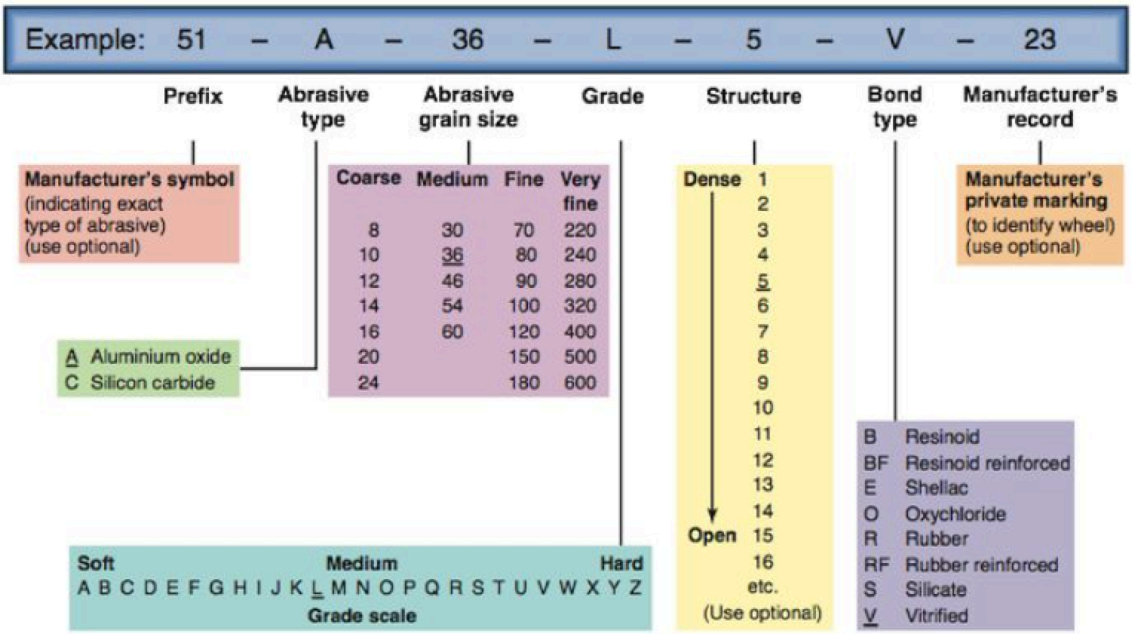

Figure 7: Marking system for aluminum oxide and silicon carbide grinding wheels as defined by ANSI

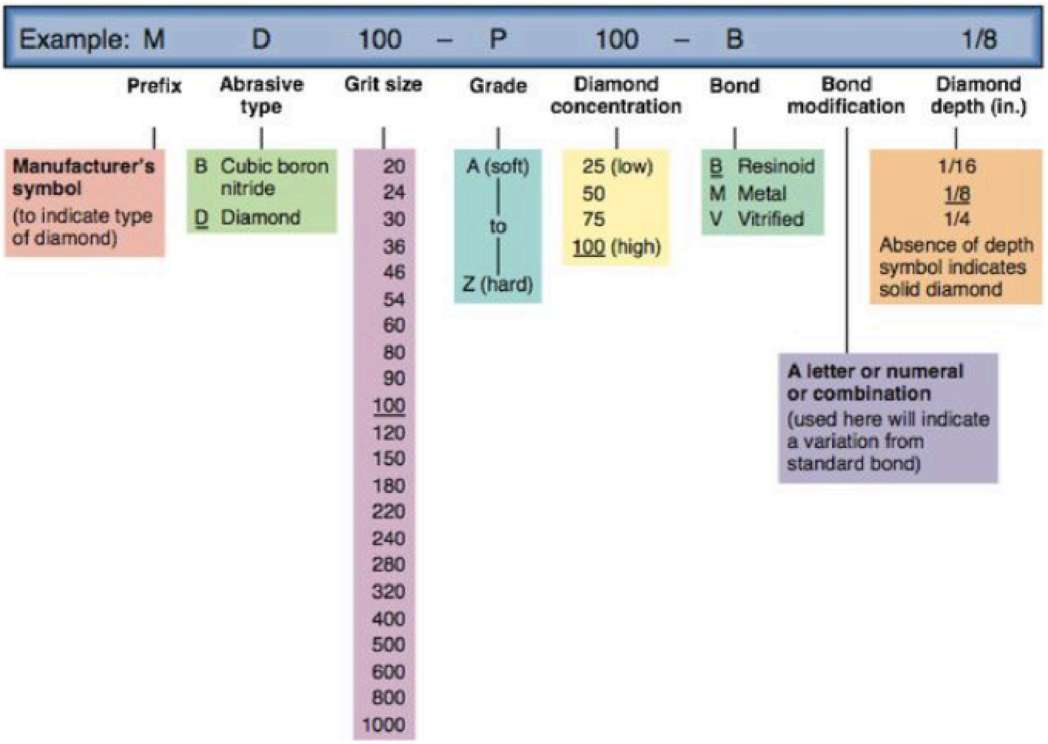

Figure 8: Marking system for diamond and cubic boron nitride grinding wheels as defined by ANSI

2.3. ANALYSIS OF THE GRINDING PROCESS

Grinding process is characterized by cutting conditions with very high speeds and small cut size compared to traditional machining processes. The grinding process and its parameters can be observed best in the surface grinding operation shown in Figure 9.

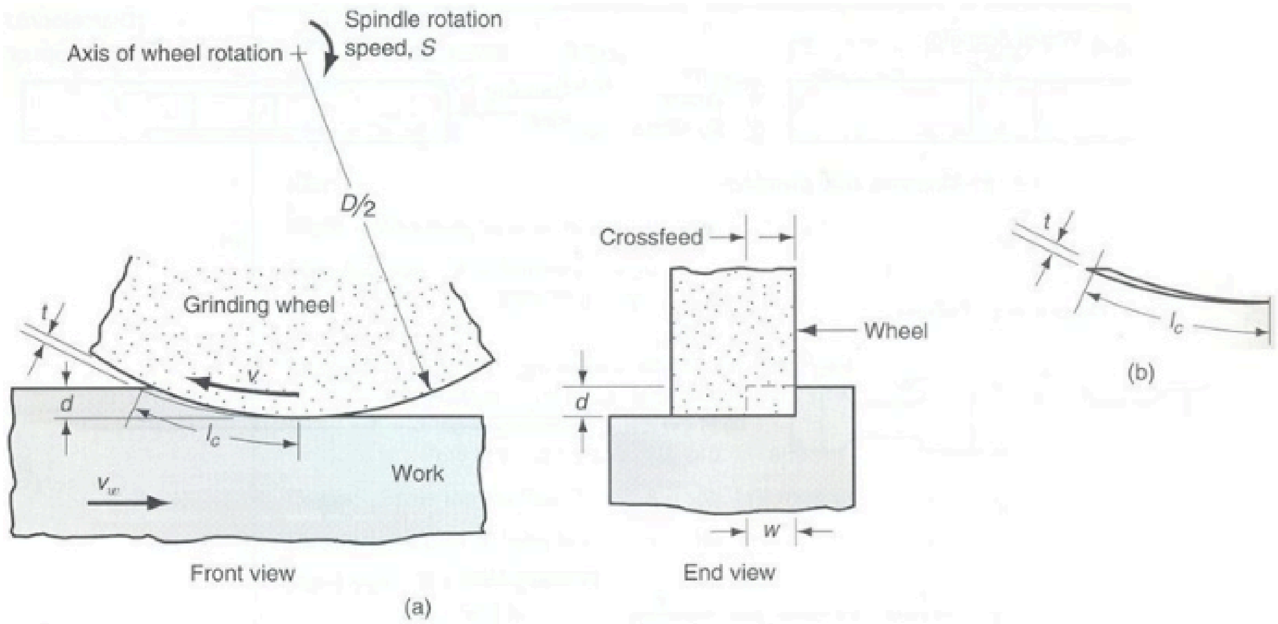

Figure 9: a) Schematic illustration of the surface-grinding process, showing the cutting conditions; b) longitudinal shape

The peripherical speed of the grinding wheel is determined by the rotational speed of the wheel (Equation 1):

$$v = \pi \cdot D \cdot N$$

Equation 1: Peripherical speed of the grinding wheel

In which:
- v is the surface speed of the wheel [m/min].
- N is the spindle speed [rev/min].
- D is the wheel diameter [m].

Depth of cut d, called the *infeed,* indicates the penetration of the wheel in the workpiece surface. As the operation progresses, the wheel is fed sideways across the surface with each pass from the workpiece. This is called **crossfeed** and defines the grinding path width w (Figure 9). This width, multiplied by depth of cut determines the cross-sectional area of the cut. In most grinding operations, the workpiece moves at a certain speed v_w, therefore the Material Removal Rate (MRR) can be evaluated through Equation 2. [2] [6]

$$MRR = v_w \cdot w \cdot d \; [^{mm^3}/_s$$

Equation 2: Material Removal Rate

In a grinding operation, it is fundamental to pay attention on how the combination between the cutting conditions and the grinding wheel parameters affects the following factors [6]:

1. **Surface finish.**
2. **Forces and energy.**
3. **Temperature of the work surface.**
4. **Wheel wear.**

2.3.1. Surface finish

Most commercial grinding is carried out to achieve a surface finish that is superior to that achievable with traditional machining. The surface finish of the workpiece is affected by the size of the individual chips obtained during grinding. An obvious factor in determining chip size is the grain size - a smaller grain allows for better finishes.
From the geometry in Figure 1 (b), the average length of a chip and the undeformed chip thickness can be measured respectively through Equation 3 and Equation 4.

$$l_C = \sqrt{D \cdot d}$$

Equation 3: Average length of the chip

Where:
l_C is the average length of the chip [mm].
D is the wheel diameter [mm].
d is the depth of cut or infeed [mm].

$$t = \sqrt{\left(\frac{4 \cdot v}{v_w \cdot C \cdot r}\right)\sqrt{\left(\frac{d}{D}\right)}}$$

Equation 4: Undeformed chip thickness

In which:
v is the wheel speed [mm/min].
C is the number of active cutting points (grits) per unit area of the periphery of the wheel [grits/mm^2].
r is the grain ratio, obtained dividing the width of the chip for the average undeformed chip thickness.
The other values have been defined previously.

In general, smaller grain sizes give larger C values. C is also related to the wheel structure. A denser structure means more grits per area. By means the value of C, the number of chips formed per time n_c can be evaluated through Equation 5.

$$n_c = v \cdot w \cdot C$$

Equation 5: Number of chips formed per time

Hence, increasing the number of chips formed per unit time on the workpiece surface for a given width, surface finish will improve. Therefore, according to Equation 5, increasing v and/or C. [2] [6]

2.3.2. Forces and Energy

A knowledge of grinding forces is essential for:

- Estimation power requirements.
- Design of grinding machines.
- Determination of the deflections that the workpiece and the grinding machine undergo. Furthermore, negatively affect the dimensional accuracy.

Forces in grinding are usually much smaller than those in the conventional machining operations. Grinding forces should be kept low in order to prevent distortion and to maintain the high dimensional accuracy of the workpiece. [2]
If the force required to move the workpiece past the grinding wheel is known, the specific energy in grinding can be determined through Equation 6.

$$SE_{grind} = \frac{F_c \cdot v}{v_w \cdot w \cdot d} = \frac{P_{grind}}{MRR}$$

Equation 6: Grinding specific energy

Where:
SE_{grind} is the grinding specific energy [J/mm^3].
F_c is the cutting force, which is the force to drive the workpiece past the wheel [N].
The others parameters have been defined previously.
By multiplying the workpiece speed, width of cut and depth of cut, the material removal rate (MRR) is obtained as shown previously in Equation 2. In addition, the multiplication between the cutting force and the wheel speed, allows to calculate the grinding power (P_{grind}).

In grinding, the specific energy is much greater than in conventional machining processes, for the following reasons which make the process inefficient in terms of energy consumption per volume of material removed [2]:

- The dimension effect in machining. As mentioned earlier, the chip thickness in grinding is much lower than in other processes, such as milling. Depending on the dimensional effect, the small size of the chips during grinding means that the energy required to remove each unit volume of material is significantly greater than in conventional machining, roughly ten times higher.

- The individual grains of a grinding wheel have extremely negative rake angles. These extremely low rake angles result in low values of shear plane angle and high shear strain, both of which lead to higher energy levels in grinding.

- The specific energy is higher in grinding because not all the individual grains are engaged in the actual cut. Due to the random positions and orientations of the grains in the wheel, some grains do not protrude far enough into the workpiece surface to perform the cut.

Three types of grain actions can be recognized ([2]), as illustrated in Figure 10:

1. **Cutting**, in which the grit projects far enough into the workpiece surface to form a chip and remove material.

2. **Plowing**, where the grit projects into the workpiece, but not far enough to perform cutting.

3. **Rubbing**, in which the grit contacts the surface during its sweep, but only rubbing friction occurs, thus energy is consumed without removing material.

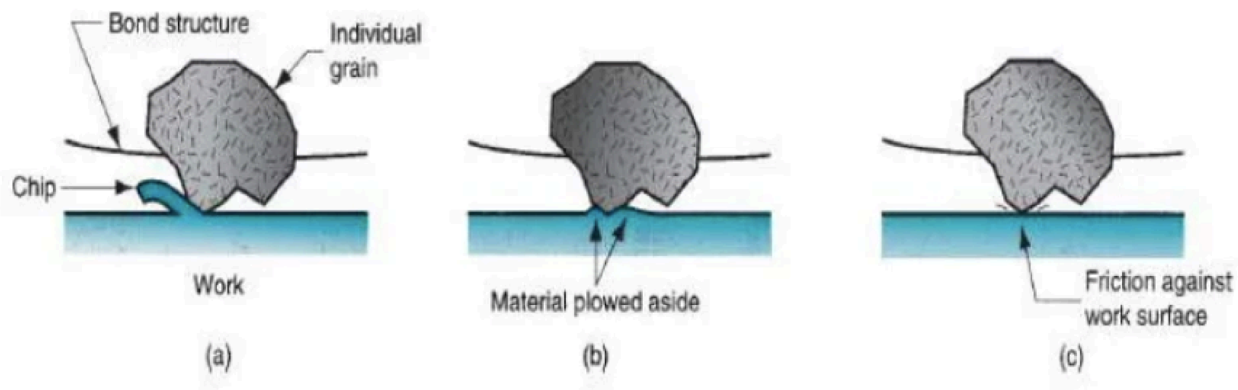

Figure 10: Three types of grain action in grinding: a) cutting; b) plowing; c) rubbing

2.3.3. Temperatures at the workpiece

Due to the size effect, high negative rake angles, and plowing and rubbing of the abrasive grits against the work surface, the grinding process is also characterized by high temperatures. Unlike conventional machining operations in which most of the heat energy generated in the process is carried off in the chip, much of the energy in grinding remains in the ground surface, resulting in high workpiece surface temperatures. [6]
The temperature rise in grinding process is essential for the following considerations:

- It can negatively affect the surface properties.
- The temperature rise can cause residual stresses on the workpiece.
- Temperature gradients in the workpiece generate distortions due to thermal expansion and contraction of the workpiece, making difficult to control dimensional accuracy.

The *surface temperature rise* in grinding can be measured by means of Equation 7.

$$Temperature\ rise\ \propto\ D^{1/4} \cdot d^{3/4} \cdot \left(\frac{v}{v_w}\right)^{1/2}$$

Equation 7: Surface temperature rise in grinding operation

Therefore, increasing wheel diameter D, depth of cut $d$and wheel speed v, temperature increases, instead it decreases with increasing workpiece speed v_w. In addition, from Equation 7 it can be noted that the temperature is most affected by the depth of cut since it has the largest exponent. [6]

High surface temperatures have several possible damaging effects:

- **Tempering** – Excessive temperature rise in grinding can cause *tempering* and *softening* of the temperature surface. Many grinding operations are performed on parts that have been heat treated to achieve high hardness and high grinding temperatures can lead to a loss of their hardness. Therefore, the correct process parameters must be selected in order to prevent excessive temperature rise.

- **Burning** – High temperatures during grinding operation may burn the surface being ground. *Burn marks* manifest as surface discoloration (bluish color) caused by oxidation. They can be detected by etching and metallurgical techniques.

- **Heat checking** – Excessive temperatures in grinding may cause the onset of cracks on the workpiece surface; this phenomenon is known as *heat checking*. Generally, the cracks are perpendicular to the grinding direction. However, also parallel cracks can occur under severe conditions. Heat checking leads to a surface with low fatigue and corrosion resistance.

- **Residual stresses** – Temperature gradients within the workpiece cause residual stresses on the surface. Grinding fluids, their method of application, as well as process parameters such as depth of cut and speeds significantly influence the entity and type of residual stresses develop. Residual stresses usually can be reduced by lowering wheel speed and increasing workpiece speed; softer-grade wheels (known as free-cutting wheels) may be used too.

Hence, it is important to understand what factors affect the surface temperatures of the part during grinding to prevent thermal damages. Furthermore, dull grinding wheels which have a hard grade and dense structure tend to cause thermal problems. [6] [7]

2.3.4. Wheel wear

Grinding wheels wear is a relevant factor because it negatively affects the shape and dimensional accuracy of ground surfaces, similar to conventional cutting tools wear. Three different mechanisms, reported in Figure 11, are recognized as the principal causes of wear in grinding wheels:

1. **Grain fracture**. It occurs when a portion of the grain breaks off, but the rest of the grain remains bonded in the wheel. The edges of the fractured area become new cutting edges on the grinding wheel. The tendency of the grain to fracture is called *friability*. High friability means that the grains fracture more easily due to the cutting forces.

2. **Attritious wear**, it involves dulling of the individual grains, resulting in flat spots and rounded edges. Wear is caused by the interaction of the grain with the workpiece, involving both physical and chemical reactions. Attritious wear is low when grain and workpiece are chemically inert. The more inert they are, the lower the tendency for reactions to occur between them. The environment and type of grinding fluid used also have an influence on grain-workpiece interactions.

3. **Bond fracture**. It occurs when the individual grains are pulled out of the bonding material. The tendency toward this mechanism depends on wheel grade (the strength of the bond), among other factors. If the bond is too strong, dull grains can’t be dislodged. This avoid the contact between the sharp grains of the grinding wheel with the workpiece to remove chip, resulting in an inefficient grinding process.
   On the other hand, if the bond is too weak, the grains are dislodged easily and the wear rate of the wheel increases.

In general, soft bonds are recommended for harder materials and for reducing residual stresses and thermal damage to the workpiece. Hard-grade wheels are used for softer materials and for removing large amounts of material at high rates. [6] [7]

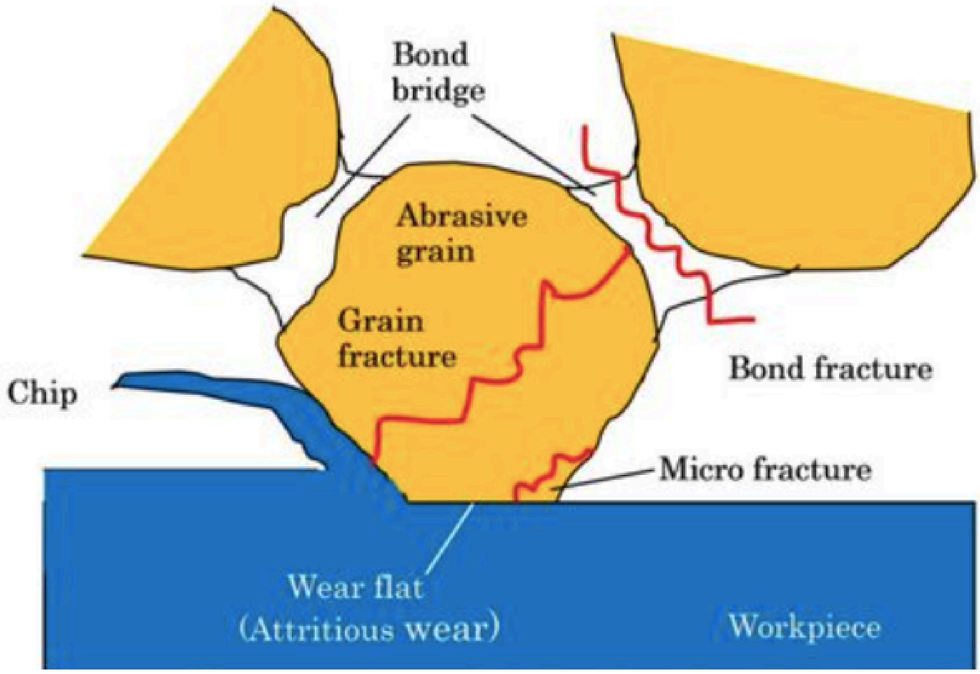

Figure 11: Principal causes of wear in grinding wheels -Grain fracture, Attritious wear and Bond fracture

The three mechanisms combine to cause the grinding wheel to wear as depicted in Figure 12, where three wear regions can be identified. In the first region, the grains are initially sharp, and wear is accelerated due to grain fracture.

In the second region, the wear rate is fairly constant, and there is a linear relationship between wheel wear and volume of material removed. In this region attritious wear occurs, with some grain and bond fracture.

In the third region of the wheel curve, the grains become dull and the amount of plowing and rubbing increases with respect to cutting. Moreover, some of the chips become clogged in the pores of the wheel. This is called *wheel loading*, and it impairs the cutting action and leads to higher heat and work surface temperatures. As consequence, grinding efficiency decreases, and the volume of wheel removed increases with respect to the volume of material removed. [6]

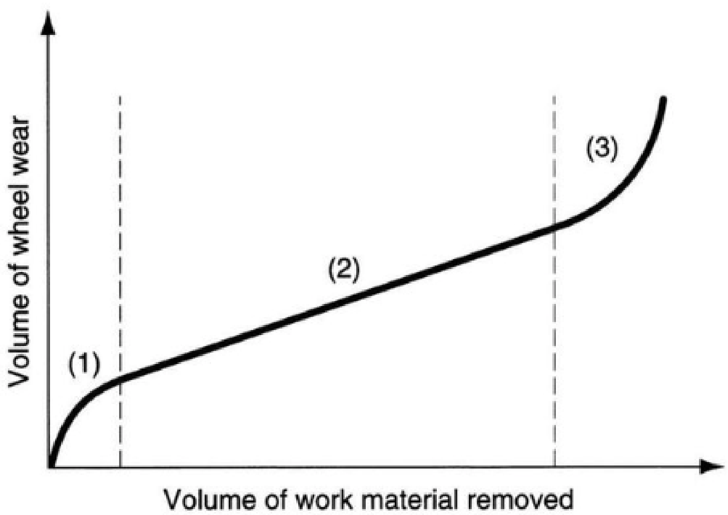

Figure 12: Typical wear curve of a grinding wheel: t is plotted as a function of volume of material removed, rather than a function of time

The **grinding ratio** (Equation 8) is a term used to indicate the slope of the wheel wear curve.

$$GR = \frac{Volume\ of\ material\ removed}{Volume\ of\ wheel\ wear}$$

Equation 8: Grinding ratio

The grinding ratio is more relevant in the linear wear region of Figure 12.
As it can be noticed in Figure 13, the grinding ratio is generally increased by increasing wheel speed, as the size of the chip formed by each grit is smaller with higher speeds, therefore the amount of grain fracture is reduced. Because higher wheel speeds also improve surface finish, there is a general advantage in operating at high grinding speeds. However, when speeds become too high, attritious wear and surface temperatures increase. Consequently, the grinding ratio decreases and the surface finish is impaired. [6]

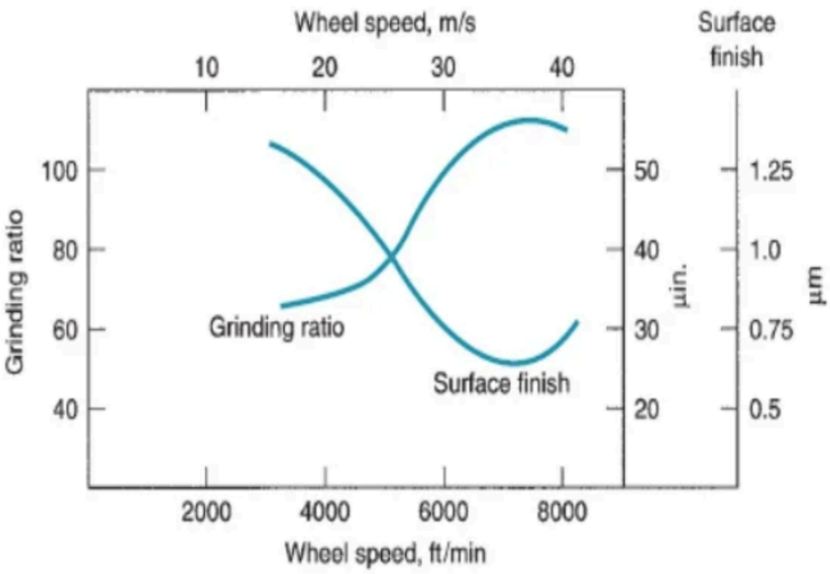

Figure 13: Grinding ratio and surface finish as a function of wheel speed

When the wheel is in the third region of the wear curve, it must be resharpened by an operation called ***dressing*** (this topic is treated in detail in the second chapter), which consist of: 1) breaking off the dulled grits on the outside periphery of the grinding wheel in order to expose fresh sharp grains; 2) removing chips that have become clogged in the wheel. It is accomplished by a rotating disk, an abrasive stick, or another grinding wheel operating at high speed, held against the wheel being dressed as it rotates.
Although dressing sharpens the wheel, it does not guarantee the shape of the wheel. ***Truing*** is an alternative procedure that not only sharpens the wheel, but also restores its cylindrical shape and ensures that it is straight across its outside perimeter. The procedure uses a diamond-pointed tool (other types of truing tools are also used) that is fed slowly and precisely across the wheel as it rotates. [6]

2.4. Application considerations in grinding

In this section it is reported the practical application of wheel parameters and theoretical analysis of grinding, taking into account also the grinding fluid, which are commonly used in grinding operations.

- **Application guidelines**: As said there are different variables that affect the performance and success of the operation. The guidelines in Table 1 are helpful in solving the many complexities and selecting the appropriate wheel parameters and grinding conditions. [6]

Application Problem	Guideline
Grinding steel and most cast irons	Select aluminum oxide as the abrasive
Grinding most nonferrous metals	Select silicon carbide as the abrasive
Grinding hardened tool steels and certain aerospace alloys	Select cubic boron nitride as the abrasive
Grinding hard abrasive materials such as ceramics, cemented carbides and glass	Select diamond as the abrasive
Grinding soft metals	Select a large grit size and harder grade wheel
Grinding hard metals	Select a small grit size and softer grade wheel
Optimize surface finish	Select a small grit size and dense wheel structure. Use high wheel speeds and lower workpiece speeds
Maximize material removal rate	Select a large grit size, more open wheel structure and vitrified bond.
To minimize heat damage, cracking and warping of the work surface	Maintain sharpness of the wheel. Dress the wheel frequently. Use lighter depths of cut, lower wheel speeds and faster workpiece speeds
If the grinding wheel glazes and burns	Select wheel with a soft grade and open structure
If the grinding wheel breaks down too rapidly	Select wheel with a hard grade and dense structure

Table 1: Application guidelines for grinding

- **Grinding fluids**: The functions of grinding fluids are similar to those of cutting fluids. Although grinding can be performed dry, the use of a fluid is useful because it:

    1. Prevents temperature rise in the workpiece, reducing the thermal damages.
    2. Reduces friction.
    3. Washes away chips.
    4. Improves part surface finish and dimensional accuracy.
    5. Improves the efficiency of the process by reducing wheel wear and loading and it lowers power consumption.

  Chemically, two types of grinding fluids can be defined: grinding oils and emulsified oils. The grinding oils are derived from petroleum and other sources. These products are interesting because friction is such an important factor in grinding. However, they present risks in terms of fire and operator health and their cost is high compared to emulsified oils.
  Furthermore, their ability to dissipate heat is inferior to water-based fluids. Thus, mixtures of oil in water are most commonly recommended as grinding fluids. These are usually mixed

with higher concentrations than the emulsified ones used as conventional cutting fluids. In this way, the friction reduction mechanism is emphasized.
In Table 2are reported general recommendations for grinding fluids. [6] [7]

Material	Grinding fluids
Aluminum	E, EP
Copper	CSN, E, MO + FO
Magnesium	D, MO
Nickel	CSN, EP
Refractory metals	EP
Steels	CSN, E
Titanium	CSN, E

Table 2: General recommendations for grinding fluids – D = dry; E = emulsions; EP = Extreme Pressure; CSN = Chemicals and Synthetic; MO = Mineral Oil; FO = Fatty Oil

- **Grinding chatter:** Different guidelines have been established to reduce the grinding chatter, which negatively affects surface finish and wheel performance:

  1. Using soft-grade wheels
  2. Dressing the wheel frequently.
  3. Changing dressing techniques.
  4. Reducing the material removal rate.
  5. Supporting the workpiece rigidly.

  The important factors to control chatter are stiffness of the grinding machine, stifness of workholding devices and damping.
  Analyzing *chatter marks* on ground surfaces is useful to identify their sources. In addition, the grinding operation itself can cause *regenerative chatter*, as it occurs in machining. [7]

- **Ductile-regime grinding:** it is a process which allows to carry out grinding on brittle materials, as ceramics, using light passes and machines with high stiffness and damping capacity. By means of these set parameters, a continuous chio and good surface integrity can be achieved.
  However, since ceramic chips are typically 1 to 10 μm in size, they are more difficult to remove from grinding fluids than metal chips and require fine filters and particular techniques.

2.5. Grinding operations and Machines

The types of grinding operations can be distinguished from each other for the type of machine that performs them, for the machined surfaces and for the direction along which the grinding wheel moves relatively to the piece. [2]
The selection of a grinding process and machine for a specific application depends on workpiece shape and features, size, ease of fixturing and the production rate required. [7]
Grinding is traditionally used to finish parts whose geometries have already been created by other operations. Consequently, grinding machines have been developed to grind flat surfaces, external and internal cylinders and contour shapes such as threads. [6]
Modern applications of grinding process are expanding to include more high speed and high material removal operations. In addition, modern grinding machines are computer controlled and are characterized by features such as automatic loading and unloading, part clamping, dressing and wheel shaping. [6] [7]
The relative movement of the wheel may be along the surface of the workpiece (*traverse* grinding, *through-feed* grinding, *cross-feeding*), or it may move radially into the workpiece (*plunge* grinding). [7]
Therefore, the main grinding operations can be distinguished as follow:

- **Surface grinding.**
- **Cylindrical grinding.**
- **Centerless griding.**
- **Creep feed grinding.**

2.5.1. Surface grinding

Surface grinding is one of the most common operations and is generally used for grinding plain flat surfaces. [2]
The workpiece is usually secured on a magnetic chuck placed and attached on the worktable of the grinder; nonmagnetic materials are kept in place through vises, vacuum chucks, or some other devices. [7]
Surface grinding is performed using the periphery of the grinding wheel or the flat face of the wheel. Since the workpiece is normally kept in a horizontal orientation, peripheral grinding is carried out by rotating the wheel around a vertical axis.
In both cases, the relative movement of the part being machined is achieved by alternately moving the workpiece past the wheel or rotating it.
In Figure 14 the four possible surface grinding machines configurations of griding wheel orientations and workpiece motions are illustrated.
Among these four types, the horizontal spindle machine with reciprocating worktable is the most common, shown in Figure 15. Grinding is carried out by reciprocating the workpiece longitudinally under the wheel at a very reduced depth (infeed) and by feeding the wheel transversally into the workpiece at certain distance between strokes.
In these operations, the width of the wheel is generally less than that one of the workpiece.
Furthermore, a grinding machine with horizontal spindle and reciprocating table can be used to obtain special contoured surfaces by means of a formed grinding wheel.
Instead of feeding the wheel crosswise to the workpiece while it reciprocates, the wheel is *plunge-fed* radially into the workpiece (Figure 16), as it is when grinding a groove. The shape of the formed wheel is then achieved on the workpiece surface.

Grinding machines with vertical spindle and reciprocating tables are arranged so that the wheel diameter is greater than the workpiece width. Consequently, these operations can be performed without using a transverse feed motion.
Instead, grinding is carried out by reciprocating moving the workpiece past the wheel and feeding the wheel vertically into the workpiece until the desired final dimension is achieved. This configuration is capable of obtaining a very flat surface on the workpiece.
With respect to the two types of rotatory table grinding in Figure 14, the vertical spindle machines are more common. By means of relatively large surface contact area between grinding wheel and workpiece, vertical grinding machines with spindle rotating table are able to obtain high metal removal rates if equipped with suitable grinding wheels. [6]

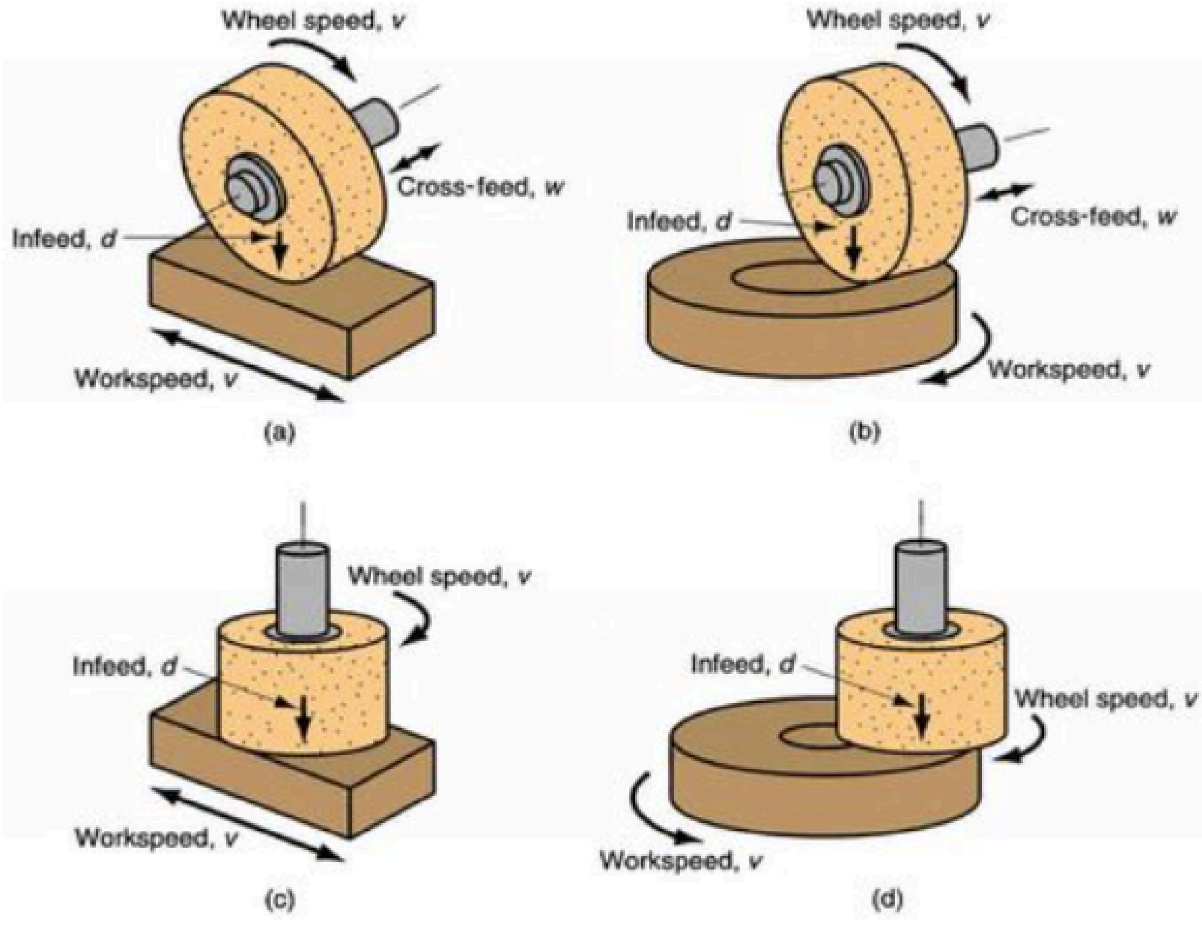

Figure 14: Four types of surface grinding - a) horizontal spindle with reciprocating worktable; b) horizontal spindle with rotating worktable; c) vertical spindle with reciprocating worktable; d) vertical spindle with rotating worktable

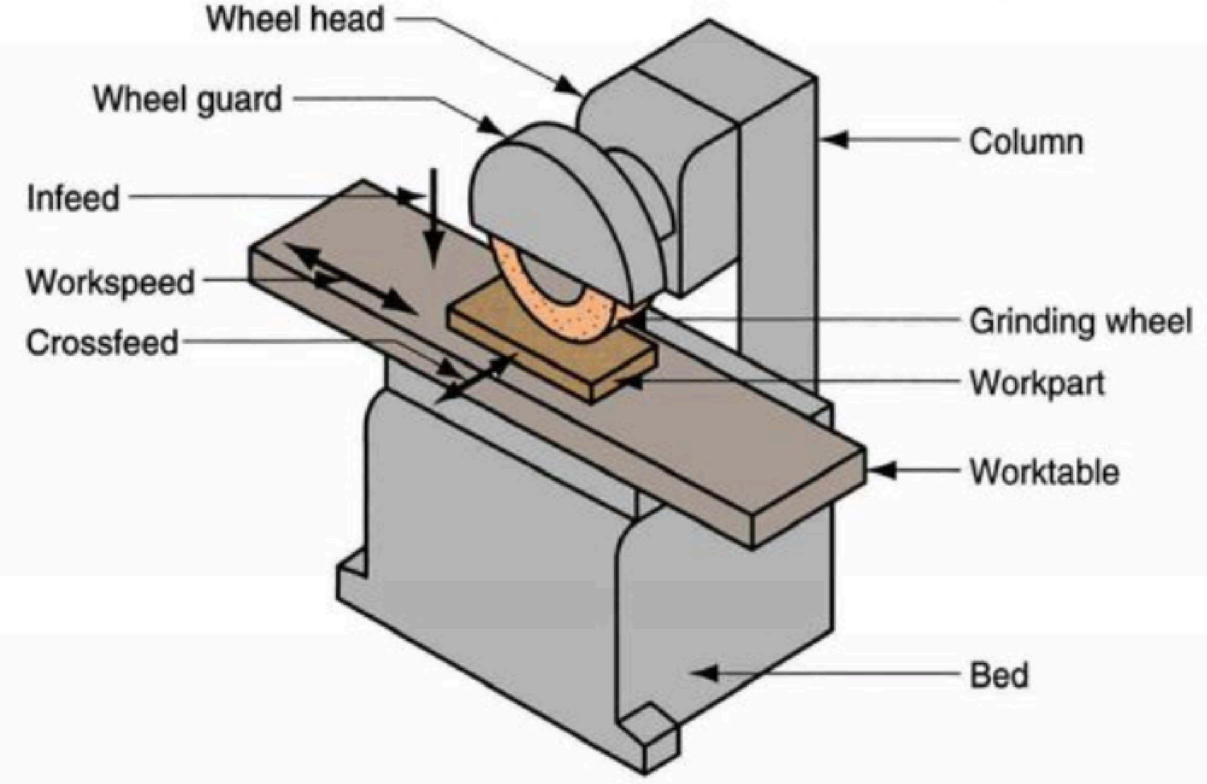

Figure 15: Surface grinder with horizontal spindle and reciprocating worktable

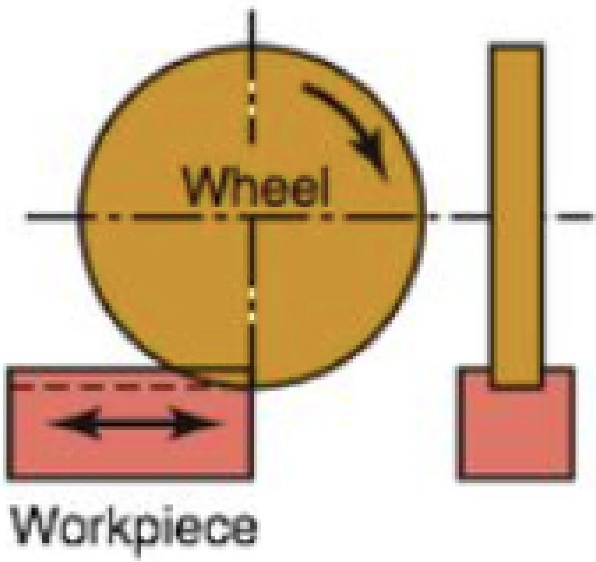

Figure 16: Horizontal-spindle surface grinder: Plunge grinding

2.5.2. Cylindrical grinding

Cylindrical grinding is used to grind rotational parts. Cylindrical grinding can be distinguished in two basic types, shown in Figure 17: external cylindrical grinding and internal cylindrical grinding.
External cylindrical grinding is similar to a turning operation: grinding machines used for these operations closely resemble a lathe in which the tool holders have been substituted by a high-speed motor to rotate the grinding wheel. The cylindrical workpiece is rotated between centers to provide a surface speed between 18 and 30 m/min, and the grinding wheel, rotating at 1200 to 2000 m/min, is engaged to perform the cut. Two types of feed motion can be defined: traverse feed and plunge-cut, shown in Figure 18.
In *traverse feed*, the grinding wheel is fed in a direction parallel to the axis of rotation of the workpiece. The infeed is arranged in a range typically between 0.0075 and 0.075 mm. Sometimes a longitudinal reciprocating motion is imparted to either the workpiece or the wheel to improve surface finish.
In plunge-cut, the grinding wheel is fed radially into the workpiece. Shaped grinding wheels use this kind of feed motion.
External cylindrical grinding is used to finish parts that have been machined to approximate size and heat treated to desired hardness. Parts include: axles, crank-shafts, spindles, bearings and bushings, and rolls for rolling mills. The grinding operation produces the final size and required surface finish on these hardened parts.
In **internal cylindrical grinding** the workpiece is generally kept in a chuck and rotated to provide surface speeds between 20 and 60 m/min. Wheel surface speeds similar to external grinding are used. The wheel can be fed in two ways: traverse feed (Figure 17 b), or plunge feed. The grinding wheel diameter in internal cylindrical grinding must be smaller than the original bore hole. Therefore, the wheel diameter is quite small, requiring very high rotational speeds to achieve the desired surface speed.
Internal cylindrical grinding is used to finish the hardened inside surfaces of bearing races and bushing surfaces.
Furthermore, it is possible to grind on rotating workpiece also *noncylindrical parts* such as cam by means of computer-control features. As Figure 19 shows, the workpiece spindle speed is synchronized such that the radial distance between the workpiece and the wheel axis is varied continuously to achieve a particular shape.
On cylindrical grinders is also performed *thread,* using specially dressed grinding wheels that match the shape of the threads, as shown in Figure 20. Although expansive, the threads manufactured by grinding are the most accurate and have a very fine surface finish with applications such as screws recirculating ball mechanisms utilized for the precise movement of machine components. The movements of the workpiece and the grinding wheel are synchronized to produce the thread pitch, usually in about six passes. [6]

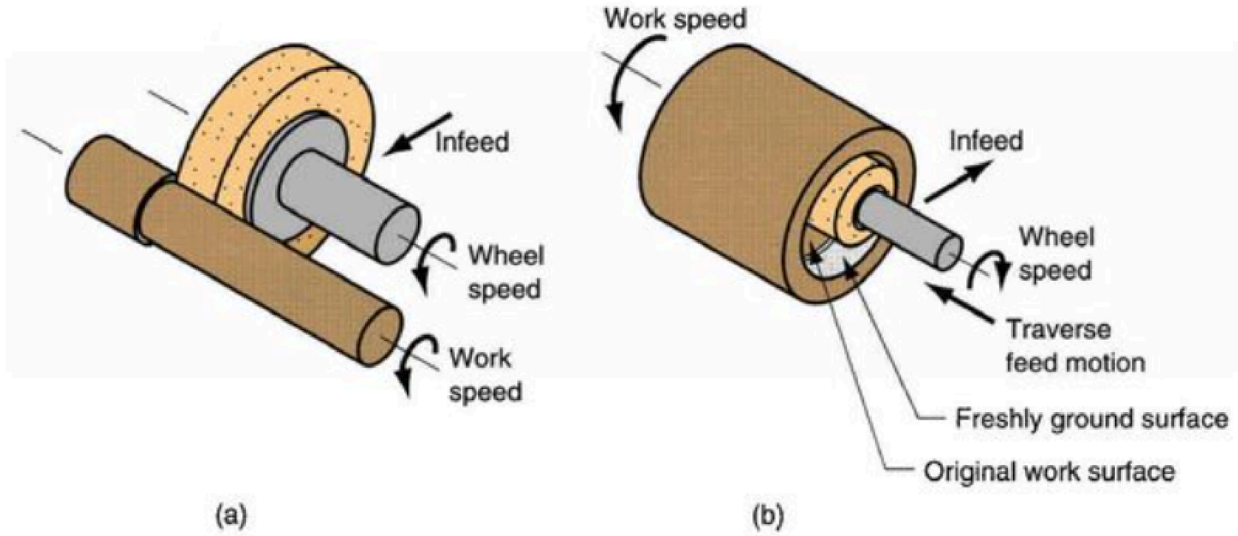

Figure 17: Two main types of cylindrical grinding - a) External cylindrical grinding; b) Internal cylindrical grinding

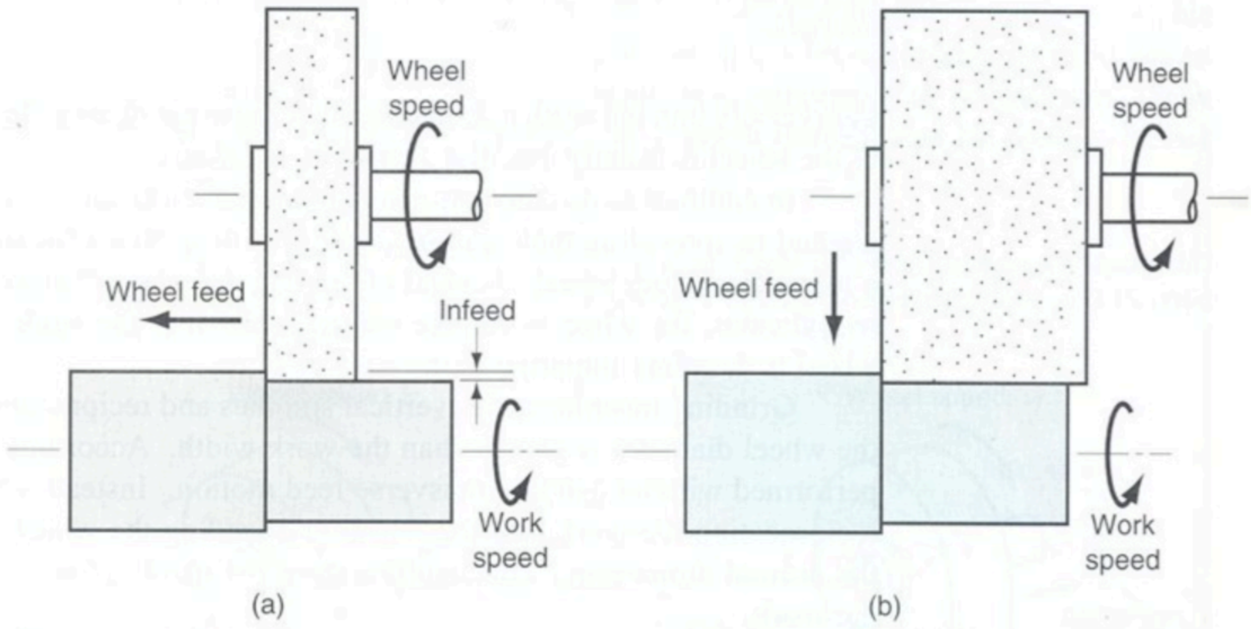

Figure 18: Two types of feed motion in external cylindrical grinding - a) Traverse feed; b) Plunge-cut

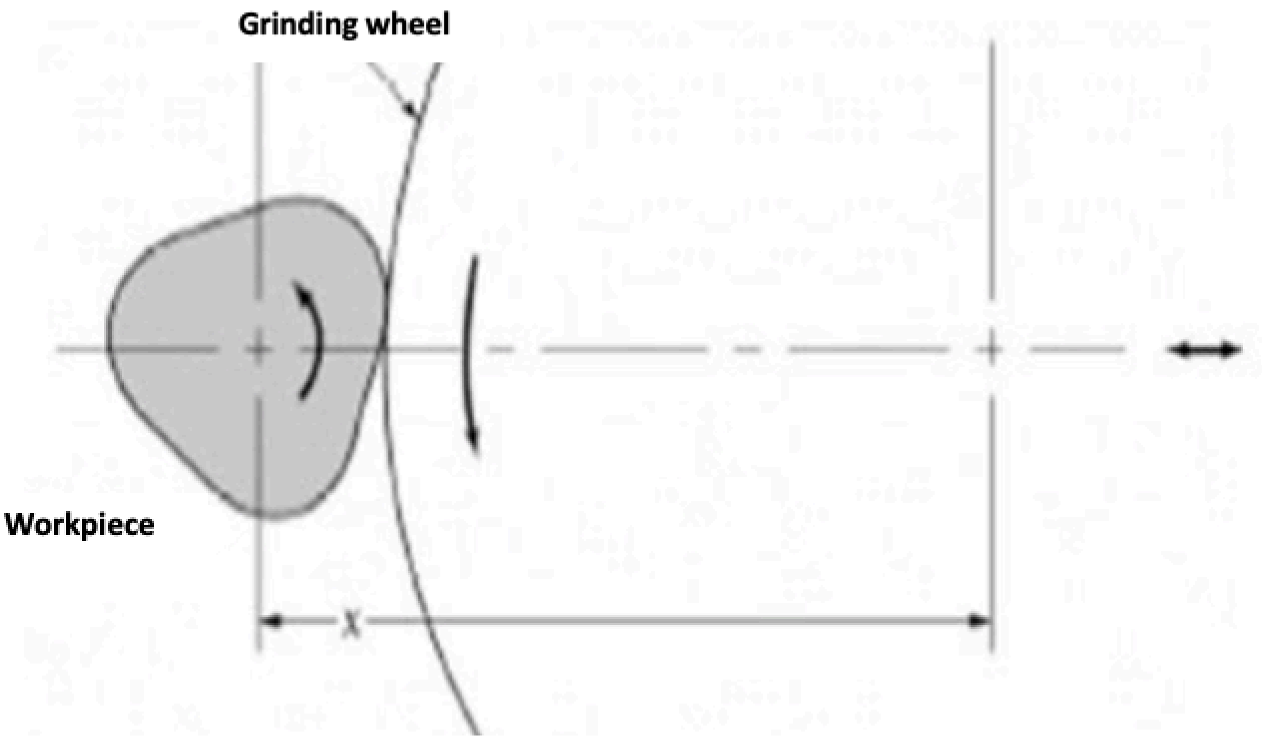

Figure 19: Schematic illustration of grinding a noncylindrical part on a cylindrical grinder with computer controls to produce the shape

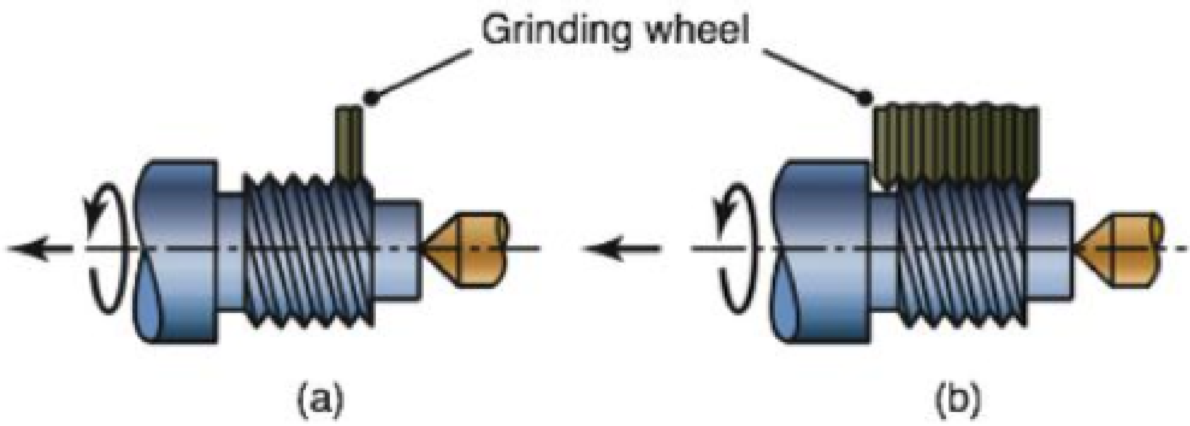

Figure 20: Thread grinding - a) Traverse thread grinding; b) Plunge thread grinding

2.5.3. Centerless grinding

Centerless grinding is a high-production alternative process for grinding external and internal cylindrical surfaces, as the workpiece is not kept between centers but is supported by *blades.* This results in a reduction in work handling time.
Centerless grinding normally is used to produce roller bearings, piston pins, engine valves and camshaft.
External centerless grinding is characterized by two wheels, the grinding wheel and regulating wheel, and the workpiece is supported by a rest blade and fed between the two wheels (Figure 21).
The grinding wheel, the larger one, performs the cutting, whereas the regulating wheel, the smaller one, rotates at lower speed than the grinding wheel and is inclined at a slight angle I (indicated in Figure 21 on the right) to regulate the axial movement of the workpiece. Furthermore, the regulating is a rubber bond wheel.
By means of Equation 9, the throughfeed rate can be predicted.

$$f_r = \pi \cdot D_r \cdot N_r \cdot \sin I$$

Equation 9: Throughfeed rate

In which:

- f_r is the throughfeed rate [mm/min].
- D_r is the diameter of the regulating wheel [mm].
- N_r is the rotational speed of the regulating wheel [rev/min].
- I is the inclination angle of the regulating wheel.

In **internal centerless grinding**, the workpiece is supported between three rolls and is ground internally, as illustrated in Figure 22. The applications of this operation are sleeve-shaped parts and rings.
The regulating wheel is tilted at a small inclination angle to control the feed of the workpiece past the grinding wheel. Due to the need to support the grinding wheel, it is not possible to feed the workpiece as in external centerless grindin. Therefore, with this grinding operation cannot be achieved the same high production rates of the external centerless operation.
The advantage of internal centerless grinding is that is capable to provide very close concentricity between internal and external diameters on a tubular part. [6] [7]
Parts with variable diameters, such as bolts, can be ground by centerless grinding by means of *plunge grinding* (Figure 23): tapered pieces are centerless ground by *end-feed grinding*. [7]

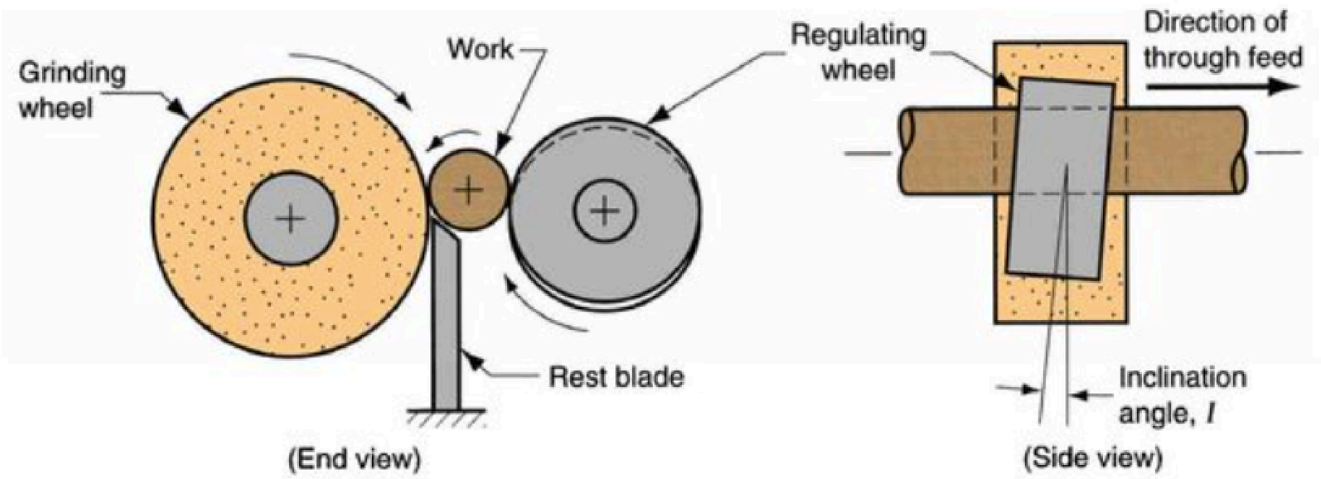

Figure 21: External centerless grinding

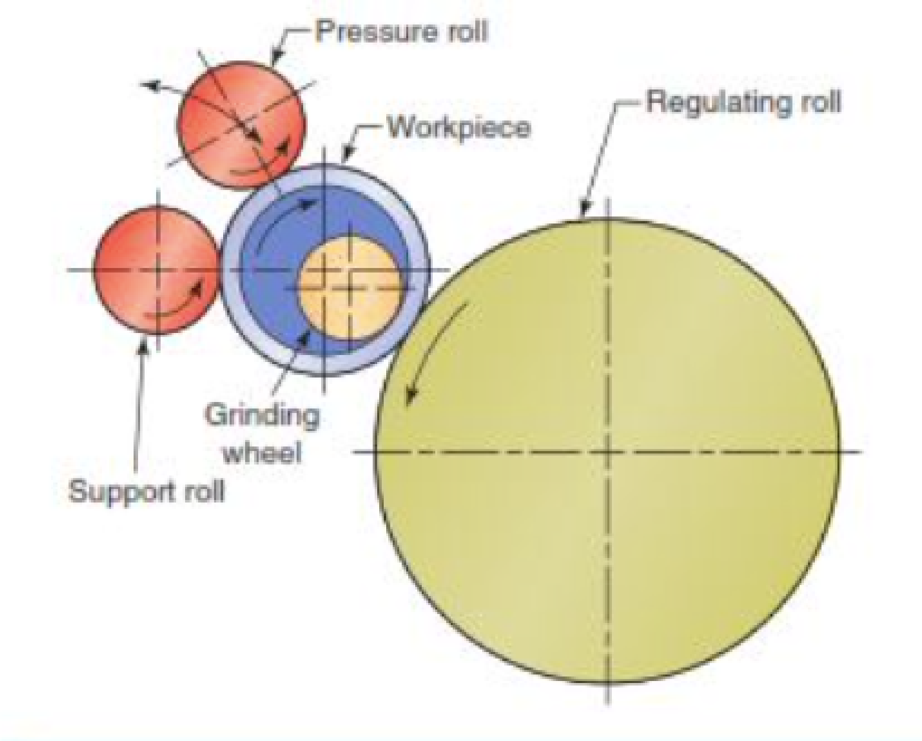

Figure 22: Internal centerless grinding

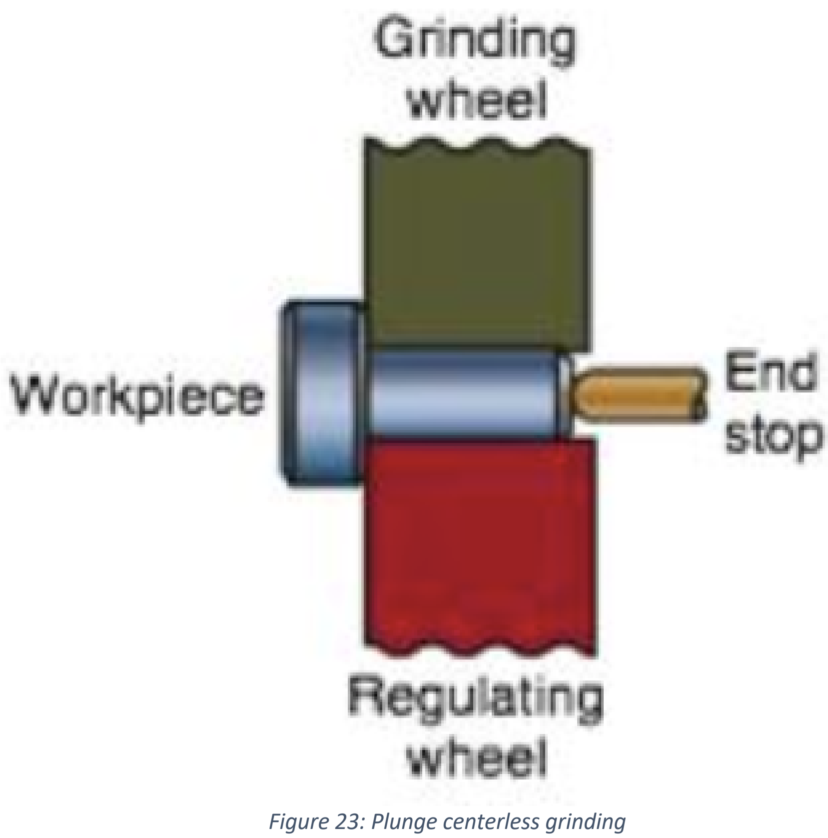

Figure 23: Plunge centerless grinding

2.5.4. Creep-feed grinding

Grinding process is usually related small rates of material removal and fine finishing operations. But it can be considered also for large-scale metal removal operations and be competitive with conventional machining processes.
Creep-feed grinding is carried out at very high depths of cut and very low feed rates. To control workpiece temperatures keeping them low and improve surface finish, the wheels are softer-grade resin bonded and they have an open structure.
The properties of creep-feed grinding machines are high stiffness (due to high forces for the large depth of material removed), high damping capacity, variable spindle and worktable speeds and ample capacity for grinding fluids.
Grinders are equipped with features for continuously dressing the wheel using a diamond roll as the dressing tool.
Typically creep-feed grinding is used to grind shaped punches, key seats, twist-drill flutes, the roots of turbine blades and several complex, superalloy parts.
Generally, in this griding operation is performed a single grinding pass, a second one may be necessary for improved surface finish. [7]
Therefore, the advantages of creep-feed grinding are [6]:

- High material removal rates.
- Improved accuracy for formed surfaces.
- Reduced temperatures at the workpiece surface.

In Figure 24 is reported a schematic comparison of conventional surface grinding and creep-feed grinding to highlight the greater depth of cut.

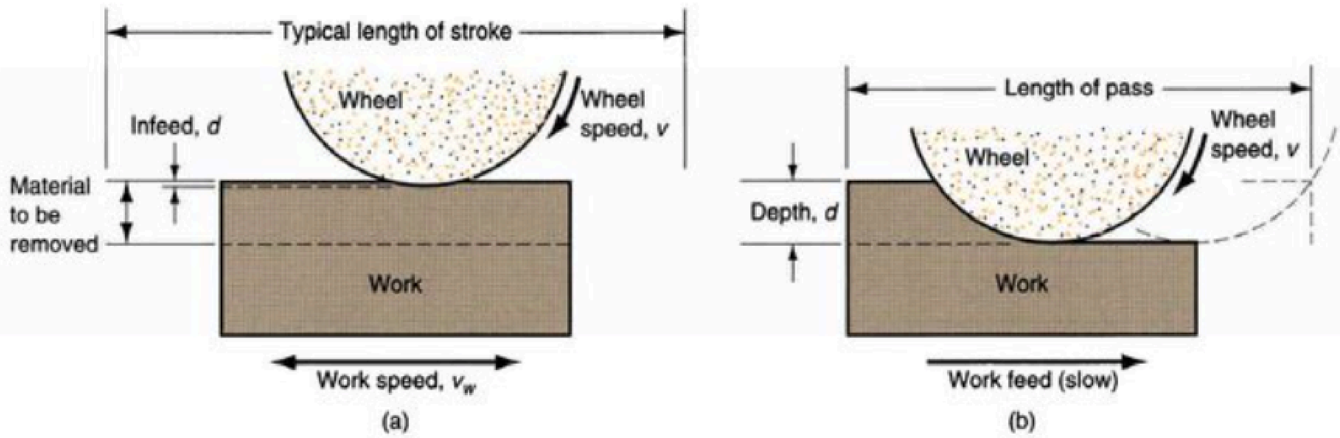

Figure 24: Comparison of a) Conventional surface grinding and b) Creep-feed grinding

2.6. Main grinding parameters

The most important parameters for grinding process to control it are [8]:

1. **The material removal rate.**
2. **Specific energy.**

2.6.1. The Material removal rate (MMR)

This parameter indicates the volume of material ground (or dressed) away in a unit time. It is measured in mm^3/s. Usually it is named Q or MRR.
For surface grinding the formula is reported in Equation 10:

$$MRR\left[\frac{mm^3}{s}\right] = Q = depth\ of\ cut\ [mm] \cdot feedrate\ \left[\frac{mm}{s}\right] \cdot width\ of\ cut\ [mm]$$

Equation 10: Material removal rate

The specific material removal rate is named Q' and is given by Equation 11:

$$Q' = \frac{Q}{width}\ [\frac{mm^2}{s}]$$

Equation 11: Specific material removal rate

2.6.2. The specific energy (SE)

The specific energy, called SE, is measured in J/mm^3 and represents the energy during the operation per unit volume. It is obtained through Equation 12:

$$SE = \frac{P}{Q}\ \left[\frac{J}{mm^3}\right]$$

Equation 12: Specific energy

Where P is the grinding (or dressing) power in Watts, obtained through Equation 13:

$$P = P_{total} - P_{idle}\ [W]$$

Equation 13: Grinding power

3. THE DRESSING PROCESS

3.1. Introduction

Dressing is a machining process which includes:

- *Conditioning* worn grains on the surface of a grinding wheel by producing sharp new edges on grains so that they cut more effectively.
- *Truing*, which refers to removal of material from the cutting surface of a grinding wheel so that the spinning wheel runs true with minimum run-out from its macroscopic shape. Truing can also include profiling of the wheel in a specific shape.

Dressing is necessary when excessive attritious wear dulls the wheel (called glazing due to the shiny appearance of the wheel surface) or when the wheel becomes loaded. [7]
With *conventional abrasive wheels*, therefore softer wheels, both truing and dressing are generally performed by the same process and the combination is commonly called **dressing**. Instead, with *superabrasive wheels*, hence harder wheels, truing and dressing may be used separately.
In the first chapter, it was seen how the wheel topography and the grinding parameters affect the kinematic interaction between the abrasive grains and the workpiece. The grinding wheel preparation, namely truing and dressing, deeply affect the grinding performance taking in account forces, power consumption, temperatures and surface finish. [9]
Wheel loading occurs when porosities on wheel surfaces become filled or clogged with chips from the workpiece. Loading can occur when grinding soft materials or when selecting wheels or process parameters incorrectly. A loaded wheel cuts inefficiently and generates a lot of frictional heat, which causes surface damage and loss of dimensional accuracy of the part. [7]
The main dressing operations can be distinguished in:

- *Dressing of conventional abrasive wheels*
  - **Single point or multipoint diamond dressing**
  - **Rotary dressing**
  - **Diamond block dressing**
  - **Crush dressing**

- *Truing followed by Dressing of superabrasive wheels*, since as mentioned before, truing and dressing usually are used separately.

3.1.1. Dressing of conventional abrasive wheels – single point or multipoint diamond dressing

Conventional abrasive wheels, as said in the first chapter, are those wheels characterized by aluminum oxide and silicon carbide as abrasive material. They are normally prepared for the grinding operation by feeding a dressing tool across the rotating wheel surface, as shown in Figure 25.
A small layer of certain depth is removed from the radius afterwards each pass of the dressing tool across the wheel surface.
This method of dressing motion is analogous to turning on a lathe. The axial feed of the dressing tool per wheel revolution is called dressing lead and is reported in Equation 14.

$$S_d = \frac{\pi \cdot d_s \cdot v_d}{V_s}$$

Equation 14: Dressing lead

In which:
- v_d is the crossfeed (traverse) velocity of the dresser across the wheel.
- V_s is the wheel velocity.
- d_s is the wheel diameter.

Normally two to five dressing passes are performed in addition to what is required to true the wheel, although it may be necessary to dress off more wheel material to remove artifacts from the previous grinding operation. As a final step, "spark-out" passes can also be performed, in which the dressing tool is moved through the wheel without further increasing the dressing depth setting. Each subsequent spark-out pass removes less material from the wheel and gives an increasingly finer wheel topography.
The dressing tool is generally a *diamond-point tool* (single point) or a *diamond cluster* (multipoint) composed by one or more layers of diamonds impregnated in a metal binder. The diamond-point tool is usually tilted relative to the wheel with a drag angle α_d (Figure 25).
Obviously, multipoint diamond tools feature the advantage to have a more consistent grinding performance during the life of the dressing tool. Instead, with a single point diamond tool, its continued use leads to make the exposed point dull, thereby changing the dressed wheel topography and the successive grinding operation. [9]

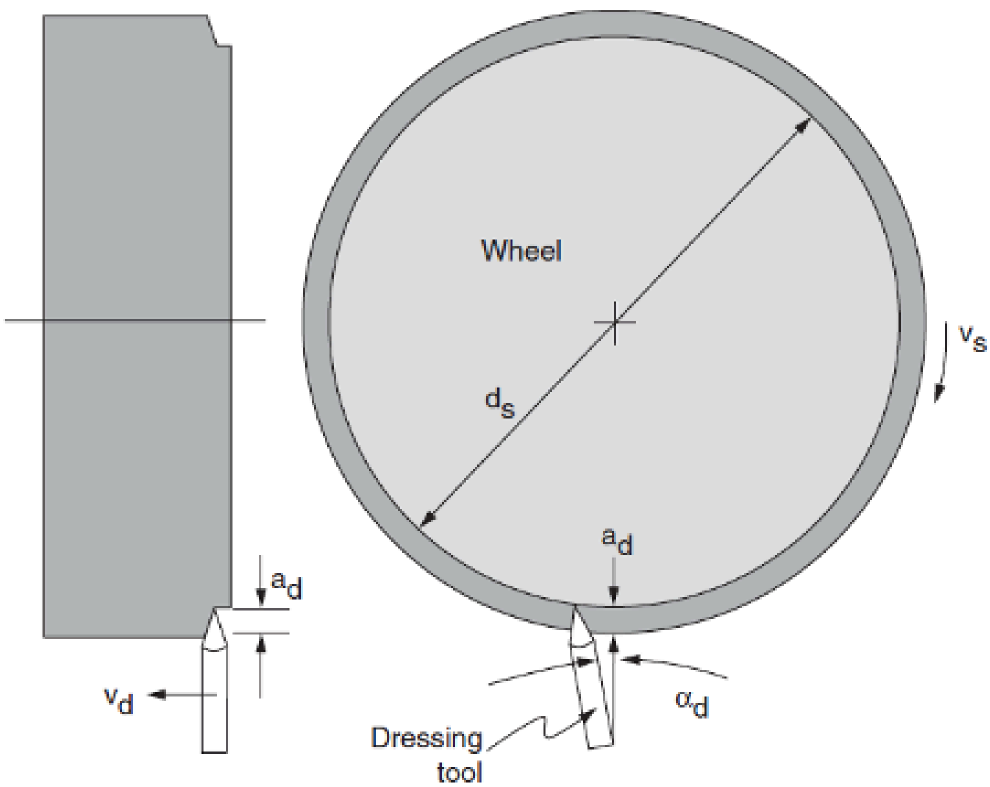

Figure 25: Single point dressing of a grinding wheel

3.1.2. Dressing of conventional abrasive wheels – Rotary dressing

Another dressing method which is particularly used for the generation of profiles is **rotary diamond dressing.** A rotary diamond dressing tool (roll) consists of an axisymmetric body with diamond particles impregnated in a metal matrix on its outer surface.

The dressing roll has the same profile as that one required on the workpiece, so the wheel is dressed with the reverse profile. For most applications, the dressing roll is driven at a peripherical velocity v_r while it is fed radially into the rotating wheel at an infeed velocity v_i corresponding to a depth per wheel revolution a_r, as illustrated in Figure 26. With this arrangement, the rotary dresser appears to grind the cylindrical grinding wheel surface. The peripheral dresser velocity v_r may be in the same (+) or opposite (-) direction (unidirectional or anti-directional mode) of the grinding wheel velocity at the dresser-wheel contact area. Typically, the rotary dresser velocity at its maximum diameter might be 20-50% if the wheel velocity is in the opposite (up) direction, although the dresser is often rotated in the same direction (down) especially with creep feed grinding at speeds up to 80% of the grinding wheel velocity. The dresser infeed per wheel revolution is typically $a_r = 10 - 30\ \mu m$ and the total wheel revolution is $50 - 200\ \mu m$. Before retracing the dressing tool, its infeed may be deliberately or unintentionally stopped (dwell), analogous to 'spark-out' with single-point dressing. Rotary dressing may also be applied continually during creep feed grinding processes, rather than intermittently, in order to maintain the wheel sharpness and profile shape. [9]

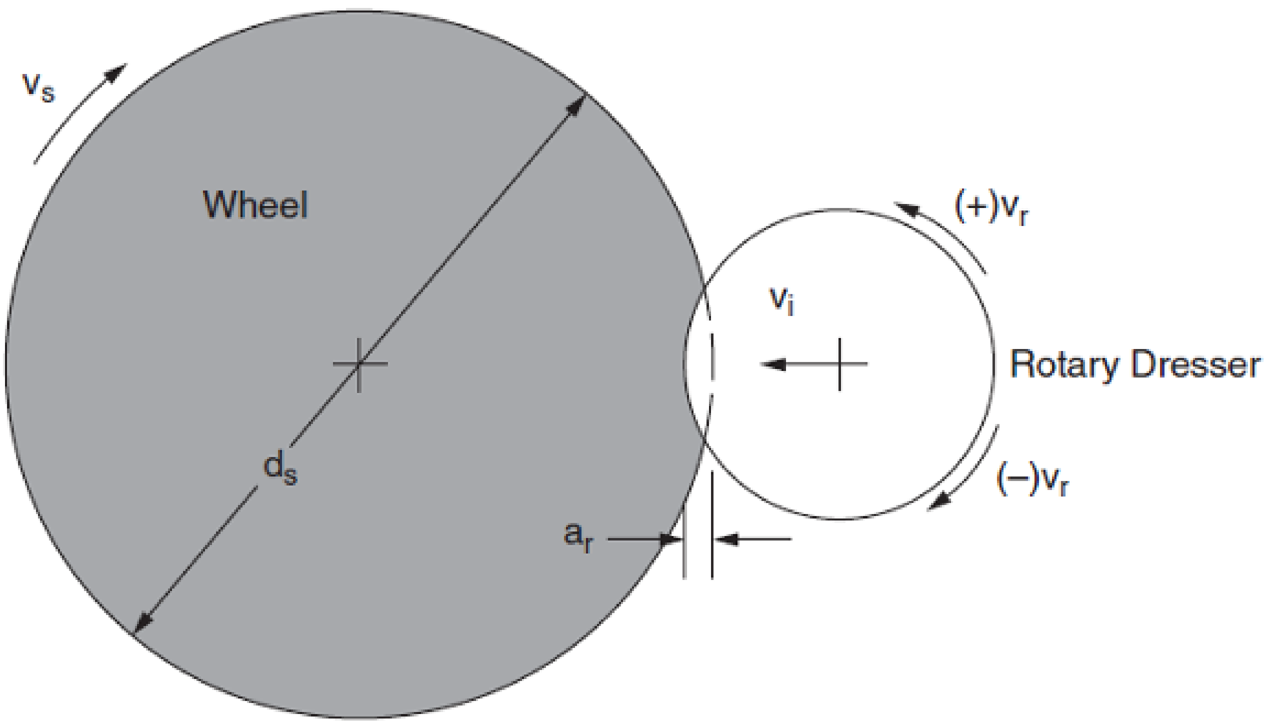

Figure 26: Rotary diamond dressing of a grinding wheel

3.1.3. Dressing of conventional abrasive wheels – Diamond block dressing and rush dressing

Diamond block dressing and **crush dressing** are not so common profile dressing methods. With diamond block dressing (Figure 27), the rotating grinding wheel is transversally feed along a fixed diamond impregnated block having the desired workpiece profile.
Crush dressing process (Figure 28), instead, consists of pressing a metal roll on the surface of the grinding wheel, which normally it is a vitrified wheel. The roll (made of high-speed steel, tungsten carbide or boron carbide) has a ground profile on its periphery. Hence, it reproduces a replica of this profile on the surface of the grinding wheel while it is dressed. [9]

3.2.1. Dressing of superabrasive wheels – Truing

Superabrasive wheel are made by two types of abrasive materials as said in the previous chapter, cubic boron nitride and diamond. Practically, on all types of superabrasive wheels is carried out a pre-grinding preparation, namely **truing**, which may be followed by **dressing**.
The only exception includes electroplated wheels which may require occasional cleaning. [9]

- A common truing method for ***diamond wheels*** consists of using a vitrified (friable) silicon carbide grinding wheel which is mounted on a brake-controlled truing device. A *'slip'* velocity between the truing wheel and the grinding wheel is obtained by means of a centrifugal brake placed on the truing wheel spindle, which resist the rotating motion of the truing wheel caused by direct contact with the diamond grinding wheel.
  With peripherical grinding wheels, the truing wheel is operated as if it cylindrically traverse grinds the grinding wheel, as illustrated in Figure 27, with the axes of the dressing wheel and grinding wheel parallel to each other.
  A diamond grinding wheel may also be undergone to truing using a silicon carbide wheel on a freely rotating shaft without any brake. In this case, the 'slip' velocity between the grinding and truing surfaces is obtained by orienting the axis of the truing wheel in a way with which its peripherical velocity is not collinear with that one of the grinding wheel at the contact point.
  Several other truing methods, similar to those utilized with conventional abrasive wheels, have been tried on diamond wheels, using diamond tools, but with poor success. Diamond truing of diamond wheels removes wheel material much quicker than silicon carbide truing, but there is the risk to damage both, the truing tool and the wheel.

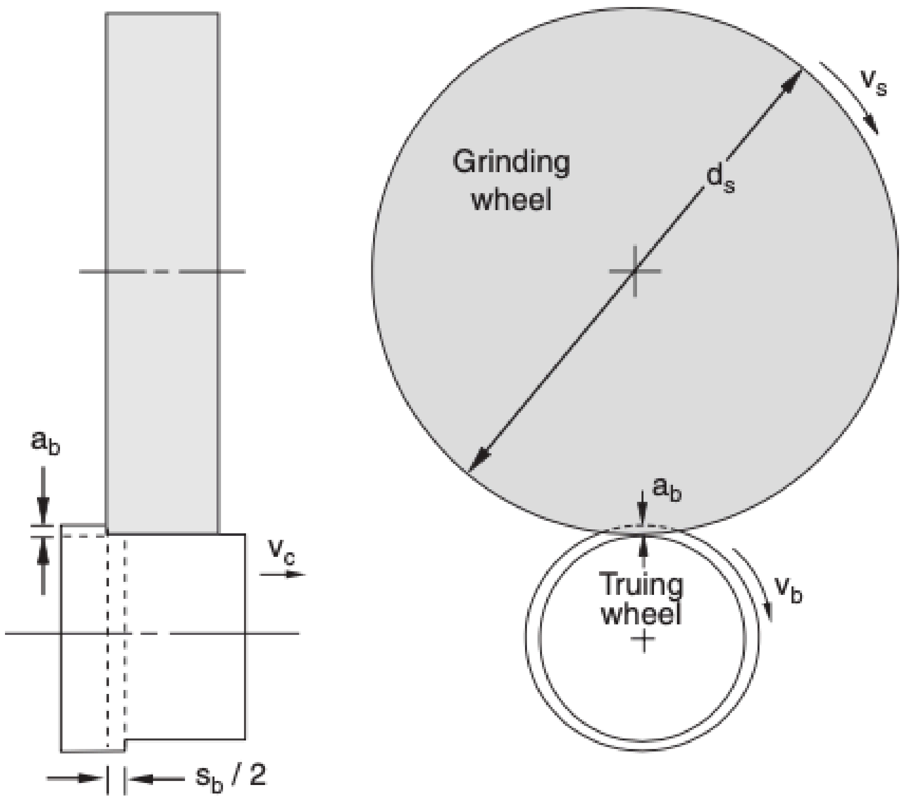

Figure 27: Brake-controlled truing arrangement for peripheral superabrasive wheels

- Diamond tool are widely used for truing of *resin and metal bonded cBN* wheels, even if it is common also the brake-controlled truing with silicon carbide wheels.
  Obviously cBN is softer than diamond, therefore diamond truing tools wear less than with diamond wheels. Single-point diamonds are generally not used except with some small vitrified cBN wheels to generate profiles. Multipoint diamond clusters are usually used, which can be manufactured with a metal binder to make them more wear resistant.

3.2.2. Dressing of superabrasive wheels – Dressing

After truing, **dressing** of *diamond wheels* and *resin and metal bonded cBN wheels* is generally performed infeeding a fine-grained vitrified abrasive stick into the wheel surface manually or with a holding device.
Silicon carbide sticks are usually used with diamond wheels and aluminium oxide sticks with cBN wheels. This process allows to “open up” the wheel surface and “expose” the abrasive grains by removing binder, without significantly affecting the abrasive grains.
With cBN wheels instead, more aggressive dressing methods are necessary to improve the sharpness of the abrasive grains which may be flattened due to truing operation. The simplest sharpening method consists of grinding a block of mild steel.
With vitrified cBN wheels, truing is easier than resin bonded cBN wheels. The most common method for truing of vitrified cBN wheels utilizes a thin diamond disk, as shown in Figure 28, which rotates with its peripherical velocity either in the same (+) or opposite (-) direction of the grinding wheel velocity. The unidirectional mode is usually used with a dressing disk speed equals to 40% or 80% of grinding wheels speed. [9]

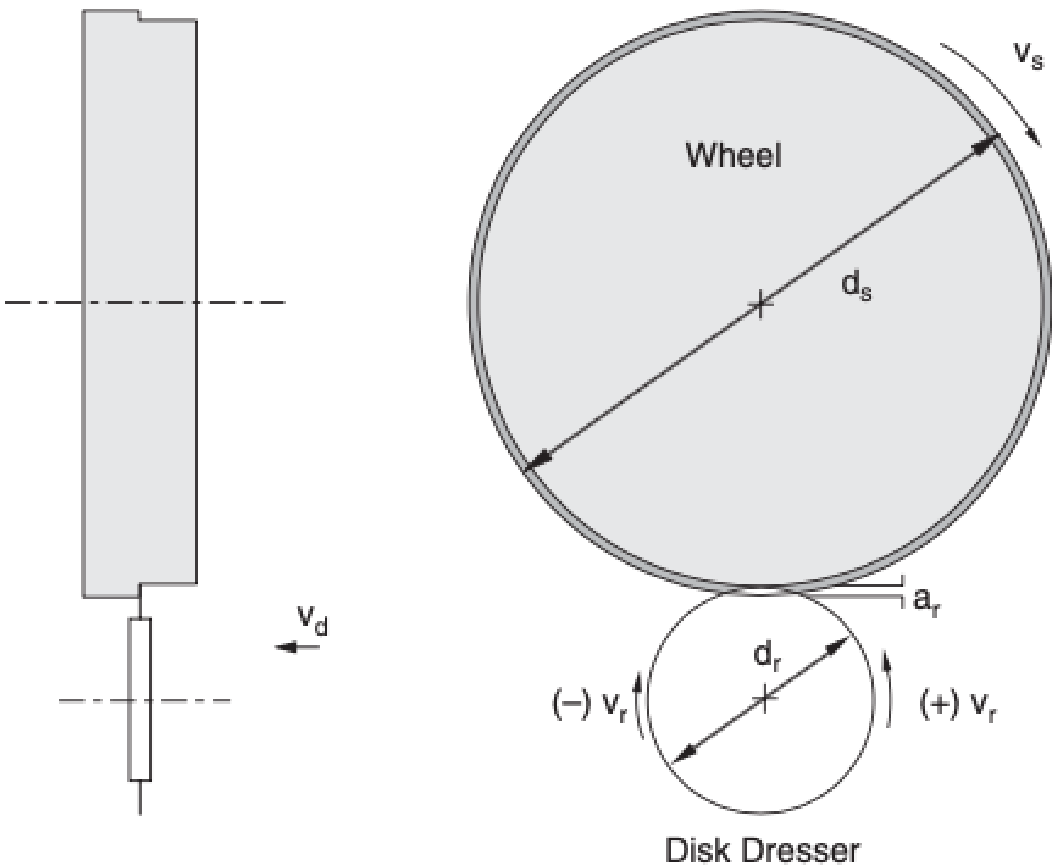

Figure 28: Diamond disk dressing of a grinding wheel

3.3. Main dressing parameters

The topography of the grinding wheel after tool preparation, hence afterwards dressing operation, largely influences its cutting properties and its performance during the process as well as the final output. By means of a precise guidance of dressing process, the grinding wheel surface can be adjusted to the required requirements. For instance, producing a rough topography is always recommendable when high cutting forces are to be expected and there are no high demands with respect to the surface quality of the workpiece. [8]
In this section, the main parameters of rotary dressing will be treated in detail since for the experimental work, *form-roll plunge dressing* has been carried out, which is a typology of rotary dressing, where the diamond roll is plunged into a grinding wheel with no traverse motion.
The most important parameters for plunge dressing process are [8]:

3. **Plunge roll effective depth.**
4. **Speed ratio.**
5. **Dwell time.**

3.3.1. Plunge roll effective depth

The way with which the wheel plunges into the workpiece it is as a spiral, as illustrated in Figure 29. The plunge roll effective depth indicates how much the dresser is plunged into the grinding wheel (or vice versa) for each grinding wheel revolution. This concept is defined also as the dressing depth, as this process can be seen like a grinding operation in which the grinding wheel is the workpiece and the dresser is the grinding wheel.
Furthermore, it is possible to identify a threshold value beyond whose, the wheel sharpness will not change. This value is for 1 $\mu m/rev$. As shown in Figure 30, the power will not decrease significantly after this threshold value.
However, by decreasing the infeed rate the heat generation will increase quickly, therefore going below 1 $\mu m/rev$ and consequently the wheel will result dull, since the grits will be dull, leading to a bigger risk of burn and chatter. [8]

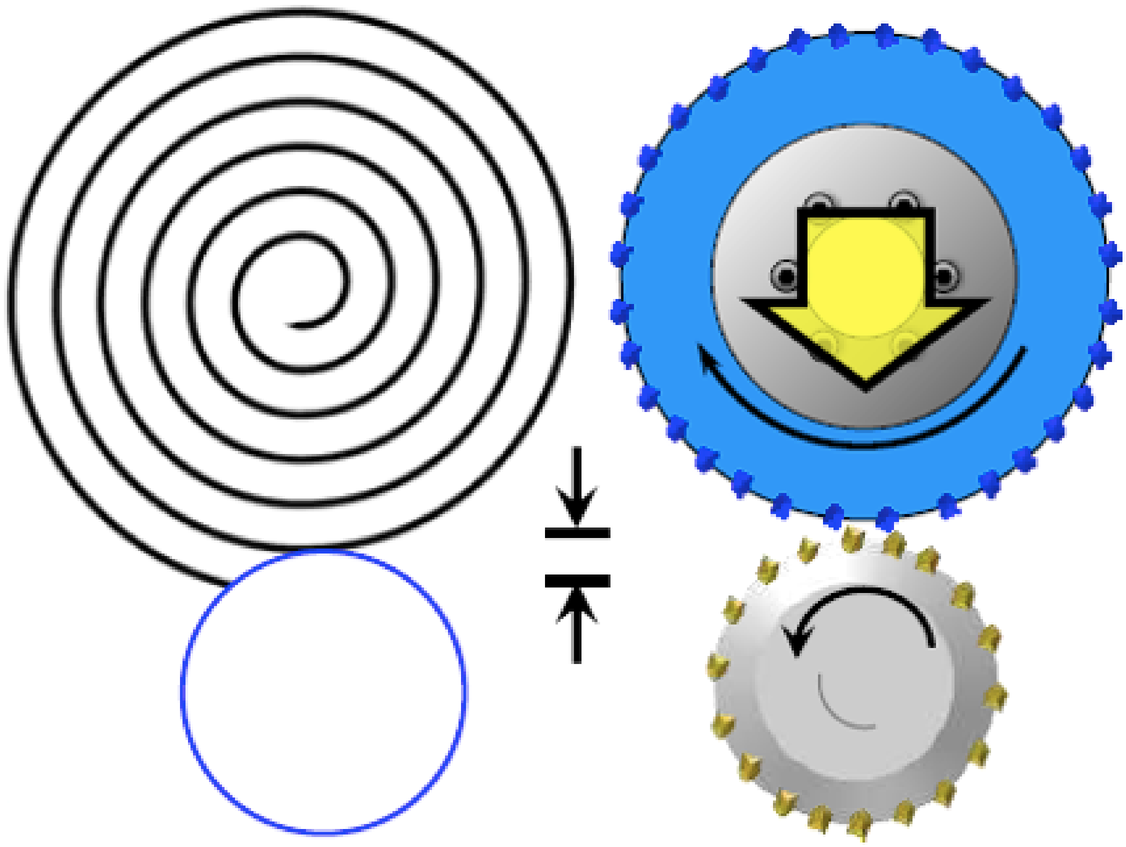

Figure 29: The wheel plunge into the workpiece with a spiral motion

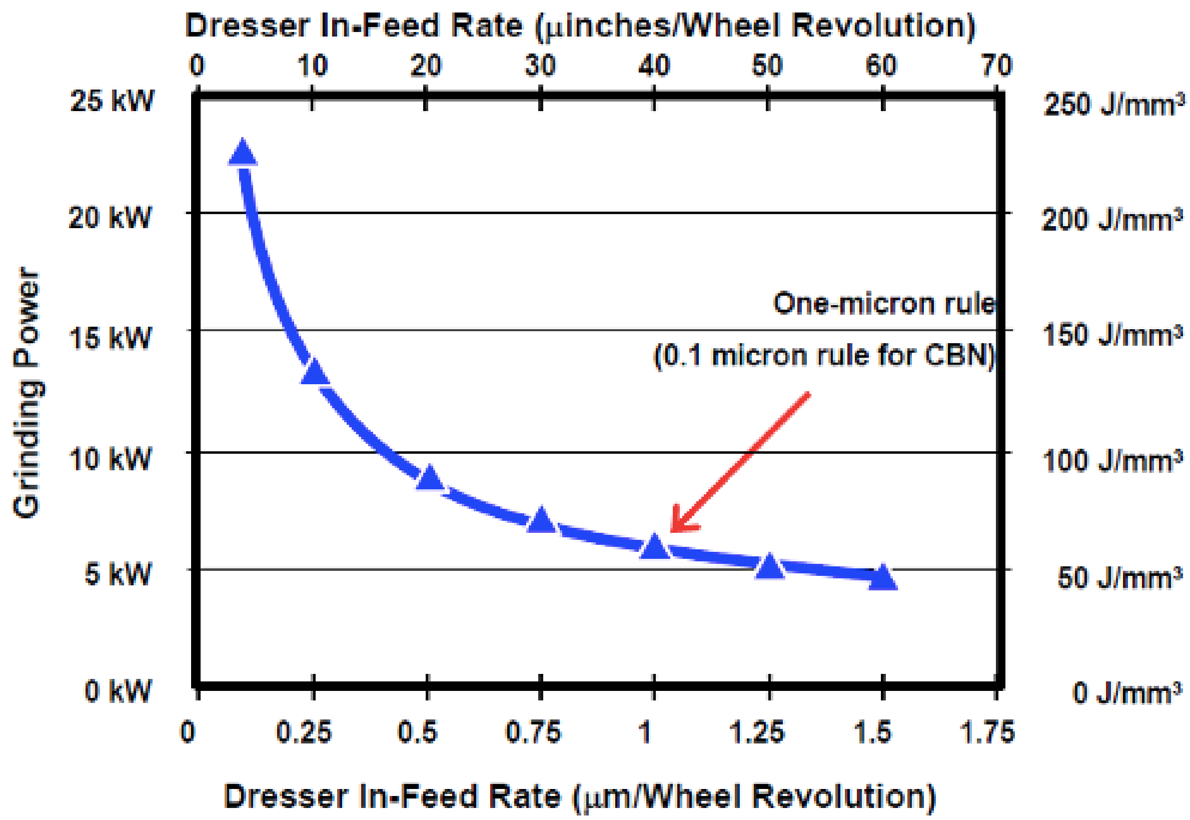

Figure 30: Grinding power plotted against the dresser infeed rate - 1 $\mu m/rev$ threshold value

3.3.2. Speed ratio

The speed ratio is the most important parameter and is measured through Equation 15.

$$q_d = \frac{v_{roll}}{v_{wheel}}$$

Equation 15: Speed ratio

Where:
q_d is the speed ratio.
v_{roll} is the dresser velocity [m/s].
v_{wheel} is the grinding wheel velocity [m/s].

Two mode of dressing operation can be distinguished depending on the direction in which the dresser and the grinding wheel move: unidirectional and anti-directional.
As it can be seen in Figure 31, in unidirectional mode, the roll and the grits move in the same direction at the point of contact; instead, if the dresser and the grinding wheel move in opposite direction, anti-directional mode is performed. The speed ratio can be higher than 1 or lower, if anti-directional mode is used, the speed ratio features a negative value.
When unidirectional mode is used, the dresser grits sort of dive bombs the grits of the grinding wheel and therefore it is much more likely to fracture them and make them very sharp (Kamikaze Dive-Bomb Dressing occurs). In anti-directional dressing instead, the roll grits come along and it just sort of clip the wheel grits and most likely make them dull (Skim Dressing occurs).
Kamikaze Dive-Bomb Dressing and Skim Dressing are reported in Figure 32.
Unidirectional mode leads less heat and risk of chatter, but also to a rougher surface (Figure 33), which can be improved using a finer grit size.
With anti-directional mode a better surface finish can be obtained but there will be a lot of heat generation (Figure 33), a bigger risk of chatter and the grinding power will be higher. The latest result can be noticed in Figure 34, in which there is a plot showing the difference in grinding power afterwards uni and anti-directional mode, the difference is about 30%.
Speed ratio equals or that gets closer to one will give a very sharp wheel and the dressing forces get large; this can cause chatter in dressing.
The best condition to use is speed ratio equals to +0.8, as it allows to avoid burn. On the other hand, as mentioned before, the dressing forces are large with this condition. Therefore, sometimes there needs to be a compromise and +0.4 as speed ratio, is a good one, which ensures an acceptable heat-surface trade-off too. [8]

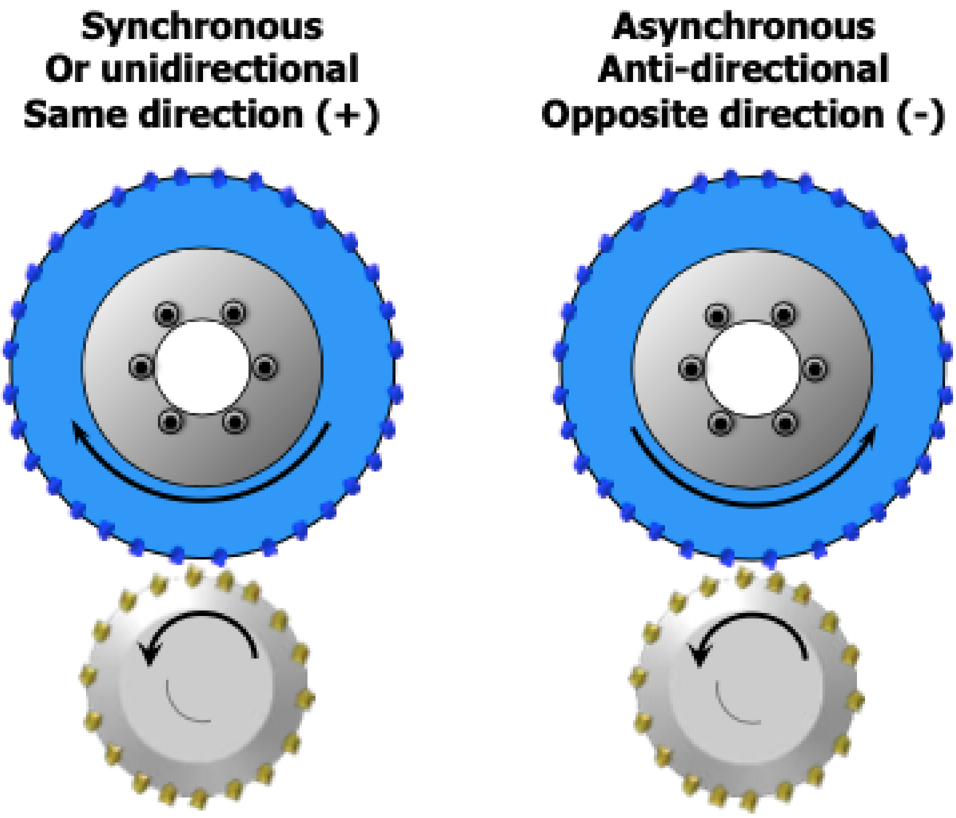

Figure 31: Speed ratio - unidirectional and anti-directional mode

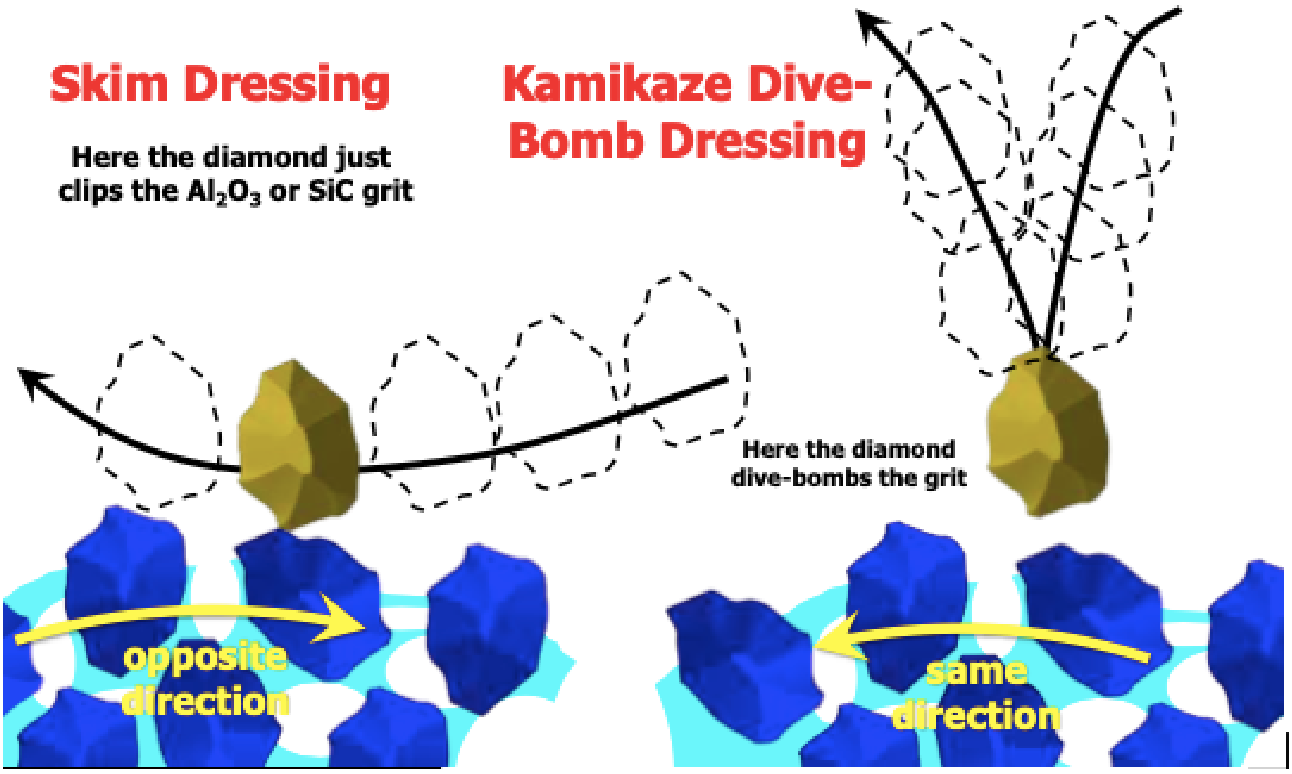

Figure 32: Kamikaze Dive-Bomb Dressing in unidirectional mode and Skim Dressing in anti-directional mode

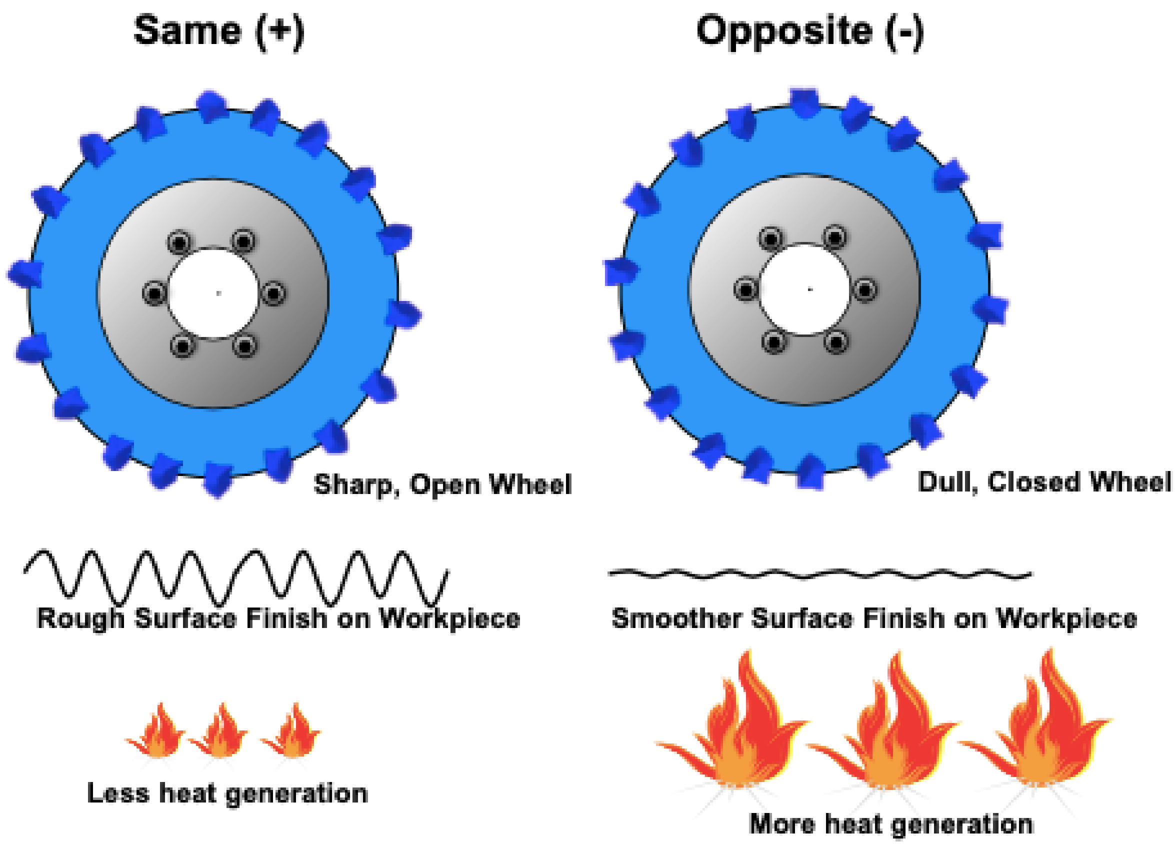

Figure 33: Unidirectional mode leads to a rough surface finish and less heat generation while anti-directional mode ensures a smoother surface finish but more heat generation

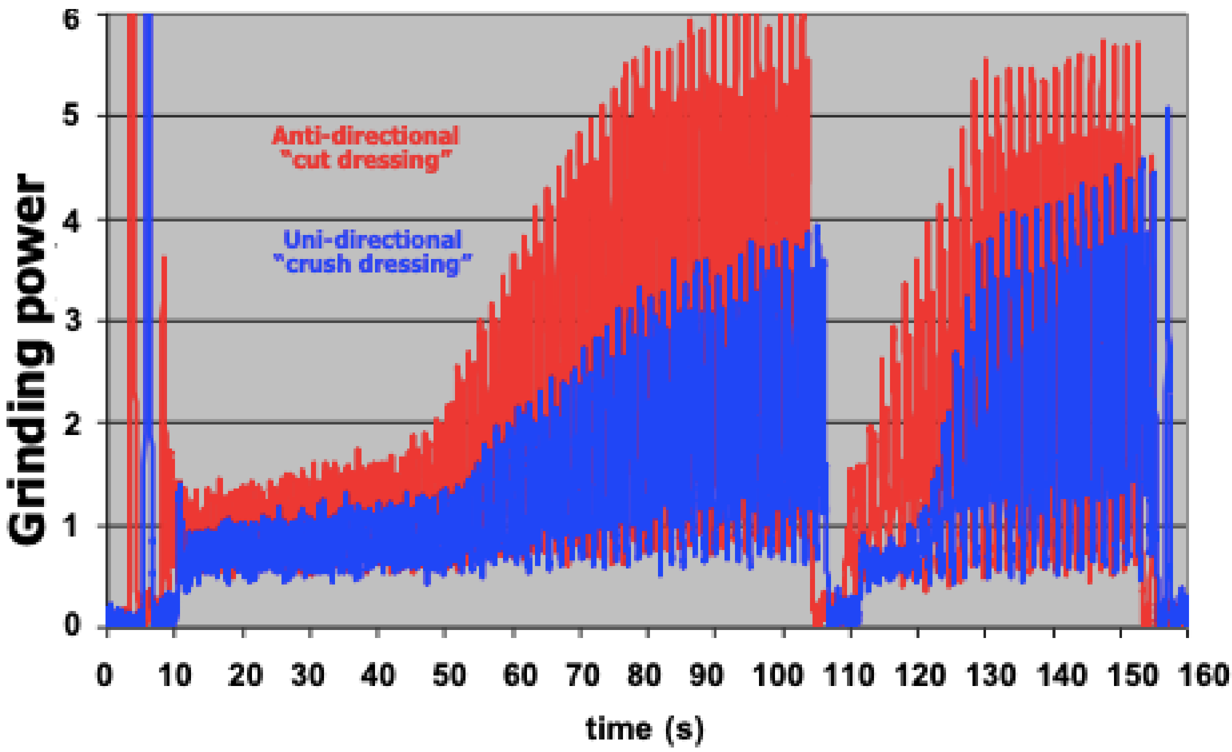

Figure 34: Grinding power is plotted against time -difference of around 30% of P_{grind} between uni and anti-directional mode

3.3.3. Dwell time

The dwell is the time necessary to achieve a perfect round shape of the grinding wheel. The dwell time is an important parameter, since, as said in the plunge roll effective depth section, when the dresser grinds away the wheel, the path it follows on the grinding wheel is a spiral. Therefore, it is fundamental to dwell otherwise the grinding wheel would feature a spiral shape if the dresser had retracted immediately, as illustrated in Figure 35.

Theoretically, it should be necessary to dwell only one revolution of the grinding, but practically there is the need to dwell more revolutions because the grinding wheel spindle and dressing spindle are not completely stiff.

A rule of thumbs advices dwelling for 20-40 wheel revolutions for a unidirectional dressing and for 10-20 wheel revolutions for an anti-directional dressing.

It is important dwelling only for the necessary time, otherwise the heat generation will increase in the subsequent grinding operation. [8]

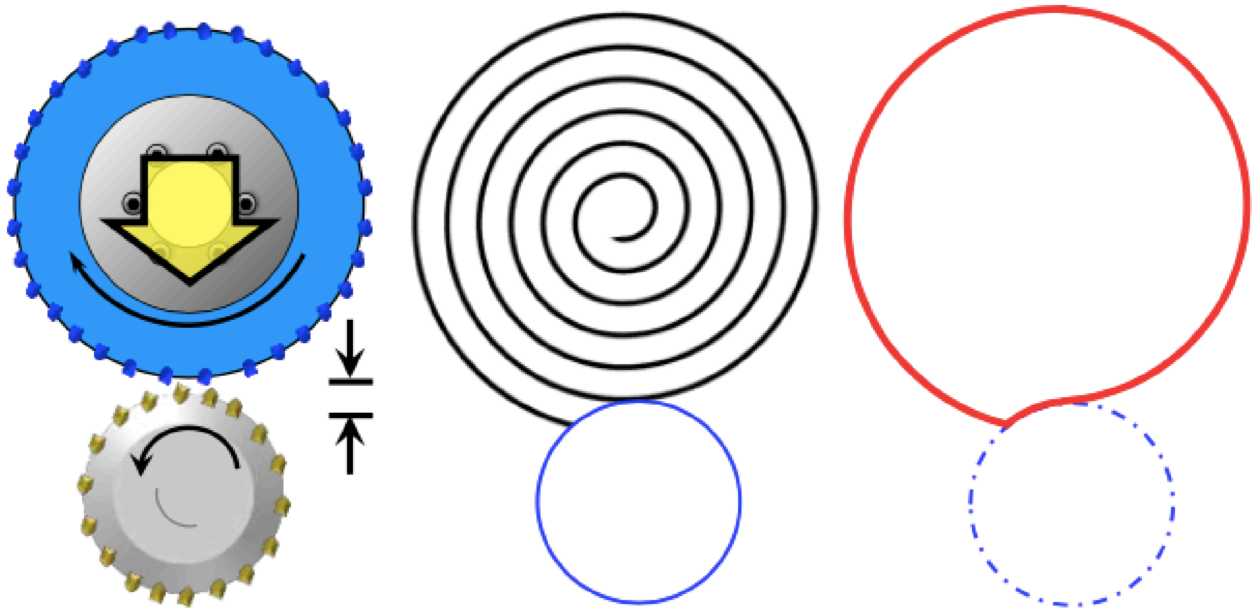

Figure 35: Spiral shape of the grinding wheel if the dresser would be retracted immediately

4. STATE OF ART

4.1. Aggressiveness number definition

The following study has been carried out by Krajnik et al. in [10].
The Aggressiveness number was defined for the first time in 2008.
It is a dimensionless number of significant importance for abrasive operations as grinding and dressing. The aim is to overcome the concept of chip thickness, which is difficult to detail in this kind of machining operations where the chip is not defined as it is in turning or milling. This is due to the undefined cutting tool geometry.
Over the years, different definitions for equivalent chip thickness were proposed.
The first one was in 1974 with Snoeys and Peters (Equation 16).

$$h_{eq} = a_e \cdot \frac{v_w}{v_s} \; [mm]$$

Equation 16: Equivalent chip thickness

(1)

where a_e indicates the depth of cut in mm, and v_w and v_s represents respectively feedrate and wheel speed in mm/s.
But there was an issue, the arc length was not considered which would give a relevant difference in operations such as cylindrical outer-diameter operation and creep-feed operation.
To overcome this issue, there is a parameter called maximum undeformed chip thickness reported in Equation 17:

$$h_m = \sqrt{\frac{4}{C \cdot r} \left(\frac{v_w}{v_s}\right) \sqrt{\frac{a_e}{d_{eq}}}} \; [mm]$$

Equation 17: Maximum undeformed chip thickness

(2)

In which C is the cutting point density, r the chip shape factor and d_{eq} is the equivalent diameter for cylindrical grinding, or the grinding wheel diameter for surface grinding.

In 2008 Jeffrey Badger defined the Aggressiveness number (Equation 18), a dimensionless parameter in which only significant variables are used: depth of cut, feedrate (workpiece speed), wheel speed and wheel diameter or equivalent diameter.

$$Aggr = 10^6 \cdot \frac{v_w}{v_s} \sqrt{\frac{a_e}{d_{eq}}} \; [-]$$

Equation 18: Aggressiveness number

(3)

In this way, the Aggressiveness number was still limited to grinding operation and geometry of plunge grinding.
In 2020, all the theories have been unified under a theory of Aggressiveness.
The point Aggressiveness was defined as shown in Equation 19:

$$Aggr^* = \frac{v_{w,N}}{v_s}\ [-]$$

Equation 19: Point Aggressiveness number

(4)

where $v_{w,N}$ is the velocity component acting normal to the point of contact, and v_s is the component acting tangentially.

The Aggressiveness number has been a revolution for the machining field since with a few adjustments it is possible to find a definition for different typologies of grinding and dressing operation, such as surface grinding, cylindrical grinding, inner-diameter and outer-diameter dressing. In particular, for dressing operation, the most useful advantage is the possibility to plot surface roughness and specific energy for different dressing variables and getting a clear and only trend for all data.

For example, in the following, two different plots are reported, the first one for the workpiece surface roughness vs the grinding Aggressiveness number for different radial infeeds and wheel speed, for cylindrical grinding of steel (Figure 36), and the second one for dressing specific energy vs dressing Aggressiveness number for different speed ratios in rotary diamond dressing (Figure 37).

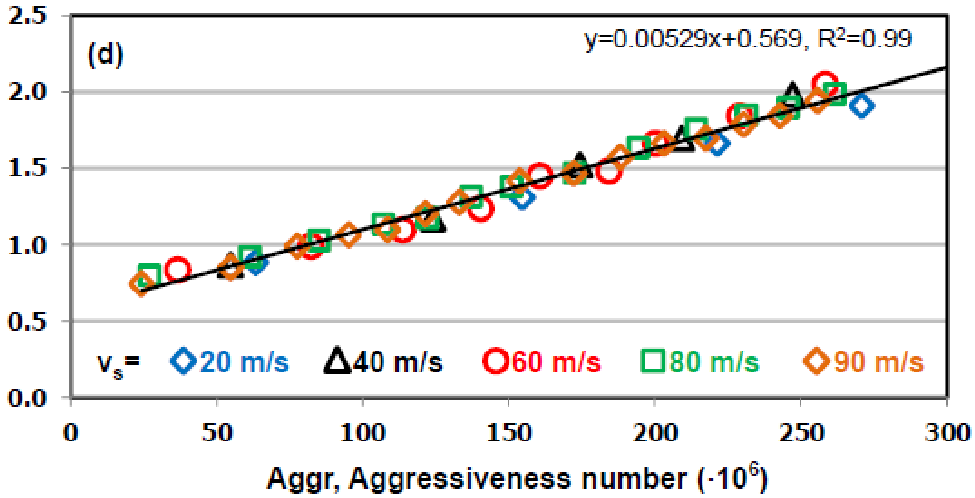

Figure 36: Workpiece surface roughness vs grinding Aggressiveness number, surface grinding

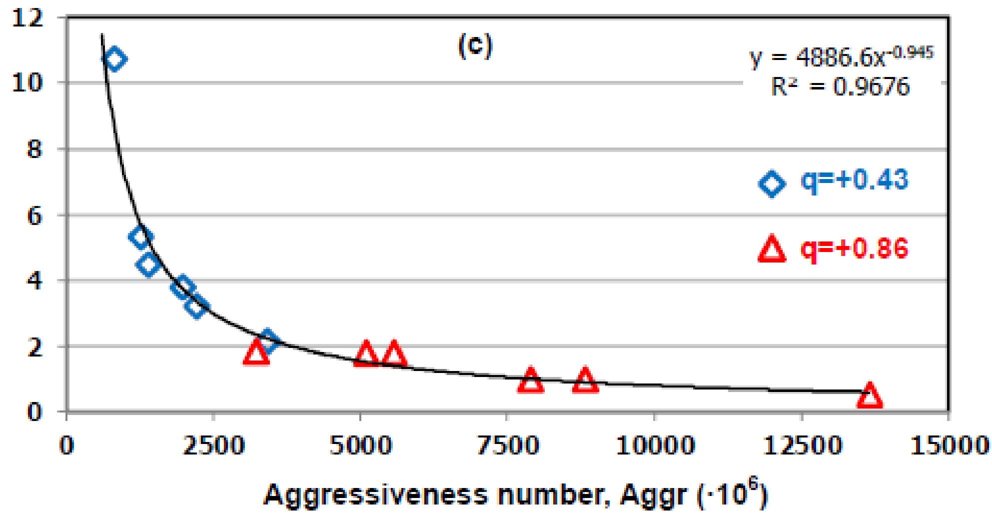

Figure 37: Dressing specific energy vs dressing Aggressiveness number, diamond dressing

It can be noticed it is easy to find correlations and trends between these variables as surface roughness, specific energy with the Aggressiveness number than with other parameters such as speed ratio or radial infeed per wheel revolutions.

4.2. Acoustic emission in dressing of grinding wheels

The following study carried on by Badger et al. in [11], is centered on acoustic emission during dressing for single-point diamond dressing.
Acoustic emission is used to know when the contact between dresser and grinding wheel occurs and to detect thermal damage.
When both cases happen, a sudden increase in the AE RMS value is registered.
The aim of this project is proving that dressing acoustic emission could be useful to predict dressing power and consequently wheel topography and grinding specific energy.
Grinding and dressing tests have been carried on a Jones and Shipman 540 surface grinder, and a single-point diamond dresser has been mounted on a holder.
Two grinding wheels have been used: a vitrified bond, monocrystalline, Aluminum-oxide, 60-mesh, J-grade wheel (32A60JVBE) and a vitrified bond, 50% ceramic-grit, 60-mesh, J-grade wheel (5SG60JVS).
As it can be seen in Figure 38, to collect the data only the 70% of the dressing pass has been considered, without considering the entry and exit of the diamond dresser in the grinding wheel.
Furthermore, in Figure 39 it can be noticed the presence of a direct proportion between the AE in Volts of a single-point diamond dressing and the dressing power in Watts (disregarding the intercept, with a value close to zero).
Through this relationship, it is possible to determine an acoustic emission power factor, which can be used to evaluate in an enough-accurate way the dressing power value, and wheel sharpness as well since the wheel sharpness is related to the power value.
In the end, a new variable has been defined: acoustic emission specific energy, measured in mV/mm3/s and obtained by means of the ratio between acoustic emission value and dressing material removal rate.
Through this variable and the acoustic emission factor, dressing specific energy can be measured.
Moreover, the acoustic emission specific energy is also related to grinding specific energy with a power-law trend (Figure 40): if one is increasing, the other is decreasing.

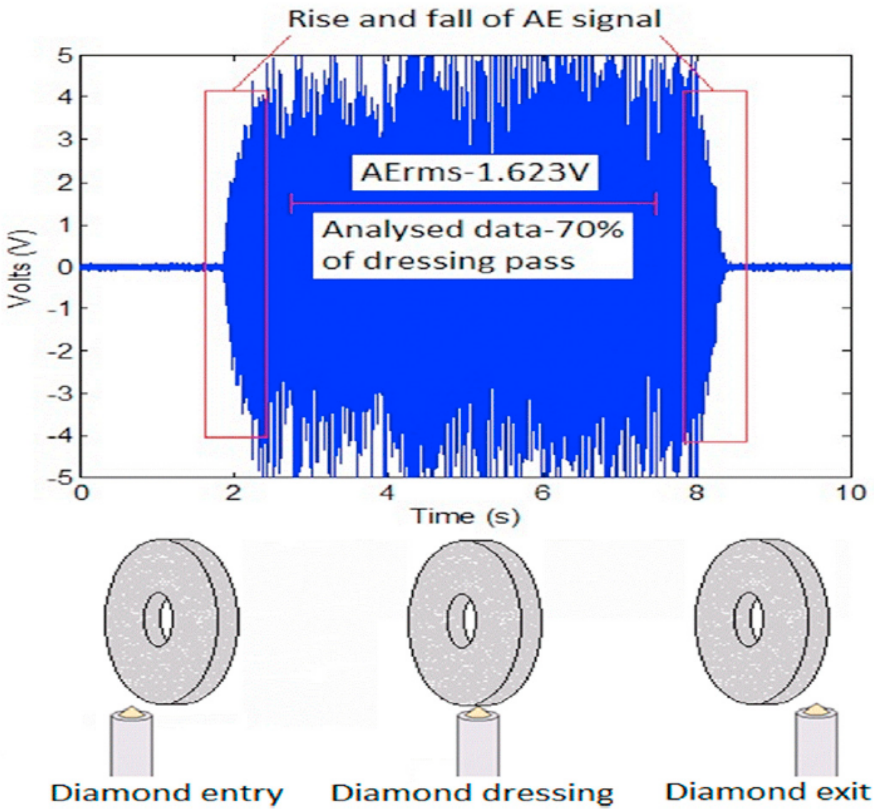

Figure 38: Dressing acoustic emission definition

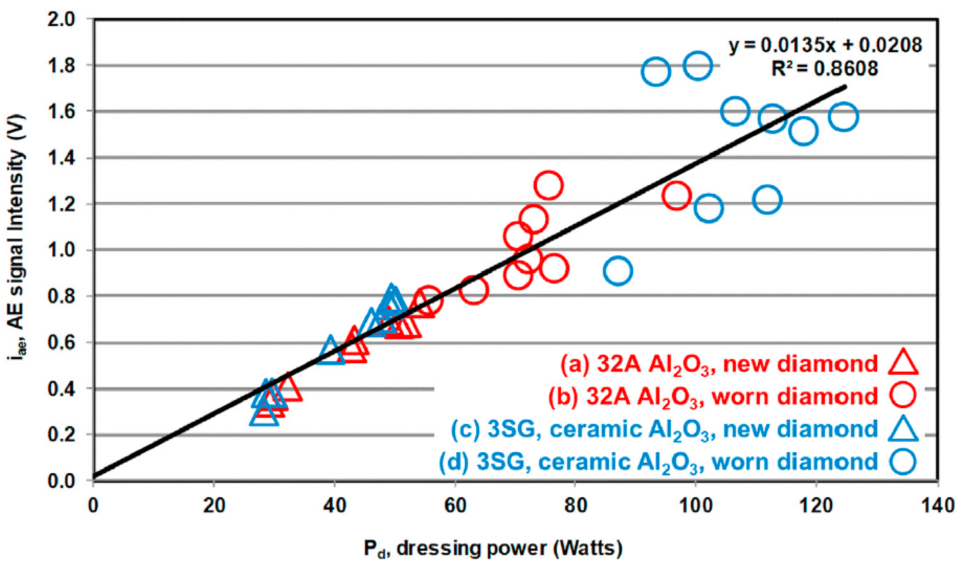

Figure 39: Dressing acoustic emission versus dressing power for different grinding wheels for different dressing parameters

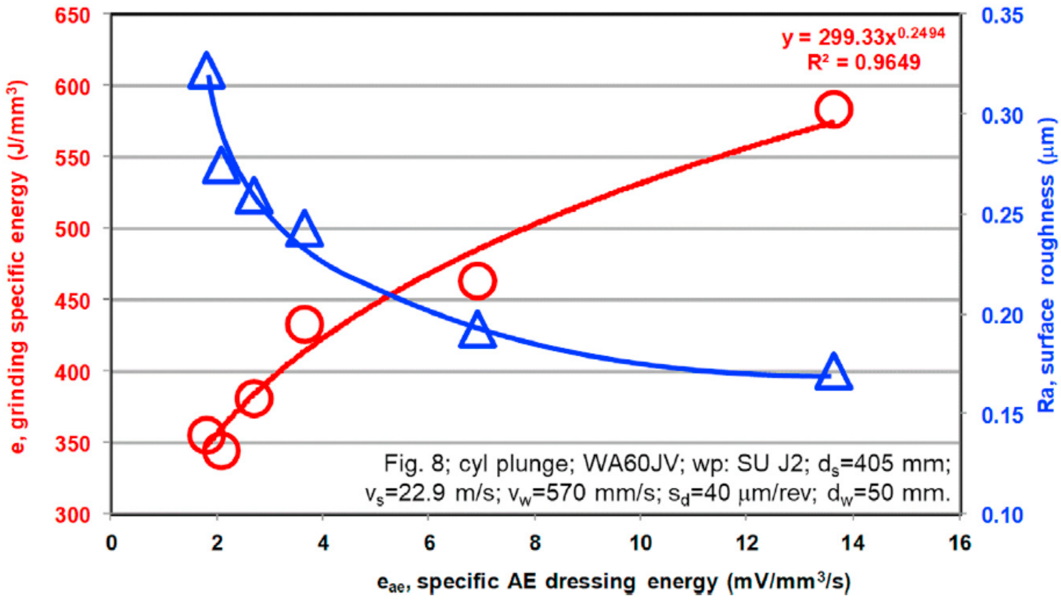

Figure 40: Grinding specific energy and surface roughness against dressing AE specific energy

5. DATA ANALYSIS

The data points have been taken from Malkin and Salmon's experiments.
The charts from the papers mentioned above have been remade using WebPlotDigitizer (https://automeris.io/WebPlotDigitizer/), and new considerations and discussions have been described by plotting variables against Aggressiveness numbers and finding new correlations.

5.1. Surface roughness analysis

The following data points are taken from Malkin's experiments on effects of rotary dressing on grinding wheel performances [12] [13]. In the chart reported in Figure 42, the surface roughness of a workpiece made of AISI 1090 hot rolled steel of hardness Rockwell 34C is plotted against the speed ratio between dressing roll velocity and grinding wheel velocity. The workpiece was ground with a grinding wheel of diameter 355.6mm and width 12.7 mm, with a speed of about 32 m/s. This wheel was designated as 32A46I8VBE, consisting of crystal Aluminum oxide abrasive in a vitreous binder. The dresser was of diameter 69.85 mm and width 19.1 mm manufactured using an infiltrated powder metal matrix for holding the diamonds, with a single layer of diamonds set with an irregular pattern. The analysis was run varying different dressing parameters: the speed ratio and the radial infeed of dresser per wheel revolution. As it can be seen, the higher are radial infeed per revolution and speed ratio, the higher will be the correspondent surface roughness on the ground workpiece.
Schematic representations are presented for dressing and grinding operations from [12] and [13] (Figure 41).

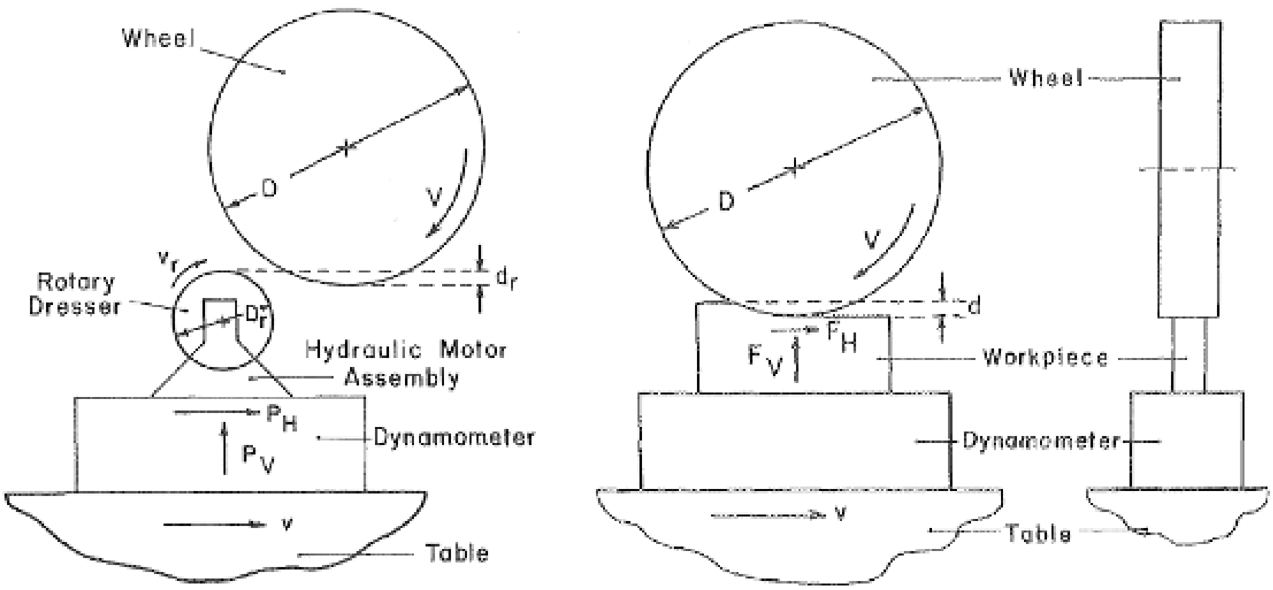

Figure 41: Plunge dressing (left) and surface (right) schematic representation

The data points are reported in Table 3 for the speed ratio and in Table 4 for the radial infeed of dresser per wheel revolution a_r [µm/rev].

Speed ratio [-]
+1.05
+0.9
+0.6
+0.2
-0.2
-0.4

Table3: Speed ratio data

a_r [µm/rev].
+1.05
+0.9
+0.6
+0.2
-0.2
-0.4

Table 4: Radial infeed of dresser per wheel revolution data

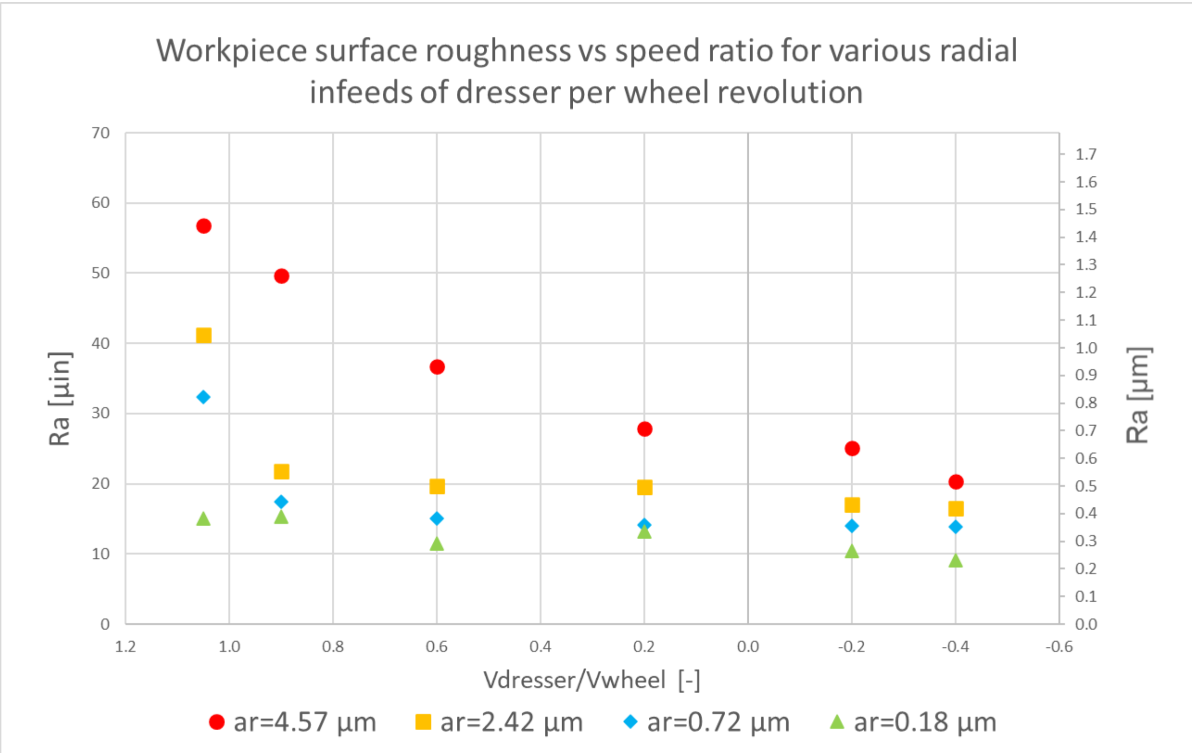

Figure 42: Surface roughness plotted against the speed ratio between dressing roll velocity and grinding wheel velocity

As shown in Figure 43, the same variable can be plotted against the ratio between grinding wheel velocity and difference between grinding wheel and dressing roll velocity (useful variable for dressing Aggressiveness number definition).

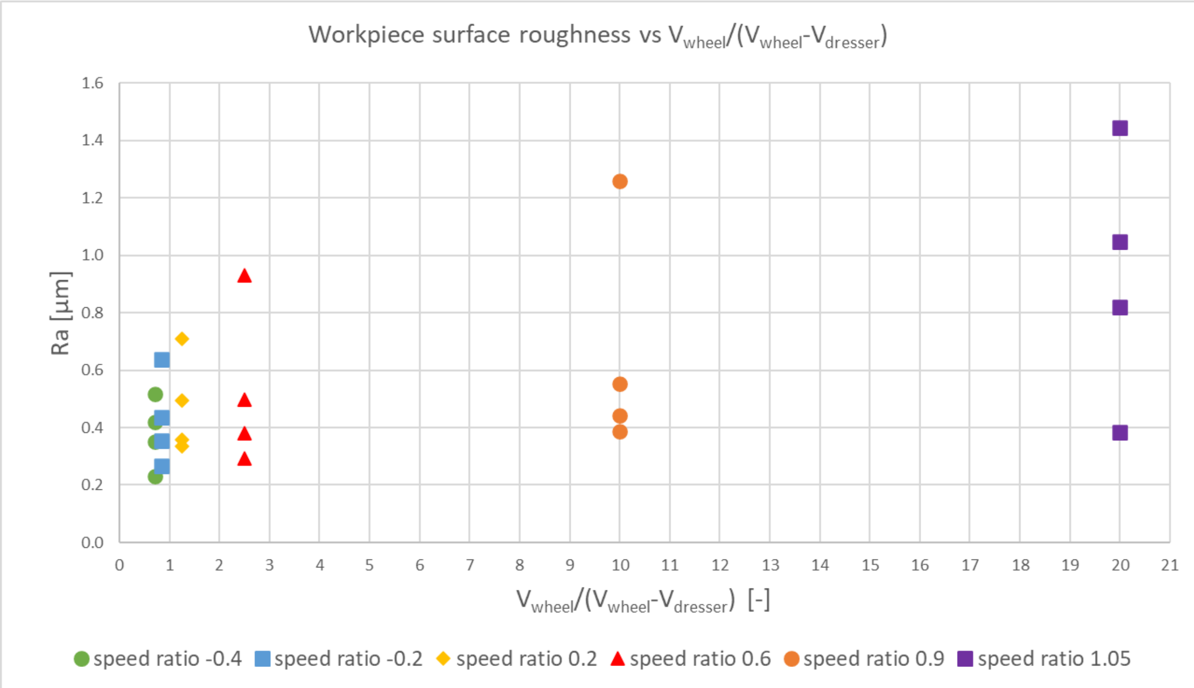

Figure 43: Surface roughness plotted against the ratio between grinding wheel velocity and difference between grinding wheel and dressing roll velocity

By means of the dressing Aggressiveness number, dimensionless number defined to have the possibility to combine the most important dressing parameters into one, it is possible to obtain a plot in which a trend can be visualized (Figure 44). In particular, the higher is the Aggressiveness, therefore the higher are speed ratio and radial infeed of dresser, the higher will be the workpiece surface roughness.

In Equation 20, the definition of Aggressiveness number from [10] is shown:

$$Aggr_d\ [-] = \frac{1}{1 - \left(\frac{v_r}{V}\right)} \cdot \sqrt{\frac{a_{eff}}{d_{eq}}} \cdot 10^6$$

Equation 20: Definition of dressing Aggressiveness number

It is possible to recognize dressing roll to grinding wheel speed ratio, radial infeed of dresser per wheel revolution (a_{eff}), and equivalent diameter calculated in Equation 21 for outer diameter (OD) dressing operation [10]:

$$d_{eq} = \frac{d_{roll} \cdot d_{wheel}}{d_{roll} + d_{wheel}} = \frac{69.85 \cdot 355.6}{69.85 + 355.6} = 58.382\ [mm]$$

Equation 21: Equivalent diameter

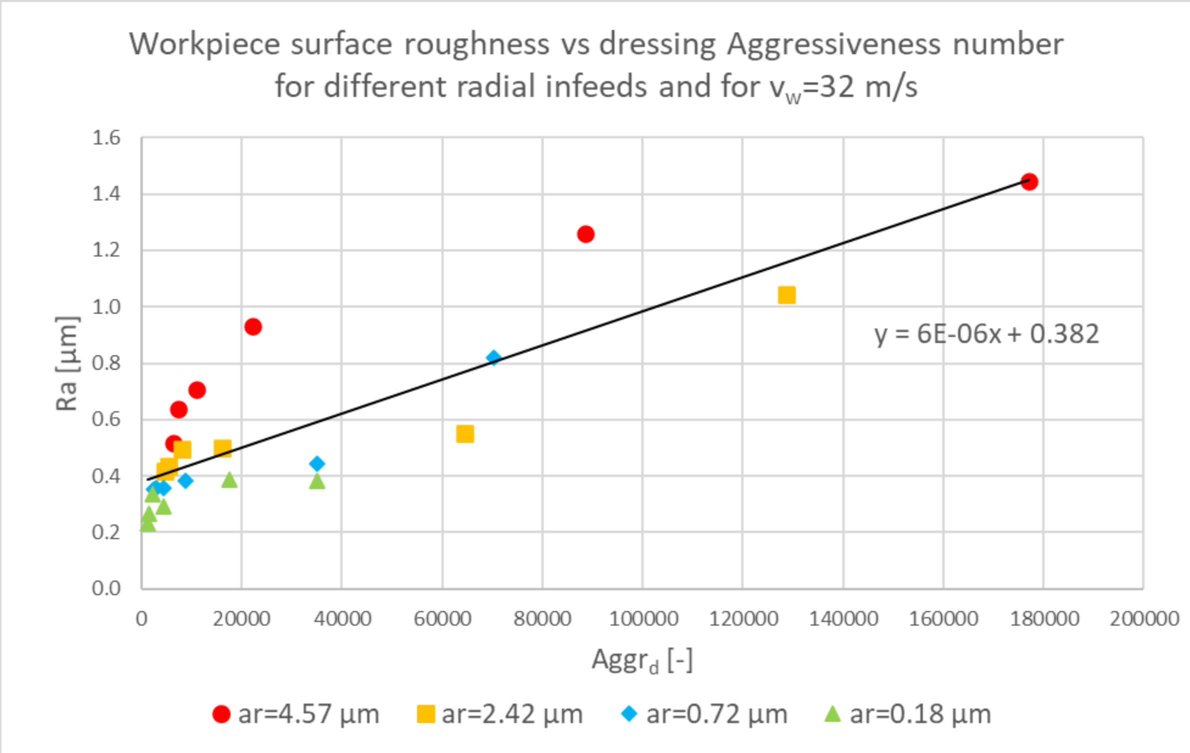

Figure 44: Surface roughness plotted against the dressing Aggressiveness number

5.2. Grinding specific energy analysis

A similar analysis to the previous one can be carried out on another fundamental variable in grinding: the specific energy. To get this value, the maximum horizontal force during grinding is needed. Once F_H is known, it is possible to get the grinding power, and finally, knowing the material removal rate, the grinding specific energy.
In the following formulas are reported.
For getting the grinding power in Watts, since the horizontal force is measured per unit width, it is necessary to multiply by the workpiece width as well, as shown in Equation 22.

$$P_{grinding}[W] = F_H \left[\frac{N}{mm}\right] \cdot V_{wheel} \left[\frac{m}{s}\right] \cdot width\ [mm]$$

Equation 22: Grinding power

Before obtaining the grinding specific energy, MRR must be calculated (Equation 23):

$$MRR \left[\frac{mm^3}{s}\right] = feedrate \left[\frac{mm}{s}\right] \cdot depth\ of\ cut\ [mm] \ \cdot width[mm]$$

Equation 23: Material Removal Rate for surface grinding

In the end, the grinding specific energy can be measured through Equation 24:

$$SE_g \left[\frac{J}{mm^3}\right] = \frac{P_{grinding}\ [W]}{MRR \left[\frac{mm^3}{s}\right]}$$

Equation 24: Grinding specific energy

The data points are presented in Table 5 for the speed ratio and in Table 6 for the radial infeed of dresser per wheel revolution a_r [µm/rev].

Speed ratio [-]
+0.9
+0.6
-0.2
-0.4

Table 5: Speed ratio data

a_r [µm/rev].
4.57
2.42
0.72
0.18

Table 6: Radial infeed of dresser per wheel revolution data

From Figure 45 it is possible to get the F_H values and evaluate the grinding specific energy.

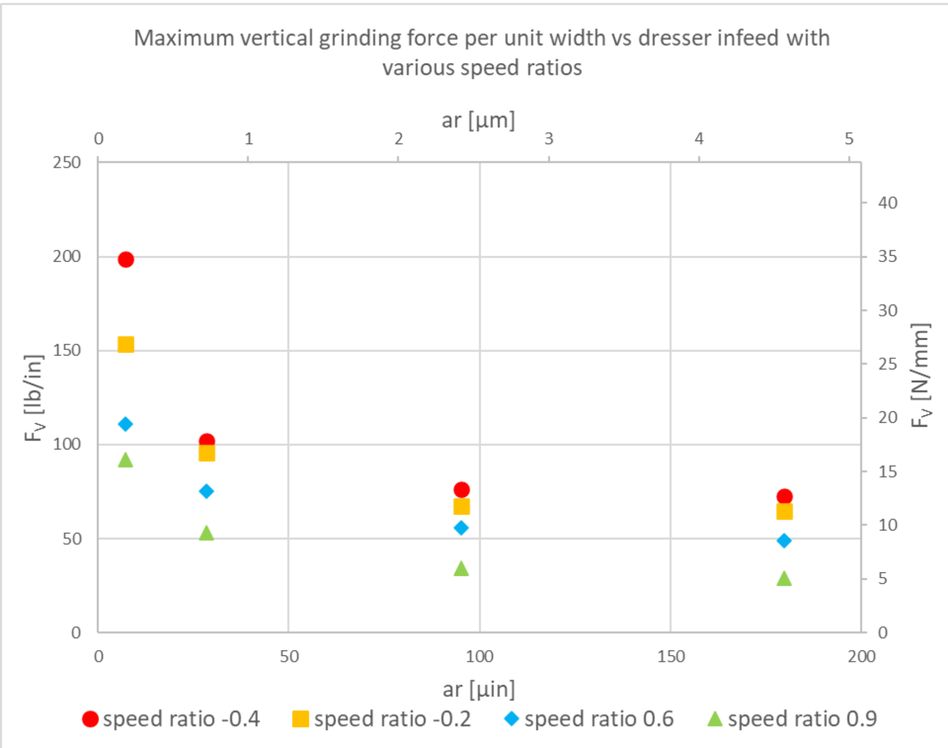

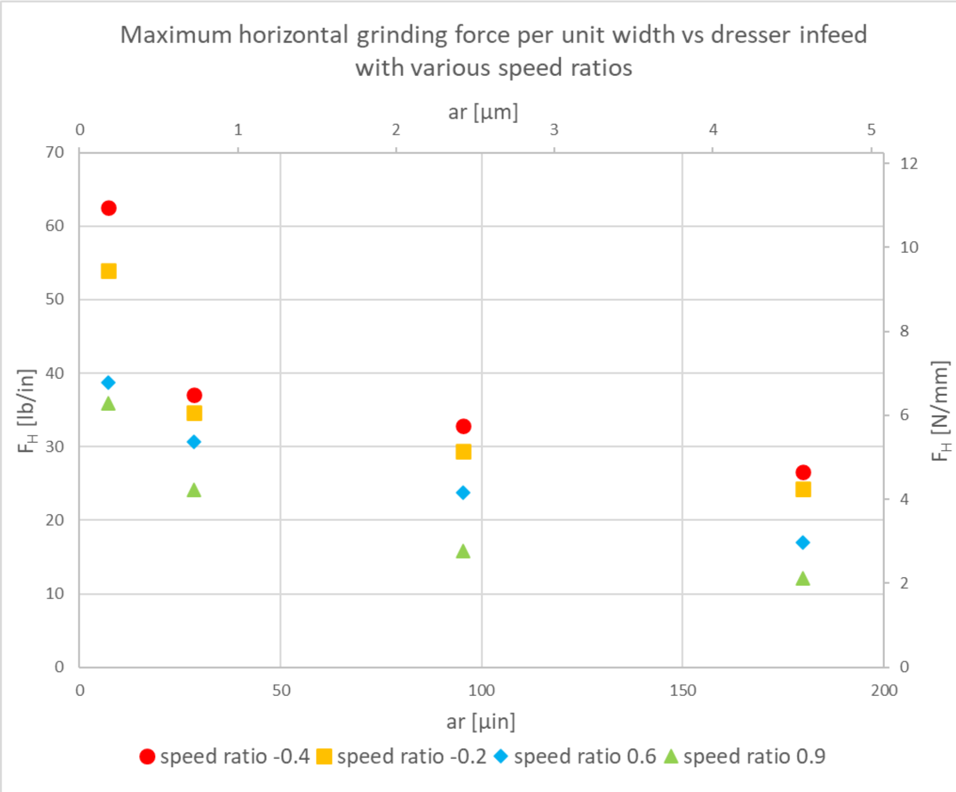

Figure 45: Vertical (above) and horizontal (below) forces during grinding plotted against the radial infeed for different speed ratio

The grinding material removal rate is calculated with Equation 23:

Then, in this case $MRR = 142.24 \left[\frac{mm}{s}\right] \cdot 0.0254\ [mm] \cdot 9.525\ [mm] = 34.41 \left[\frac{mm^3}{s}\right]$

If interested in the specific material removal rate, it can be calculated simply by dividing the material removal rate by the width, as shown in Equation 25for the specific case.

$$Q' = \frac{MRR}{width} = \frac{34.41}{9.525} = 3.61 \left[\frac{mm^2}{s}\right]$$

Equation 25: Specific material removal rate

The dressing Aggressiveness number has been calculated in the same way as in the surface roughness analysis.
In Figure 46 the grinding specific energy is plotted against the dressing Aggressiveness number: a power law trend can be identified, and it will be similar to the one found in the following experimental part.

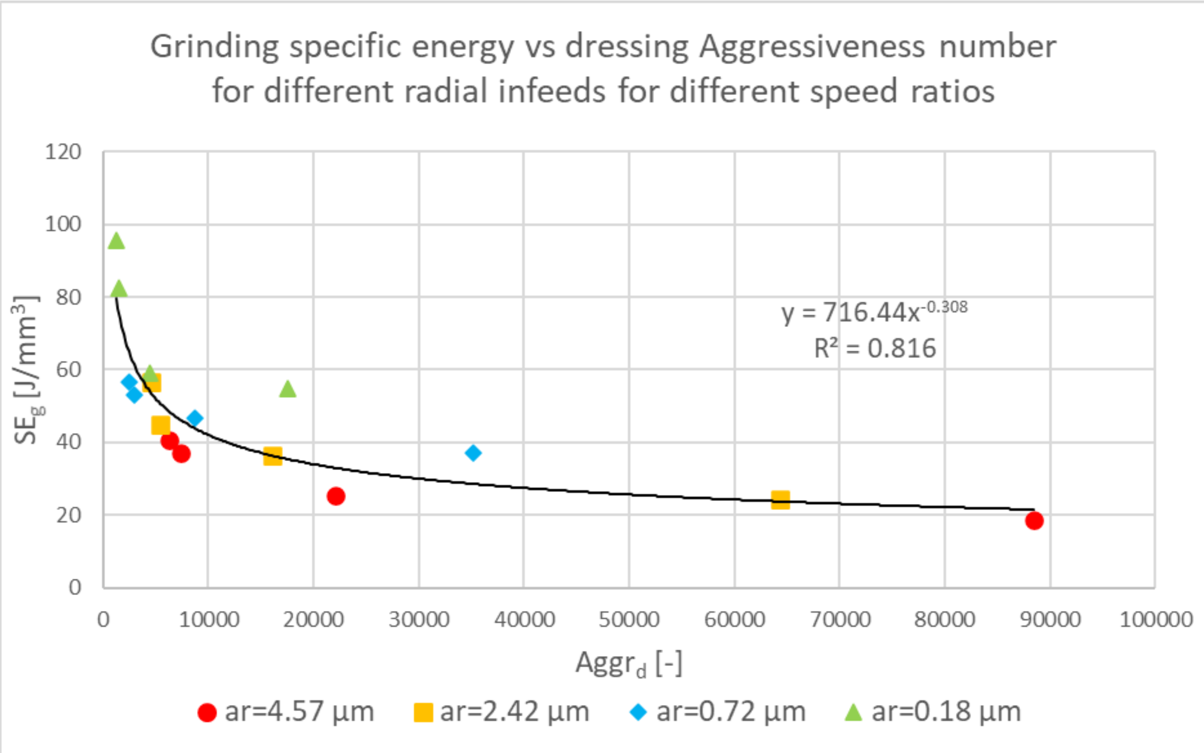

Figure 46: Grinding specific energy is plotted against the dressing Aggressiveness number - a power law trend can be seen

5.3. Surface roughness versus grinding specific analysis

Continuing the above work, since the data points were taken for the same speed ratios (+0.9 +0.6 -0.2 -0.4) and radial infeeds (4.57 2.42 0.72 0.18 [μm/rev]), surface roughness and grinding specific energy can be plotted together in the same chart, for different radial infeeds (Figure 47). A power law trend is recognized. From this image it can be seen as these two variables are connected: for higher specific energy during grinding a finer surface finish will come as consequence, therefore dressing dull there is higher heat generation but better surface finish.

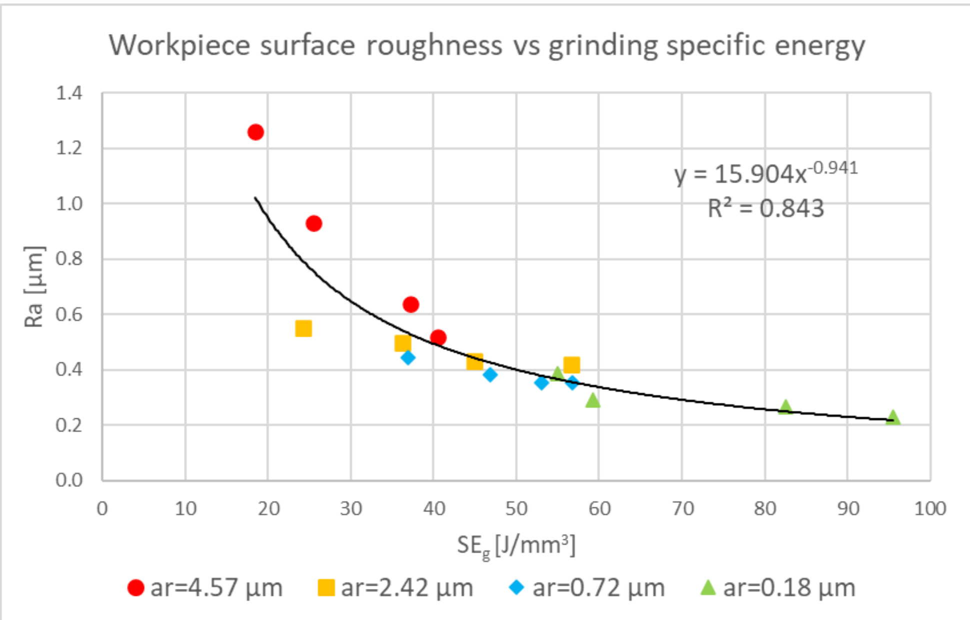

Figure 47: Surface roughness is plotted against the grinding specific energy - a power law trend can be identified

5.4. Force ratio during grinding (F_V/F_H) analysis

The next evaluation is about the ratio between maximum vertical grinding force and maximum horizontal grinding force. The data points shown in the previous figures for these forces, were both given for the same speed ratios (+0.9 +0.6 -0.2 -0.4) and radial infeeds (4.57 2.42 0.72 0.18 [µm/rev]), thus a new chart in which the ratio between the forces is plotted versus the dressing Aggressiveness number for different radial infeeds, it is presented in Figure 48. The higher is the dressing Aggressiveness, the lower is the ratio between the two forces.

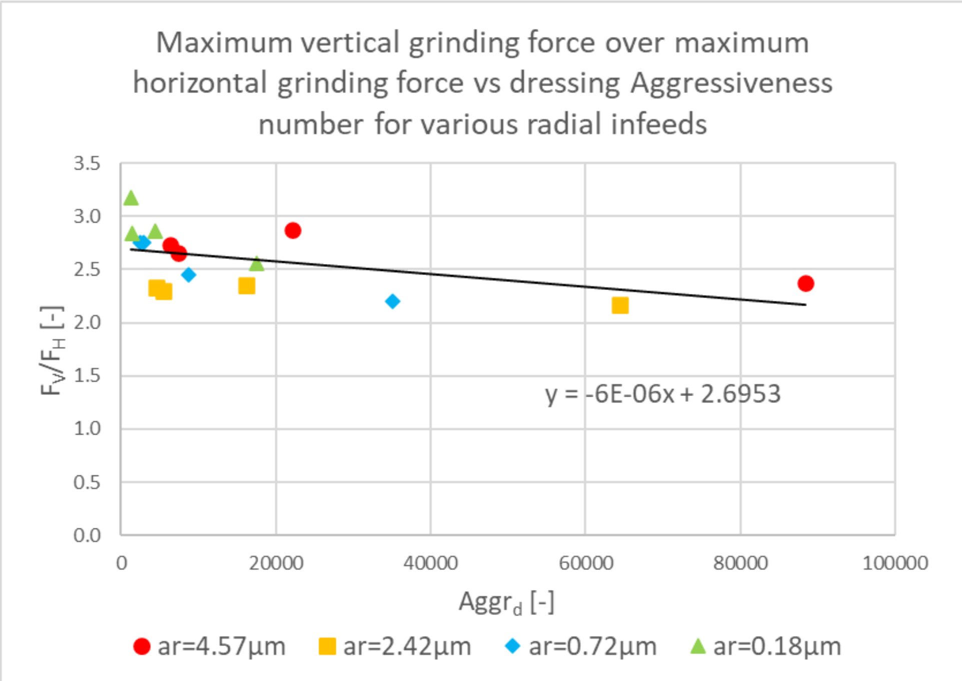

Figure 48: The ratio between the maximum vertical and horizontal grinding forces is plotted against the dressing Aggressiveness number

5.5. Continuous rotary dressing analysis

In the following analysis, data from Salmon's experiments on continuous rotary dressing effects on grinding specific energy [14] are analyzed.
First, the effect of dressing speed ratio on grinding specific energy is shown. In Figure 49, the radial infeed of dresser per wheel revolution was fixed at 0.14 µm/rev.

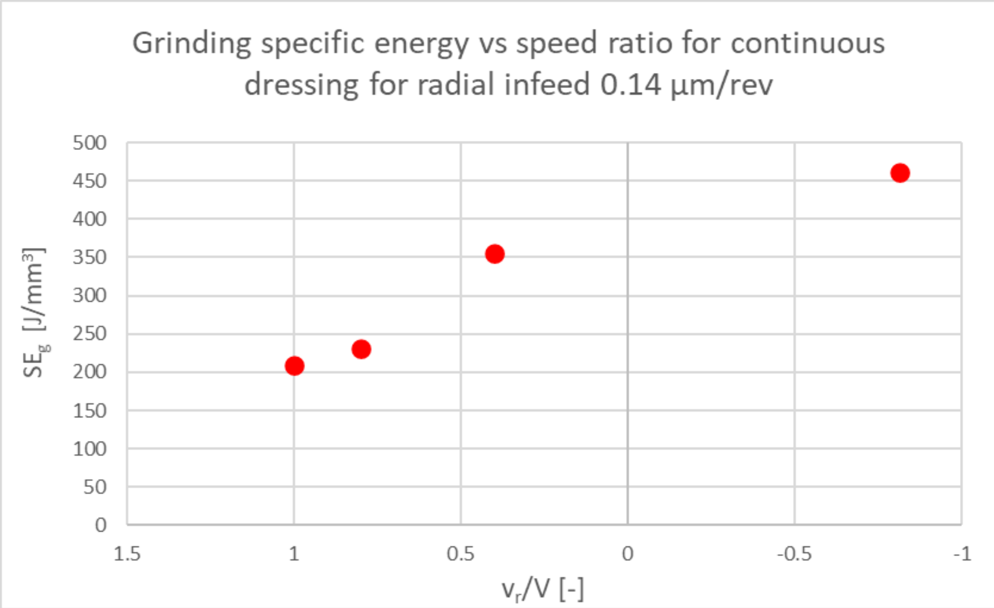

Figure 49: Grinding specific energy is plotted against the speed ratio for continuous dressing with fixed radial infeed 0.14 µm/rev

Furthermore, the test is run now by fixing the speed ratio (+0.8) and changing the radial infeed of dresser per wheel revolution. From this following plot, shown in Figure 50, it is clear that increasing the radial infeed over 1.5 µm/rev would not lead to a significant decrease in grinding specific energy as excepted.

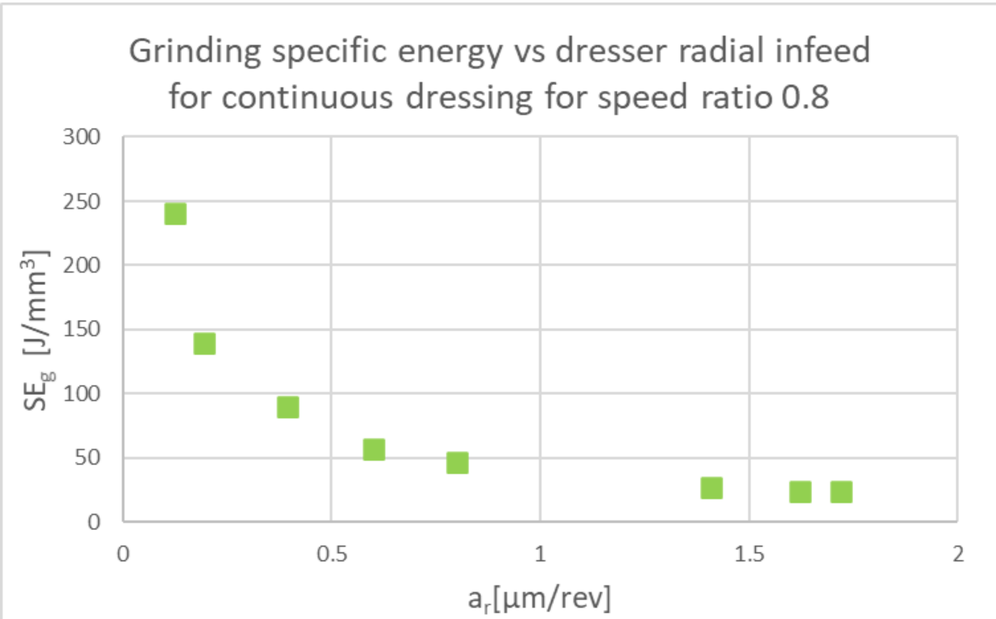

Figure 50: Grinding specific energy is plotted against the dressing radial infeed for continuous dressing with fixed speed ratio 0.8

Both the tests were run with the same dresser, grinding wheel and workpiece. [14]
The grinding wheel was coded as WA 60 80 F P2 V, and the workpiece was C 1023 nickel-base alloy. For both cases, the wheel speed was 30 m/s, and speed ratios and radial infeeds of dresser per wheel revolution were varying. The dresser was a diamond roller dresser coded DIAMESH 82971 IPE DD150.
Grinding wheel diameter was 600 mm, and dressing roll diameter was 100 mm.
Knowing these parameters, it has been possible to calculate equivalent diameter and consequently dressing Aggressiveness number, respectively through Equation 26 and Equation 27.

$$d_{eq} = \frac{d_{roll} \cdot d_{wheel}}{d_{roll} + d_{wheel}} = \frac{100 \cdot 600}{100 + 600} = 85.714\ [mm]$$

Equation 26: Equivalent diameter

$$Aggr_d\ [-] = \frac{1}{1 - \left(\frac{v_r}{V}\right)} \cdot \sqrt{\frac{a_{eff}}{d_{eq}}} \cdot 10^6$$

Equation 27: Dressing Aggressiveness number

Finally, the two previous plots are combined in only one in Figure 51, in which the grinding specific energy is plotted versus the dressing Aggressiveness number.

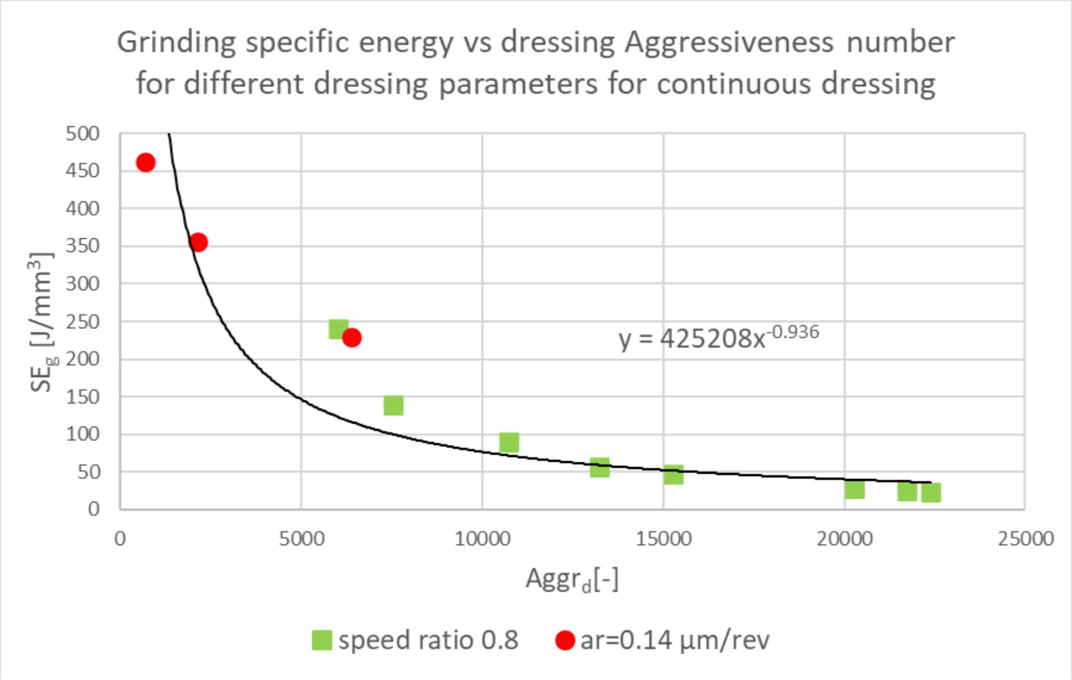

Figure 51: Grinding specific energy is plotted against the dressing Aggressiveness number for different dressing parameters for continuous dressing - a power law trend can be observed

The point correspondent to speed ratio equals to 1 is missing in this figure, since this would lead to an infinite Aggressiveness number value, given the definition of this dimensionless number.
A power law trend can be seen; however, the specific energy values result different from the ones presented in Figure 46, probably because of the too different material for the grinding operation.

5.6. Grinding specific energy plotted against dressing specific energy analysis

In the described work [15], Malkin and Murray found a correlation between rotary dressing and single point dressing. Grinding conditions after the two different kinds of dressing resulted similar.
In particular, in Figure 52, there is a plot for grinding specific energy vs dressing specific energy for rotary dressing performed with the same dressing roll as mentioned in "section 5.1"; they are proportional (as seen also in [11]), specifically there is power law trend.

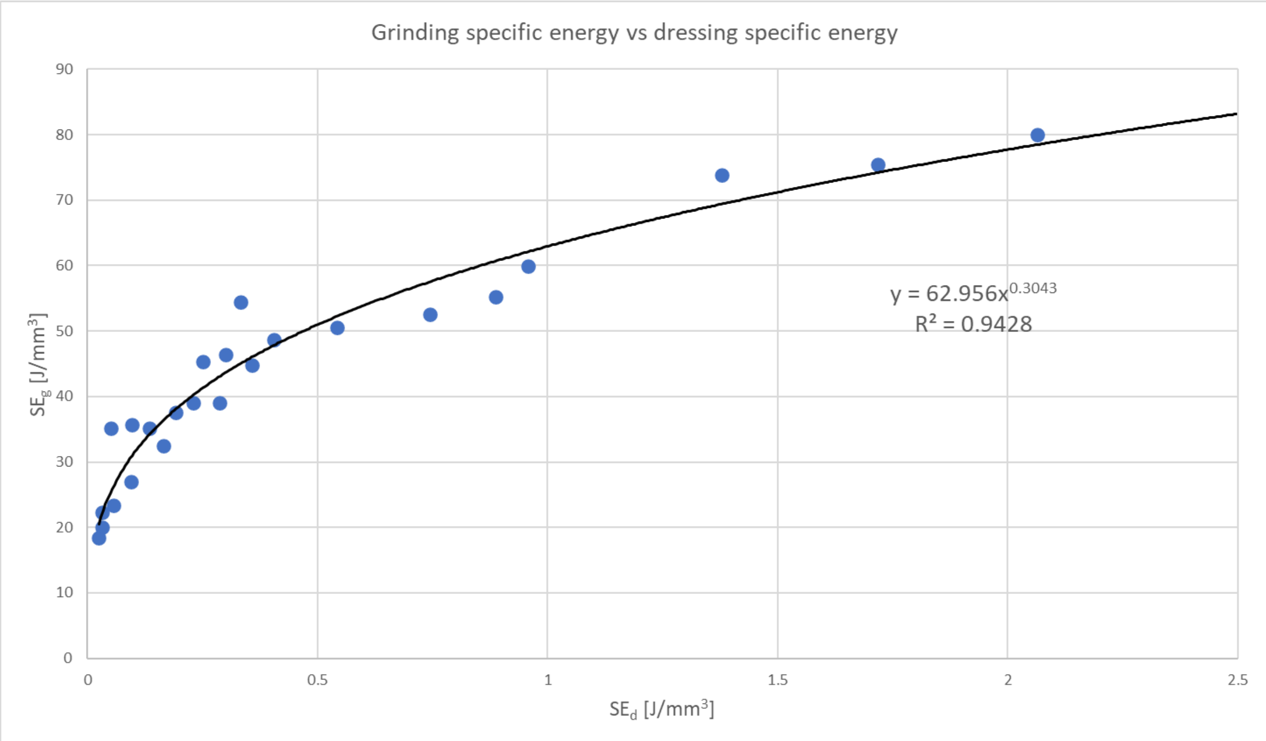

Figure 52: Grinding specific energy is plotted against the dressing specific energy - a power law trend can be identified

6. EXPERIMETAL SETUP

6.1. Machine description

For the experimental analysis a CNC BLOHM PLANOMAT HP 408 machine has been utilized, shown in Figure 53.
It is a profile grinding machine with excellent speed, robustness and efficiency and it enables the possibility of dressing station attachment, indeed a spindle for a diamond roll dresser has been mounted.
The machine consists of the following accessories (Figure 54):

- A magnetic chuck for holding the workpiece while grinding.
- An automatic balancing system for the grinding wheel.
- Acoustic sensors for acoustic emission data collection during dressing operation.
- Coolant filtration units.

It has liner guideways, and it is characterized by three driven axes which allows to reach all working points in the machine workspace, as it can be seen in Figure 55. [16]

Figure 53: PLANOMAT HP 408

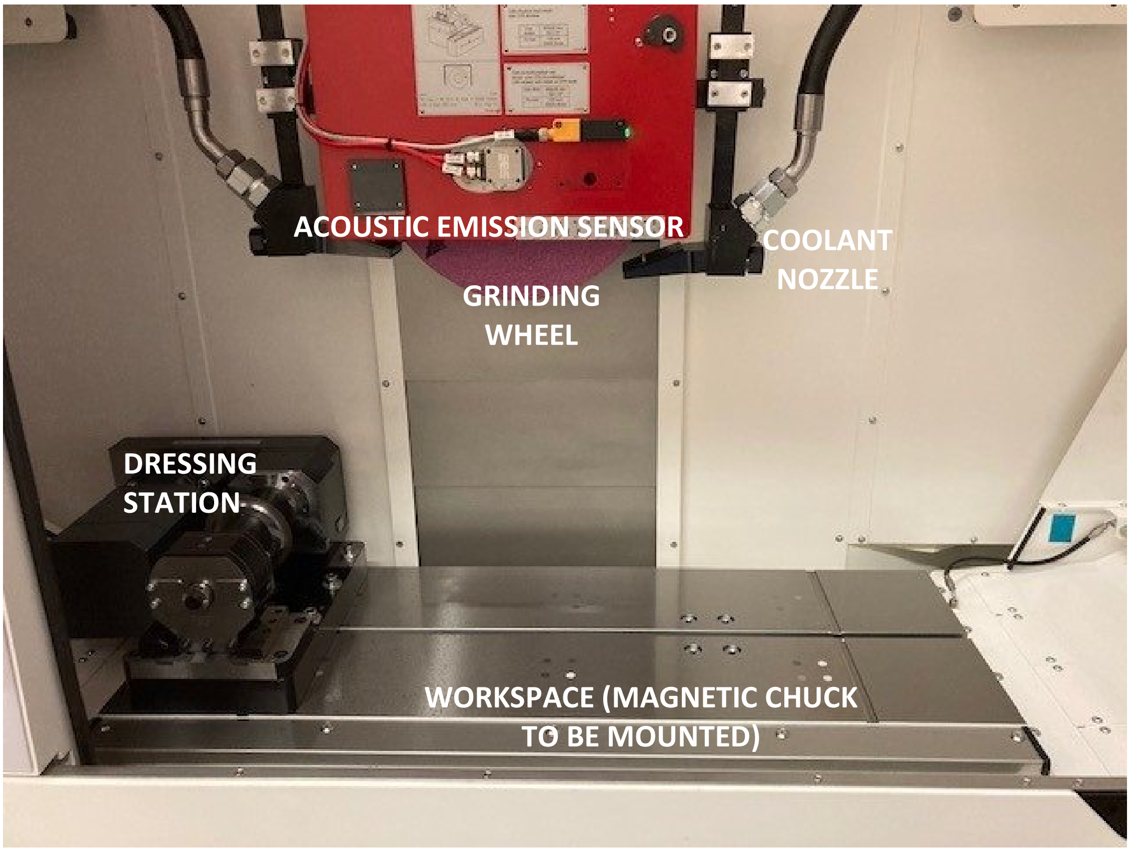

Figure 54: BLOHM machine setup and accessories

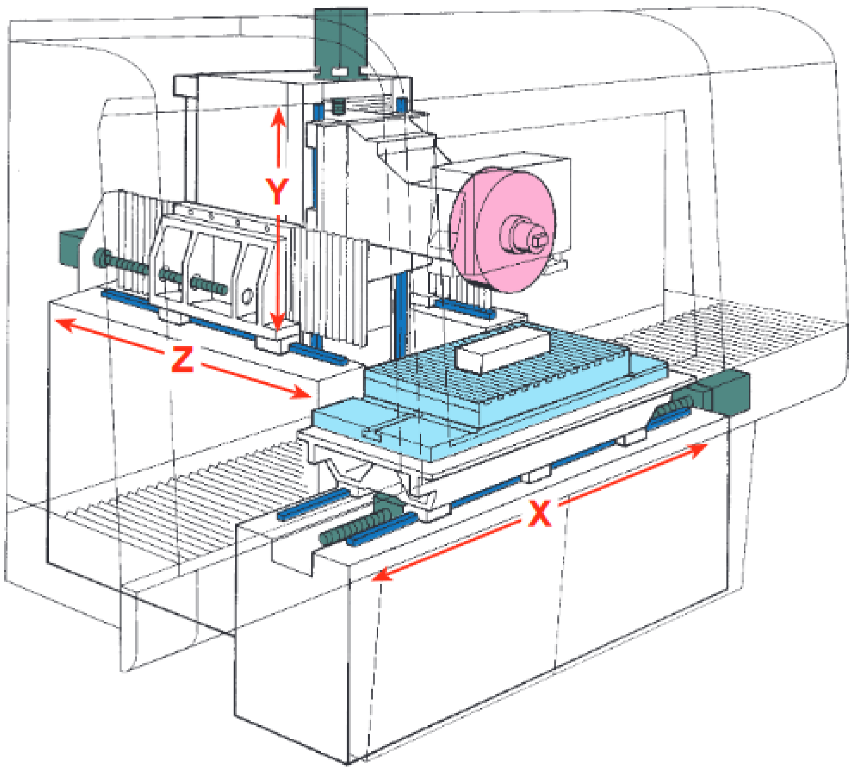

Figure 55: PLANOMAT HP 408 sketch

In addition, a user interface on Siemens platform with a touch screen enables to use easily the machine and import and export data (Figure 56).

Figure 56: BLOHM machine interface

6.2. Machine description

6.2.1. Diamond dressing roll from Meister Abrasives

The plunge-roll dresser (Figure 57) has been purchased from Meister Abrasives. The roll diameter is 150mm and the roll width 12.83mm.
A diamond coating 5mm radially thick is mounted on a steel body. The bond for the diamond grits is an innovative hybrid bond: in the matrix of the dressing coating there is a selected combination of metal and ceramic properties, which improve the wear resistance.

Figure 57: Diamond dressing roll from Meister Abrasives

6.2.2. Diamond dressing disk for traverse dressing from Meister Abrasives

The diamond dressing disk (Figure 58) has been acquired from Meister Abrasives too. It has been utilized to perform profile dressing and traverse dressing. The diamond coating is 5 mm radially thick and mounted on a steel body. It is characterized by the same bond of the diamond dressing roll.

Figure 58: Diamond disk for traverse dressing from Meister Abrasives [17]

6.2.3. Aluminum oxide grinding wheel from Hermes

The Aluminum oxide grinding wheel has been purchased from Hermes Abrasives.
Following the grinding wheel designations, the wheel is coded EWD46G7VHK. Wheel width is 50 mm and initial diameter is 400 mm.
Afterwards, the wheel specifications are reported [5]:

- EDW: friable Aluminum oxide with mixtures.
- 46: medium grit size (Figure 59).
- G: very soft considering hardness.
- 7: medium density for the structure.
- VHK: vitrified-high performance bonds.

The wheel has been profiled to obtain a step as wide as the dressing roll.

Figure 59: Grit size for the Hermes grinding wheel [8, 5, 8]

6.2.4. Flat steel workpiece

The workpiece that will be ground are taken from a bigger bar made of 38MnSiVS5 with hardness 217 HV5. The thickness for this surface grinding operation is not a relevant parameter, the length was 68mm.

7. EXPERIMETAL ANALYSIS

In this section the results of the experimental analysis are reported and discussed in detail.
The tests have been performed varying dressing parameters and keeping fixed grinding conditions to evaluate the influence of dressing operation on grinding performance, and finally varying both dressing and grinding conditions to see combined effects.

7.1. Plunge-roll dressing effects on Aluminum oxide grinding wheel performances

Twenty plunge-roll dressing conditions have been performed with the Meister Abrasives dressing roll on the Hermes Abrasives friable Aluminum oxide grinding wheel, and the dressing amount has been set at 0.2mm radially for each condition.
One of the main parameters to calculate is the dressing Aggressiveness number, given by Equation 27.

$$Aggr_d = \frac{1}{1-\left(\frac{v_r}{V}\right)} \cdot \sqrt{\frac{a_r}{d_{eff}}} \cdot 10^6$$

Equation 27: Dressing Aggressiveness number

With d_{eff} obtained through Equation 26:

$$d_{eff} = \frac{d_{roll} \cdot d_{wheel}}{d_{roll} + d_{wheel}}$$

Equation 26: Equivalent diameter

Where:

$$d_{roll} = 150mm \; and \; d_{wheel} = 184.5 \cdot 2 = 369.14\; mm$$

In Table 7 the different dressing parameters set and the relative dressing Aggressiveness number are reported. The higher are speed ratio and radial infeed per wheel revolution, the higher is the Aggressiveness number

speed ratio [-]	radial infeed [µm/rev]	dressing Aggressiveness number [-]
0.8	0.1	4841
0.8	0.3	8386
0.8	0.7	12809
0.8	1	15310
0.8	1.5	18751
0.4	0.1	1614
0.4	0.3	2795
0.4	0.7	4270
0.4	1	5103

0.4	1.5	6250
-0.4	0.1	692
-0.4	0.3	1198
-0.4	0.7	1830
-0.4	1	2187
-0.4	1.5	2679
-0.8	0.1	538
-0.8	0.3	932
-0.8	0.7	1423
-0.8	1	1701
-0.8	1.5	2083

Table 7: Different dressing parameters set and the relative dressing Aggressiveness number

After realizing each condition by dressing, surface grinding on a steel workpiece in 38MnSiVS5 with average hardness 217 HV5 have been performed with the following parameters:

- Number of passes for overcoming transient: 10 passes
- Depth of cut per pass: 0.025 mm
- Wheel step width: 12.83 mm
- Workpiece feedrate: 50 mm/s
- Material removal rate:

$$MRR = width \cdot depth\ of\ cut \cdot feedrate = 12.83 \cdot 0.025 \cdot 50 = 16.0375\frac{mm^3}{s}$$

- Specific material removal rate:

$$Q' = depth\ of\ cut \cdot feedrate = 1.25\frac{mm^2}{s}$$

7.2. Grinding specific energy experimental analysis

Starting from the grinding power plot, after 10 passes the transient can be considered over, and therefore the correct grinding power is evaluated.

A measured grinding power (called ‘P1’, green line) is obtained considering the peak value of the last pass, and an idle grinding power (called ‘P2’, red line) is read as well. Once they are defined, it is possible to proceed by subtracting P2 from P1 and get the actual grinding power.

For instance, for the case with speed ratio -0.4 and ar=1.5μm/rev, the plot is presented in Figure 60, and the grinding power is given by 1022-193=829W.

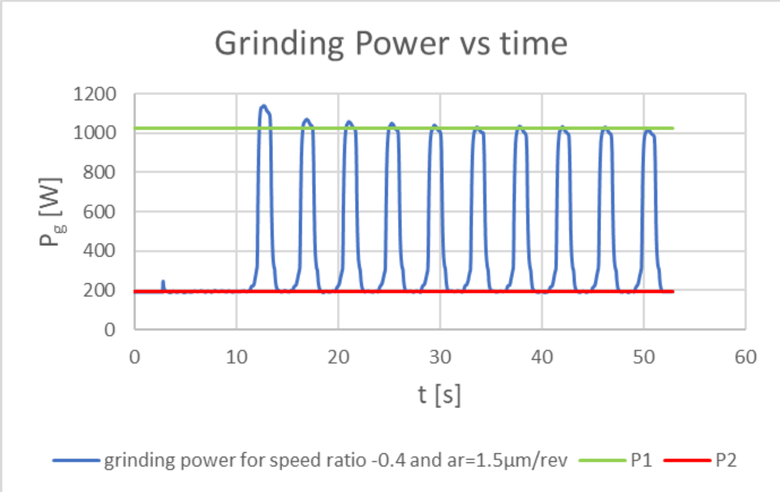

Figure 60: Grinding power is plotted against time for speed ratio -0.4 and radial infeed 1.5 µm/rev

For visualizing the difference between the operations, there are plots for different dressing radial infeeds for same speed ratio. For instance, the plot in Figure 61 is for speed ratio 0.8. It is clear such as a more aggressive dressing condition (if speed ratio constant is obtained with higher radial infeed value) would lead to lower grinding power. First passes are to be disregarded because of slight errors on evaluating the zero-position for the grinding operation start.

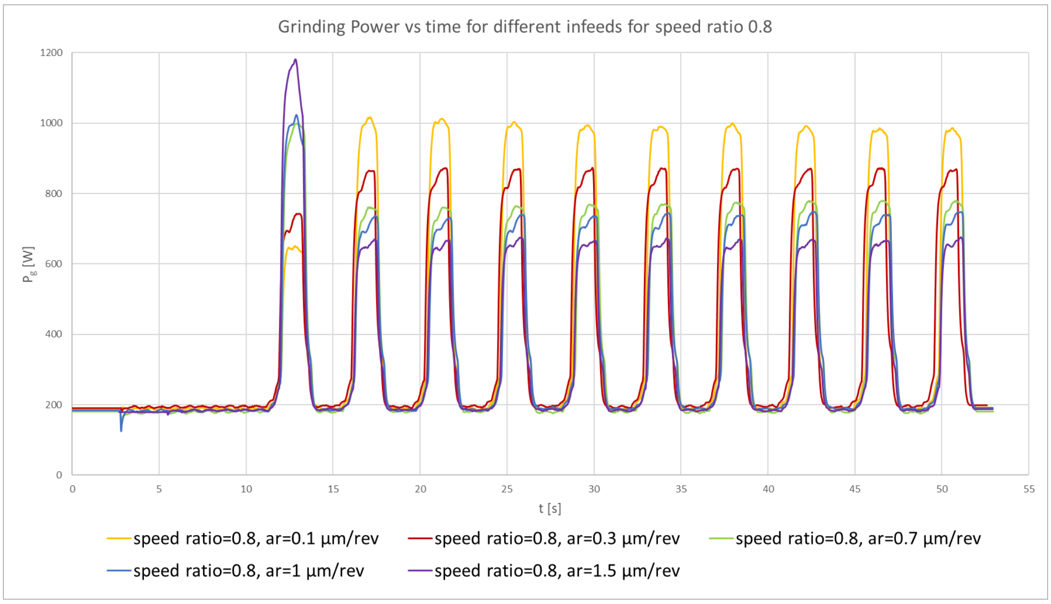

Figure 61: Grinding power is plotted against time for different radial infeeds and speed ratio 0.8

Once the grinding power has been calculated, it has been possible to get the grinding specific energy, obtained by dividing grinding power by grinding material removal rate.
In Table 8 there are the grinding results for all the dressing conditions.

speed ratio [-]	radial infeed [µm/rev]	Measured power [W]	P idle [W]	P grinding [W]	SE_g [J/mm^3]	$Aggr_d$ [-]
0.8	0.1	986	188	798	49.76	4841
0.8	0.3	869	194	675	42.09	8386
0.8	0.7	780	179	601	37.47	12809
0.8	1	748	183	565	35.23	15310
0.8	1.5	676	184	492	30.68	18751
0.4	0.1	1213	189	1024	63.85	1614

0.4	0.3	864	182	682	42.53	2795
0.4	0.7	960	189	771	48.07	4270
0.4	1	770	182	588	36.66	5103
0.4	1.5	788	184	604	37.66	6250
-0.4	0.1	1398	191	1207	75.26	692
-0.4	0.3	1048	176	872	54.37	1198
-0.4	0.7	1001	191	810	50.51	1830
-0.4	1	947	181	766	47.76	2187
-0.4	1.5	1022	193	829	51.69	2679
-0.8	0.1	1627	174	1453	90.60	538
-0.8	0.3	1261	191	1070	66.72	932
-0.8	0.7	1050	181	869	54.19	1423
-0.8	1	914	188	726	45.27	1701
-0.8	1.5	929	183	746	46.52	2083

Table 8: Grinding results collected for all the dressing conditions

Proceeding with representing all the points in the same chart, the expected trends can be seen by plotting grinding specific energy versus radial infeed for different speed ratios in Figure 62.

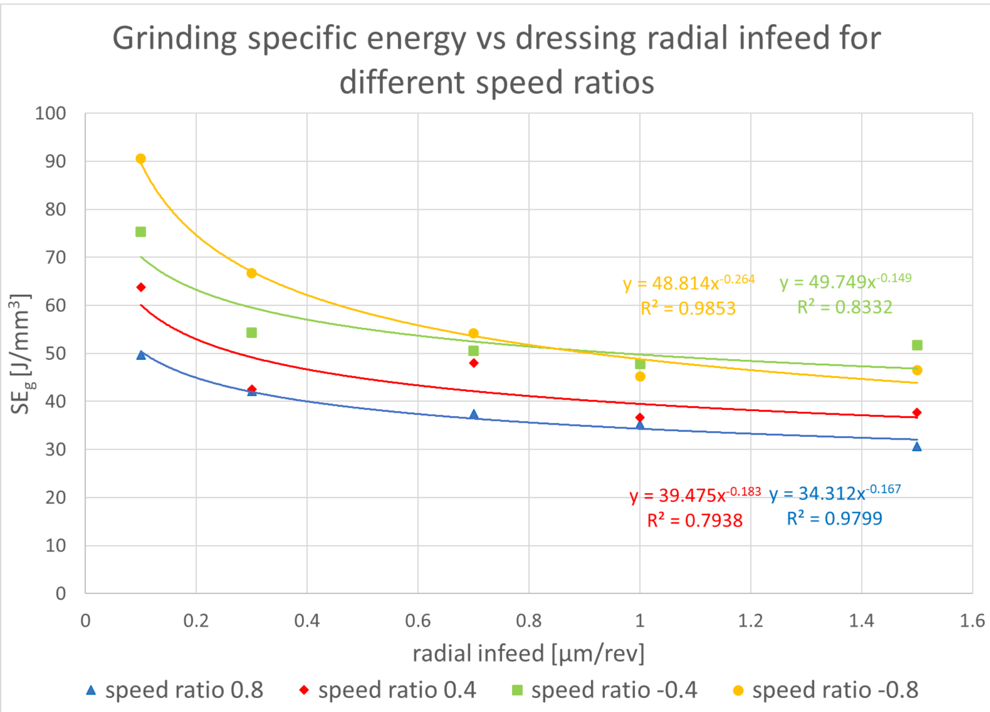

Figure 62: Grinding specific energy vs dressing radial infeed for different speed ratios - power law trends for each speed ratio value

In order to fully understand the process, the grinding specific energy can be plotted versus the dressing Aggressiveness number, which is reuniting the main dressing parameters (Figure 63).

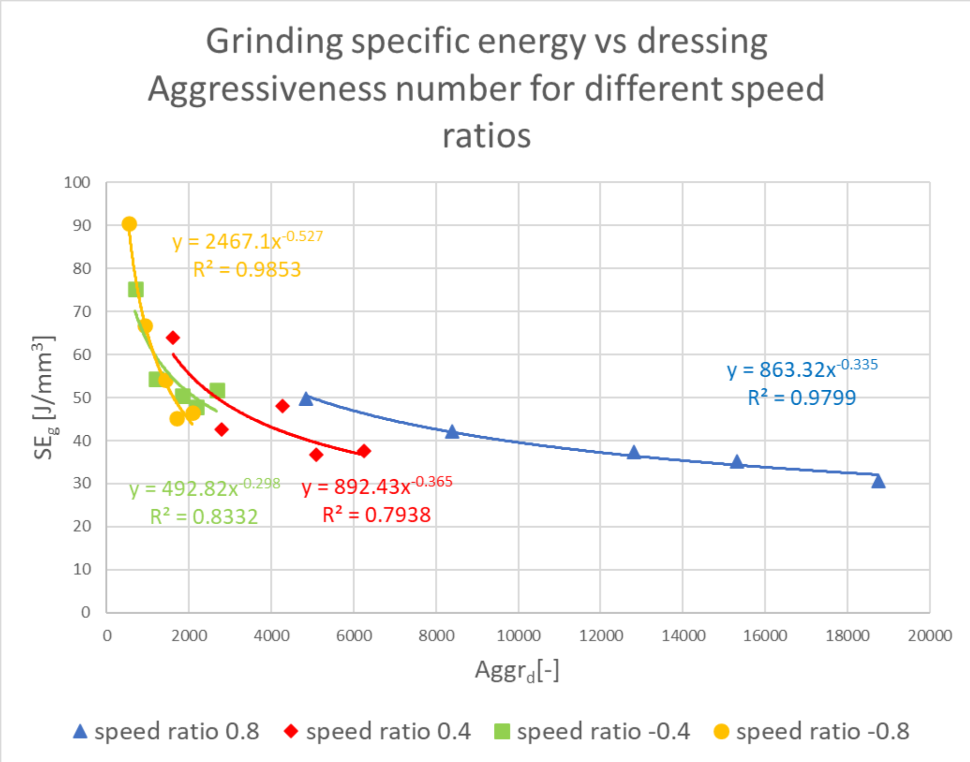

Figure 63: Grinding specific energy is plotted against the dressing Aggressiveness number for different speed ratios - a power-law trend for each speed ratio can be seen

To make the concept even clearer, in Figure 64, for different speed ratios, the data are fit in one trend with a power law equation, which results in an enough-precise approximation. This plot reminds of the one in Figure 46 and Figure 51.

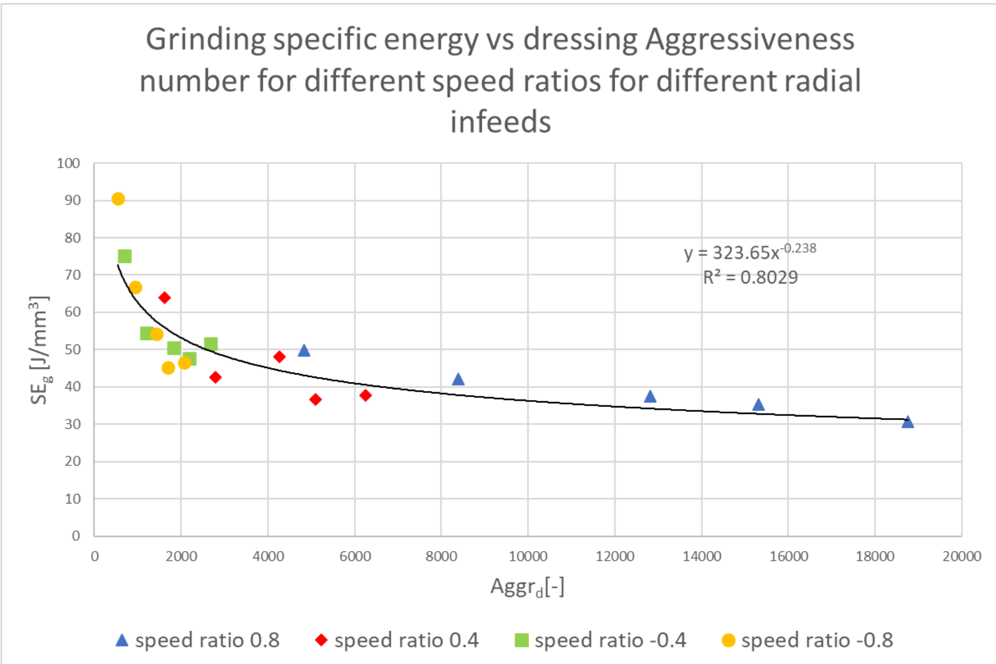

Figure 64: Grinding specific energy is plotted against the dressing Aggressiveness number for different speed ratios - a power-law trend can be observed

In particular, if visualizing in the same plot Malkin and Murray's results (Figure) and the experimental results for grinding specific energy versus dressing Aggressiveness number, there are similarities (Figure 65).

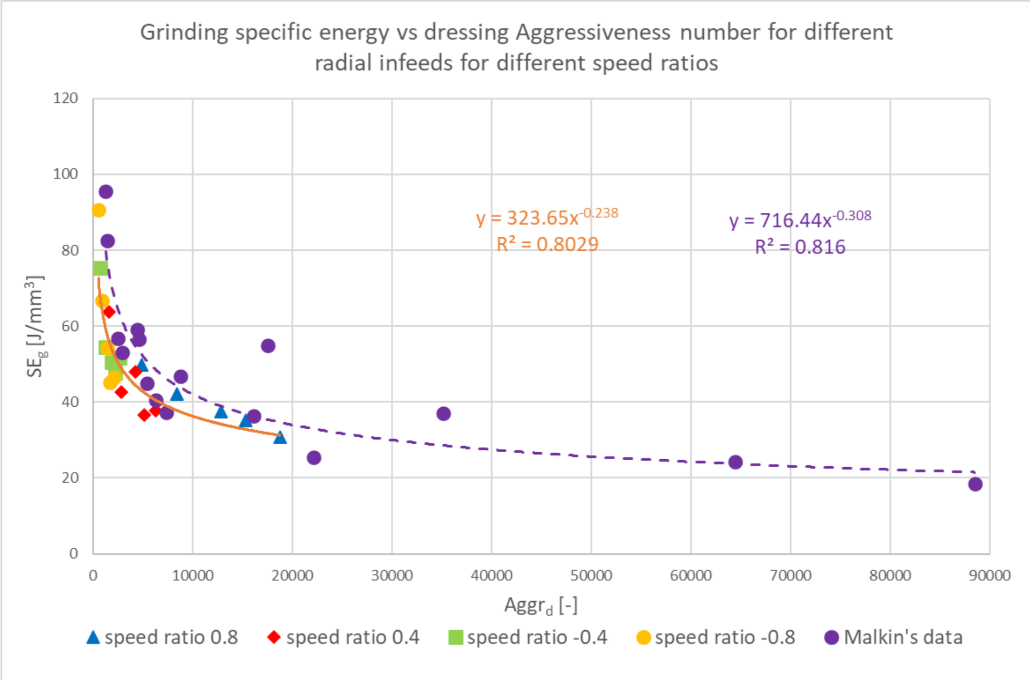

Figure 65: Grinding specific energy is plotted against dressing Aggressiveness number: comparison with Malkin's data

Since Malkin's data were for a larger range of dressing Aggressiveness, by restricting the analysis, an even better correlation is found regardless eventual differences between grinding wheels, dressing rolls and workpiece materials used (Figure 66).

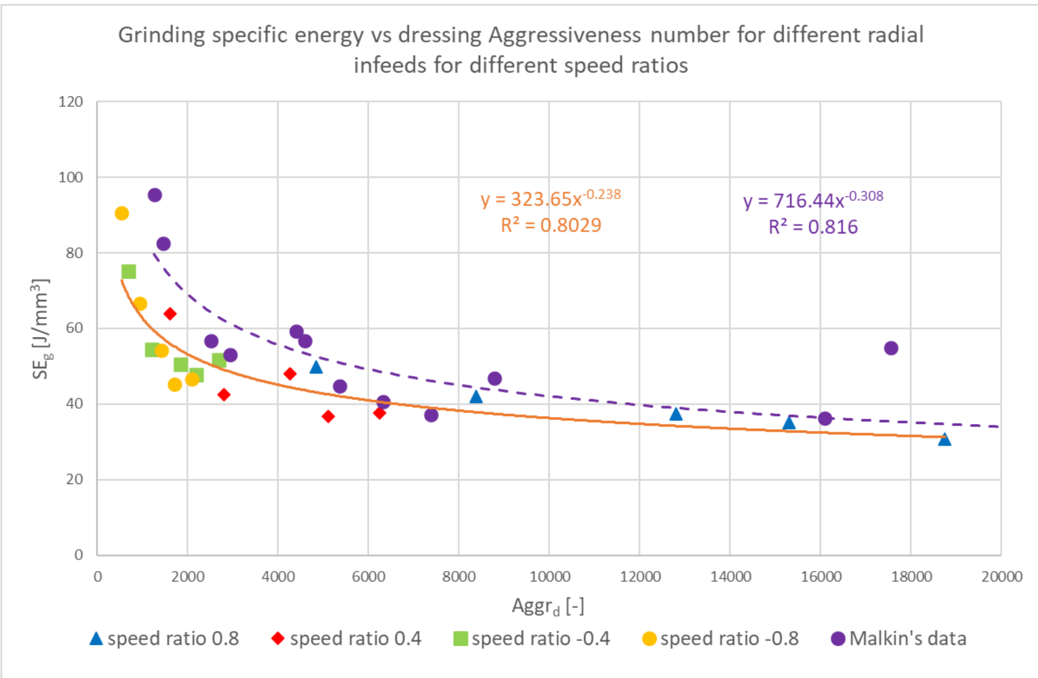

Figure 66: Grinding specific energy is plotted against dressing Aggressiveness number: comparison with Malkin's data in a restricted area

7.3. Dressing power and dressing specific energy experimental analysis

One of the goals is to plot dressing acoustic emission vs dressing power, thus dressing power should be calculated. The latter has been defined according to the following equations, and by considering the value of power in the plot towards the end of the dressing operation, where eventual transients would be over.
In order to get this variable, the charts are including dressing roll power and grinding wheel power during dressing, indeed the total power results as a combination of both.
For instance, for the unidirectional case with speed ratio 0.4 and radial infeed 1.5 µm/rev (Figure 67), the dressing power has been defined in Equation 28, as the difference between (P1-P2) and (P3-P4).

$$P_{dressing} = (P1 - P2) - (P3 - P4)$$

Equation 28: Dressing power in uni-directional case

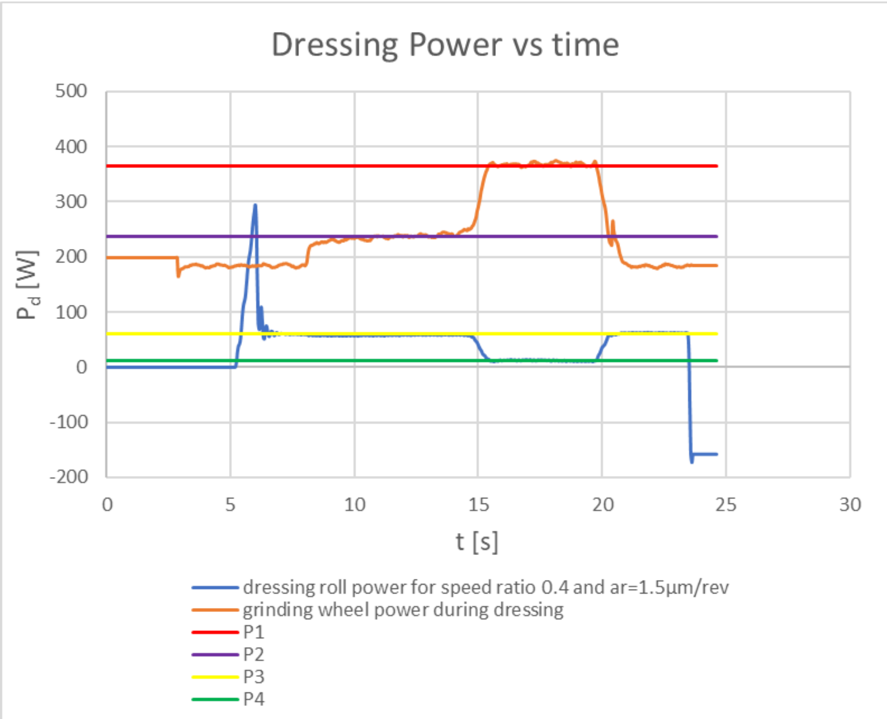

Figure 67: Dressing power is plotted against time with speed ratio 0.4 and radial infeed 1.5 µm/rev

In Figure 68, a similar procedure has been adopted for calculating dressing power for anti-directional dressing mode, however in this case both powers are defined as positive, as it can be seen in Equation 29:

$$P_{dressing} = (P1 - P2) + (P3 - P4)$$

Equation 29: Dressing power in anti-directional case

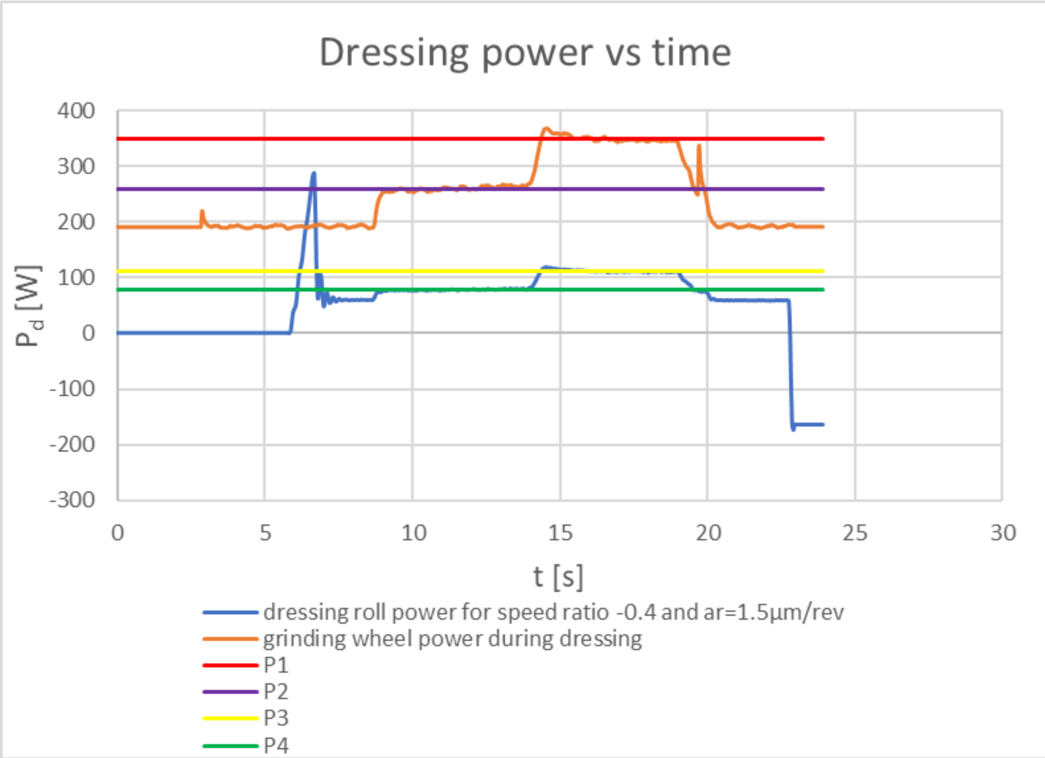

Figure 68: Dressing power is plotted against time with speed ratio -0.4 and radial infeed 1.5 µm/rev

Finally, the dressing specific energy can be defined. It is given by dressing power divided by dressing material removal rate.
The dressing material removal rate for outside diameter (OD) dressing is defined in Equation 30:

$$MRR = 2\pi \cdot grinding\ wheel\ radius \cdot width \cdot \frac{radial\ infeed\ in \frac{\mu m}{s}}{1000} \left[\frac{mm^3}{s}\right]$$

Equation 30: Dressing material removal rate

In Table 9 all the data are collected. Wheel speed was 30 m/s and width was 12.83 mm for all cases.

speed ratio [-]	radial infeed [µm/rev]	P total dressing [W]	Wheel rpm [rpm]	Wheel radius [mm]	radial infeed [µm/s]	Dressing MRR [mm^3/s]	SE_d [J/mm^3]	$Aggr_d$ [-]
0.8	0.1	8.5	1579	181.43	2.63	38.49	0.221	4841
0.8	0.3	21.0	1575	181.88	7.88	115.47	0.182	8386
0.8	0.7	35.0	1569	182.56	18.31	269.43	0.130	12809
0.8	1	48.0	1562	183.37	26.04	384.90	0.125	15310
0.8	1.5	82.0	1559	183.72	38.98	577.35	0.142	18751
0.4	0.1	13.5	1581	181.20	2.64	38.49	0.351	1614
0.4	0.3	21.5	1561	183.52	7.81	115.47	0.186	2795
0.4	0.7	53.5	1582	181.09	18.46	269.43	0.199	4270
0.4	1	49.5	1552	184.56	25.87	384.90	0.129	5103
0.4	1.5	86.0	1566	182.92	39.15	577.35	0.149	6250
-0.4	0.1	15.0	1584	180.85	2.64	38.49	0.390	692
-0.4	0.3	30.5	1556	184.11	7.78	115.47	0.264	1198
-0.4	0.7	61.0	1574	182.00	18.36	269.43	0.226	1830
-0.4	1	72.5	1567	182.79	26.12	384.90	0.188	2187
-0.4	1.5	116.5	1586	180.59	39.66	577.35	0.202	2679
-0.8	0.1	33.0	1557	183.99	2.60	38.49	0.857	538
-0.8	0.3	41.5	1577	181.65	7.89	115.47	0.359	932
-0.8	0.7	50.5	1554	184.32	18.13	269.43	0.187	1423
-0.8	1	62.0	1564	183.14	26.07	384.90	0.161	1701
-0.8	1.5	94.5	1571	182.32	39.28	577.35	0.164	2083

Table 9: All data of dressing power and dressing specific energy analysis

In Figure 69, all the data are reported in a single chart, but it is not possible to fit them in a single trend even if each one of them has a linear behavior if considering fixed speed ratio.

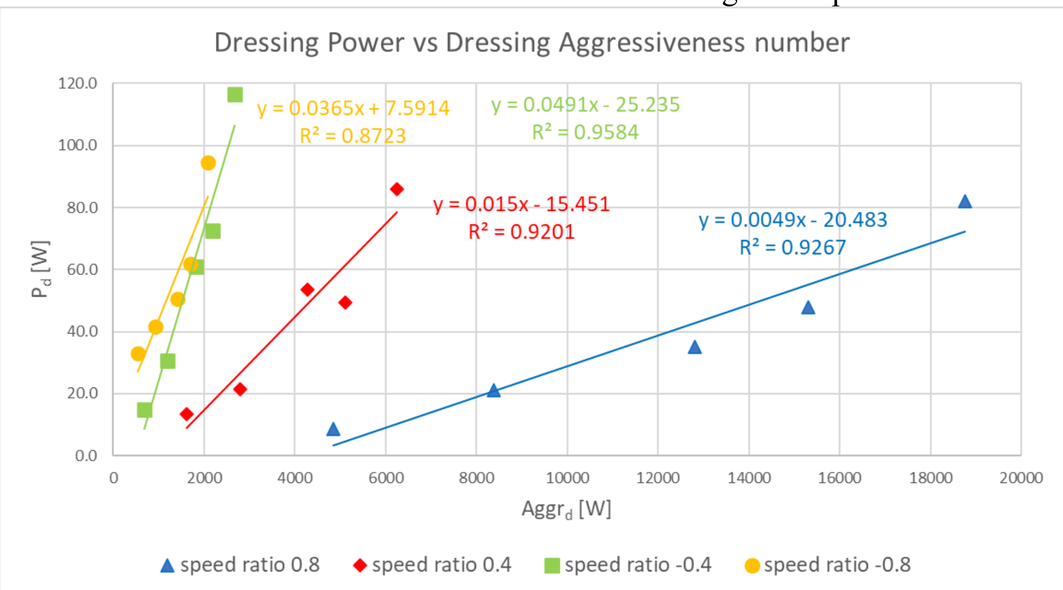

Figure 69: Dressing power is plotted against the dressing Aggressiveness number for different speed ratios - linear trend for each case

Since it is physically clear that for 0 as Aggressiveness, a power of 0 Watts would correspond, by setting the intercept at 0 W it is possible to state that the less aggressive is the condition (lower speed ratio if plotting for different speed ratios), the higher is the slope value (Figure 70). Therefore, if having fixed speed ratio, for speeding up the production it would be beneficial to increase radial infeed value, however if considering anti-directional dressing modes it would result inconvenient because of high increase rates of the dressing power.

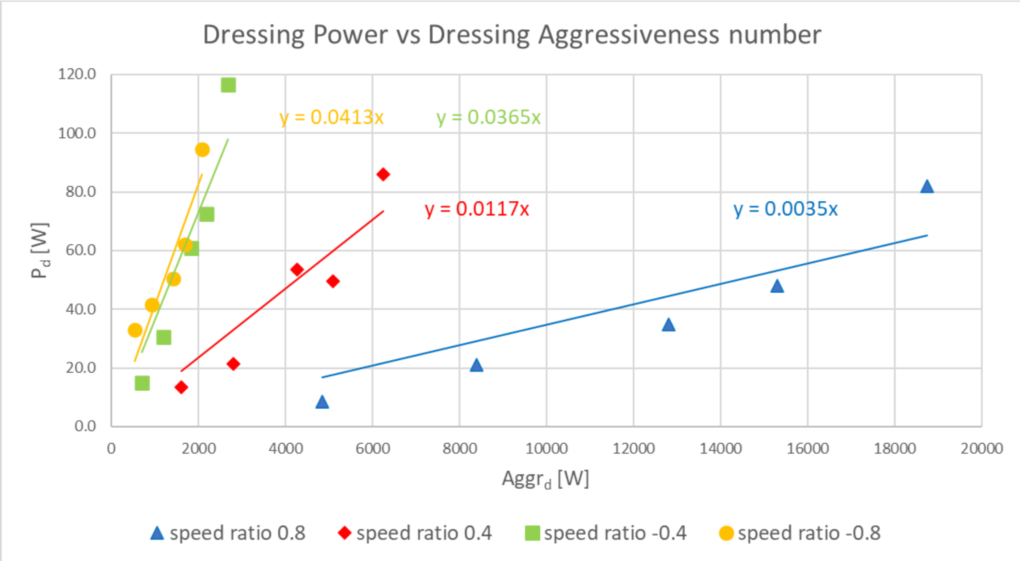

Figure 70: Dressing power is plotted against the dressing Aggressiveness number for different speed ratios - linear trend for each case with intercept 0 Watts

By means of the dressing specific energy, a better-defined behavior can be observed in Figure 71. In this plot the dullest dressing case, where burning has occurred during dressing, has not been considered.

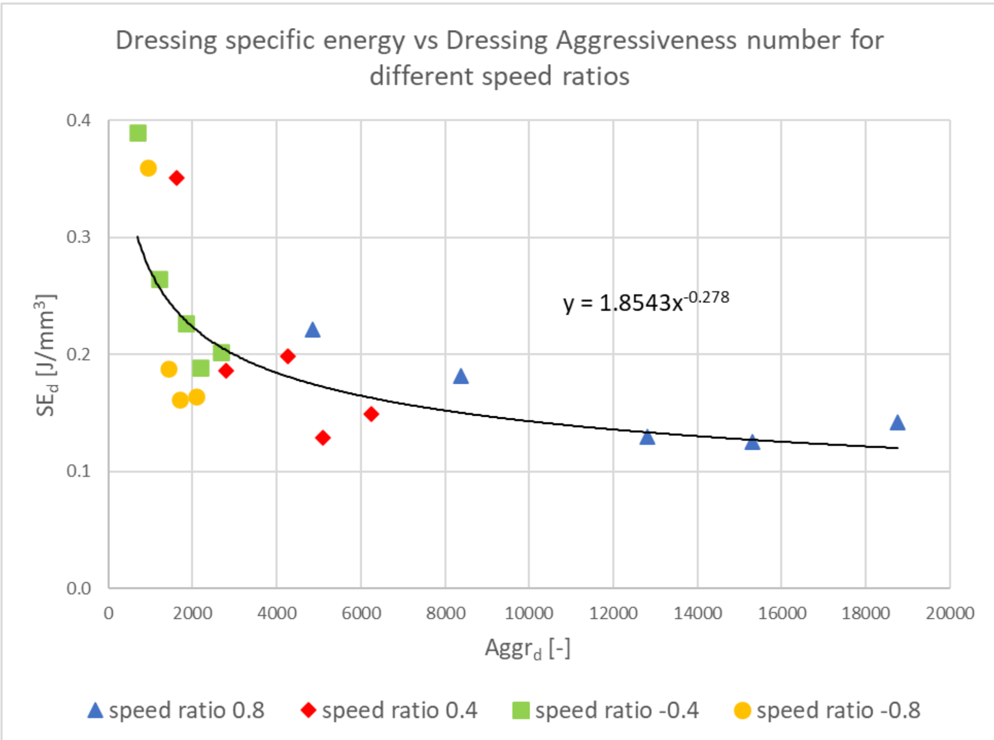

Figure 71: Dressing specific energy is plotted against the dressing Aggressiveness number for different speed ratios – a power law trend can be seen

In Figure 72, there is a plot for different speed ratios of grinding specific energy vs dressing specific energy. A good trend could be the linear one. Thus, grinding specific energy and dressing specific energy would appear to be proportional and 20 J/mm^3 could be defined as the minimum grinding

specific energy that is possible to reach by dressing with an “infinite sharp” condition with this diamond dressing roll, Aluminum oxide grinding wheel and steel workpiece.
As for the previous case, considering that during the grinding operation for the dullest dressing condition (for speed ratio -0.8 and radial infeed 0.1 µm/rev) burning occurred, it is better not to consider it for the fitting curve since it led to too high specific energies for the data point itself.
On the other hand, by using a power law fitting curve, the result is shown in the same Figure and it leads to a higher R^2 value, hence this is the proposed trend for fitting properly the data points.

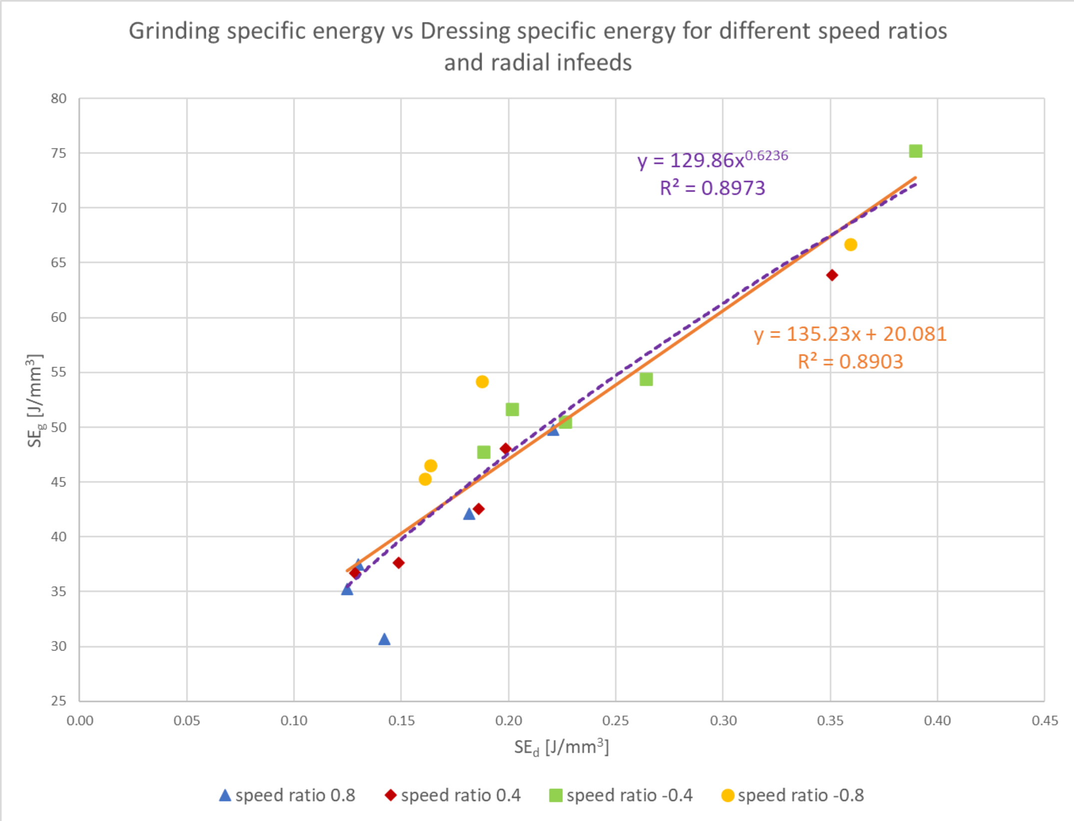

Figure 72: Grinding specific energy is plotted against the dressing specific energy - a linear trend is found

In Figure 73, there is a comparison of the experimental power law trend with the plot shown in Figure 52, coming from Malkin and Murray’s analysis.

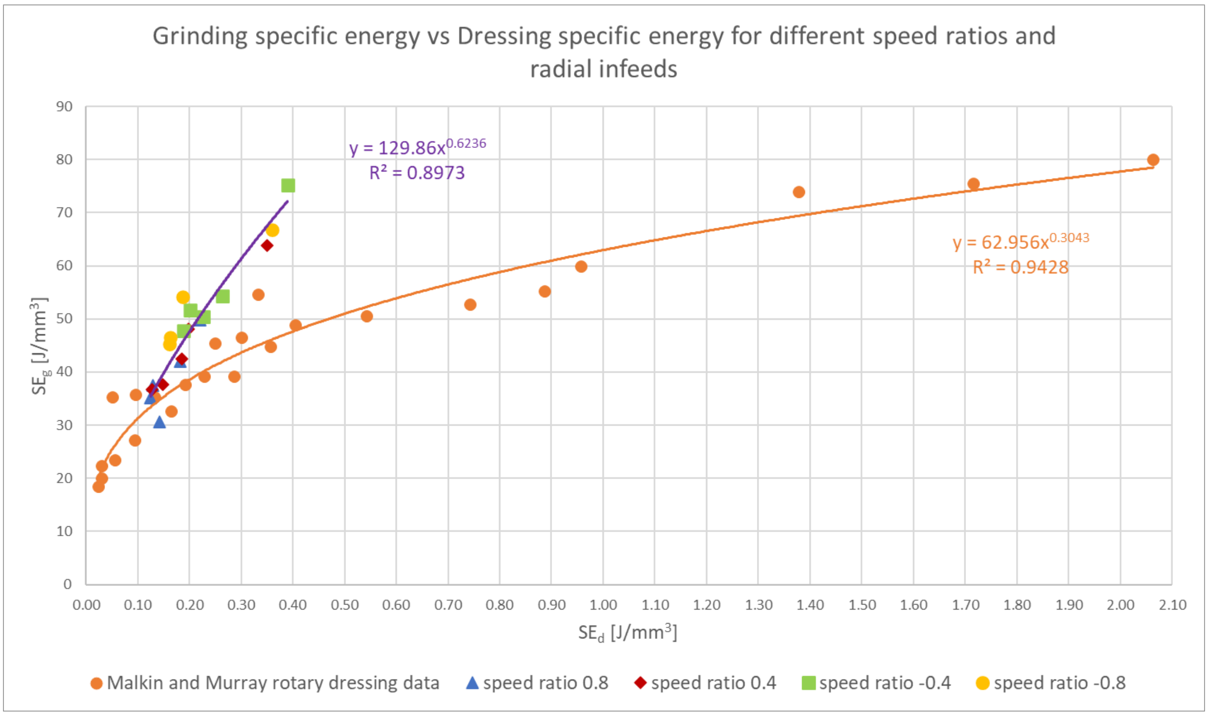

Figure 73: Comparison between experimental data and Malkin and Murray data for SE_g against SE_d

And more specifically in a SE_d values region in which the experimental tests have been focused (Figure 74).

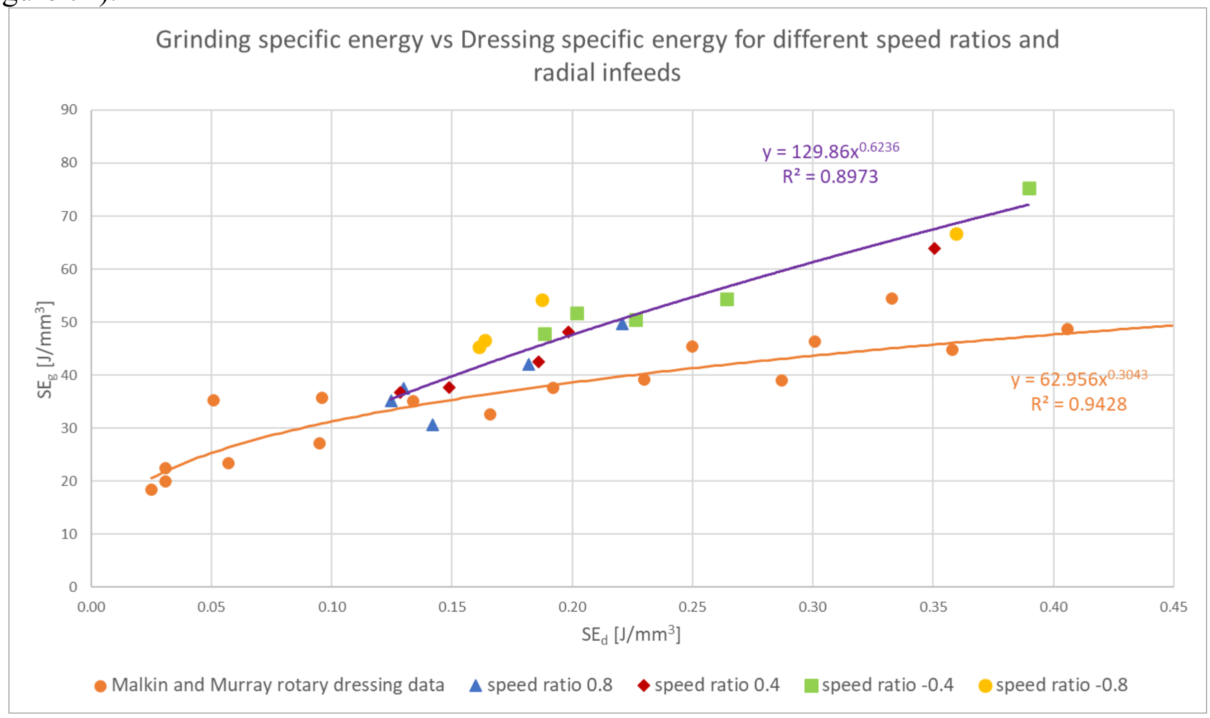

Figure 74: Comparison between experimental data and Malkin and Murray data for SE_g against SE_d, restricted region for SE_d values

7.4. Dressing acoustic emission experimental analysis

During the dressing operation, the dressing acoustic emission monitoring has been possible with sampling time of 0.004s.
An “idle acoustic emission” was identified in each case, and it was always around 2.3%.

Here there are two examples of how the acoustic emission has been identified: basically, an acoustic emission value during the operation has been taken, and finally from this value the idle value of 2.3% has been subtracted.
For instance, in Figure 75 and in Figure 76, the two cases of speed ratio +0.4 and radial infeed 1.5 µm/rev and speed ratio -0.4 and radial infeed 0.3 µm/rev are reported.

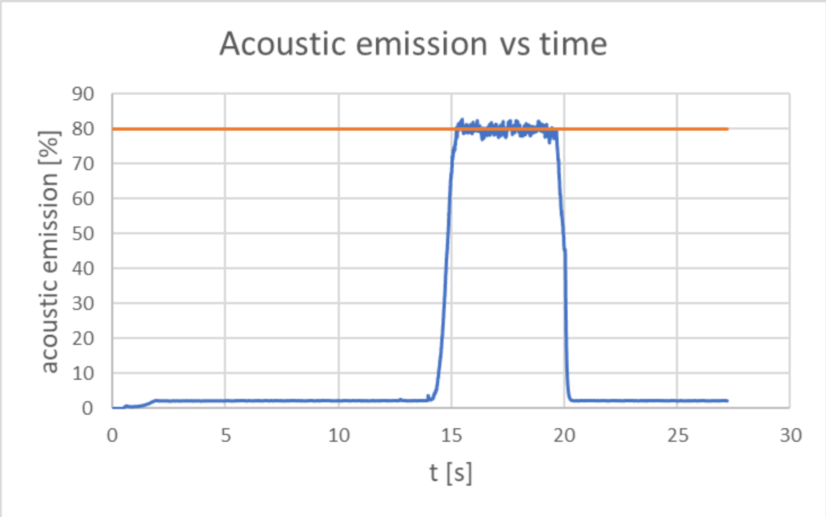

Figure 75: Acoustic emission during dressing is plotted against the time for speed ratio 0.4 and radial infeed 1.5 µm/rev: orange line is the acoustic emission value taken during the operation and P_{idle} is 2.3 %

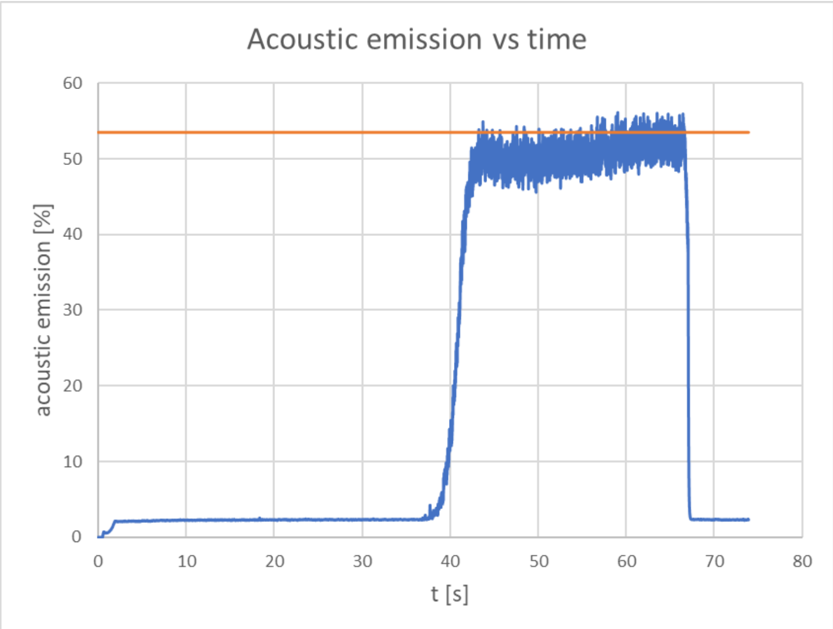

Figure 76: Acoustic emission during dressing is plotted against the time for speed ratio -0.4 and radial infeed 0.3 µm/rev: orange line is acoustic emission value taken during the operation and P_{idle} is 2.3 %

In the following, since both dressing material removal rate and the acoustic emission are known for each dressing case, it has been possible to determine ***specific energy for acoustic emission***, given by acoustic emission over dressing material removal rate, as can be seen in Equation 31:

$$SE_a = \frac{AE}{MRR_d} \left[\frac{\%}{\frac{mm^3}{s}}\right]$$

Equation 31: Specific energy for acoustic emission

In Table 10 all data are reported.

speed ratio [-]	radial infeed [μm/rev]	Idle acoustic emission [%]	measured acoustic emission [%]	acoustic emission [%]	Dressing power [W]	Dressing MRR [mm³/s]	SE_d [J/mm³]	SE_a [%/mm³*s⁻¹]	SE_g [J/mm³]
0.8	0.1	2.3	15.9	13.6	8.5	38.49	0.221	0.35	49.76
0.8	0.3	2.3	25.2	22.9	21.0	115.47	0.182	0.20	42.09
0.8	0.7	2.3	37.2	34.9	35.0	269.43	0.130	0.13	37.47
0.8	1	2.3	43.8	41.5	48.0	384.90	0.125	0.11	35.23
0.8	1.5	2.3	54	51.7	82.0	577.35	0.142	0.09	30.68
0.4	0.1	2.3	28.2	25.9	13.5	38.49	0.351	0.67	63.85
0.4	0.3	2.3	38.4	36.1	21.5	115.47	0.186	0.31	42.53
0.4	0.7	2.3	65.3	63	53.5	269.43	0.199	0.23	48.07
0.4	1	2.3	64.5	62.2	49.5	384.90	0.129	0.16	36.66
0.4	1.5	2.3	80	77.7	86.0	577.35	0.149	0.13	37.66
-0.4	0.1	2.3	34	31.7	15.0	38.49	0.390	0.82	75.26
-0.4	0.3	2.3	50.8	48.5	30.5	115.47	0.264	0.42	54.37
-0.4	0.7	2.3	69.6	67.3	61.0	269.43	0.226	0.25	50.51
-0.4	1	2.3	82.2	79.9	72.5	384.90	0.188	0.21	47.76
-0.4	1.5	2.3	99	96.7	116.5	577.35	0.202	0.17	51.69
-0.8	0.1	2.3	35.4	33.1	33.0	38.49	0.857	0.86	90.60
-0.8	0.3	2.3	56	53.7	41.5	115.47	0.359	0.47	66.72
-0.8	0.7	2.3	72.7	70.4	50.5	269.43	0.187	0.26	54.19
-0.8	1	2.3	84.4	82.1	62.0	384.90	0.161	0.21	45.27
-0.8	1.5	2.3	96.8	94.5	94.5	577.35	0.164	0.16	46.52

Table 10: All data of dressing acoustic emission experimental analysis

About the acoustic emission, now it can be plotted versus the dressing power (Figure 77).
Both a power law trend and a linear trend could be defined, but the power law seems to fit the data in a better way, hence the choice is again for a power law equation for describing the phenomenon.

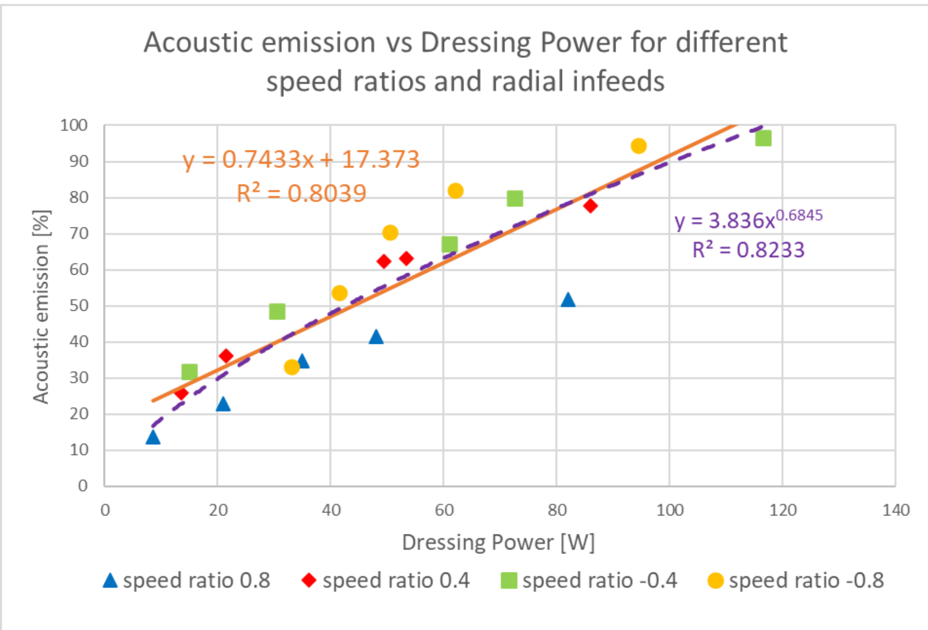

Figure 77: Acoustic emission is plotted against the dressing power for different speed ratios – power law trend fits better the data

If not considering the data coming from speed ratio +0.8 (blue triangles), the R^2 value results higher, as can be seen in Figure 78.

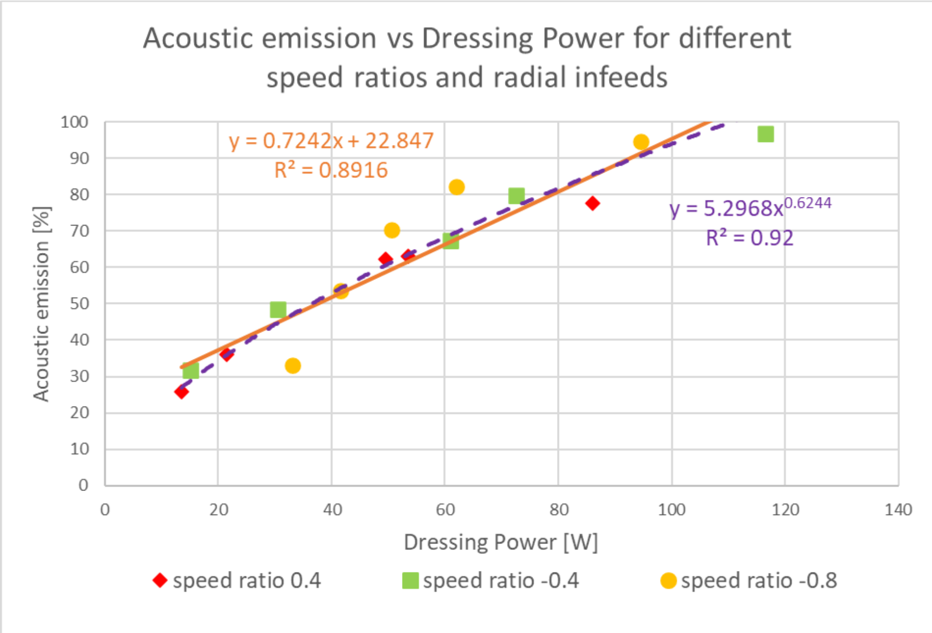

Figure 78: Acoustic emission is plotted against the dressing power for different speed ratios, without +0.8 – power law trend fits better the data

Nevertheless, it would be possible to define a "calibrated power", $P_{AE,c}$ in order to get a power in Watts by knowing the acoustic emission value: this calculation could be done by setting 0 as intercept of a linear trend, and taking the slope of this line as a conversion factor. The distortion between this trend and a power law trend would not be evident, as shown in Figure 79. In conclusion, for sake of simplicity there is the option to define this linear trend with intercept 0, and the more interesting conclusion is that the conversion factor would result close to 1, hence 45° slope for the trendline.

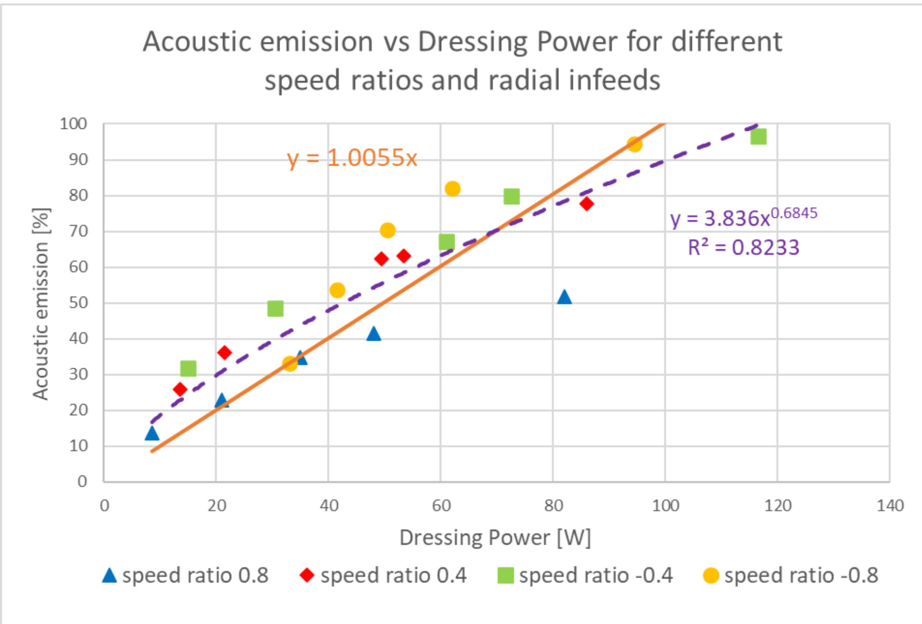

Figure 79: Acoustic emission is plotted against dressing power for different speed ratios – linear trendline with zero as intercept and power law trend

By means of the dressing Aggressiveness number, similar plots to Figure 69 and Figure 70 can be presented for dressing acoustic emission instead of dressing power.
Therefore, in Figure 80 and in Figure 81 linear trends and linear trends with 0% as intercept for different speed ratios are respectively presented.

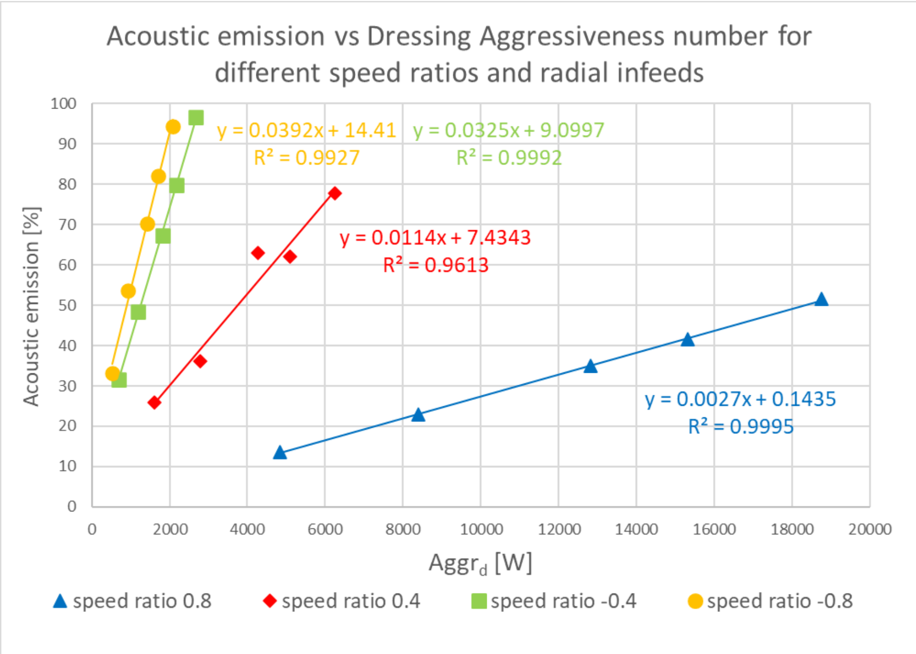

Figure 80: Acoustic emission is plotted against the dressing Aggressiveness number for different speed ratios - linear trend for each case

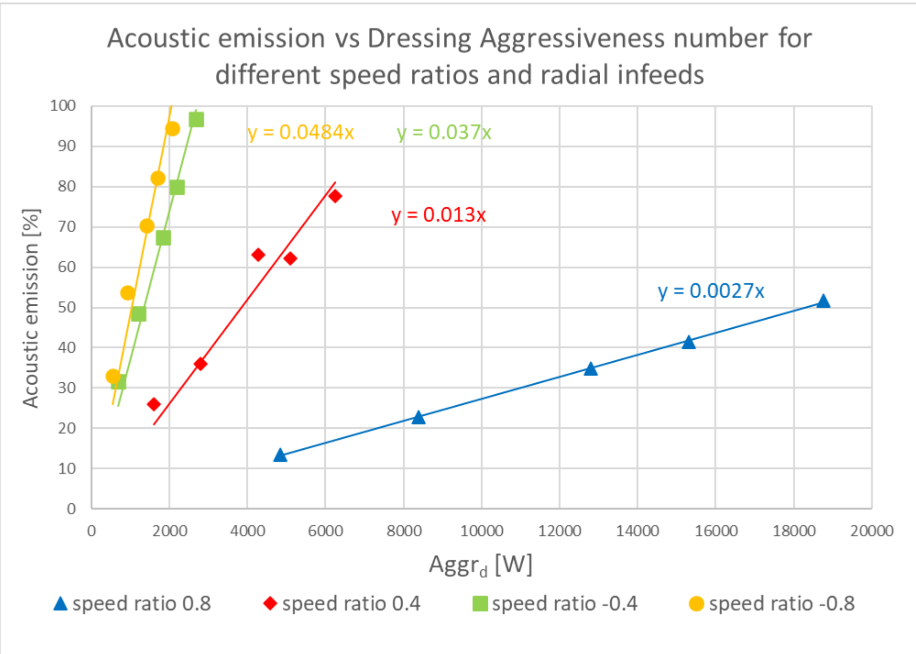

Figure 81: Acoustic emission is plotted against the dressing Aggressiveness number for different speed ratios - linear trend for each case with 0% as intercept

From Figure 80 it can be noticed as the slopes result very similar to the ones coming from the plot for dressing power vs dressing Aggressiveness number (Figure 70).
In Figure 82 it is proposed the dressing specific energy plotted against the acoustic emission specific energy. A linear trendline can be recognized with an intercept value of 0.0999. Therefore, the chart in Figure 82 shows that the dressing specific energy and the acoustic emission specific energy are

proportional. Furthermore, in the same Figure a power law trend is proposed and chosen as the best fitting curve since the R^2 value is proven to be higher. Nevertheless, the linear trend is still a possible choice for easier understanding.

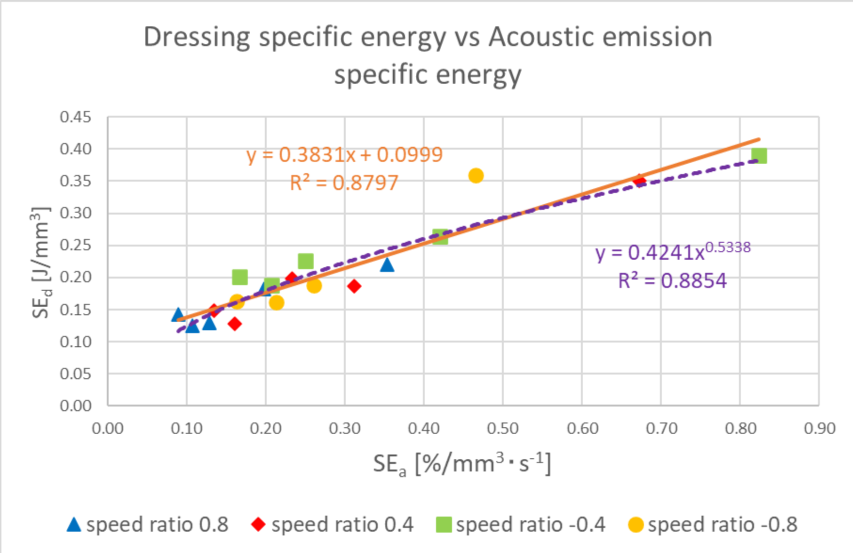

Figure 82: Dressing specific energy is plotted against the acoustic emission specific energy for different speed ratios – linear trend and power law trend

In addition, in Figure 83, there is a plot for grinding specific energy vs acoustic emission specific energy. A power law is fitting properly the data as well as a linear trend, that is convenient for simplified analysis.

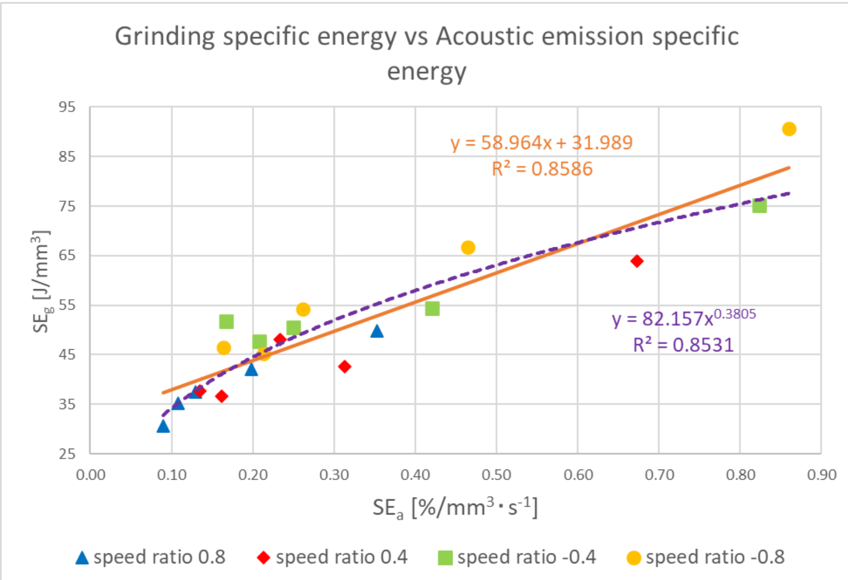

Figure 83: Grinding specific energy is plotted against the acoustic emission specific energy for different speed ratios - a power law trend and linear trend can be identified

In Figure 84, it is displayed a plot including acoustic emission specific energy and dressing specific energy in the same chart, plotted versus dressing Aggressiveness number.

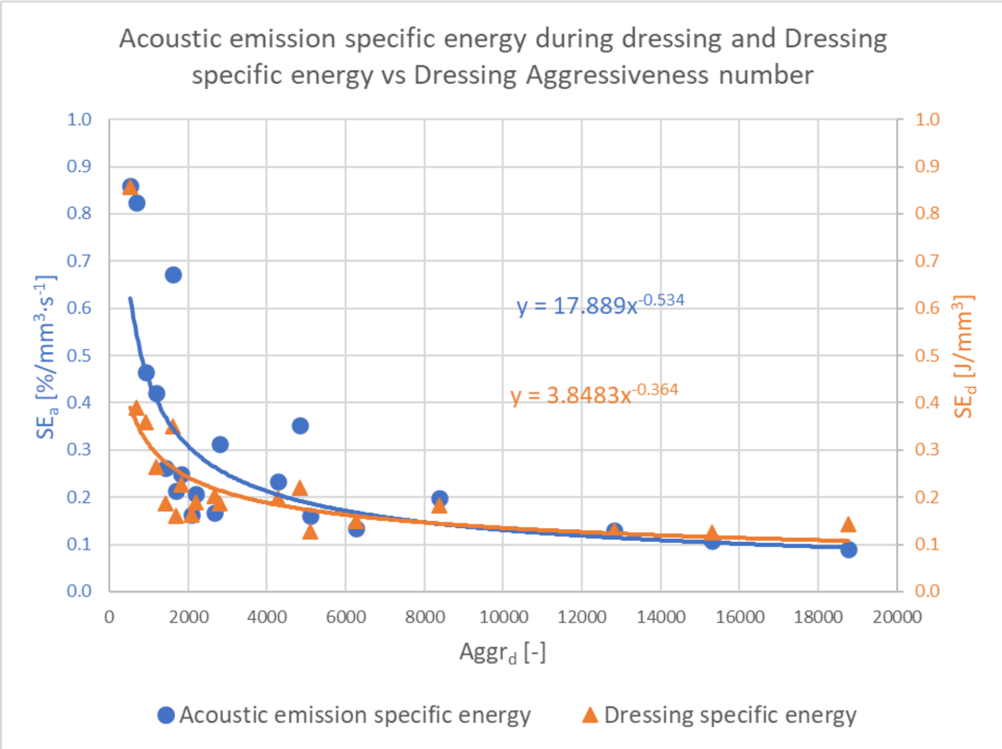

Figure 84: Acoustic emission specific energy and dressing specific energy are plotted against the dressing Aggressiveness number

Finally, there are plots for dressing roll power during dressing, grinding wheel power during dressing and acoustic emission value during dressing vs time. In Figure 85 and in Figure 86, examples for unidirectional dressing and anti-directional dressing are shown. It can be seen that acoustic emission and dressing power have the same behavior, thus acoustic emission could be used instead of dressing power for the same analyses.

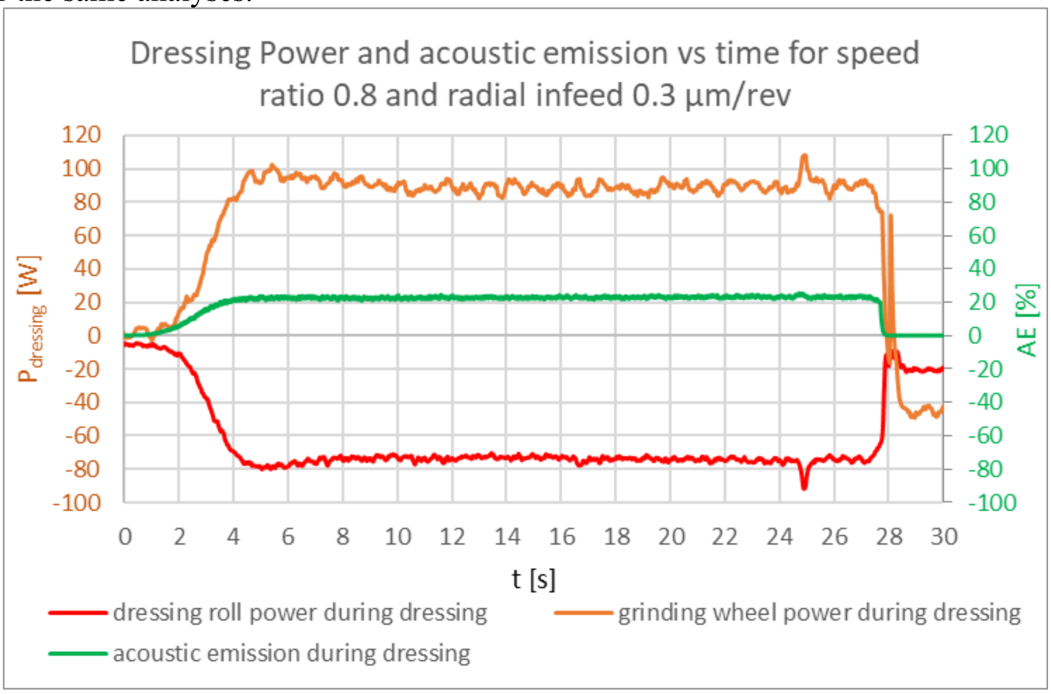

Figure 85: Dressing power and acoustic emission are plotted against the time for speed ratio 0.8 and radial infeed 0.3 µm/rev

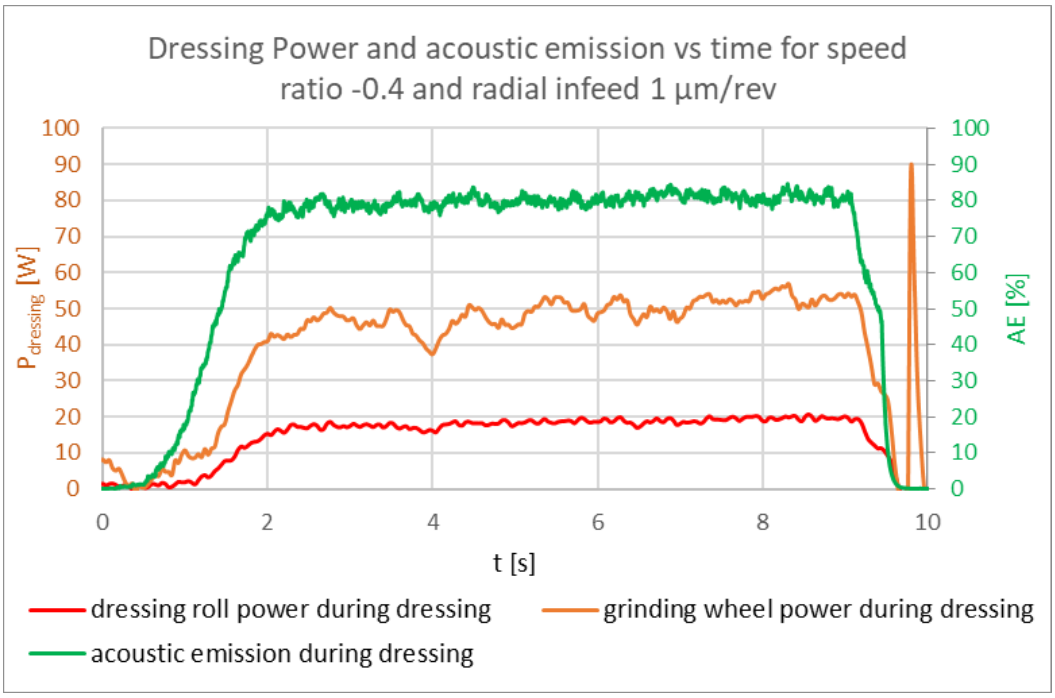

Figure 86: Dressing power and acoustic emission are plotted against the time for speed ratio -0.4 and radial infeed 1 µm/rev

7.5. Tangential forces, normal forces and grinding wheel spindle displacement experimental analysis

In order to calculate tangential forces, the total dressing power has been considered and divided by a Δspeed, defined based on dressing condition (unidirectional or anti-directional).
It would have been possible to consider the amount of dressing power generated in the grinding wheel during the dressing operation, and divide it by the grinding wheel speed, obtaining again a tangential force.
The first mentioned definition has been preferred because data are coming from both spindles, and therefore the method results more robust.
The used equation is Equation 32:

$$F_{T_{dressing}} = \frac{P_{total_{dressing}}}{V_s \pm V_r} \; [N]$$

Equation 32: Tangential force with total dressing power, - for unidirectional case and + for anti-directional case

In the following there is a table showing all different tangential forces, normal forces and grinding wheel spindle deflections during the dressing operation.
The wheel speed as mentioned is 30m/s and the grinding wheel spindle stiffness is K=30000N/mm.
The normal force is calculated through Equation 33:

$$F_{N_{dressing}} = 1.5 \cdot F_{T_{dressing}} \; [N]$$

Equation 33: Normal force

By means of the ratio between normal dressing force and tangential dressing force defined as stated by Linke B. et al in [17]
The grinding wheel spindle displacement is gotten from Equation 34:

$$h = \frac{F_{N_{dressing}}}{K} \cdot 1000\ [\mu m]$$

Equation 34: Grinding wheel spindle displacement during dressing

All the data are collected in Table 11.

speed ratio [-]	radial infeed [µm/rev]	P total dressing [W]	F_T[N]	F_N[N]	grinding wheel spindle displacement during dressing [µm]
0.8	0.1	8.5	1.42	2.13	0.071
0.8	0.3	21.0	3.50	5.25	0.175
0.8	0.7	35.0	5.83	8.75	0.292
0.8	1.0	48.0	8.00	12.00	0.400
0.8	1.5	82.0	13.67	20.50	0.683
0.4	0.1	13.5	0.75	1.13	0.038
0.4	0.3	21.5	1.19	1.79	0.060
0.4	0.7	53.5	2.97	4.46	0.149
0.4	1.0	49.5	2.75	4.13	0.138
0.4	1.5	86.0	4.78	7.17	0.239
-0.4	0.1	15.0	0.36	0.54	0.018
-0.4	0.3	30.5	0.73	1.09	0.036
-0.4	0.7	61.0	1.45	2.18	0.073
-0.4	1.0	72.5	1.73	2.59	0.086
-0.4	1.5	116.5	2.77	4.16	0.139
-0.8	0.1	33.0	0.61	0.92	0.031
-0.8	0.3	41.5	0.77	1.15	0.038
-0.8	0.7	50.5	0.94	1.40	0.047
-0.8	1.0	62.0	1.15	1.72	0.057
-0.8	1.5	94.5	1.75	2.63	0.088

Table 11: All data for tangential forces, normal forces and grinding wheel spindle displacement

Once knowing the normal forces, plots for absolute acoustic emission decrease, relative acoustic emission decrease and acoustic emission slope (defined respectively with Equation 35, Equation 36 and Equation 37) vs normal force during dressing, are displayed in Figure 87 – Figure 91.

$$Absolute\ AE\ decrease = AE\ before\ dwelling\ starts - AE\ end\ of\ dwelling\ [\%]$$

Equation 35: Absolute AE decrease

$$Relative\ AE\ decrease = \frac{AE\ before\ dwelling\ starts - AE\ end\ of\ dwelling}{AE\ before\ dwelling\ starts} \cdot 100\ [\%]$$

Equation 36: Relative AE decrease

$$AE\ slope = \frac{AE\ before\ dwelling\ starts - AE\ end\ of\ dwelling}{considered\ \Delta t}\left[\frac{\%}{s}\right]$$

Equation 37: AE slope

The data points in the next plots are taken from the Table 12.

speed ratio [-]	radial infeed [µm/rev]	$Aggr_d$ [-]	considered Δt [s]	absolute decrease [%]	slope [%/s]	relative decrease [%]	F_N[N]
0.8	0.1	4841	0.412	1.34	3.26	8.25	2.13
0.8	0.3	8386	0.392	2.93	7.47	11.57	5.25
0.8	0.7	12809	0.364	10.31	28.33	28.33	8.75
0.8	1	15310	0.416	14.38	34.57	33.64	12.00
0.8	1.5	18751	0.368	19.57	53.17	37.69	20.50
0.4	0.1	1614	0.400	3.45	8.63	11.82	1.13
0.4	0.3	2795	0.420	7.48	17.81	18.88	1.79
0.4	0.7	4270	0.312	20.30	65.06	32.71	4.46
0.4	1	5103	0.364	22.74	62.47	34.12	4.13
0.4	1.5	6250	0.368	32.18	87.45	41.54	7.17
-0.4	0.1	692	0.272	7.08	26.03	18.94	0.54
-0.4	0.3	1198	0.344	13.33	38.75	25.27	1.09
-0.4	0.7	1830	0.352	26.20	74.43	34.19	2.18
-0.4	1	2187	0.372	35.28	94.84	41.89	2.59
-0.4	1.5	2679	0.336	43.78	130.30	45.53	4.16
-0.8	0.1	538	0.388	7.69	19.82	19.12	0.92
-0.8	0.3	932	0.352	14.47	41.11	23.71	1.15
-0.8	0.7	1423	0.368	31.34	85.16	40.23	1.40
-0.8	1	1701	0.380	36.52	96.11	41.08	1.72
-0.8	1.5	2083	0.404	45.12	111.68	46.16	2.63

Table 12: All data for Absolute AE decrease, Relative AE decrease and AE slope

For AE absolute decrease (Figure 87), for each speed ratio a linear trend is visible, and moreover the intercepts are all close to zero as expected.

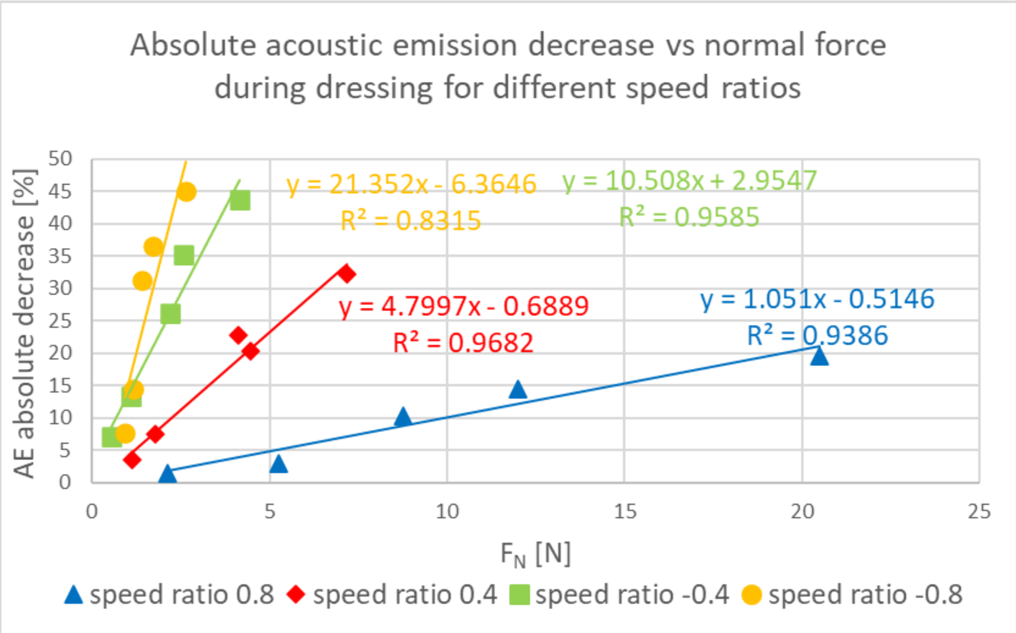

Figure 87: Absolute acoustic emission decrease is plotted against the normal force during dressing for different speed ratio - linear trend for each speed ratio

By reporting AE absolute decrease versus F_N for different speed ratios and imposing as 0% the intercept on the acoustic emission axis, Figure 88 is proving that for lower speed ratios (thus duller conditions in general), the line slope in the plot has higher value.

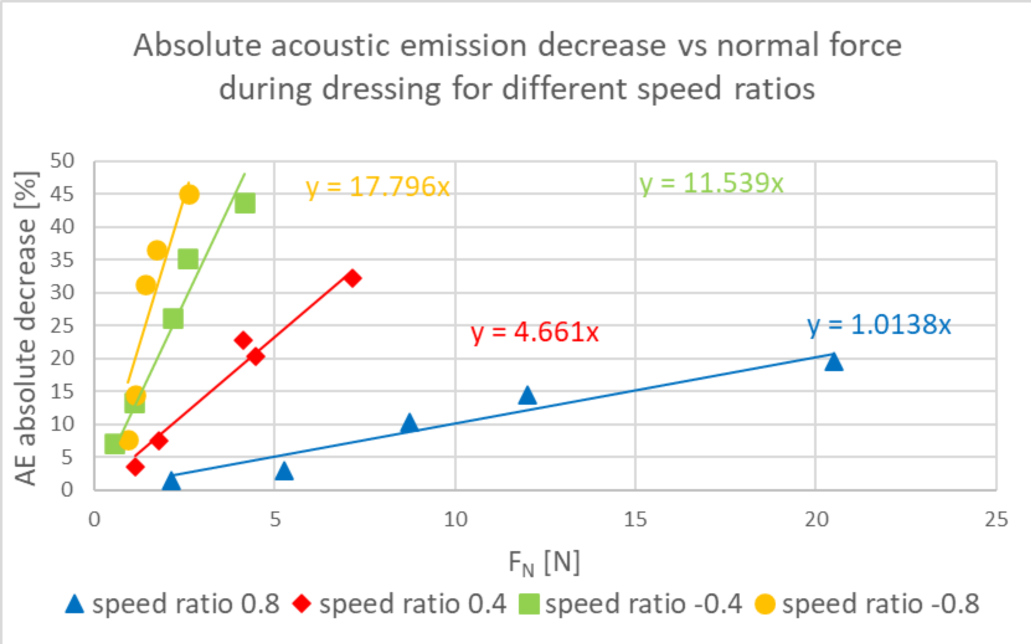

Figure 88: Absolute acoustic emission decrease is plotted against the normal force during dressing for different speed ratios - linear trends for each speed ratio and intercepts set at 0%

For AE relative decrease, for each speed ratio a power law trend is recognized (Figure 89):

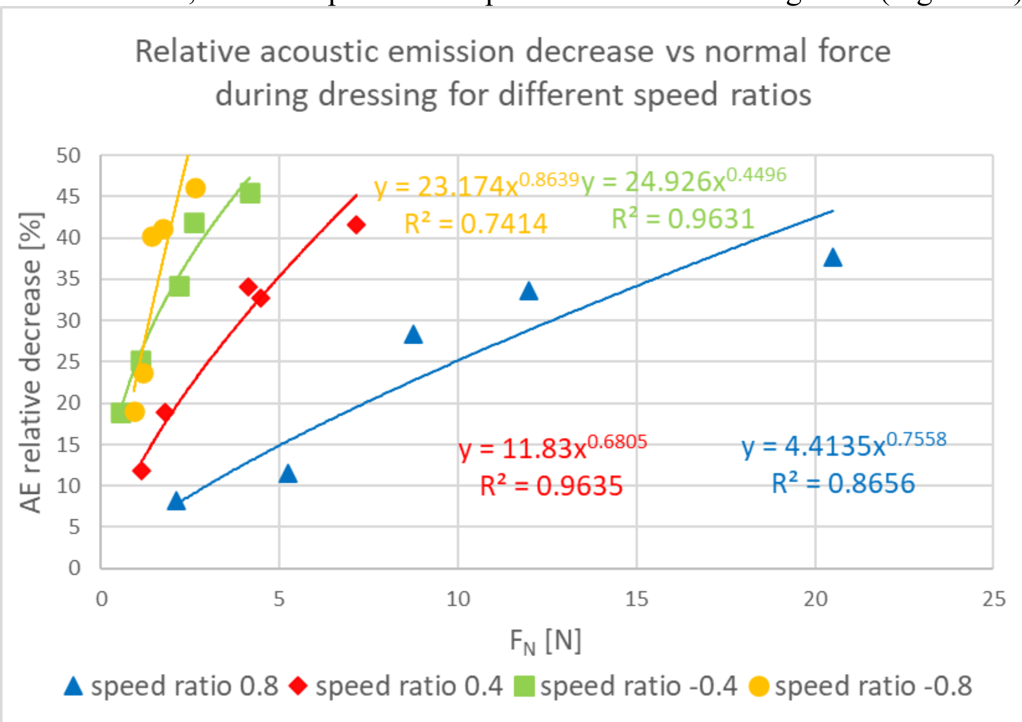

Figure 89: Relative acoustic emission decrease is plotted against the normal force during dressing for different speed ratios - power law trend for each speed ratio

For AE slope for each speed ratio a linear trend is evident, and furthermore the intercepts are all close to zero (Figure 90):

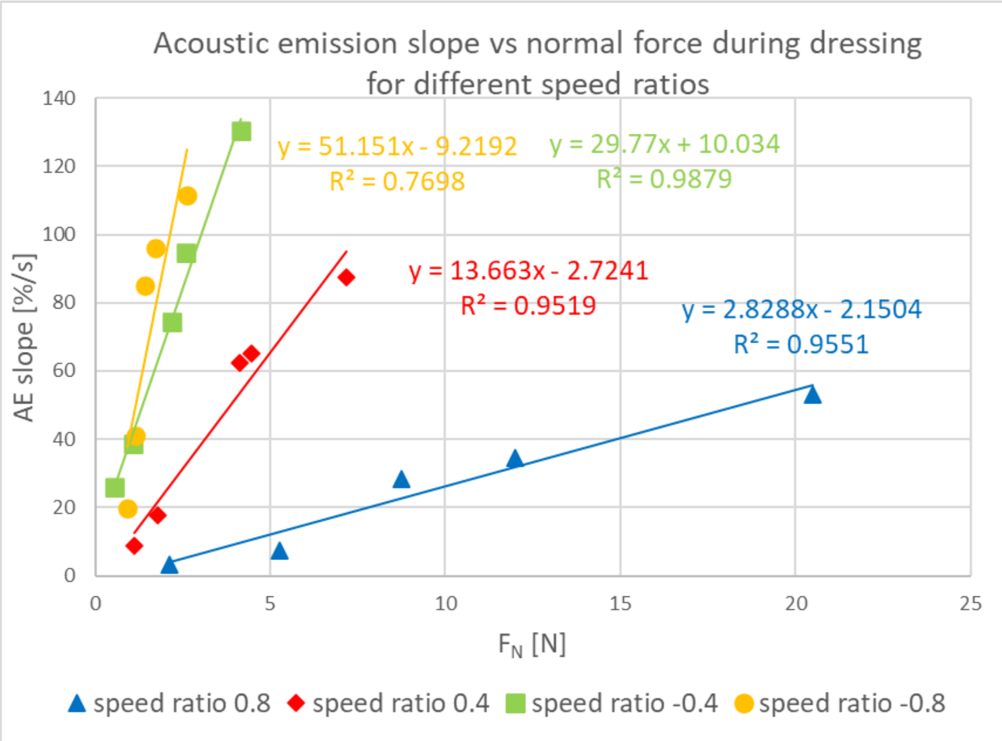

Figure 90: Acoustic emission slope is plotted against the normal force during dressing for different speed ratios - linear trend for each speed ratio

In Figure 91, given the previous statement, plots for the same variables as in Figure 90 are displayed and the intercept is set at 0%/s. As for Figure 88, higher slopes are associated to lower speed ratios.

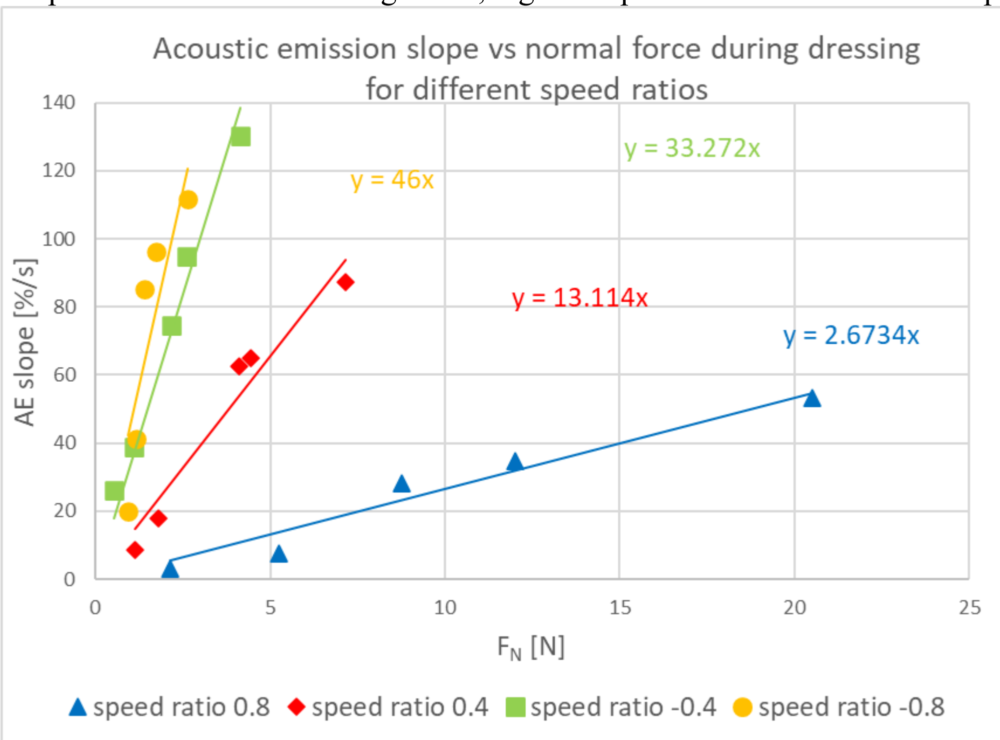

Figure 91: Acoustic emission slope is plotted against the normal force during dressing for different speed ratios - linear trend for each speed ratio and intercepts set at 0 %/s

7.6. Different grinding conditions experimental analysis

The following tests have been run by using four different grinding aggressiveness conditions and five different dressing conditions. The grinding parameters have been kept constant apart from varying the depth of cut per pass to differ grinding aggressiveness.
Grinding parameters:

- Workpiece feedrate: 50mm/s
- Number of passes for different depths of cut: 8 for 0.05mm, 10 for 0.025mm, 15 for 0.01mm and 20 for 0.005mm.

The grinding Aggressiveness number for surface grinding is defined in the following Equation 38:

$$Aggr_g = \sqrt{\frac{a_e}{d_{wheel}} \cdot \frac{v_{workpiece}}{v_{wheel}}} \; [-]$$

Equation 38: Grinding Aggressiveness number for surface grinding

The parameters and results are summarized in Table 13.

Speed ratio [-]	radial infeed [µm/rev]	$Aggr_d$ [-]	depth of cut per pass [mm]	$Aggr_g$ [-]	Grinding MRR [mm^3/s]	Grinding power [W]	SE_g [J/mm^3]
0.8	1	15370	0.05	19.63	32.08	912	28.43
0.8	1	15370	0.025	13.88	16.04	554	34.54
0.8	1	15370	0.01	8.78	6.42	308	48.01
0.8	1	15370	0.005	6.21	3.21	182	56.74
0.4	1	5123	0.05	19.64	32.08	1106	34.48
0.4	1	5123	0.025	13.89	16.04	612	38.16
0.4	1	5123	0.01	8.78	6.42	330	51.44
0.4	1	5123	0.005	6.21	3.21	253	78.88
-0.4	1	2195	0.05	19.65	32.08	1280	39.91
-0.4	1	2195	0.025	13.90	16.04	696	43.40
-0.4	1	2195	0.01	8.79	6.42	407	63.45
-0.4	1	2195	0.005	6.21	3.21	303	94.47
0.4	0.1	1620	0.05	19.66	32.08	1430	44.58
0.4	0.1	1620	0.025	13.90	16.04	761	47.45
0.4	0.1	1620	0.01	8.79	6.42	399	62.20
0.4	0.1	1620	0.005	6.22	3.21	292	91.04
-0.4	0.1	694	0.05	19.67	32.08	3208	100.02
-0.4	0.1	694	0.025	13.91	16.04	1132	70.58
-0.4	0.1	694	0.01	8.80	6.42	449	69.99
-0.4	0.1	694	0.005	6.22	3.21	284	88.54

Table 13: All data of different grinding conditions

The goal was to find out the behavior of grinding specific energy plotted vs grinding Aggressiveness number. In Figure there is a first image for showing how specific energy is varying going from sharper to duller condition; going into details, sorting from sharper to duller condition, there are:

1) Speed ratio 0.8 and radial infeed 1 µm/rev
2) Speed ratio 0.4 and radial infeed 1 µm/rev
3) Speed ratio -0.4 and radial infeed 1 µm/rev
4) Speed ratio 0.4 and radial infeed 0.1 µm/rev
5) Speed ratio -0.4 and radial infeed 0.1 µm/rev

Hence, through the plot in Figure 92, it is possible to state that duller conditions lead to higher generation and burning risk.

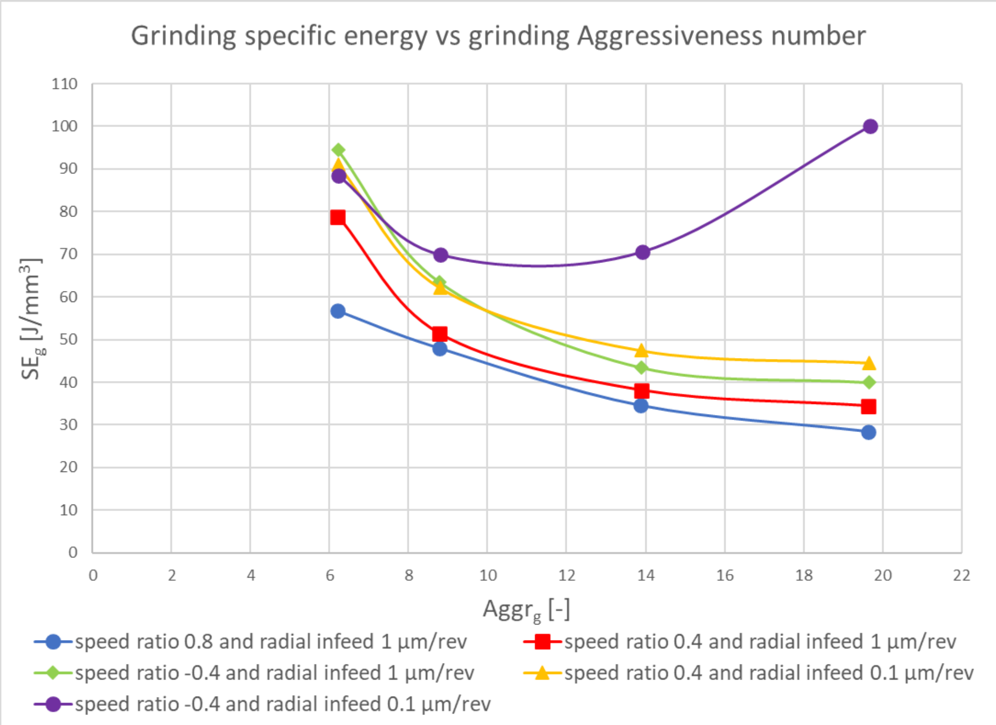

Figure 92: Grinding specific energy is plotted against grinding Aggressiveness number for different dressing parameters

For almost all dressing conditions, a power law trend can be recognized as shown in Figure 93.

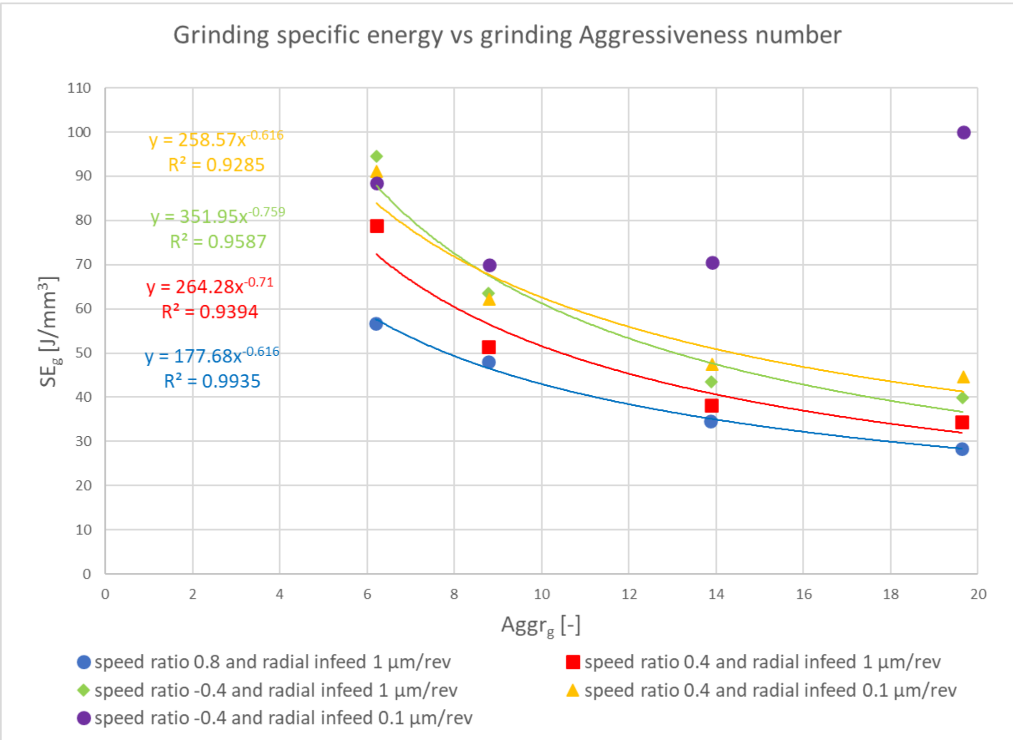

Figure 93: Grinding specific energy is plotted against grinding Aggressiveness number for different speed ratios and radial infeeds: power laws can be seen

For the dullest dressing condition combined with the two most aggressive grinding conditions (larger depths of cut: 0.025mm and 0.05mm), burning has been detected as can be seen in Figure 94, hence no trend is reported for this case (purple data points).

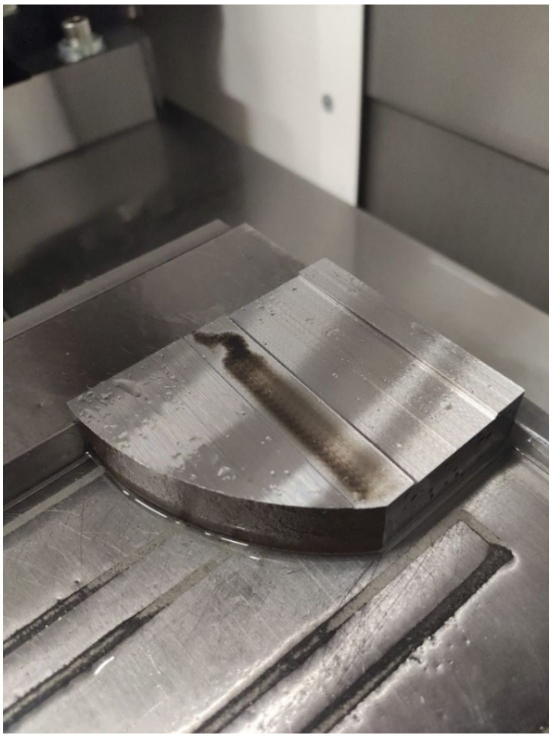

Figure 94: Burning occurred for the dullest dressing condition combined with the most aggressive grinding condition in this case (left track)

7.7. Dwell time experimental analysis

New tests have been run by performing a sharp and a dull dressing condition, respectively +0.8 as speed ratio and 1 μm/rev as radial infeed, and -0.8 as speed ratio and 0.1μm/rev as radial infeed.
Six data points have been collected by using 3 different dwell times for each dressing condition; in particular: 0, 10 and 100 dwell revolutions of grinding wheel.
In Figure 95 and Figure 96, plots are displayed showing a comparison for each dressing condition.

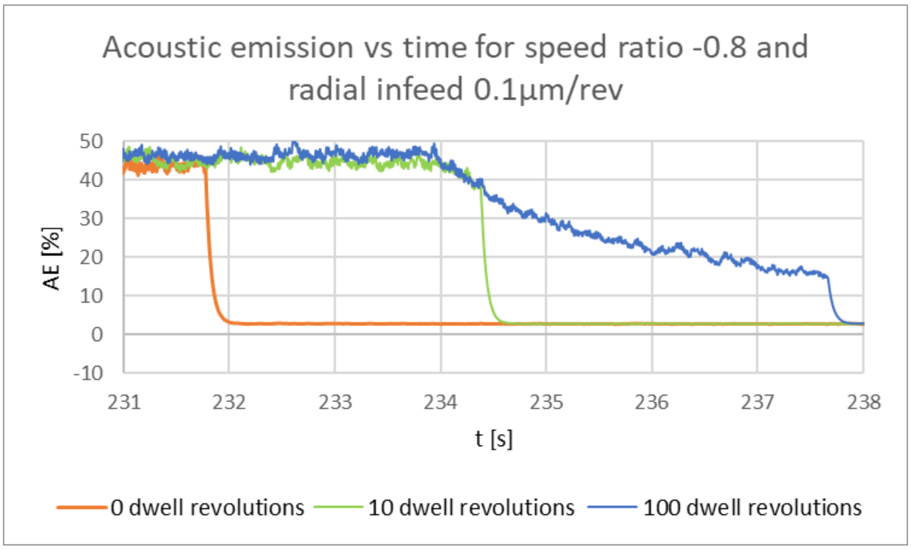

Figure 95: Acoustic emission is plotted against time for speed ratio -0.8 and radial infeed 0.1 µm/rev with 0, 10 and 100 dwell revolutions

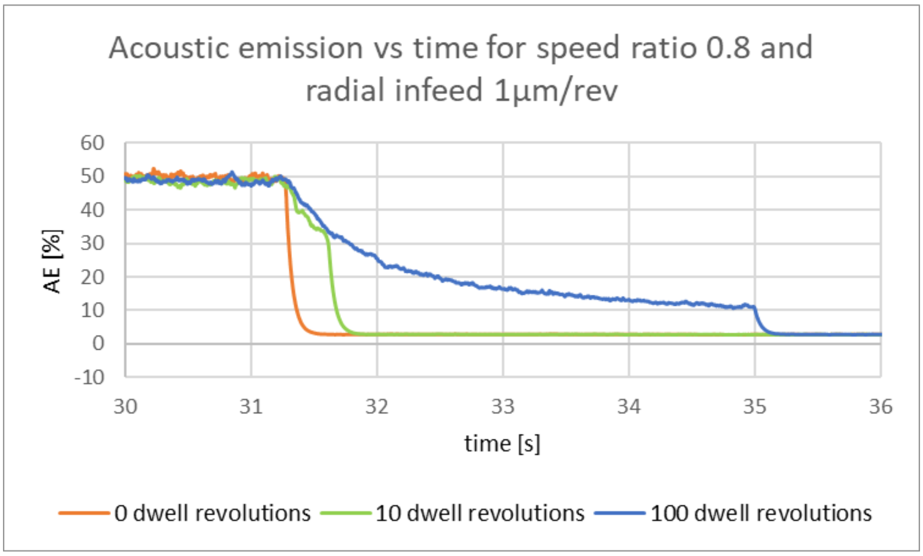

Figure 96: Acoustic emission is plotted against time for speed ratio 0.8 and radial infeed 1 µm/rev with 0, 10 and 100 dwell revolutions

7.8. SEM analysis

Scanning electron microscope (SEM) analysis has been carried out to analyze the topography of the grinding wheel surface: the grinding wheel step has been dressed with speed ratio 0.8 and 1 μm/rev of radial infeed on one half, and for speed ratio -0.8 and 0.1 μm/rev of radial infeed on the other half. Furthermore, the step, 12.83 mm wide, has been ground in the central part for a width of 6.415 mm, with the purpose to analyze and identify differences between the ground and not ground regions processed with different parameters. Hence, overall, four different conditions can be identified: dull dressing, dull dressing + grinding, sharp dressing + grinding, sharp dressing. These regions are indicated in Figure 100 and Figure 101.

7.8.1. SEM analysis setup

To obtain a sample small enough to fit in the scanning electron microscope, a chunk of the grinding wheel step has been broken away with a hammer. The sample has been coated with a thin gold layer in order to proceed with the analysis properly, since made of Aluminum oxide, a ceramic material therefore non-conductive material. Without applying the coating, it would have been challenging to get relevant and clear SEM images, since an accumulation of charge (electrons) would have occurred, which would have disturbed the detection of secondary electrons.
The interaction between the electrons of the beam and the atoms of the sample describes a volume of interaction that is gradually larger with increasing beam voltage. For the SEM analysis two different types of electrons have been used:

- secondary electrons, which are the electrons linked to the outermost atomic levels; they are emitted with an energy between 0 and 50 eV.
- Backscattered electrons, reflected with an energy ranging from 50 eV up to incidence energy.

The first are used for studying surface morphology of the samples, instead the latter are carrier mainly of topographical signals.
In Figure 97 is presented the utilized SEM station (Philips XL30 ESEM) at Chalmers university. During the analysis different holders have been used with the purpose to facilitate the view high tilt angles. Moreover, contrast and brightness have been adjusted time by time to have the most clear image possible.

Figure 97: Chalmers scanning electron microscope

7.8.2. SEM analysis images

In the following the most relevant SEM images of the sample are shown, which have been observed with Different magnifications, and the high tension has been set to 20kV.
In Figure 98, it is shown a comparison between the dull and sharp parts of the grinding wheel step. As expected, the part of the wheel dressed with speed ratio -0.8 and 0.1 µm/rev of radial infeed (on the left) exhibits a quite flat surface overall; instead the other side dressed with speed ratio 0.8 and 1 µm/rev of radial infeed (on the right) reveals an irregular and sharp surface.
In addition, by looking at the red circles it can be noticed that in the left SEM image (dull conditions) there are more flat surfaces areas than in the SEM image on the right (sharp conditions), for the same considered mm^2.

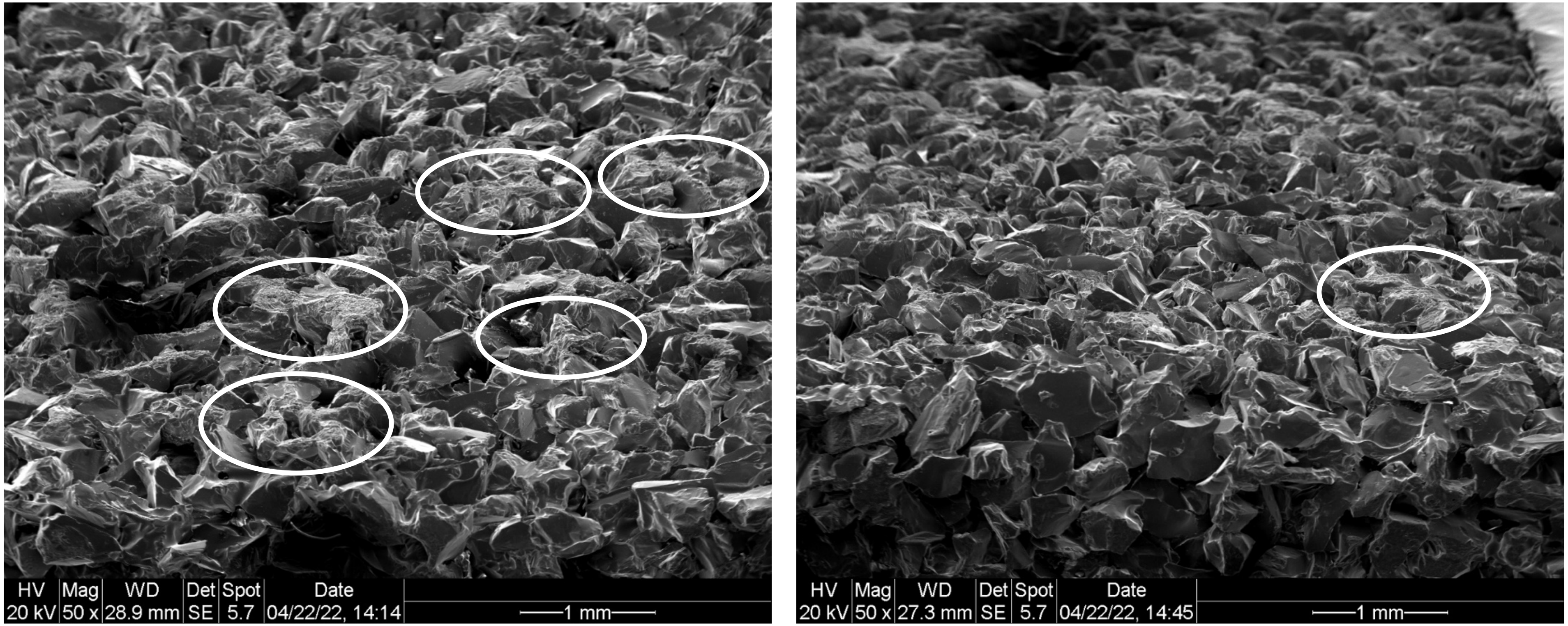

Figure 98: Comparison between the dull (on the left) and sharp (on the right) regions of the grinding wheel step (low tilt angle)

In Figure 99 a significant zoom of Figure 98 is presented to better exhibit the dull and sharp areas of the grinding wheel step dressed with different conditions.

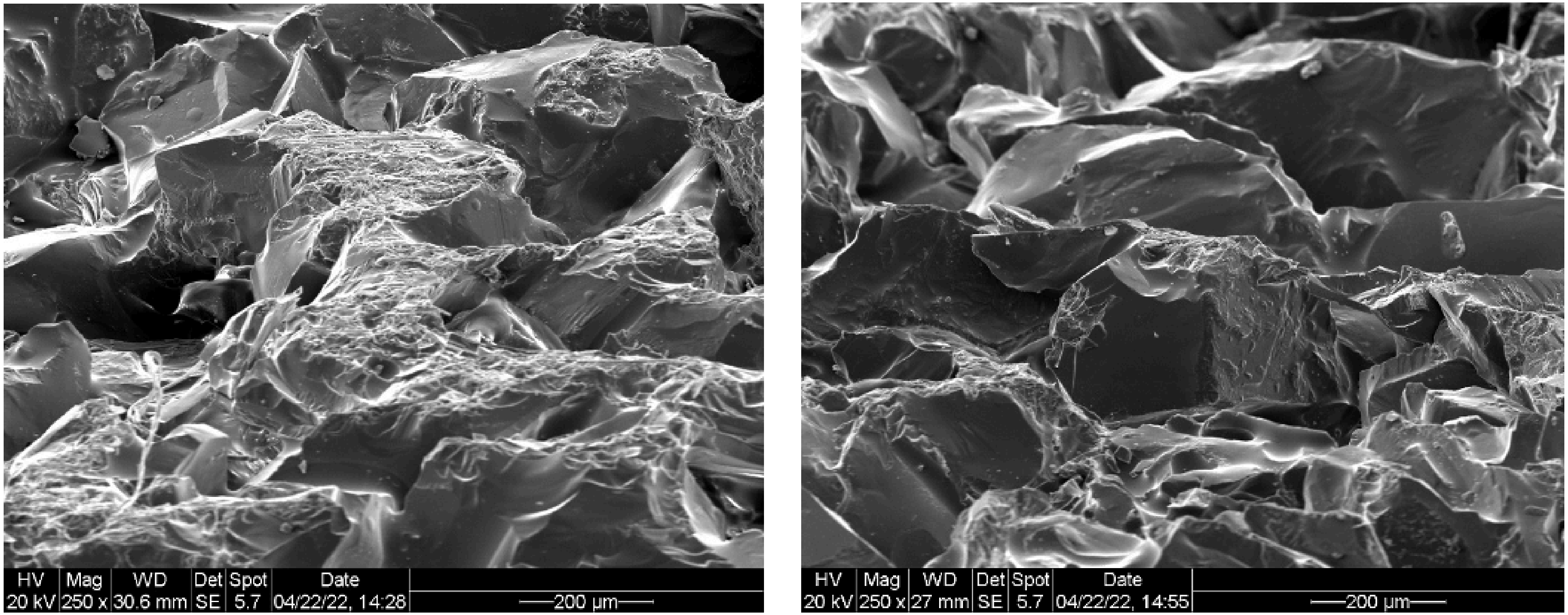

Figure 99: Comparison between dull (on the left) and sharp (on the right) regions of the grinding wheel step with high magnification

The differences between the regions of the grinding wheel step can be seen in Figure 100, in which the dressed and dressed-ground parts are defined and distinguished, taking into account an overview of the sample with a high tilt angle. Figure 101 shows the same image with 90° observing angle. In these pictures the steel presence on the ground part can be recognized by means of backscattered electrons, in particular in the second one it is clear as for duller dressing condition, the steel presence (material loading) will be larger, thus the heat generation as well.

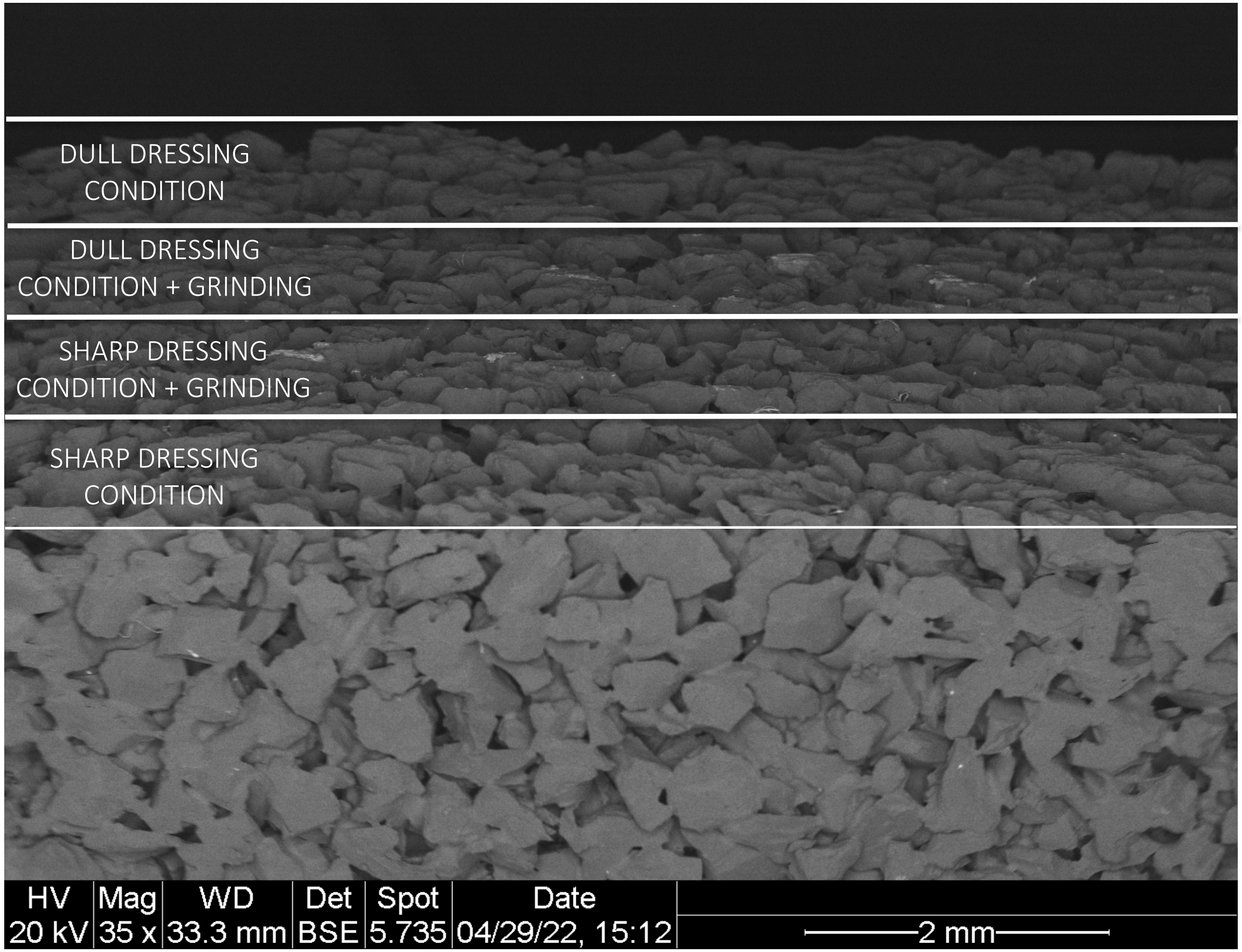

Figure 100: Distinction of the 4 sections of the grinding wheel step – sharp dressing condition, sharp condition + grinding, dull dressing condition + grinding, dull dressing condition

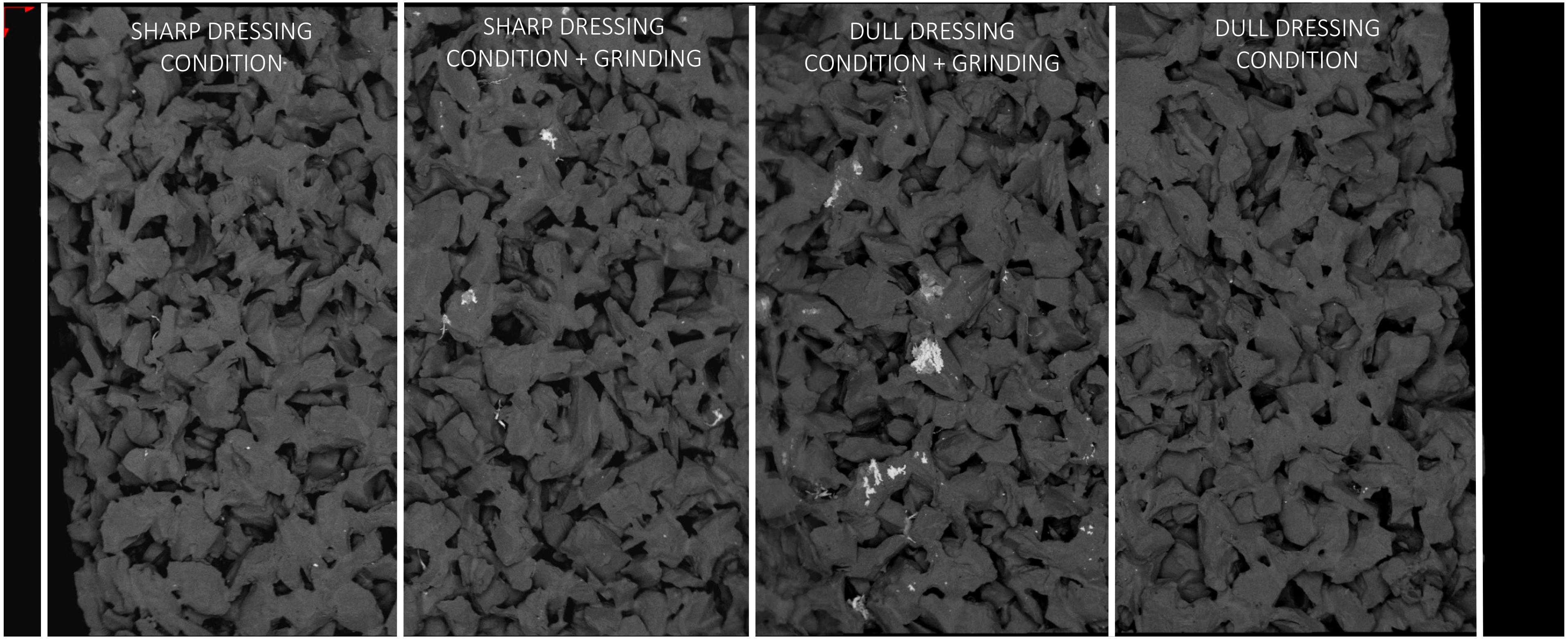

Figure 101: Distinction of the 4 sections of the grinding wheel step using 90° observing angle – sharp dressing condition, sharp condition + grinding, dull dressing condition + grinding, dull dressing condition

In the next pages, several SEM images (obtained with high tilt angle) of the dull and sharp parts of the grinding wheel step are reported, showing furthermore for both conditions the areas in which steel is present with a larger magnification and reporting a comparison between BSE and SE of each zoom area as well (proceeding from left to right BSE and then SE).

In Figure 102, the sharp part of the sample is shown with high tilt angle, and in Figure 103 – Figure 107, the zoomed areas showing steel presence are proposed.

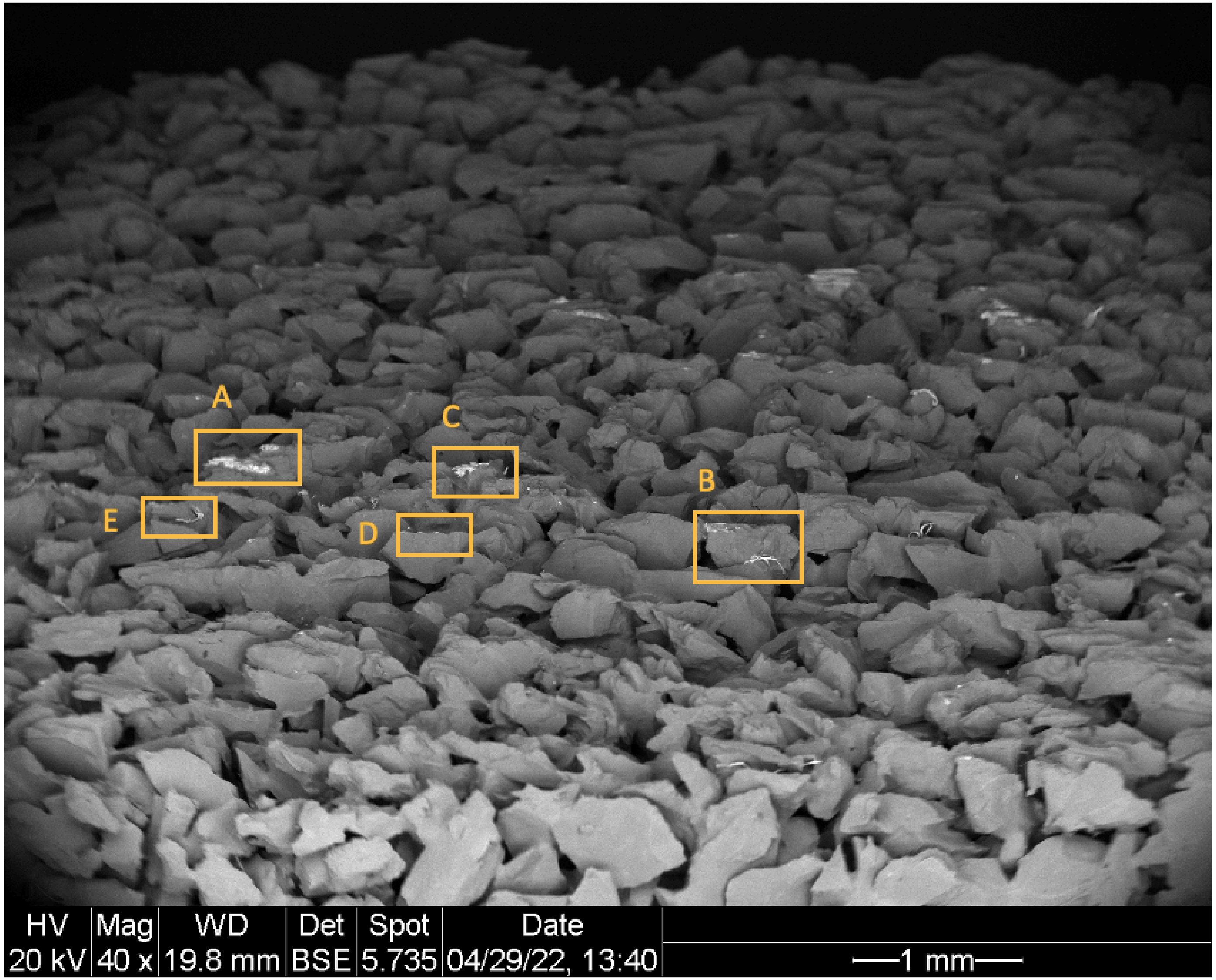

Figure 102: Sharp part of the grinding wheel step (high tilt angle)

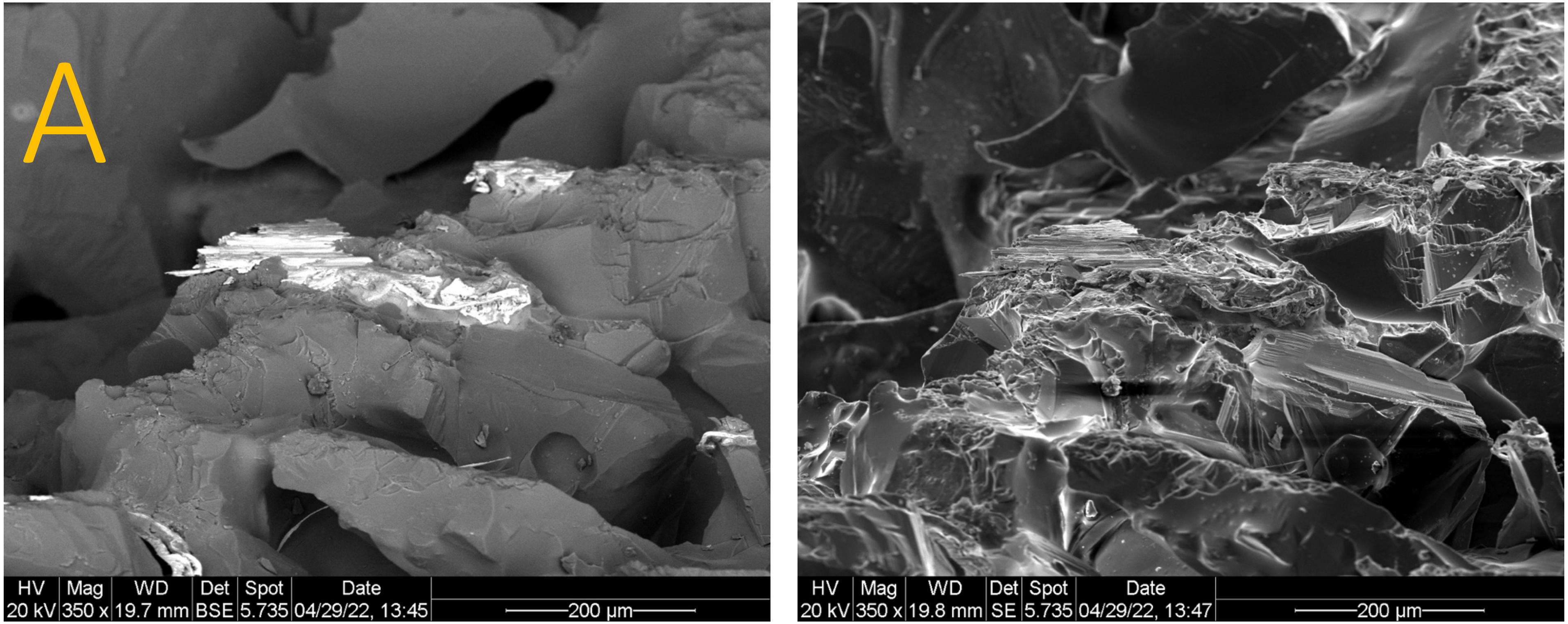

Figure 103: Zoom sharp part rectangle A - comparison BSE and SE

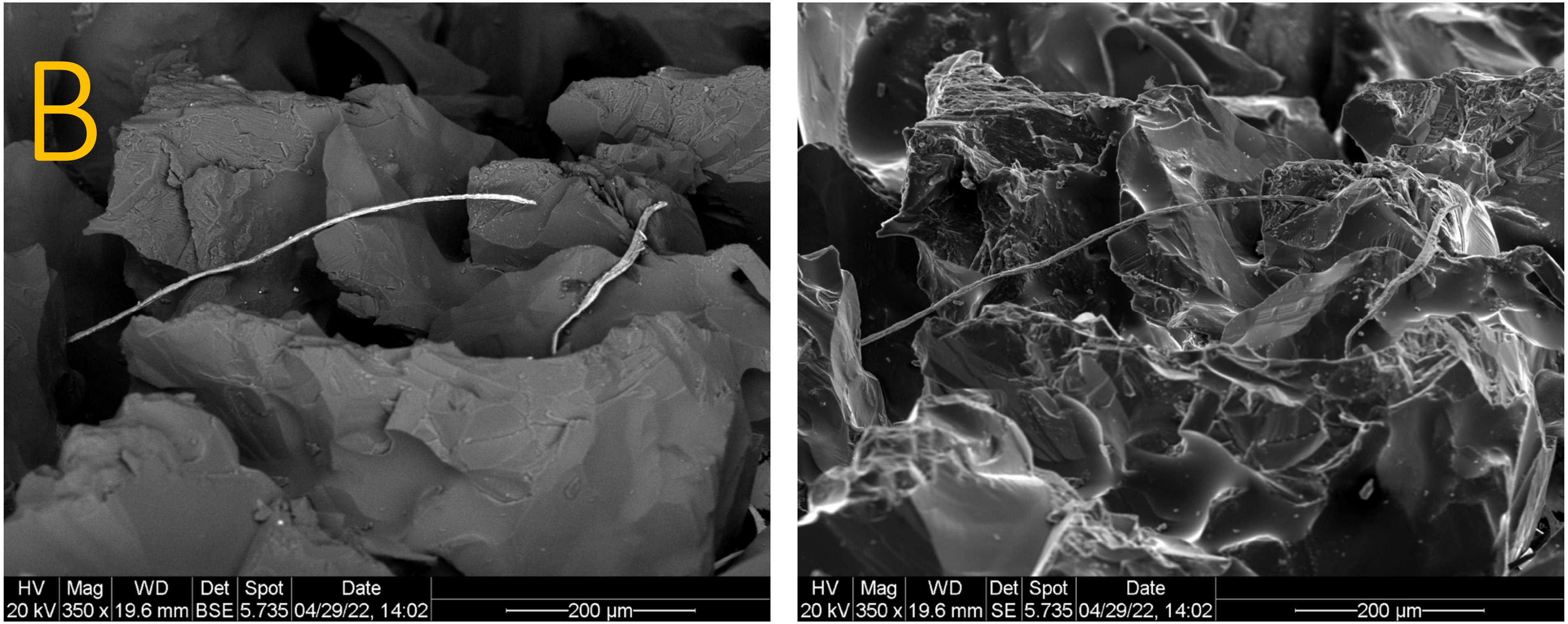

Figure 104: Zoom sharp part rectangle B - comparison BSE and SE

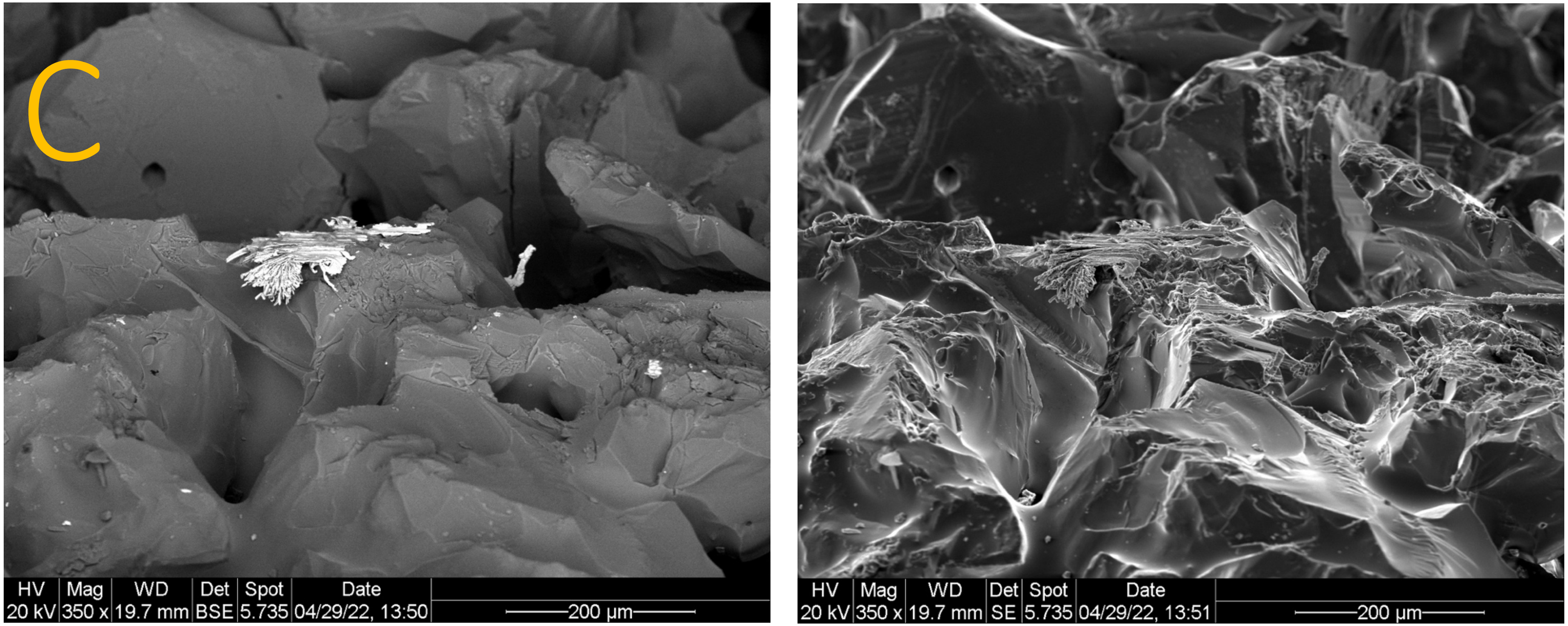

Figure 105: Zoom sharp part rectangle C - comparison BSE and SE

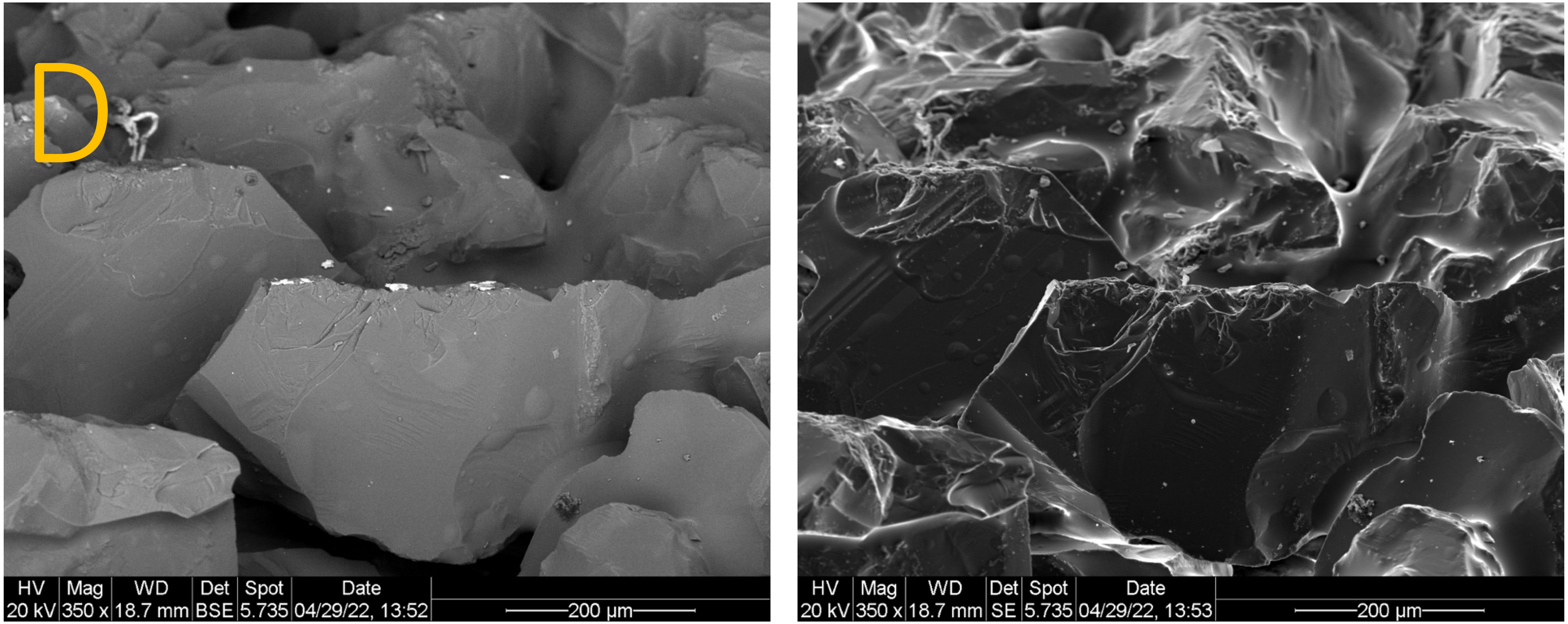

Figure 106: Zoom sharp part rectangle D - comparison BSE and SE

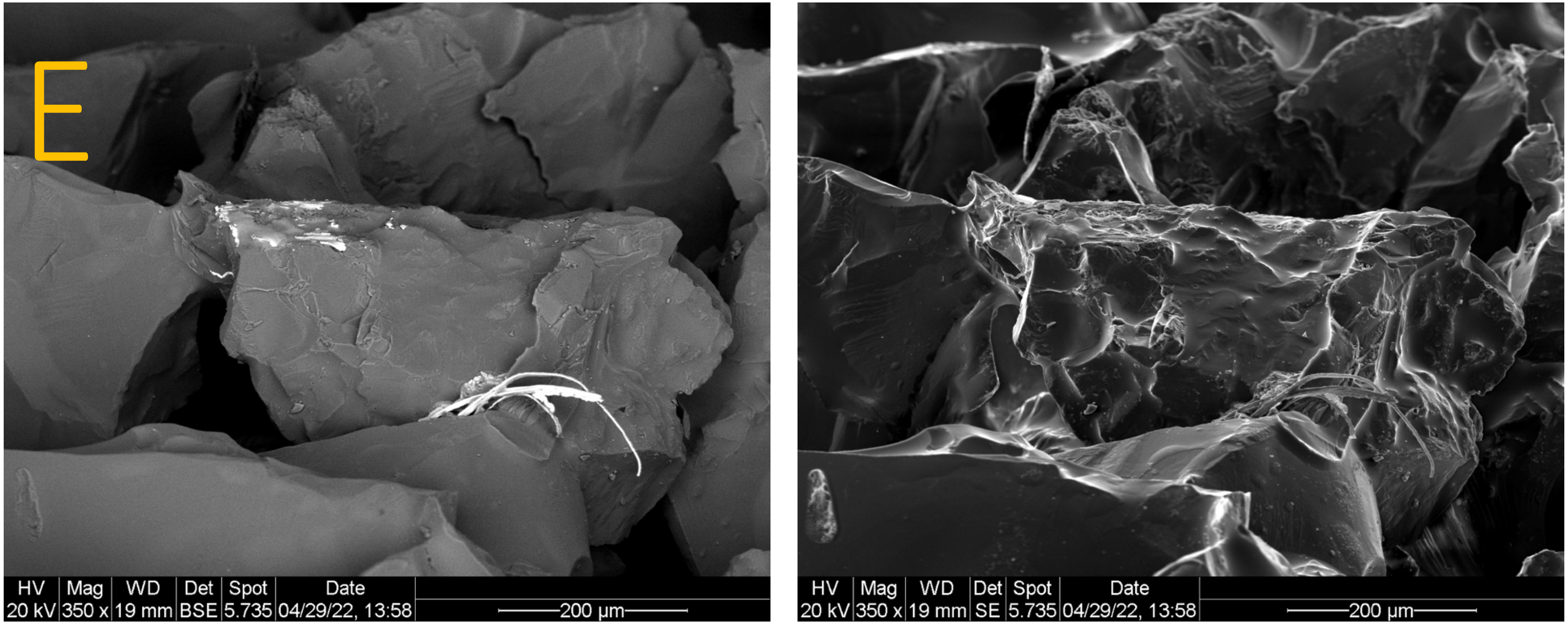

Figure 107: Zoom sharp part rectangle E - comparison BSE and SE

In Figure 108 there is a zoom of the sharp dressing condition of the step taken with high tilt angle, which shows the differences between BSE and SE of a very irregular grains area.

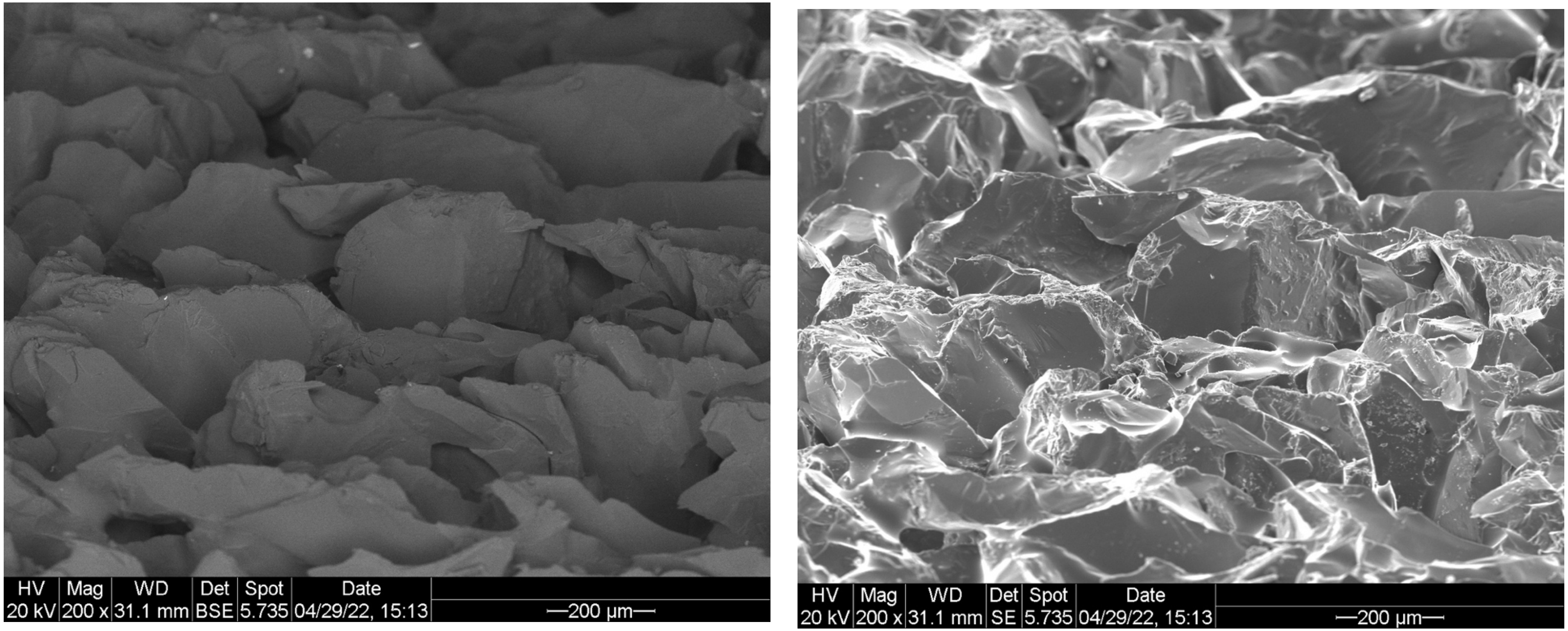

Figure 108: Very irregular grains area, sharp part of the grinding wheel step - comparison BSE and SE

In Figure 109, a picture of the dull dressing condition of the sample got with high tilt angle is presented, and in the figures below (Figure 110 – Figure 114), the zoomed areas revealing steel presence are shown as well.

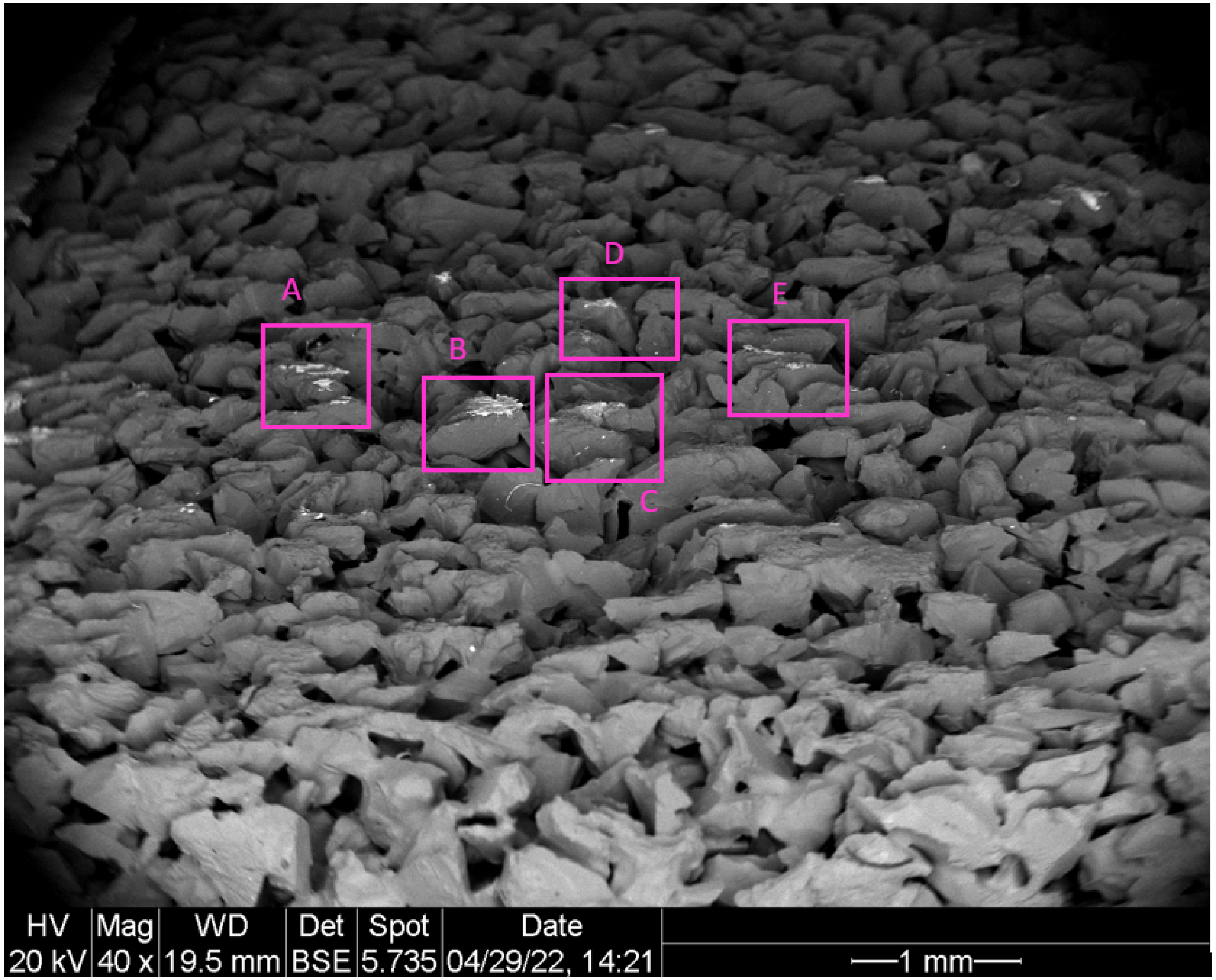

Figure 109: Dull part of the grinding wheel step (high tilt angle)

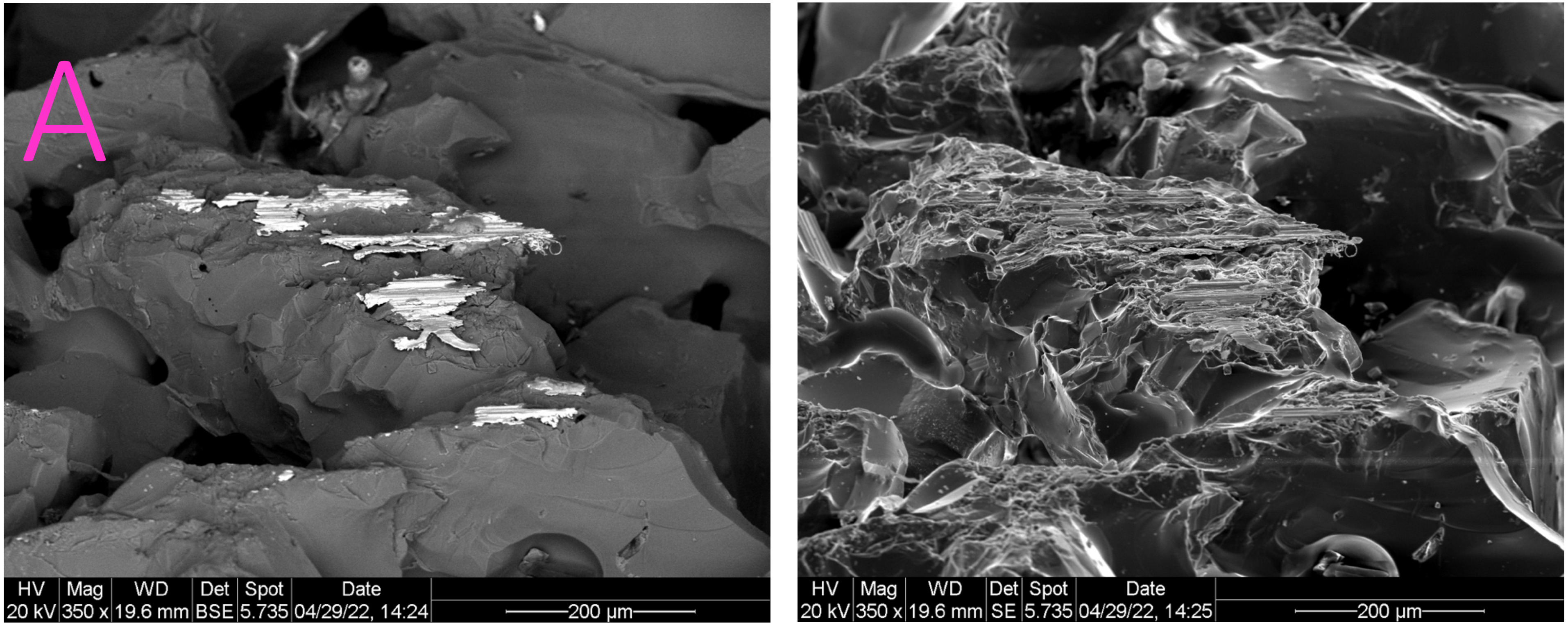

Figure 110: Zoom Dull part rectangle A - comparison BSE and SE

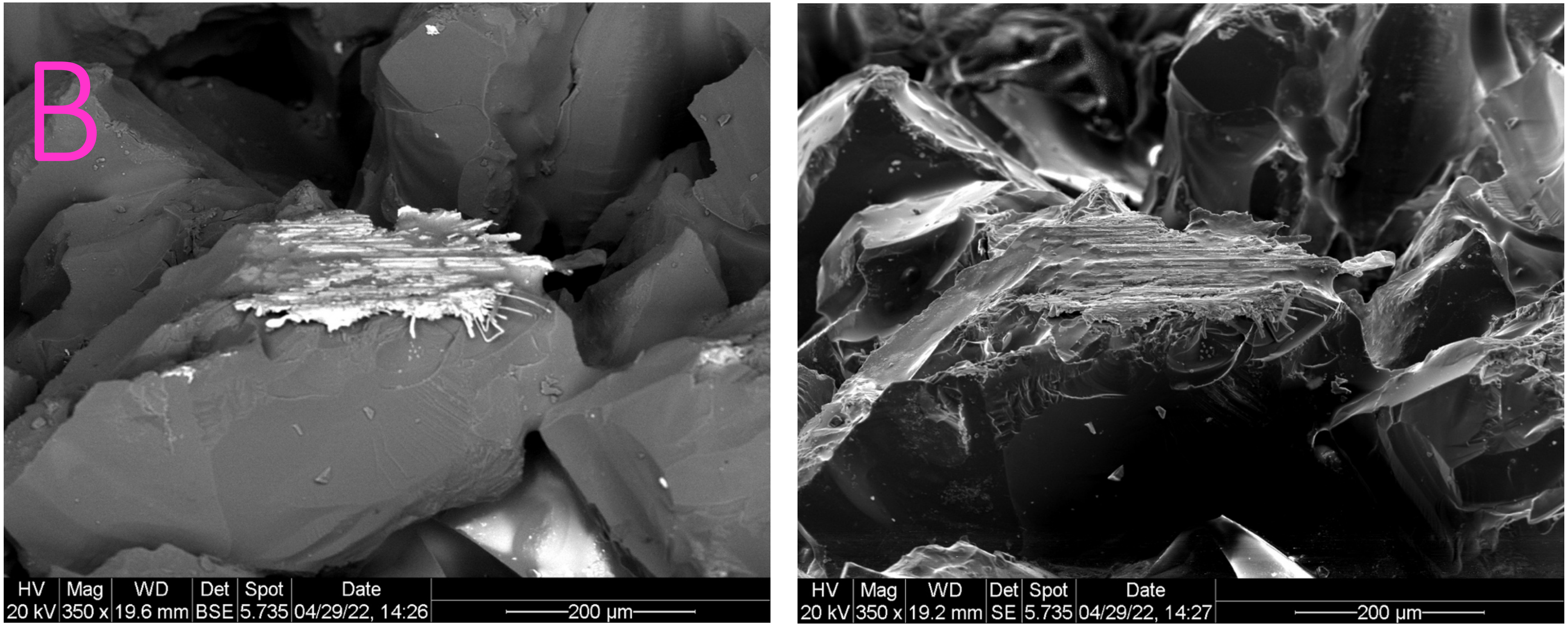

Figure 111: Zoom Dull part rectangle B - comparison BSE and SE

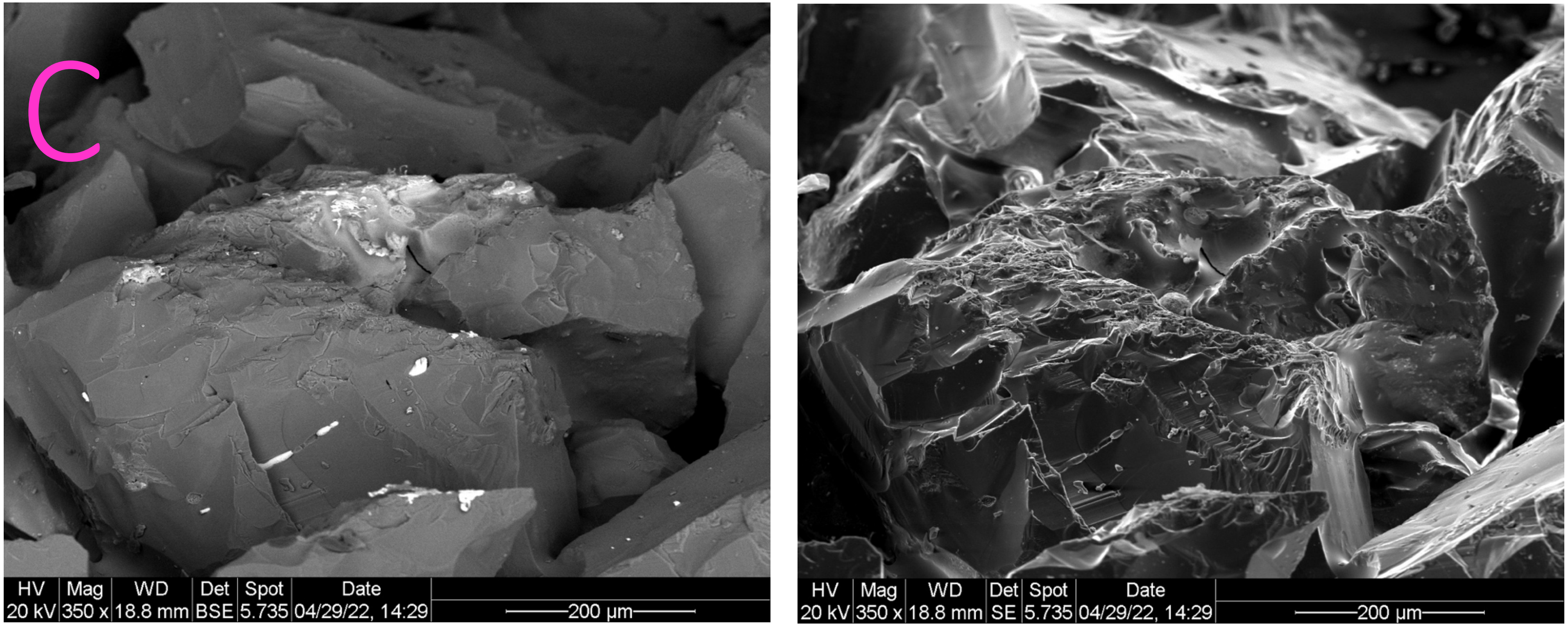

Figure 112: Zoom Dull part rectangle C - comparison BSE and SE

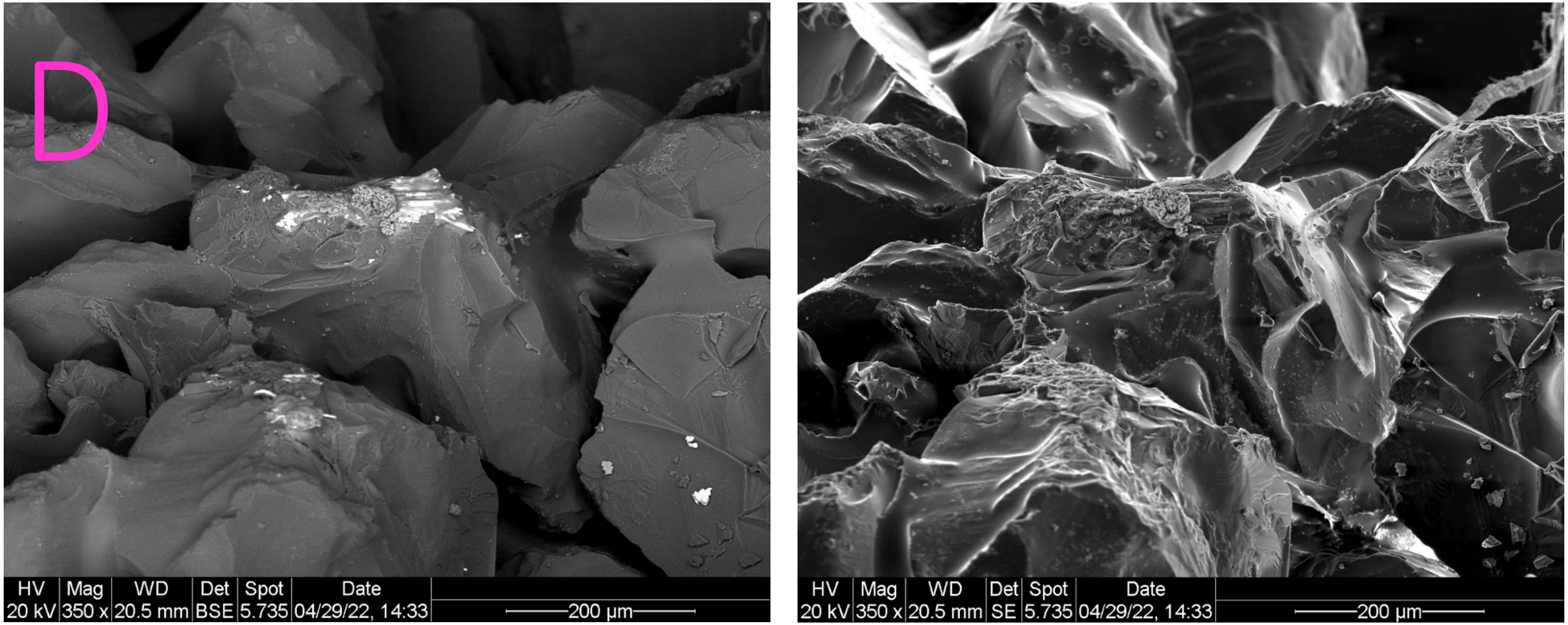

Figure 113: Zoom Dull part rectangle D - comparison BSE and SE

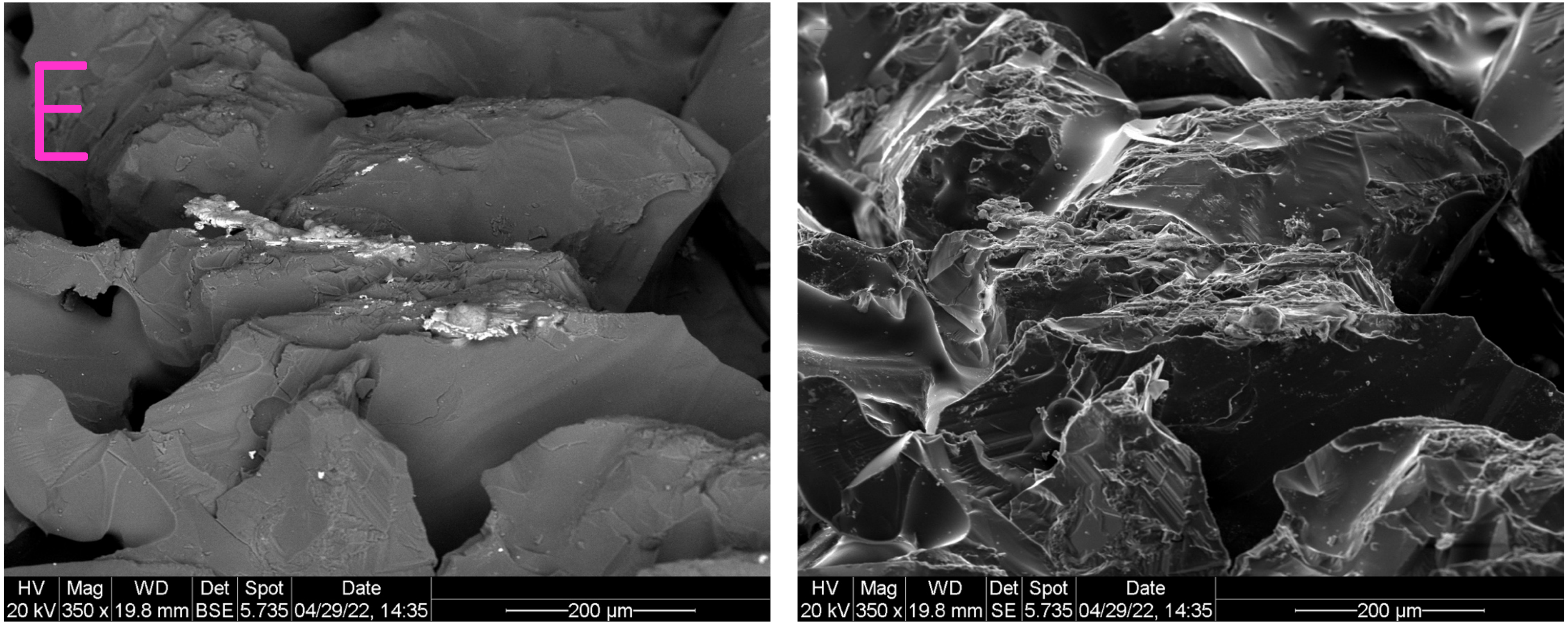

Figure 114: Zoom Dull part rectangle E - comparison BSE and SE

In conclusion, in Figure 115 there is an interesting zoom of the dull part of the step, which shows the comparison between BSE and SE of a very flat surface, taken with high tilt angle.

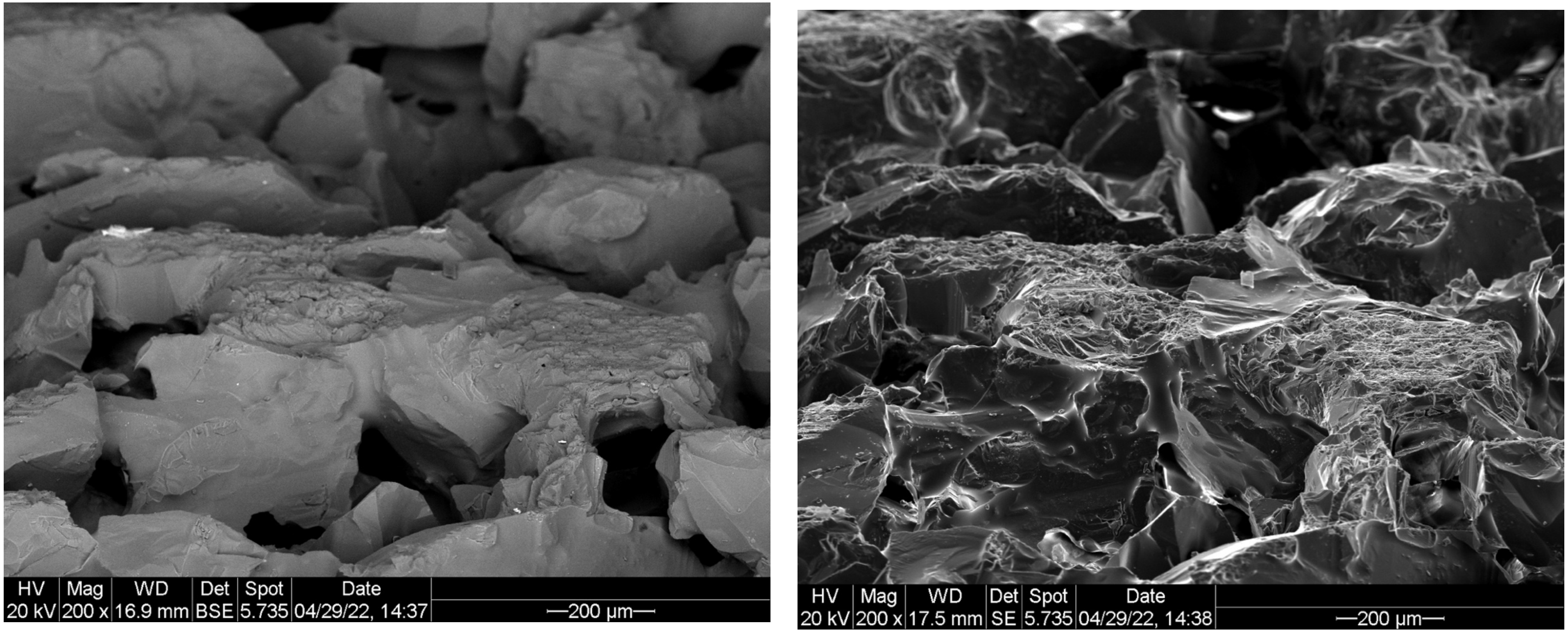

Figure 115: Very flat area, dull part of the grinding wheel step - comparison BSE and SE

8. RESULTS DISCUSSIONS AND CONCLUSIONS

8.1. Consistency with Malkin and Murray’s results

The charts in which the grinding specific energy is plotted against the dressing Aggressiveness number and against the dressing specific energy (reproposed in Figure 116) show results which are comparable with Malkin and Murray's experiments. Indeed, the behaviors of the involved variables are consistent overall, despite different conditions and tools have been used, such as dressing roll, grinding wheel and steel workpiece.

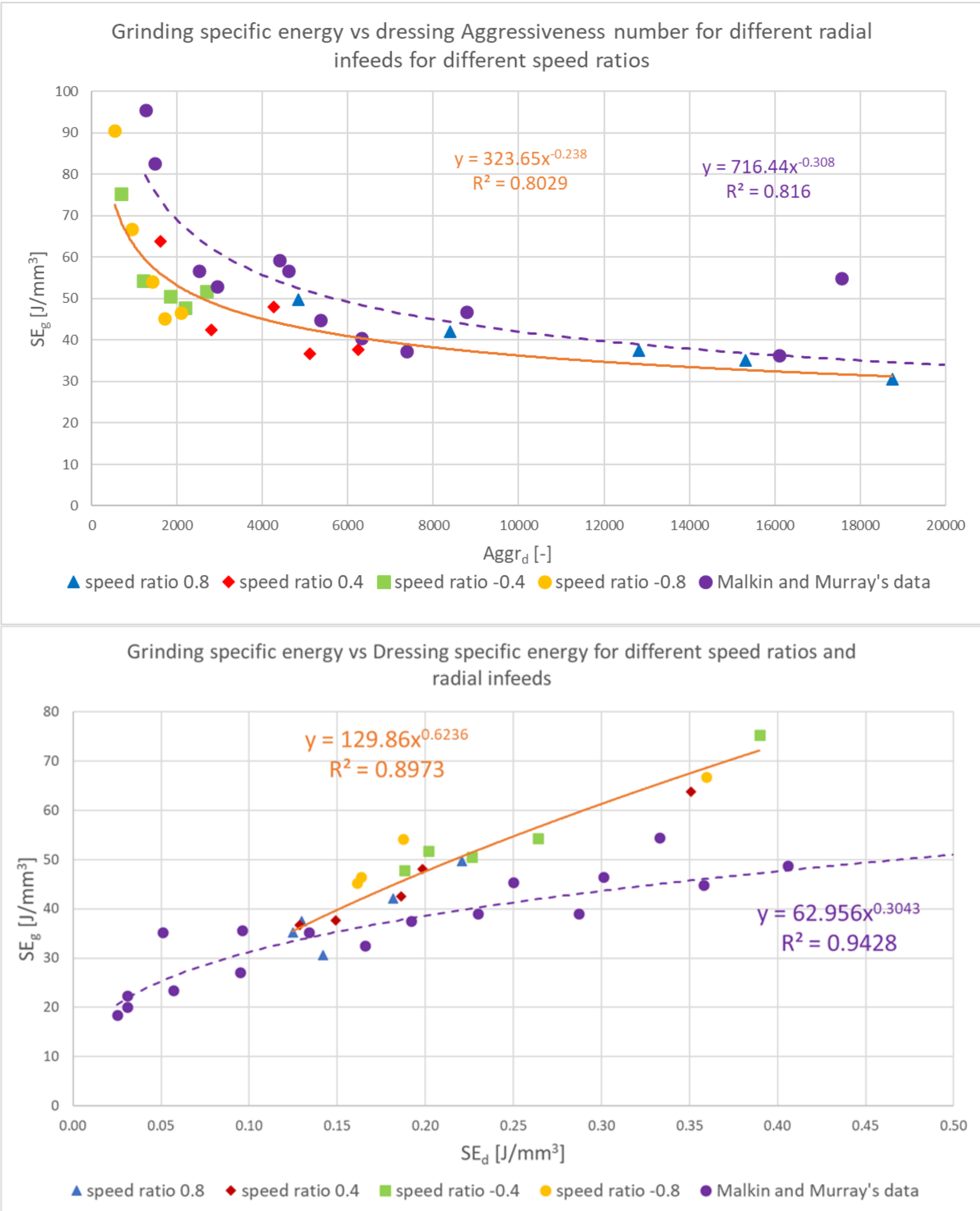

Figure 116: Experimental plots similar to Malkin and Murray's results

In the first chart, case data points for grinding specific energy versus dressing Aggressiveness number have the same behavior and similar values too.
On the other hand, in the second plot, it is more difficult to find an evident similarity, even if, considering the behavior, it is possible to state both for Malkin and Murray's results both for the new experiments that, for higher dressing specific energy, higher grinding specific energy corresponds.
This is due to many factors involved in the operations carried out such as: material type, grit size and type for grinding wheel grits, coolant type and grinding parameters. Therefore, in this case the main result is that for given grinding operation, grinding specific energy increases with dressing specific energy.

8.2. Dressing Aggressiveness number importance

Another key point is the utility of the dressing Aggressiveness number to predict thermal damages, indeed burning is caused by the combination of too dull dressing (low dressing Aggressiveness number) and too large grinding Aggressiveness (e.g. large depth of cut, high workpiece federate). In In Figure 117, for fixed grinding conditions, only one dressing condition (the dullest) led to burning, therefore a threshold can be defined.
A similar reasoning for variable dressing and grinding conditions is presented in Figure 118, and once again, burning can be easily individuated.

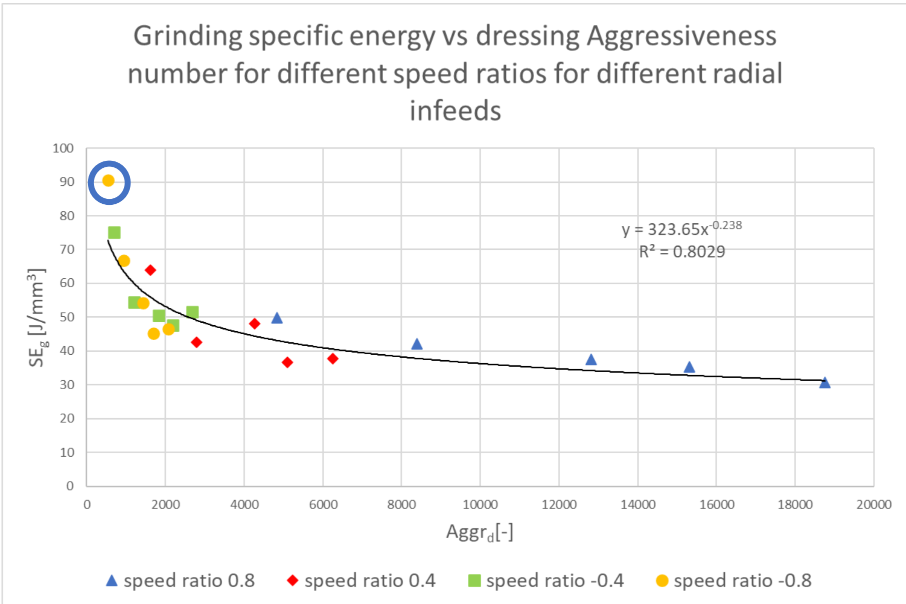

Figure 117: Grinding specific energy versus dressing Aggressiveness number, burning threshold

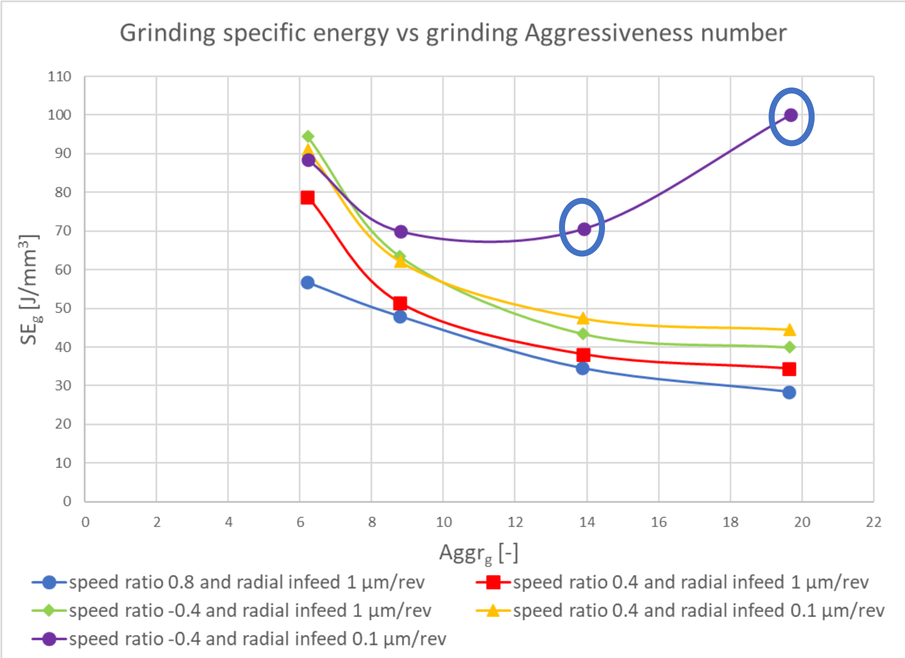

Figure 118: Grinding specific energy against grinding Aggressiveness number, burning occurred

Furthermore, through the dressing Aggressiveness number it is possible to assess the wheel sharpness, indeed to establish if the dressing condition is dull or sharp, therefore if the grinding wheel will have more or less flattened areas, the same plot as the one shown in Figure 115 can be used: duller dressing condition will lead to higher specific energy, and vice-versa for sharp condition.
In addition, the SEM images have shown evident differences between dull and sharp condition, and considering the images in Figure 119, where a comparison between two of the zooms on dull and sharp areas with steel loading is presented, it can be seen that in the dull condition the steel presence results higher and the material is practically molten, indicating larger rubbing and plowing with respect to cutting, thus higher heat generation. On the other hand, in the sharp case, some chips are visible through the backscattered electrons, hence the grains edges are sharper, and cutting is occurring.

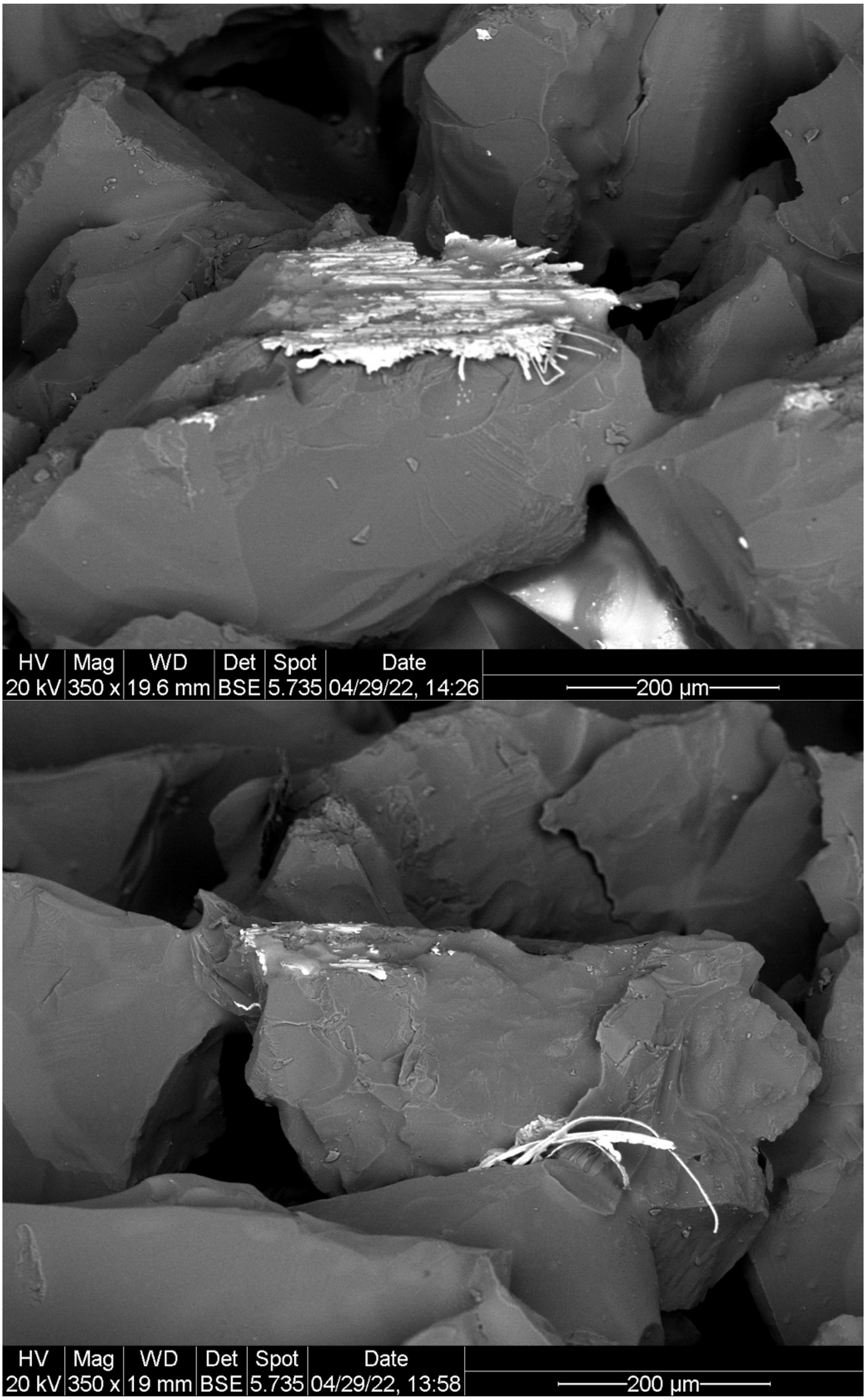

Figure 119: Dull (above) and sharp (below) conditions comparison

8.3. Acoustic emission signal during dressing

Acoustic emission has been another important study factor in the tests.
By means of the acoustic emission sensor mounted in the machine, it was possible to collect AE data coming from the dressing operations and draw conclusions.
First, it has been proven that it was possible to find a correlation between acoustic emission and dressing power (Figure 120), or an even better between the corresponding specific energies (Figure 121).
In Figure 122 and Figure 123 there is a proof that dressing power and acoustic emission have the same behavior during the process.
Finally, there is the possibility of defining an acoustic emission calibrated power, and in Figure 124 it has been noticed that the accuracy will not be too low with respect to the one coming from following a power law trend, the one with the highest R2. The acoustic emission value was given in percentage of a certain Volt value, not known; nevertheless, it is possible to say that the Volt value was "calibrated" as well to have a correlation between AE and dressing power giving a possible linear proportionality with slope close to 1: hence a percentage value of acoustic emission would correspond to the same value in Watts for the dressing power.

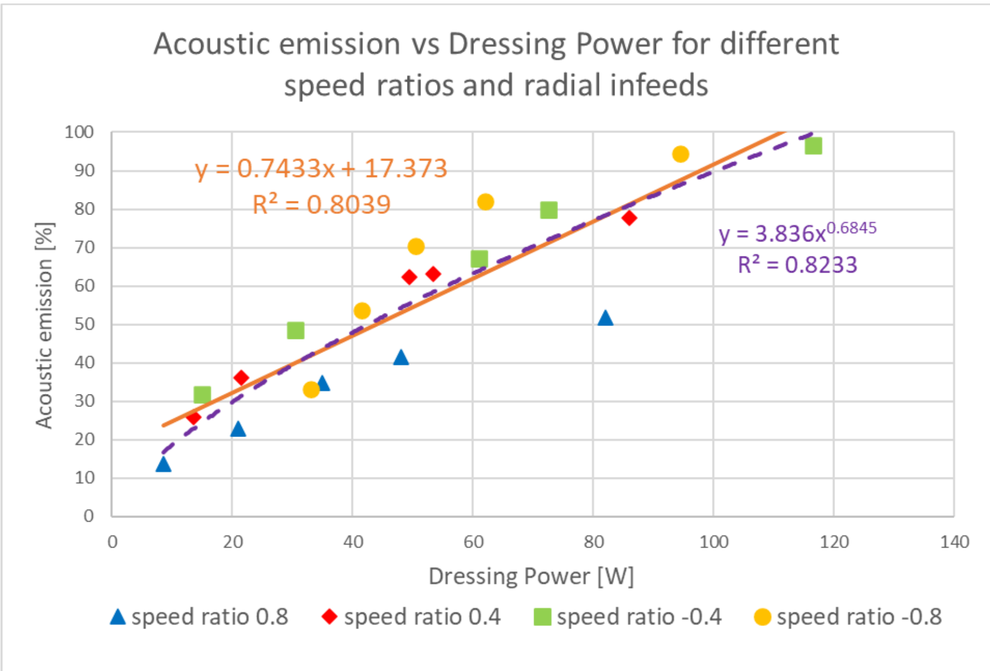

Figure 120: Acoustic emission is plotted against the dressing power for different speed ratios – power law trend fits better the data

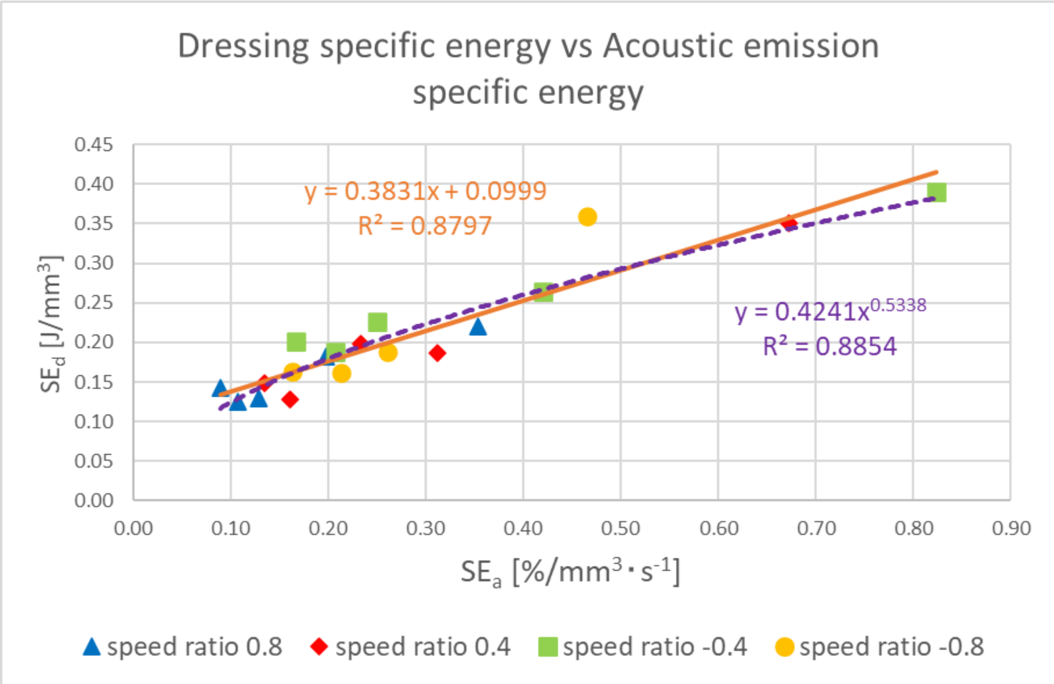

Figure 121: Dressing specific energy is plotted against the acoustic emission specific energy for different speed ratios – linear trend and power law trend

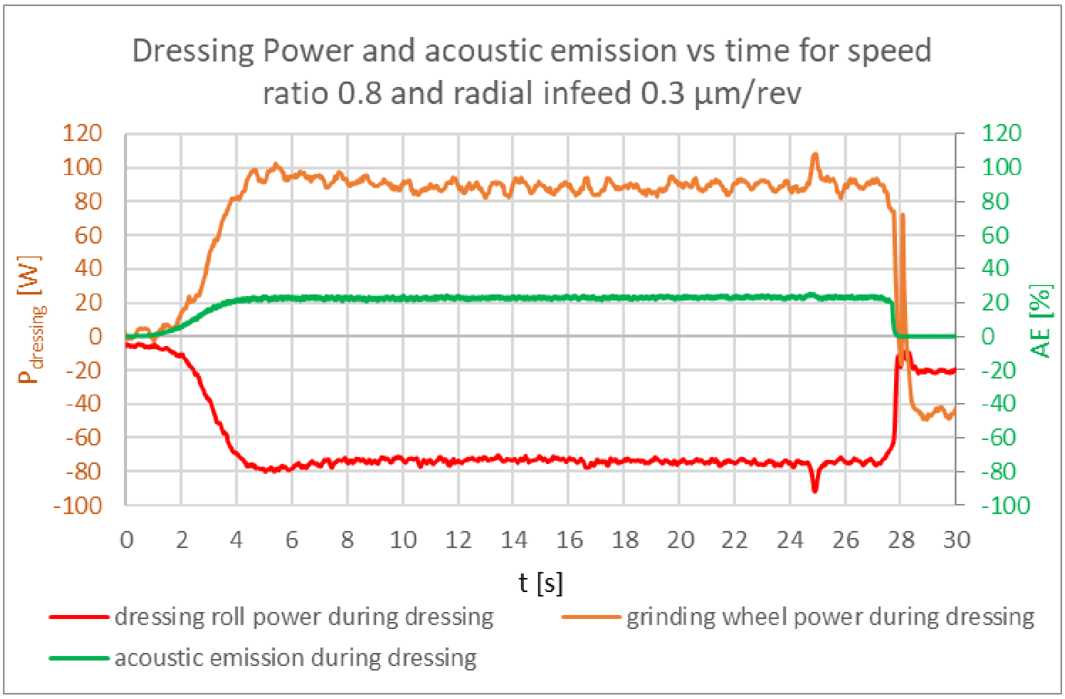

Figure 122: Dressing power and acoustic emission are plotted against the time for speed ratio 0.8 and radial infeed 0.3 µm/rev

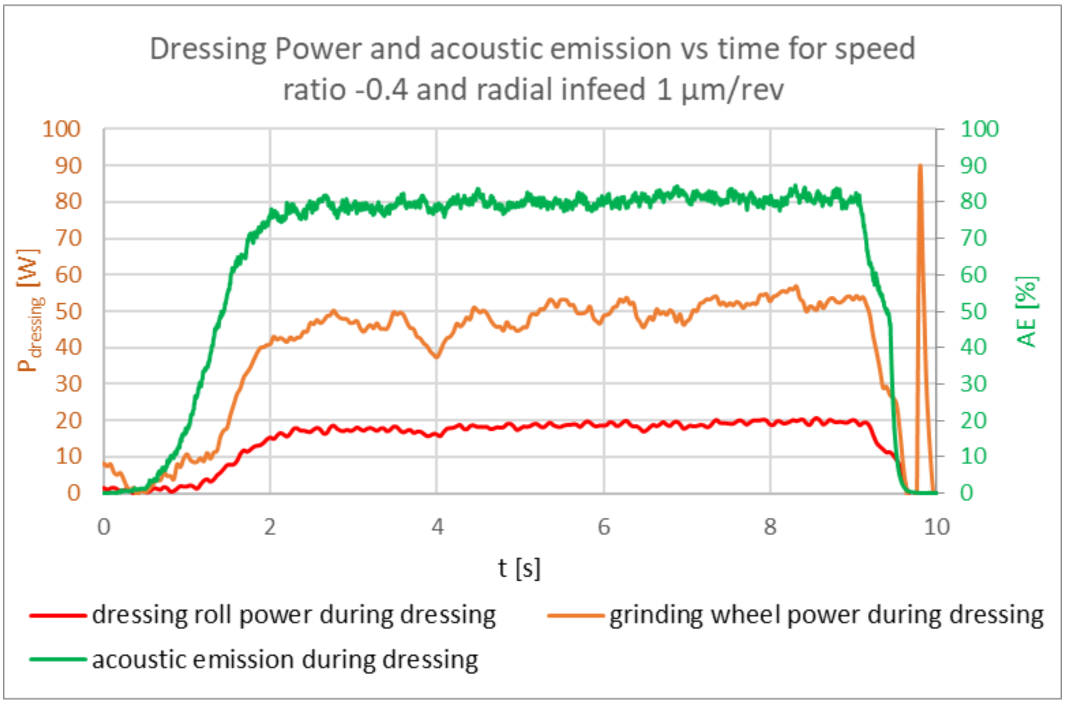

Figure 123: Dressing power and acoustic emission are plotted against the time for speed ratio -0.4 and radial infeed 1 µm/rev

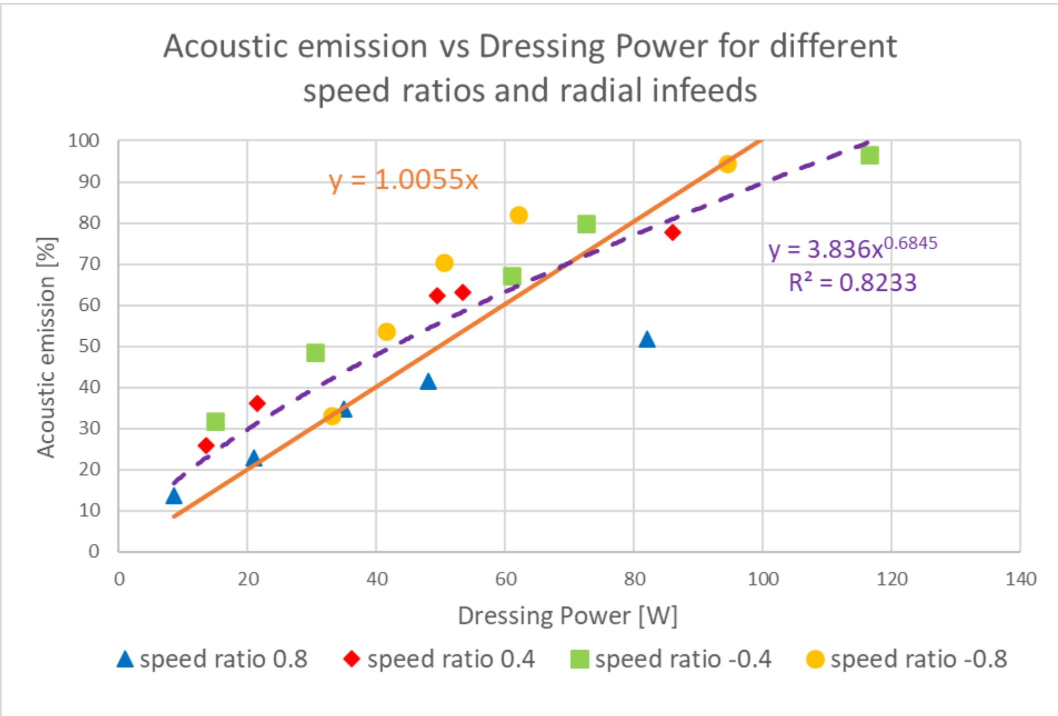

Figure 124: Acoustic emission is plotted against dressing power for different speed ratios – linear trendline with zero as intercept and power law trend

References

[1] R. L. McKee, Machining with Abrasives, New York: Van Nostrand Reihnhold.

[2] P. Krajnik, «Manufacturing processes course slides,» Sweden, 2021.

[3] R. W. Bolz, Manufacturing processes, New York: McGRAW-HILL BOOK COMPANY, INC.

[4] B. H. Amsted, P. F. Ostwald e M. L. Begemman, Manufactirunig processes.

[5] H. Company, «Basic of bonded abrasives».

[6] M. P. Groover, Principles of Moder Manufacturing 4° Edition.

[7] S. Kalpakjian e S. S. R., Manufacturing Engineering Technology ifth Edition, Pearson Education, Inc.

[8] J. Badger, The Grinding Book.

[9] S. Malkin, «Wheel Truing, Dressing, and Topography,» in *Grinding process*, Springer Link.

[10] J. Badger, P. Krajnik e R. Dražumerič, «Application of the dimensionless Aggressiveness number in abrasive processes,» *Elsevier: Internal Journal of Machine Tools and Manifacture.*

[11] J. Badger, S. Murphy e G. E. O'Donnell, «Acoustic emission in dressing of grinding wheels: AE intensity, dressing energy, and quantification of dressing sharpness and increase in diamond wear-flat size,» *Elsevier: Internal Journal of Machine Tools and Manifacture.*

[12] T. Murray e S. Malkin, «Effects of Rotary Dressing on Grinding Wheel Performance,» *Journal of Engineering for Industry.*

[13] S. Malkin e T. Murray, «Mechanics of Rotary Dressing of Grinding Wheels,» *Journal of Engineering for Industry.*

[14] «Creep feed grinding - Continuous dressing».

[15] S. Malkin e T. Murray, «Comparison of single point and rotary dressing of grinding wheels».

[16] «PLANOMAT HP | BLOHM,» [Online]. Available: https://www.blohm-machines.com/en/grinding-machines/detail-view/product/planomat-hp/.

[17] B. Linke, «“Wirkmechanismen beim Abrichten keramisch gebundener Schleifscheiben”».